Characterisation of Lactose in the Liquid and Solid State using Nuclear Magnetic Resonance and Other Methods

A thesis presented in partial fulfilment
of the requirements for the degree of

Doctor of Philosophy

at

Massey University

Jim Hargreaves

1995

Abstract

The anomeric composition of lactose is studied using polarimetry, gas liquid chromatography and a variety of nuclear magnetic resonance (NMR) methods and the results compared. As a result reliable characterisation based on solution methods is obtained. The measurement of the spectrum of nuclear spin-lattice relaxation times (T_1) of lactose powders demonstrate significant differences between crystalline and amorphous species and between the different crystalline forms of lactose. These differences form the basis of a new characterisation methodology of powdered lactose where measurements are performed in the solid state. The use of linear multi-exponential curve fitting algorithms (NNLS and Contin) to deduce the "relaxation spectrum" from the multiexponential decay curve (obtained using a low-cost wideline NMR machine) allows for the reliable interpretation of noisy and drift-affected inversion recovery data. The absence of spin-diffusion between crystalline and amorphous species enables the determination of the relative weight fractions of several lactose species in a mixed powder sample with a simple correlation to the relative intensities of relaxation time components of the T_1 spectrum. The T_1 values of amorphous lactoseareshown to be sensitive to moisture content and the glass transition process. The quantitative results gained from using the T_1 method to characterise lactose can be applied to improve the functionality of lactose and lactose-containing powders.

Acknowledgments

I wish to thank Professor Paul Callaghan for his enthusiasm and positive guidance as first-principal supervisor and whose advice and inspiration helped make this work a success, and secondly, my second-principal supervisor Associate Professor Ken Jolley whose experience and positive criticism provided much-needed guidance during the development stages of the research work and the writing of this thesis. Thanks go to my other supervisors, Dr John Smart, Dr Richard Archer, and Dr Eric Ainscough for their contribution and positive support during our many meetings.

I would like to thank the staff of the Milkfat Products Section of the NZDRI for allowing endless use of the BRUKER minispec NMR machine. In particular, I thank Alastair MacGibbon who was never too busy to help when things went wrong, and to my special friends Sally Hewson and Yvonne van der Does who made my work in the Milkfat laboratory truly a pleasure. I thank Dong Chen and Richard Lloyd of the Milkpowders Section for their contribution to the work on amorphous lactose.

Thanks go to Keith Morgan and Richard Meinhold of Industrial Research Limited, Gracefield for the solid-state high-resolution 13C spectra of the crystalline species of lactose.

Thanks go to the staff and students of the Department of Physics at Massey University for advice and support when needed and for maintaining an enjoyable and lively working atmosphere.

I would like to thank my Father and Grandmother for their constant encouragement and to all my friends for helping me to stay on top of things.

Table of Contents

List of Figures

List of Tables

List of Symbols

Chapter 1.

S	: magnitude of the reciprocal space vector ($S = 2\sin\vartheta/\lambda$).
λ	: wavelength of the X-rays.
$I_{cr}(S)$	: coherent scattering intensity of the crystalline regions.
$I(S)$	: coherent scattering intensity of the crystalline and amorphous regions.
$\overline{f^2}$	: mean square amplitude of the atomic scattering factor.
D	: disorder function.
k	: disorder parameter.
X_{cr}	: crystallinity of the material.
ΔH_{cr}	: crystallisation enthalpy.

Chapter 3.

L	: length of the polarimeter tube in decimeters.
c	: anhydrous concentration of lactose in g/100 ml.
R_t	: polarimeter reading at time t.
R_∞	: polarimeter reading at equilibrium.
$[R]$	: the specific optical rotation.
w_∞	: weight of lactose sample used to determine R_∞.
W_a	: anhydrous weight fraction.
α	: percentage of alpha lactose present in the sample.
$[\alpha]$	: specific optical rotation of alpha lactose.
$[\beta]$	: specific optical rotation of alpha lactose.
$R_t^{\cdot}$	: normalised optical rotation reading.
E_a	: activation energy.
R	: universal gas constant.
T	: temperature (in Kelvin).
A	: pre-exponential factor.

Chapter 4.

H	: Zeeman Hamiltonian operator.
γ	: gyromagnetic ratio.
$\hbar$	: *Plank's constant*$(h)/2\pi$.

B_0	: polarising magnetic field.
$I_{x,y,z}$	: angular momentum operator.
B_1	: oscillating magnetic field.
ω	: frequency.
$U(t)$	: evolution operator.
H_{rot}	: Hamiltonian operator in the rotating frame.
$M_{x,y,z}$	: components of the spin magnetisation vector, **M**.
M_0	: magnitude of $M_z(t)$ as $t \rightarrow \infty$.
T_1	: spin lattice relaxation time.
T_2	: spin spin relaxation time.
μ_0	: permeability of free space.
I	: vector operator representing angular momentum.
$\mathbf{r}_{ij}$	: internuclear vector.
r_{ij}	: magnitude of the internuclear vector.
H_D	: dipolar Hamiltonian operator.
W_{nm}	: transition rate.
$E_{n,m}$	: energies of states n and m.
i	: $\sqrt{-1}$.
τ_c	: average correlation time.
$J^{(q)}(\omega)$	: spectral density function.
$\rho^*(t)$	: density operator in the rotating frame.
$H_D^*(t)$	: dipolar Hamiltonian operator in the rotating frame.
ω_0	: Larmor frequency.
$M(t)$	: equal to $M_z(t)$
A_i	: amplitude of component i.
$y(t_i)$	: amplitude of multiexponential relaxation function at time t_i.
$s(T)$	: unknown amplitude of relaxation time T.
t_i	: time.
χ^2	: error function.
y_i	: equal to $y(t_i)$.
$\dot{y_i}$	: datum point.
σ_i	: variance of datum points $\dot{y_i}$.
$\mathbf{x}_m$	: column vector representing the true solution.
x	: column vector of the current estimate to $\mathbf{x}_m$.
$x_{i,j}$	: components of the column vector **x**.
A	: Hessian matrix.
b	: gradient vector.
a	: finite step required to find the minimum ($\mathbf{a} = \mathbf{x} - \mathbf{x}_m$).

$a_{i,j}$: components of vector **a**.
β_i : first partial derivative of χ^2 with respect to **x**.
α_{ij} : second partial derivative of χ^2 with respect to **x**.
$\mathbf{x}_{next}$: next estimate of **x**.
λ : constant.
s_j : spectral amplitude of component j.
T_j : relaxation time component j.
Q : Householder transformation matrix.
$\mathbf{R}_k$: upper triangular matrix.
u : an m vector
$\mathbf{u}^T$: transpose of **u**
μ : constant.
H : matrix representing additional constraints used in continuum formulation.
c : an n vector.
$M'(t)$: corrected magnetisation.

Chapter 6.

C_p : heat capacity at constant pressure.
α_p : volume expansivity at constant pressure.
H : enthalpy.
V : volume.
p : pressure.
z : order parameter.
$w_{1,2}$: weight fraction of components 1 and 2.
T_g : glass transition temperature.
k : constant.
T_1 : spin lattice relaxation time.
μ_0 : permeability of free space.
γ : gyromagnetic ratio.
$\hbar$: *Plank's constant*$(h)/2\pi$.
r_{ij} : average intermolecular distance.
I : angular momentum operator.
τ_c : average correlation time.
ω : frequency.
$\tau(T)$: mechanical and electrical relaxation time at temperature T.
$C^g_{1,2}$: arbitrary constants.

T_g : glass transition temperature.

$\phi_{CR,g}$: relaxation times of crystallisation at temperatures T and T_g respectively.

Chapter 7.

$M(t)$: amplitude of the inversion recovery signal at time t.

M_0 : amplitude of the inversion recovery signal at t = 0.

$A_{am,cr}$: relative amplitude of the amorphous and crystalline parts of the inversion recovery signal respectively.

T_{1CR} : spin lattice relaxation time of the crystalline part of the sample.

1. Introduction

1.1 Problem definition

Lactose (4-O-ß-galactopyranosyl-D-glucopyranose) is a naturally occurring disaccharide of glucose and galactose found almost exclusively in mammalian milk[1]. It constitutes the largest dry matter component of bovine milk (approximately 33%). Commercially, lactose is isolated[1] from whole or deproteinised whey obtained as a waste product of cheese and casein manufacture. Crystallisation of the preconcentrated whey solution yields alpha lactose monohydrate, a white, water soluble powder of moderately sweet taste[1] and no odour.

Lactose is most commonly used in the food processing and pharmaceutical industries[2,3,4]. In the food industry, it is used as an ingredient in human milk substitutes because breast milk has a higher lactose content than cow's milk. It is also used in baby foods, in the production of reconstituted and modified milk products, and as an anticaking agent in powdered foods. Lactose improves the consistency and shelf life of candies, and in bakery products improves flavour, appearance, and baking ability. The amorphous form of lactose provides an ideal tabletting excipient for use in pharmaceutical preparations as it is chemically inactive towards most types of active ingredient, and mechanically binds the mixture under compression[5].

As an ingredient, lactose plays a significant role in determining the physical properties of food powders and mixtures. The state of the lactose component of powders determines the flowability, dispersibility and instant solubility when added to water[6,7,8]. These properties, known as the functional properties, are of importance to the consumer and reflect the perceived quality of the product. They are determined, in part, by the physical and chemical state of lactose[8]. In spray-dried milk powders, lactose is formed in an amorphous state. However, partial crystallisation of lactose may cause a loss of colloidal stability upon reconstitution and reduce the solubility of the powder in water. Crystallisation may occur during manufacture, or later in storage where moderate temperatures and humidity may be experienced. The extent of crystallisation is usually small, yet the effect on functional properties is potentially large.

Detection and quantisation of these low concentrations of unwanted lactose phases is necessary for improved quality control of all lactose-containing powders. Literature reviews show no single methodology capable of detecting and quantifying all known species of lactose. Many methods characterise lactose in aqueous solution[9,10,11] in which the identity of the crystalline structure is lost. Solid-state methods, including Near Infrared Reflectance (NIR)[12], Differential Scanning Calorimetry (DSC)[13,14] and X-ray powder diffraction[15,16,17], are insensitive to the dilute contaminating lactose forms known to exist in milk powders (as seed crystals) and predicted to occur[15,18,19] in commercially manufactured alpha lactose monohydrate (as amorphous and crystalline beta lactose). The aim here is to develop a solid state methodology

which has the ability to differentiate all structural variations of lactose, and which has the sensitivity to detect very low concentrations of any lactose form. The method described will measure the spectrum of spin-lattice relaxation time values of lactose powders and determine the relative weight fractions of each lactose form.

1.2 Structure of the thesis

In this chapter, the physical properties of lactose are described in some detail, and commercial production of the common forms of lactose, alpha lactose monohydrate, beta lactose, and spray-dried amorphous lactose is discussed. A general literature review of the existing methods for characterising lactose in the solid and solution states follows this.

Chapter 2 describes laboratory preparation of several crystalline modifications of lactose not produced commercially. These preparations involve conversion of crystalline alpha lactose monohydrate to crystalline species of beta lactose and "mixed crystal" forms of alpha and beta lactose by acid or alkaline methanolic reflux[20-25]. Removal of the water of crystallisation at elevated temperatures produces several anhydrous forms of alpha lactose[26-28]. Their isolation provides a test to determine whether the spin-lattice relaxation method can differentiate these crystalline species of lactose (Chapter 5).

Chapter 3 reviews the existing solution state methods[9,10,11] available for the characterisation of lactose. Polarimetry, GLC and high resolution ^{1}H and ^{13}C NMR methods provide the basis of solution measurements performed here. These methods determine the ratio of alpha:beta lactose existing in the powder by measuring the anomeric ratio in solution. The experimental protocol requires continuous monitoring of the anomeric ratio after initial dissolution because of the process known as mutarotation (Section 1.3.1). The anomeric ratio existing in the powder is determined by back-extrapolation of the ratio to the point of initial powder dissolution (t=0, or the point of solvent contact).

Chapter 4 is concerned with the solid state characterisation of lactose powders by spin-lattice relaxation time measurement. The basic concepts of spin relaxation are introduced, and the protocol required for powder analysis is described. The theories surrounding some of the well-known expressions used to describe spin-spin and spin-lattice relaxation in solids are reviewed. The Bloemberger-Purcell-Pound (BPP)[29] relaxation theory is discussed, and equations describing the dependence of relaxation rates upon average internuclear distances and molecular motions (which have relevance to the detection of the glass transition phenomenon (Chapter 6)) are presented. The use of linear (non-negative least squares (NNLS (and referred to here as Lawson-Hanson[30] (LH))) and Contin[57]) and nonlinear (Marquardt-Levenberg[32] (ML)) inversion algorithms to recover the spectrum of relaxation times from relaxation data is

described. Preliminary relaxation experiments demonstrated the feasibility of using the relaxation time method to characterise the crystalline composition of lactose powders.

Measurement of the spin-lattice relaxation time spectra of the crystalline forms of lactose prepared in Chapter 2 are described in Chapter 5 and the sensitivity of T_1 spectra to variations in crystal structure discussed. Both the LH and Contin algorithms are used to determine the spectra of relaxation times and the advantages of each in terms of sensitivity to noise and to dilute relaxation time components is discussed. The accuracy of the T_1 method is determined by determining the anomeric composition of a series of lactose powders.

Lactose contained in powders manufactured by spray drying exists in an amorphous state. The functionality of amorphous lactose is known to be determined largely by the glass transition temperature T_g which is traditionally determined by DSC[13,14]. Chapter 6 investigates the response of the T_1 values as the material passes through the glass transition temperature. Solid state crystallisation of amorphous lactose is investigated and the onset temperature of crystallisation determined and compared to DSC analyses.

In chapter 7 T_1 spectra of crystalline/amorphous mixtures of lactose are used to determine the crystalline:amorphous ratio or crystallinity. A methodology is developed with enhanced sensitivity to detect very dilute concentrations of seed crystals (<0.5 %) in spray dried milk powders and dilute concentrations of amorphous lactose (<0.5 %) in crystalline alpha lactose monohydrate.

An overall summary of lactose characterisation and the T_1 methodology is presented in Chapter 8 and possible applications of the method are discussed.

1.3 Lactose chemistry

1.3.1 Mutarotation

Alpha and beta lactose are isomers which differ mainly in the orientation of the glucose C[1] hydroxyl group (Figure 1.1). Either species may mutate to the other through rotation of the hydroxyl group about the C[1]-C[2] bond: a process known as mutarotation. This reaction occurs quickly in water and is accelerated by the presence of proton donor/acceptor species. Non-dissociating solvents such as DMSO inhibit mutarotation[9,34,35]. In the solid state mutarotation may occur at elevated temperatures or by mechanical activation[15]. The mutarotation process is believed to be initiated by cleavage of the glucose ring at the C[1]-C[2] bond with formation of the open-chain intermediate species.

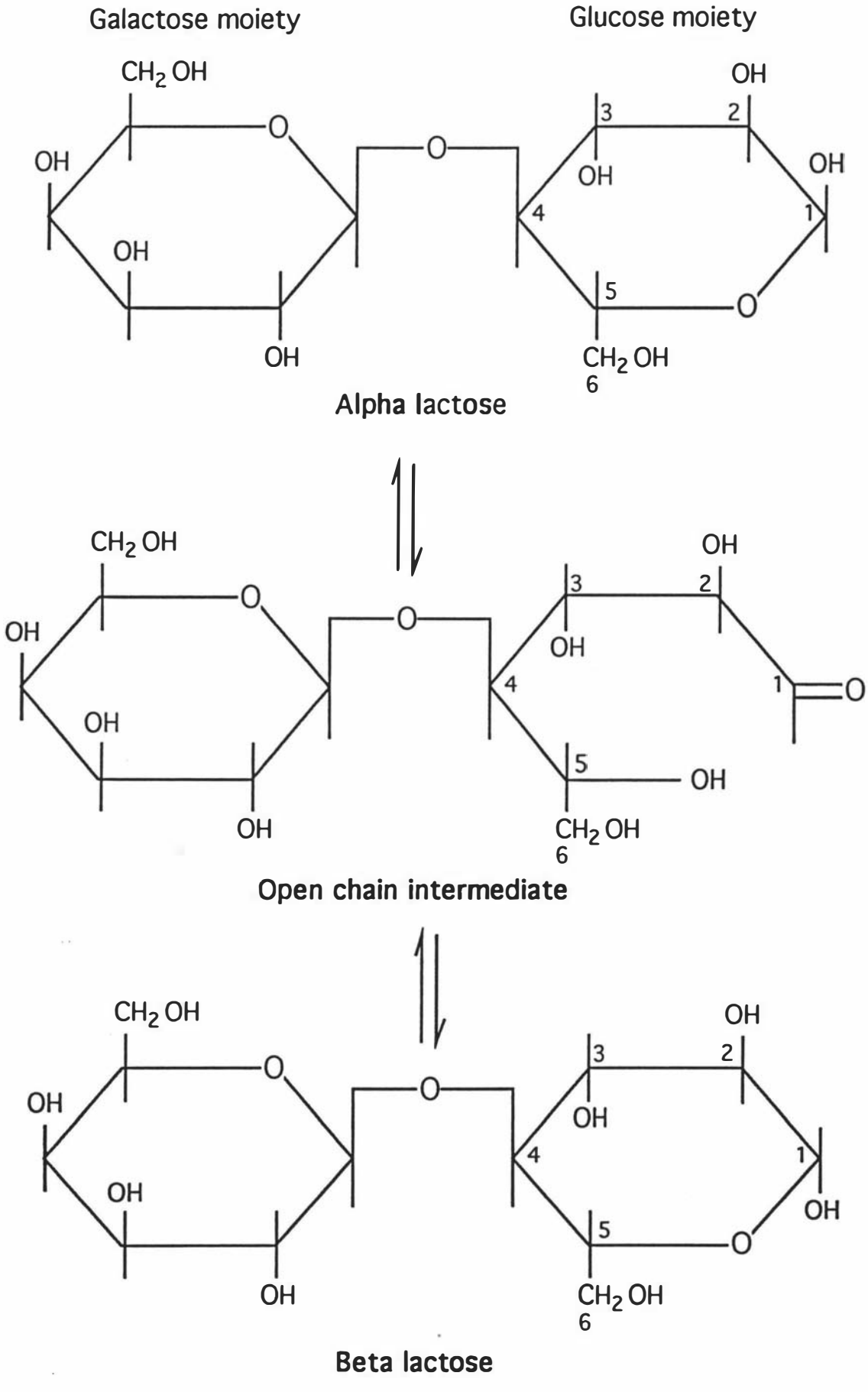

Figure 1.1. The mutarotation reaction of lactose

The activation energy of bond cleavage is lowered by the association of H^+ and OH^- about the oxygen atom. Rotation of the hydroxyl group about the C[1]-C[2] bond is terminated by closure of the glucose ring and the new chemical species is formed.

The rate determining step of mutarotation is bond cleavage because the intermediate form is virtually undetectable in solution. The mutarotation rate of lactose is first order[36], and strongly temperature dependent. At room temperature (20 °C), equilibrium is established in about 5 hours, whereas at 75 °C, it occurs in a few minutes

1.3.2 Commercial production of lactose

Whey, once a waste product of cheese and casein manufacture, provides a naturally rich source of dissolved lactose (the dry-matter (DM) content of whey consists of nearly 70% lactose). The principal means of lactose separation and purification is by aqueous crystallisation. Lactose may be separated from whey either in the presence or absence of whey proteins.

The extraction of crude lactose from whey in the presence of protein consists of the following processes[37] (Figure 1.2): evaporation and concentration of the original whey, crystallisation of lactose, first crystal separation, second crystal separation, drying, grinding, sifting, and packaging. From deproteinised whey, lactose separation is essentially the same, but only a single separation step is required following the first crystallisation stage. Since whey proteins reduce the evaporation rate during concentration and disturb both crystallisation and separation of crystals from the mother liquor, it is better to use deproteinised whey as the starting material.

Evaporation of whey is performed in multistage vacuum evaporators which yield a DM content of 60-65% from whole whey, and 70% from deproteinised whey. Further evaporation and concentration is not practicable as the resultant increase in viscosity inhibits mass transport and crystallisation of the syrup.

The crystallisation of lactose is initiated either spontaneously by supersaturation of the syrup, or by seeding with fine seed crystals of alpha lactose monohydrate. The objective is to produce a large number of similarly sized crystals averaging 0.2 mm in diameter and which are easy to separate from the remaining liquid. The number and size of crystals (and therefore the yield) increase with increasing supersaturation. Crystallisation is carried out in crystallisers which consist of large water-cooled tanks fitted with a slowly revolving mixing paddle. Continual agitation promotes nucleation and prevents the crystal shower from settling and caking in the bottom of the tank. On average, crystallisation is complete in about 30 hr, during which time the mass is cooled to 18 °C. Crystallisation time is crucial to the quality of the final product. Fast crystallisation leads to the formation of small and uneven lactose crystals, whereas

excessively long crystallisation leads to increased viscosity of the syrup and a consequent difficulty in removing the product from the tank.

The lactose crystals are separated from the mother liquor in continuous centrifuges. Usually two centrifuges operate in series providing a centripetal acceleration of 600 G and 1200 G and crystals are simultaneously washed using countercurrent wash water. Crude lactose which is not destined for refining is dried at 70 °C in large fluid bed driers to a moisture content of 0.1-0.5% w/w. The drying temperature is kept moderately low (and slow) to inhibit the formation of amorphous or beta lactose. The crystalline product is ground, sieved and packaged. The final product contains about 98% lactose.

Lactose which is destined for pharmaceutical uses must be further refined to remove contaminants such as protein (from whole whey), salts and coloured substances. Crude lactose is dissolved in hot water to create a 30% w/w solution (alternatively, a 50-60% w/w solution is sometimes formed) and the following reagents are added: (1) 1% w/w active carbon to absorb coloured substances, ash, nonprotein nitrogen, proteose-peptone components, and other impurities, (2) an acid such as HCl, to regulate pH and activate the carbon, dissolve insoluble salts, and remove possible protein contamination, (3) substances that facilitate filtration such as 0.1% w/w diatomaceous earth, and (4) bleaching agents such as 0.02% w/w sodium bisulphite. The contents of the tank are brought to boiling point, the pH adjusted to 5.4-5.8 by addition of alkali such as lime, and boiled for several minutes causing flocculation of proteins and settling of the carbon and insoluble salts.

The sediment is removed by filtration to yield a sparkling clear solution of pure lactose. This is evaporated to a concentration of 65-70% total solids (TS) in the presence of sodium bisulphite and seeded with 90% TS lactose paste which encourages formation of crystals of uniform size. The precipitated crystals are separated by centrifugation, washed in water and dried at 150 °C. High drying temperatures may be used since the lactose is now chemically pure, and there is little risk of browning. Crystals are ground, sieved and packaged to yield a product consisting of 99.9% lactose (predominantly alpha lactose monohydrate).

The manufacture of amorphous lactose may be achieved by the spray- or roller-drying of a saturated aqueous solution of lactose, or, alternatively by extensive milling of crystalline alpha lactose monohydrate (the process is essentially the same as for the drying of milk powder[38]). Rapid drying of the lactose solution causes a sharp increase in viscosity, and crystallisation, a diffusion dependent process, is inhibited. The extent of mutarotation during drying is negligible[39]. Subsequently, the anomeric ratio of the dry powder is approximately the same as in solution. At a drying temperature of 80-90°C the anomeric ratio equals alpha:beta = 1:1.2-1.3[39].

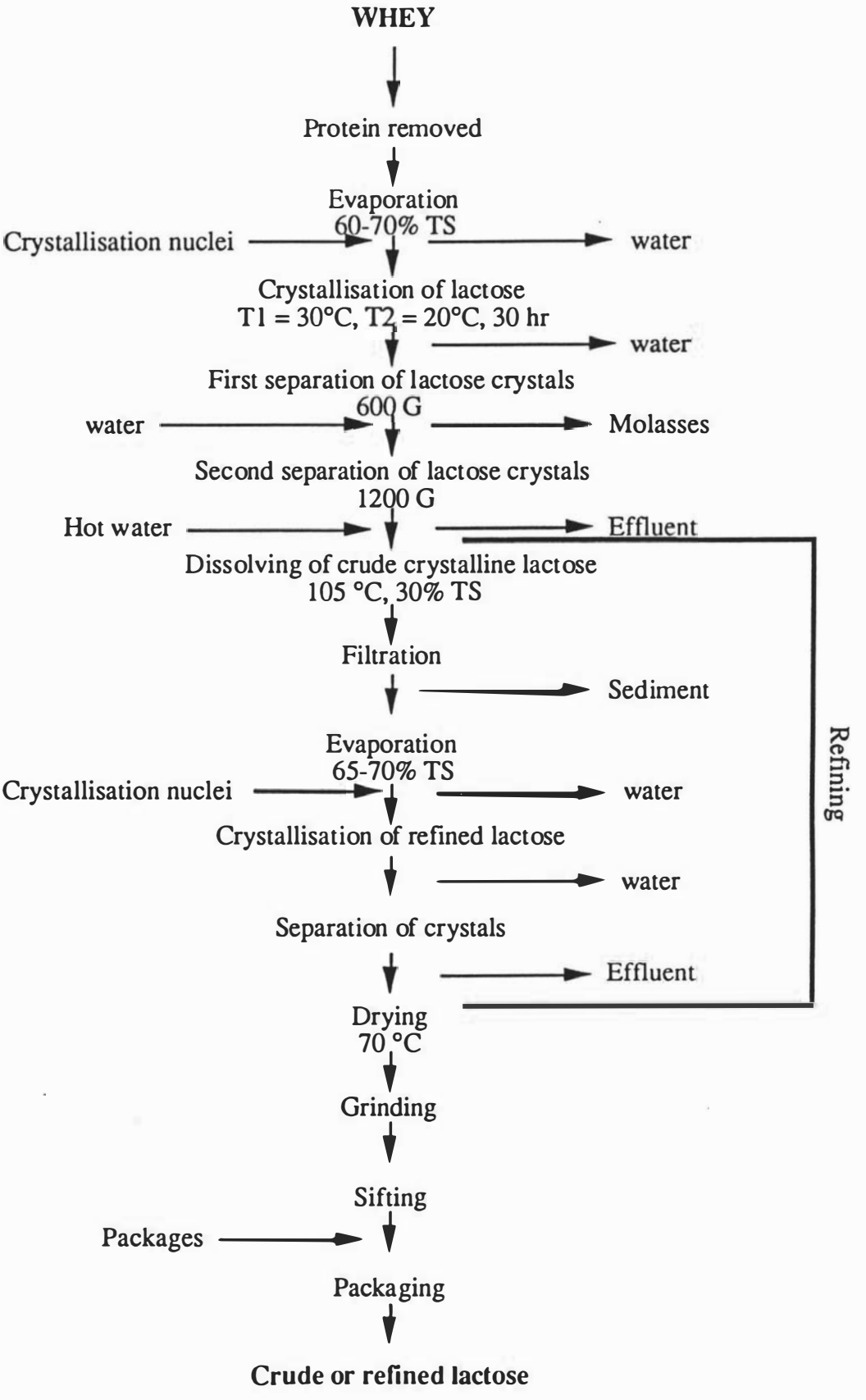

Figure 1.2. The steps involved in separating and refining lactose from whey. The bracketed refining stage is absent during the production of crude lactose. TS = total solids, T1 and T2 = initial and final crystallisation temperatures respectively. (Reproduced from Reference [1]).

In the spray drying of lactose, spray atomisation is achieved either by pumping the solution under high pressure through a specially designed nozzle (nozzle atomisation), or by allowing the solution to fall upon a disk rotating at high speed (disk atomisation). The spray descends under gravity through a countercurrent of heated air and the droplets quickly dry. The freshly formed powder descends into the conical shaped fluidised drying section at the bottom of the spray drier. From here, the powder is conveyed to a second external fluid bed where the final traces of moisture are removed.

Spray drying of lactose yields powder particles which are spherical in shape and have a size distribution typically in the range of 10-100 microns. The surface of particles may be smooth, or alternatively, covered in deep wrinkles[38], the cause of which remains unknown. Large central vacuoles or smaller, evenly distributed vacuoles which may retain moisture after drying and packaging are often formed from disk atomisation[38].

The roller-drying of lactose solutions is achieved by direct heat transfer from a hot drum into a thin layer of evaporating lactose solution[38]. The solids are scraped off the drum, and pulverised in a hammer mill. This action gives rise to the irregular shapes and sharp edges of powder particles[38]. In comparison to spray dried material, the powder particles are compact, and contain no occluded air because the lactose solution is effectively deaerated as it passes over the hot rollers.

Beta lactose is formed by aqueous crystallisation at elevated temperatures[2,40] (>93.5°C). A solution of alpha lactose monohydrate is evaporated at 105 °C to supersaturation. The thick lactose syrup is seeded with fine beta lactose crystals and allowed to crystallise. The temperature of the syrup during crystallisation is critical, and must not fall below 93.5 °C as alpha lactose monohydrate will form (Figure 1.3). The crystallisation of beta lactose depletes the solution phase of beta lactose, and disturbs the anomeric ratio from equilibrium. Mutarotation quickly restores equilibrium at these elevated temperatures, and beta lactose continues to crystallise as long as the syrup is maintained in a supersaturated state and above 93.5 °C.

The above schematic diagrams (Figure 1.3) show the dependence of solubility of each anomer on the concentration of the other, and collectively, they demonstrate the relative solubilities as a function of temperature. The progress of evaporation and solution concentration towards saturation is represented by the equilibrium line which shows a constant anomeric equilibrium ratio independent of concentration of either species.

Below 93.5 °C, it is observed that increasing solution concentration results in supersaturation with respect to the alpha anomer, and alpha lactose monohydrate crystallises out of solution. Conversely, solution temperatures greater than 93.5 °C causes supersaturation of the beta anomer and beta lactose crystallises out of solution.

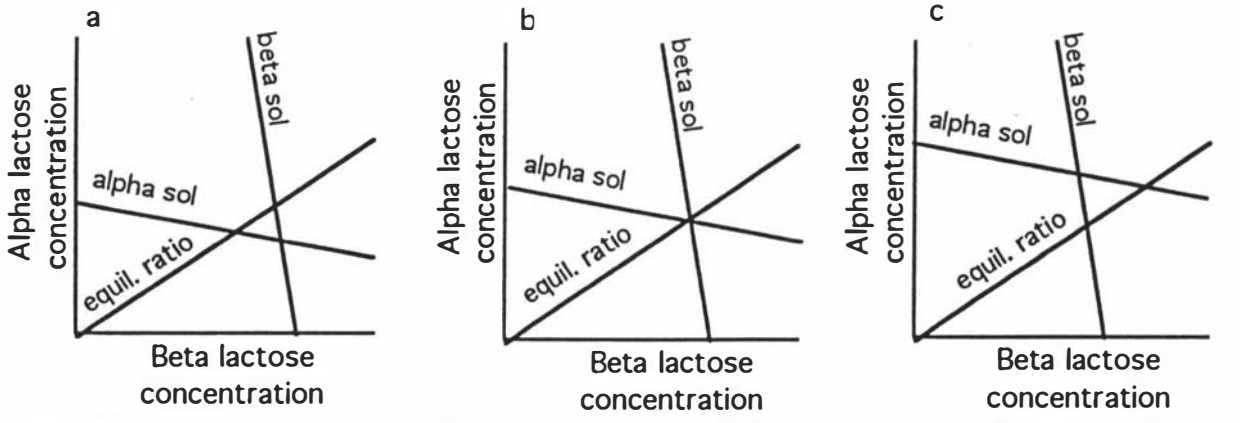

Figure 1.3. Schematic representation of the relative solubilities of alpha and beta lactose in water as a function of lactose concentration and temperature, T. a: T<93.5 °C, b: T=93.5 °C, c: T>93.5 °C.

Crystals of alpha lactose monohydrate and beta lactose differ substantially in shape, and are easily identified under a light microscope. The shape of alpha lactose monohydrate crystals is dependent upon the preferred direction of crystal growth[41,42] but the most common form is the tomahawk shape (Figure 1.4). Beta lactose tends to form diamond shaped plates, but may also exist in other forms depending upon the growing conditions.

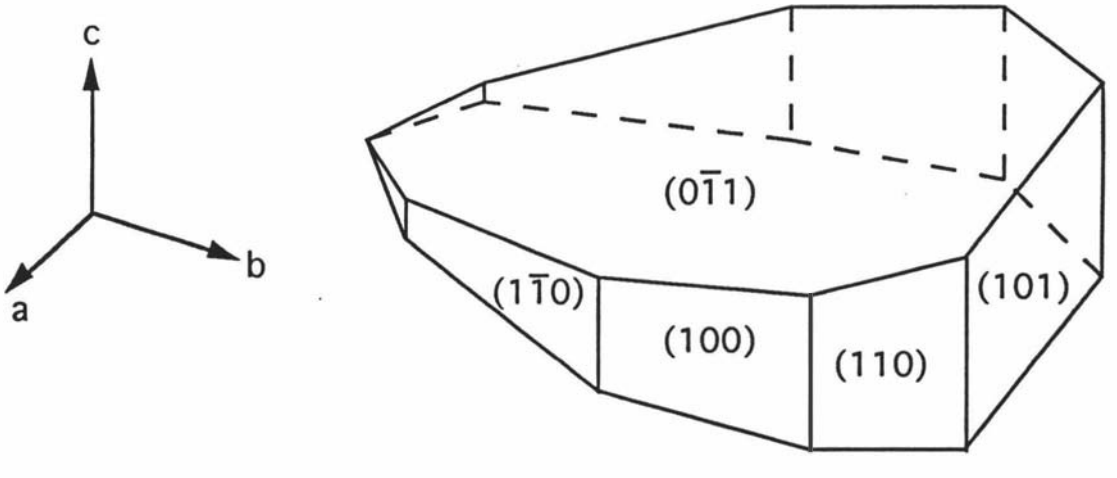

Figure 1.4. The common tomahawk crystalline shape of alpha lactose monohydrate. (Reproduced from Ref[26]).

1.3.3 "Non-commercial" crystalline forms of lactose

Aqueous crystallisation remains the major technique used for the commercial extraction and refining of lactose. Despite the high energy consumption involved in the evaporation steps, the overall cost of lactose production in energy terms is low. Beta lactose, which exhibits superior solubility[1] to alpha monohydrate is not commercially manufactured in large quantities because

of the higher energy requirements associated with high temperature aqueous crystallisation (>93.5°C). Undoubtedly, the poor solubility of alpha lactose monohydrate[1] (7.2g/100ml water at 20 °C) and its slowness to dissolve make it inferior to beta lactose (solubility of 50g/100ml) particularly where large quantities of lactose must be solubilised in water. There is much in favour of the widespread use of beta lactose in industry[23], yet the higher production costs largely offset the advantages.

Crystalline beta lactose can be produced from alpha lactose monohydrate by methanolic reflux[23-25] (Figure 1.5) more efficiently than by aqueous crystallisation. Anomeric conversion of alpha lactose monohydrate is carried out in a reaction mixture of methanol alkalised with NaOH (0.0006% w/w) which is refluxed for 2 hours. The yield of beta lactose is typically over 90% w/w.

Acidification of the methanolic refluxing solution with HCl or alkalisation with NH_4OH yields "mixed crystal" species of lactose containing both anomers[20-22] (Figure 1.5). Dehydration of alpha lactose monohydrate by variations of methanolic dehydration[26], heat[26] and vacuum[27,28] yield several anhydrous species of alpha lactose. These anhydrous alpha lactose forms exhibit superior binding of volatile flavour and aromatic enhancing compounds over alpha lactose monohydrate[43] and would find widespread uses as a food ingredient.

The detailed reaction conditions necessary to form these crystalline species of lactose are described in Chapter 2.

1.4 LITERATURE REVIEW OF THE TRADITIONAL CHARACTERISATION METHODOLOGIES

Methodologies are currently available to determine the anomeric ratio of lactose in solution, and, by extrapolation, the ratio existing in the powders, to differentiate the different crystalline forms of lactose, to determine the crystallinity of powders, and to detect the glass transition and crystallisation processes and measure their associated temperatures T_g and T_c. These methodologies are now described.

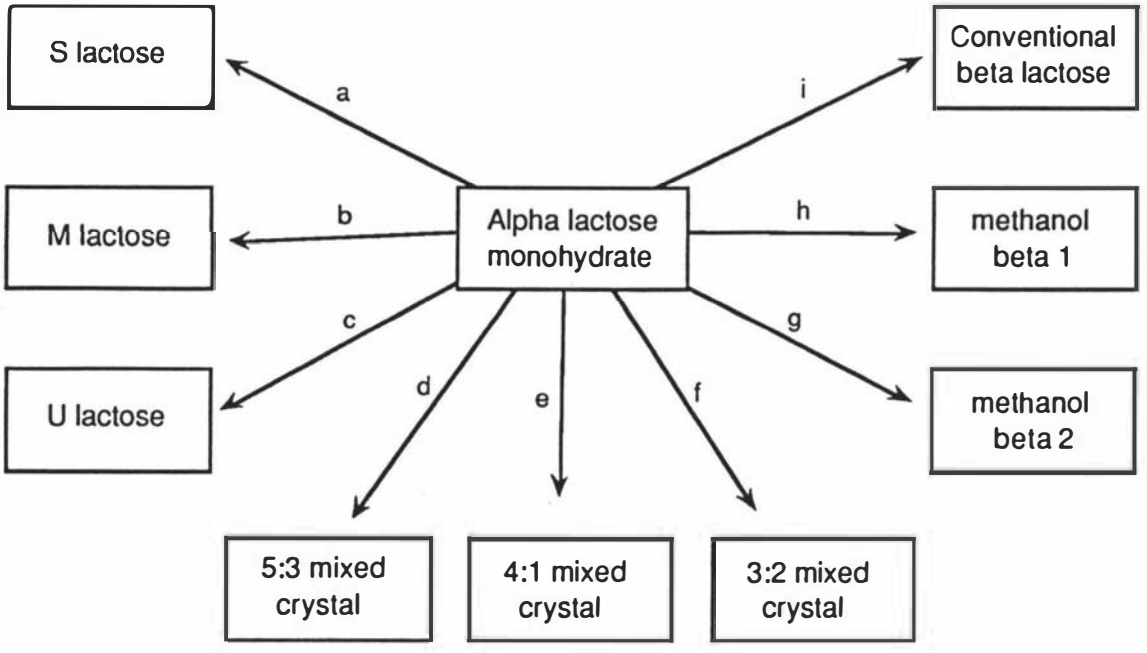

a	Dehydration at 130°C for 3 hours[25]
b	Dehydration using anhydrous methanol at refluxing temperature[26]
c	Dehydration at 130°C for 48 hours at 10^{-1} torr[25]
d	Reflux with acidic (HCl) aqueous methanol for 2 hours[20,21]
e	Reflux with acidic (HCl) anhydrous methanol for 2 hours[21]
f	Reflux with alkaline (NH_4OH) anhydrous methanol for 2 hours[22]
g,h	Reflux with alkaline (NaOH) aqueous methanol for 2 hours[23-25]
i	Crystallisation from an aqueous solution at a temperature greater than 93.5°C[31].

Figure 1.5. Reaction conditions required for the preparation of different crystalline forms of lactose from alpha lactose monohydrate.

1.4.1 Determination of the anomeric ratio

During dissolution, all crystalline modifications of lactose degenerate to alpha and beta lactose. The anomeric ratio immediately after dissolution is unchanged from that existing in the solid state, however, once in solution, the anomeric ratio immediately begins to evolve towards equilibrium due to the process of mutarotation. Since both anomers of lactose are optically active, the technique of polarimetry has traditionally been used to characterise the relative abundance of each anomer in solution. Each anomer exhibits specific dextro-rotatory power of 91.1° and 38.7° for alpha and beta lactose respectively[9]. The measurement of the specific optical rotation of a mixture of lactose anomers in solution provides a relatively simple and efficient means of determining the anomeric ratio. By following the mutarotation curve over time after dissolution, it is possible to extrapolate the resulting curve back to the time of initial dissolution and therefore establish the anomeric ratio in the powder.

Polarimetry was first used to determine the anomeric ratio of lactose by Sharp and Doob[10] in 1941. Their method, still in wide use today, measures the optical rotation of a lactose solution of precisely known concentration. The optical rotation expressed by a solution of both anomers is simply the linear summation of the rotatory power of each anomer weighted by the relative concentration of each. Firstly, the specific dextro-rotatory power of each pure anomer must be accurately determined. Sharp and Doob used aqueous crystallisation to separate and purify alpha lactose monohydrate and beta lactose and measured the rotatory power of each assuming 100% purity. However, the isolation of one anomer by aqueous crystallisation invariably results in incorporation of the other anomer into the crystalline structure. For example, the crystallisation of alpha lactose monohydrate from water around 20 °C incorporates about 2-4% beta lactose[9]. Buma and Van der Veen[9] used Gas Liquid Chromatography (GLC) to determine the purity of the crystallised anomeric species. In this way, the contribution of the contaminating anomer to the optical rotation of the lactose solution could be deconvoluted, and the error eliminated. The methodology of Sharp and Doob[10], and the revised anomeric optical rotations of Buma and Van der Veen[9] form the standard polarimetric method of measuring the anomeric ratio of lactose in solution.

Dwivedi et al[11] used the GLC method to determine the anomeric ratio of a series of prepared lactose samples. They showed the "response" of each anomeric species at the flame ionisation detector to be equal. Repeat measurements of samples showed excellent reproducibility (precision) although the accuracy of analyses was not determined. In Chapter 3, the accuracy of the GLC method will be established by comparative analyses of the anomeric ratio of powders with polarimetry.

1.4.2 Identification and quantification of crystalline species

Single crystal X-ray diffraction has been used to determine the crystal structures of several species of lactose produced by aqueous crystallisation[44-46]. Many of the refluxing preparations used in Chapter 2 precipitate fine crystals which do not achieve the dimensions necessary for single-crystal X-ray diffraction (of the order of 0.1 mm)[44-46]. In such cases, powder X-ray diffraction is a more suitable methodology. Inevitably, there is some loss of structural information where a large number of randomly orientated crystallites are simultaneously diffracting, but this loss is not crucial. Lerk et al[18] used powder diffraction to examine several crystalline forms of powdered lactose. They demonstrated large "spectroscopic" differences between different crystalline species and suggested the method was suitable as a general characterisation methodology for lactose powders. Relative peak integrals may be loosely used to determine the relative abundance of each crystalline species. However, the relative integral ratio is not necessarily proportional to the weight fraction of crystalline species present. For the method to be used quantitatively, it is necessary to perform a series of diffraction measurements

on samples of "known" composition (perhaps from polarimetry) and then calibrate the relative peak integrals to the established weight fraction.

Cross-Polarisation Magic Angle Spinning (CP-MAS) ^{13}C NMR has been used by Earl et al[47] to determine the structures of crystalline species of lactose including several "mixed crystal" species discussed earlier. They demonstrated spectroscopic features specific to each crystalline specie, and the possibility, therefore, of using the method to quantify crystalline species in a powdered mixture. CP-MAS NMR will be used here (Chapter 5) to characterise several of the crystalline species of lactose produced in Chapter 2.

1.4.3 Determination of crystallinity

X-ray powder diffraction is a well established technique used to determine the crystallinity (crystalline:amorphous ratio) of carbohydrate powders. Otsuka et al[15] demonstrated the resulting decrease in crystallinity that occurs from the grinding of crystalline alpha lactose monohydrate. Morita et al[16] studied the effect of the removal of water of crystallisation (by high temperature dehydration) upon crystal structures and the resulting destruction of local crystal order and the formation of amorphous regions.

The quantitative interpretation of X-ray diffraction patterns may be achieved in several ways. All methods rely on the correlation of the relative intensity of "crystalline peaks" and "diffuse background" to the relative concentrations of crystalline and amorphous parts of the sample. Those that assume a simple proportionality between peak intensities and crystalline abundance, as in the case of the commonly used "Herman's method[16]", are subject to large systematic errors. This is because minor lattice imperfections and thermal agitation of the crystalline phase lead to a reduction in crystalline intensity with corresponding increase in the intensity of the diffuse background.

Ruland's method[17] modulates the simple proportionality with a "disorder function" which contains the contributing effects of thermal vibrations and short and long range lattice imperfections to the reduction in crystalline intensity. According to Ruland, the degree of crystallinity, X_{cr} is

$$X_{cr} = \frac{\int_0^\infty S^2 I_{cr}(S)dS}{\int_0^\infty S^2 I(S)dS} \times \frac{\int_0^\infty S^2 \overline{f^2}dS}{\int_0^\infty S^2 \overline{f^2} D dS} \qquad [1.1]$$

where S is the magnitude of the reciprocal space vector $(S = 2\sin\vartheta/\lambda)$, ϑ the angle between the atomic plane and both the incident and reflected beams, λ the wavelength of the X-rays,

and $I_{cr}(S)$ and $I(S)$ the coherent scattering intensities at S in the crystalline and total regions respectively. $\overline{f^2}$ is the mean squared amplitude of the atomic scattering factor, and D the disorder function. Integration limits are determined experimentally[16].

The first ratio of Equation[1.1] represents the intensity ratio of "crystalline" and "total" (crystalline + amorphous) regions integrated over all angles of S. In practice, integration limits are narrowed to where X_{cr} just remains independent of S_0 and S_1. This first ratio represents the simple proportionality assumed in Herman's method. The second ratio term of Equation [1.1] represents the adjustment necessary due to motion and lattice disorder. It describes the expected intensity ratio for a material of crystallinity X_{cr} and exhibiting disorder as described by the disorder function

$$D = \exp\left(-kS^2\right) \qquad \textit{where} \quad k = k_T + k_1 + k_2 \qquad [1.2]$$

where k, the disorder parameter consists of contributions from thermal motions short and long range imperfections (k_T, k_1 and k_2 respectively).

Ruland's method is more theoretically rigorous than Herman's method, but the correction inherent in Equation[1.1] is not exact. Furthermore, the outcome of Rulands method is still dependent on the choice of integration limits and this is a possible source of error[16].

DSC has been used to measure the crystallinity of lactose powders with some success. Roos and Karel[13,14] determined the crystallinity of amorphous lactose undergoing crystallisation, and were able to map the time dependence of crystallisation as a function of the temperature above the glass transition temperature (T-Tg). The method compares crystallisation enthalpy of the unknown sample to that of a purely amorphous standard, and crystallinity is determined by

$$X_{cr} = 1 - \frac{\Delta H_{cr}(mixture)}{\Delta H_{cr}(amorphous)} \qquad [1.3]$$

where $\Delta H_{cr}(mixture)$ and $\Delta H_{cr}(amorphous)$ are the crystallisation enthalpies of the unknown sample and amorphous standard respectively.

The integrity of the method depends on the amorphous standard being 100% pure. This can generally be guaranteed by careful preparation. However, because of the possible dependence of ΔH_{cr} on humidity and crystallisation temperature (Chapter 6), Equation[1.3] does not necessarily represent all possible crystallisation conditions.

Near infrared reflectance (NIR) is commonly used to identify carbohydrates. Adsorbances are in the region corresponding to C-H, O-H, and N-H bond vibrations, which characterise most food product constituents. Susi and Ard[12] describe a procedure for evaluating the presence of crystalline alpha lactose in amorphous lactose based on the observation of strong absorption bands around 15.9 microns, amorphous lactose over the same region exhibits a flat background. Quantitative information is gained by integration of the "crystalline" peaks, and comparison to a pure crystalline standard. However, the NIR methodology requires calibration to a "known" standard whose composition is measured by an independent method.

1.4.4 Determination of the glass transition and crystallisation temperatures of amorphous powders

The phenomenon of the glass transition in lactose is detectible by many physical changes (Chapter 6). Recently, DSC has gained popularity as a means of detecting the glass transition and solid state crystallisation in single and multiple component food systems. In lactose, Roos and Karel[13] used DSC to study the plasticising effect of adsorbed water on the glass transition and crystallisation temperatures of amorphous powders (T_g and T_c respectively). The method is accurate and reproducible. It is used extensively here to measure the T_g and T_c of pure lactose powders.

1.5 Summary

Lactose has traditionally been perceived as an inert, unreactive compound which may be adequately characterised by measurement of the anomeric ratio in solution, or the crystallinity of powders. However, in the solid state, lactose may exist in a wide variety of crystalline forms. Each crystalline form exhibits markedly different physical properties, and the inclusion of minute quantities of the anhydrous alpha forms may substantially affect the functionality of powders. For the comprehensive characterisation of lactose powders, the methods used must be capable of differentiating the variety of different crystalline (and amorphous) forms and be sensitive to the changing molecular dynamics which occur at the glass transition.

The traditional methodologies which include polarimetry and GLC appear to be accurate, but are limited to the measurement of the anomeric ratio. Solid state methods used to identify the various crystalline species such as DSC and X-ray powder diffraction are not truly quantitative. It is shown that the spin-lattice relaxation method to be described in this thesis will provide the single means of characterising all forms of lactose with the accuracy that is required to achieve better product control during manufacture and storage.

2. Preparation of crystalline species of lactose

2.1 Introduction

Several reports in the literature describe methods that convert crystalline alpha lactose monohydrate to different crystalline forms of alpha, beta, and co-crystallised mixtures of alpha and beta lactose[20-28]. The reaction conditions necessary to bring about these anomeric and structural modifications were briefly introduced in Chapter 1 (Figure 1.5). Some of these conditions are not unlike those encountered during conventional lactose manufacture (Figure 1.2 and the processes of drying (dehydration) and milling[15]), and the formation of different crystalline forms (apart from alpha monohydrate and conventional beta) during processing is subsequently possible[15,18]. Here, the preparation of these crystalline forms in the laboratory is described. Spin-lattice relaxation time measurements will be performed on crystalline products in Chapter 5.

The mechanisms of crystalline modification are not currently well understood. The presence of water of crystallisation in the starting product (alpha lactose) is necessary for crystalline conversion[23]. The removal of the water of crystallisation by methanolic dehydration initiates structural rearrangement, and anomeric conversion may take place depending on the pH of the solution. The partial anomeric conversion of alpha lactose monohydrate yields "mixed" crystalline species with anomeric ratios of alpha:beta = 4:1[21], 5:3[20,21], and 3:2[22]. Complete anomeric conversion yields beta lactose with an apparently different crystal form[26] (see T_1 measurements in Chapter 5) from that produced by aqueous crystallisation. Dehydration of alpha lactose monohydrate by heat, heat and vacuum, or neutral methanolic reflux produces anhydrous forms of alpha lactose with different crystalline structures[26-28] (see T_1 measurements in Chapter 5). The different crystalline forms of lactose produced here were confirmed by melting point measurement[3] in some cases, and the anomeric composition determined by polarimetry.

2.2 Preparation of crystalline forms of lactose

All materials used in these preparations were analytical grade (AR) unless otherwise stated. The anomeric composition of all crystalline products was determined by polarimetry. The freshly prepared product was stored at low temperature (4 °C) until required.

2.2.1 Alpha lactose monohydrate

Alpha lactose monohydrate (United States Pharmacopoeia (USP) grade) was obtained from Lactose New Zealand (LNZ). All samples had been milled and sieved to 100 mesh.

2.2.2 Conventional beta lactose

A concentrated aqueous solution of lactose was formed by slowly adding 400 grams of alpha lactose monohydrate to 250 ml of boiling distilled water in a glass beaker. The agitated solution was concentrated at a temperature of 95-98 °C and allowed to crystallise. The crystalline slurry was spread over an open aluminium foil dish and transferred to a well ventilated oven maintained at 100 °C to remove final traces of water.

After several hours the lactose crystals were removed, cooled to room temperature, and gently ground in a mortar and pestle. The powder was sieved to 100 mesh, and lumps returned for further grinding. To remove amorphous and alpha lactose monohydrate impurities coating the surface, crystals were washed in a solution of acetone and ethanol 50:50(v/v). The powder was returned to a vacuum oven and dried at 40 °C overnight to remove all traces of solvent.

The purity of beta lactose was determined by polarimetry (Chapter 3). Measurements showed contamination with 15% alpha lactose monohydrate. The low yield was attributed to crystallisation of alpha lactose on cooler regions of the glass beaker which may have been below 93.5°C. This was rectified by subsequently concentrating the lactose solution in a ventilated oven maintained at 105 °C. Crystals were further processed as previously described. Polarimetry yielded 94% beta lactose. Some browning of the crystalline product was noted although high resolution proton NMR failed to detect any degradation products. The melting point was 234 °C.

2.2.3 Beta lactose from a NaOH/methanol solution

Originally described by Olano and Rios[24] , this method refluxes alpha lactose monohydrate in a methanolic solution containing 0.0006% w/w sodium hydroxide for approximately two hours. The reaction mixture was prepared by dissolving 0.08 grams of freshly ground NaOH pellets in about 200 ml of methanol, and adding 10 grams of alpha lactose monohydrate. A tube packed with anhydrous calcium chloride was fixed to the condenser to prevent the ingress of moisture during reflux. The mixture was agitated with a magnetic stirrer.

After two hours, the reaction mixture was vacuum filtered to separate the crystalline product. Crystals were washed with 200 ml of cold anhydrous methanol and dried in air. Drying was completed in a vacuum oven maintained at 40 °C for 24 hours. The crystals were then cooled, carefully ground and sieved to 100 mesh.

2.2.4 Mixed crystal (5:3) from a HCl/methanol solution

Hockett and Hudson[20] in their 1931 communication described the modification of alpha lactose monohydrate to a crystalline product with an anomeric ratio of alpha:beta = 5:3. Recently Simpson et al[21] showed that the presence of water (which unknowingly contaminated the

Hockett/Hudson reaction mixture) is an essential component for the reaction. The method used here is that described by Simpson et al.

Dry HCl gas was prepared by dropwise addition of concentrated hydrochloric acid to a concentrated solution of sulphuric acid (Figure 2.1). The reaction mixture was agitated, and released HCl gas was dried by passing through concentrated sulphuric acid.

HCl gas was bubbled through dry methanol to a final concentration of between 1-5% w/w. This was determined by titrating a 10 ml sample of the methanolic solution with a standard NaOH solution. Final concentration was 3.2%.

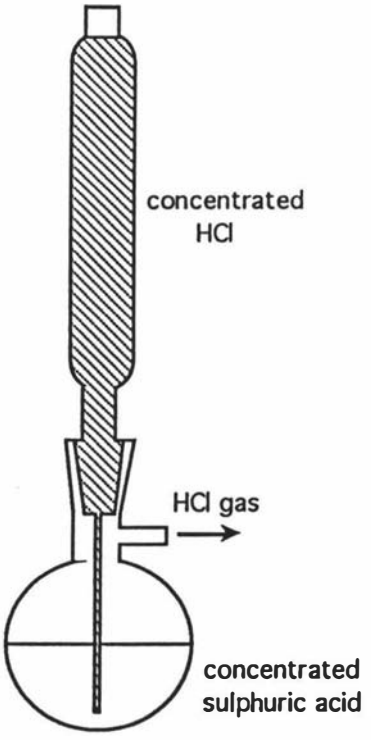

Figure 2.1. The apparatus used to generate anhydrous hydrogen chloride gas

Approximately 2 ml of distilled water was added to the methanolic solution and transferred to the refluxing apparatus. The solution was heated and 10 grams of alpha lactose monohydrate added slowly. A drying tube was fixed to the condenser as described, and the mixture refluxed for one hour. The crystalline product was recovered by vacuum filtration and dried for 24

hours in a vacuum oven at 40 °C. The anomeric ratio was determined by polarimetry to be alpha:beta = 4.9:3. Two melting points were registered at 211 and 218 °C.

2.2.5 Mixed crystal (4:1) from a HCl/methanol solution

The procedure used here[21] uses completely dry methanol and yields a crystalline product with an anomeric ratio of alpha:beta = 4:1. Preparation follows that described in 2.2.4 with some minor changes as follows.

The methanol was dehydrated by refluxing over anhydrous calcium chloride for about an hour and collecting the dry product by distillation. Moisture ingress into the condenser was prevented by installing a drying tube. The first 100 ml of distillate was discarded, and the following one litre of anhydrous methanol collected and stored in an air tight container over molecular sieve.

The reaction mixture was refluxed for one hour, and the crystalline product collected and dried as previously described. Analysis by polarimetry showed an anomeric ratio of alpha:beta = 20:1. A repeated run gave similar results. The product is not that described by the literature. It is possible that the dehydration procedure may not have sufficiently dried the methanolic solution.

2.2.6 Mixed crystal (3:2) from an ammonia/methanol solution

Originally described by Olano et al[22], this method utilises a reaction mixture containing 1% w/w concentrated ammonium hydroxide in methanol. Alpha lactose monohydrate is added and the solution refluxed for one hour. The crystalline product is filtered, ground and sieved.

Polarimetric measurements of the product yielded an anomeric ratio of alpha:beta = 18:1, and a repeat preparation gave a similar result. An explanation of this discrepancy is not presently available.

2.2.7 S lactose

One of the many anhydrous forms of alpha lactose, S (stable) lactose, is formed by dehydration of alpha lactose monohydrate with heat. About 10 grams of alpha lactose monohydrate was thinly spread over a glass petri dish and heated to 130 °C for about two hours. The product was removed and allowed to cool. Gravimetric analysis revealed a weight loss corresponding to 95% of the calculated weight of the water of crystallisation. The melting point was 216.5 °C.

2.2.8 U lactose

U (unstable) lactose is formed from alpha lactose monohydrate by the combination of heat and vacuum. As U lactose is hygroscopic, preparation was carried out in an NMR tube which

could be readily sealed. About 10 grams of alpha lactose monohydrate was heated to 130 °C for a period of 48 hours at a reduced pressure of 10^{-1} torr. The vacuum was released with air dried over concentrated sulphuric acid. The NMR tube was immediately stoppered and sealed with plastic parafilm™. Gravimetric analysis indicated a removal of 95% of the water of crystallisation.

2.3 Summary

Preparations of U-lactose, S-lactose, conventional and methanolic beta lactose, and the mixed crystal having an anomeric ratio of 5:3 gave good yields. Literature methods for the preparation of the 4:1 and 3:2 crystals yielded 20:1 and 18:1 products respectively, not the product reported in the literature. Contamination of the solvent by ambient moisture may have been responsible.

3. Analysis of the anomeric composition of lactose powders using "solution" methodologies

3.1 Introduction

Many of the methodologies discussed in Chapter 1 concern the characterisation of lactose in the solution state. Lactose powders begin mutarotation immediately on contact with water and the onset of dissolution, with the anomeric ratio evolving over several hours to an equilibrium ratio of alpha:beta of 35:65 at 20 °C[9]. Since complete dissolution of powders may take some minutes, it is not practical to measure the ratio precisely at the point of solvent contact. Instead, the mutarotation curve must be measured over time, and extrapolated to the point of solvent contact to determine the anomeric ratio existing in the powder[9]. This is the approach adopted here in applying the polarimetric and high resolution proton and carbon-13 NMR spectroscopy methods to measure the anomeric ratio of lactose solutions.

Recently, the solvent Dimethyl Sulphoxide (DMSO) has been reported to inhibit the mutarotation of lactose in solution[9]. The anomeric ratio is therefore held constant after dissolution in this solvent, and a single measurement can be used to characterise the anomeric ratio of the powder. The advantage in using DMSO, as will be shown, is that experimental protocol is considerably simplified.

In this chapter, the accuracy and reproducibility offered by the various solution methodologies in determining the anomeric ratio (or alternatively, the anomeric composition) of lactose powders is described. Polarimetry is used to measure the anomeric composition of powdered lactose dissolved in water. By contrast GLC requires the use of pure DMSO and DMSO/pyridine mixtures. This ensures that the anomeric composition is fixed in solution until derivatisation, a necessary precursor to GLC measurement, is complete. Proton and carbon-13 high resolution NMR spectroscopy are carried out both in D_2O and in deuterated DMSO (DMSO-d6) and the advantages of each described. In order to characterise the samples used in this comparative study, some method must be chosen *a priori* for the initial calibration. For this purpose polarimetry is chosen for the simple reason that this method is well-established in the literature. By using the alternative methods on the same sample series it will be possible to test for consistency of results between methods. In taking this approach, no assumption is made that polarimetry is necessarily accurate. However, in the event that all methods yield consistent results, this will tend to confirm the validity of each method, including polarimetry.

3.2 Preparation of samples

To test the accuracy of each methodology, a series of lactose powders was created using accurately known anomeric compositions. In all this work, polarimetry is used to provide the *a priori* reference values of the anomeric composition. Alpha lactose monohydrate and beta

lactose of known purity (as obtained by polarimetry) were blended by appropriate gravimetric ratios to the anomeric compositions depicted in Table 3.1.

Table 3.1 Alpha content of prepared lactose samples. Note, the anomeric composition has been determined using polarimetry according to the method outlined in Section 3.3. Polarimetry is used to provide an *a priori* reference which is to be compared with the results of other methods.

SAMPLE NUMBER	ALPHA CONTENT±0.3%
Sample 1	95.6%
Sample 2	94.6%
Sample 3	60.9%
Sample 4	17.2%
Sample 5	15.7%
Sample 6	5.5%

The small compositional differences created at the extremes of the anomeric range were intended to test the sensitivity of each method to minor fluctuations in the anomeric composition of lactose powders. Sample 6 was added at a later date following improvements in beta lactose preparation (section 2.2.2). Samples were sealed and stored at low temperature (4 °C) until required for measurement.

3.3 Polarimetry

3.3.1 Materials and method

Polarimetric measurements were performed on an OPTICAL ACTIVITY AA-10 polarimeter equipped with a water jacketed 20 cm sample tube. Temperature control was by open circuit water circulation from a HAAKE water bath which maintained a temperature of 20 ± 0.2 °C as measured by a calibrated mercury thermometer. Polarimeter readings were at 589 nm wavelength.

The general procedure begins with temperature equilibration of all chemicals and glassware in the waterbath. About 5 g of lactose powder is accurately weighed into a 100 ml volumetric flask and distilled water added to the mark. When completely dissolved, the lactose solution is transferred to the polarimeter cell which is flushed three times and filled. Polarimetric readings commence immediately.

For the mutarotation curve to accurately reflect the anomeric composition of the sample, the lactose used must be chemically pure and contain no optically active species such as glucose, a

common impurity of lactose. As the method to be described assumes a two component system (alpha and beta lactose) the presence of significant quantities of other optically active species will change the optical rotation of the entire solution and cause systematic errors in the calculation of the anomeric composition. The purity of lactose used in these measurements is greater than 99.8%.

The solvation delay between the point of solvent contact (t=0) and the completion of dissolution is another source of systematic error. This delay affects the intercept at t=0 and can influence the calculated anomeric composition. The effects of solvation delay are investigated next.

3.3.2 Effect of solvation delay upon the mutarotation curve

Figure 3.3 depicts the simulated effect (Appendix 1) of solvation delay on the early stages of polarimetric measurements of alpha lactose monohydrate. Solvation delay displaces the curve to longer times and raises the intercept. A delay of 3 minutes raises the intercept 1 degree and increases the calculated alpha content by 3%. Reduction of the delay to 30 seconds by fine grinding of the sample improves accuracy without excessive grinding which may alter the composition of some powders[15]. All lactose samples were subsequently ground and sieved to 100 mesh.

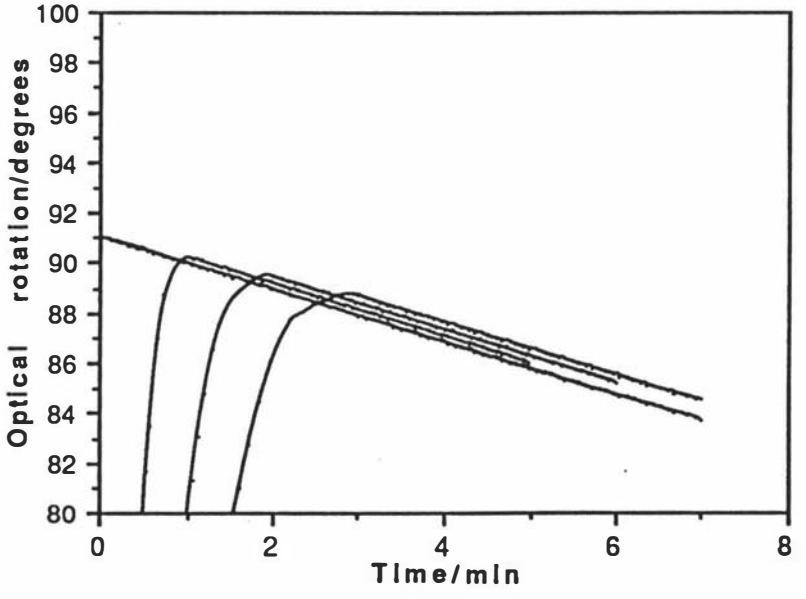

Figure 3.1. Effect of the solvation delay (0, 1, 2 and 3 min) upon the determination of the initial optical rotation of a solution of alpha lactose immediately prior to mutarotation (ie. extrapolation to t=0). The solvation delay of each curve represents the time for complete dissolution.

3.3.3 Polarimetric measurements and anomeric calculations

Optical rotation is dependent on solute concentration and polarimeter cell path length. These dependencies may be normalised (Equation [3.1]) to yield the specific optical rotation at fixed temperature and wavelength. It is therefore important that the concentration of lactose in solution be accurately known. In cases where concentration is calculated from the gravimetric addition of lactose to a known volume of solvent, the moisture content of powder samples must be determined. The method developed here was to measure the optical rotation of an equilibrium solution of lactose. Comparison to literature values[9] enabled the anhydrous weight fraction to be easily determined.

To measure the optical rotation at equilibrium, 5 grams of lactose was accurately weighed (w_∞) into a 200 ml beaker in the 20 °C waterbath. About 80 ml of distilled water and 3-4 drops of 6 N aqueous ammonia solution[10,48] were added and the solution vigorously agitated to dissolve the powder. Addition of ammonia solution establishes equilibrium in about 30 minutes. The solution was transferred to a 100 ml volumetric flask and made to the mark. After 30 minutes, the polarimeter tube was flushed three times, filled with lactose solution and purged of air. A flow-through system as depicted in Figure 3.2 quickened sample loading. The equilibrium optical rotation was recorded (R_∞).

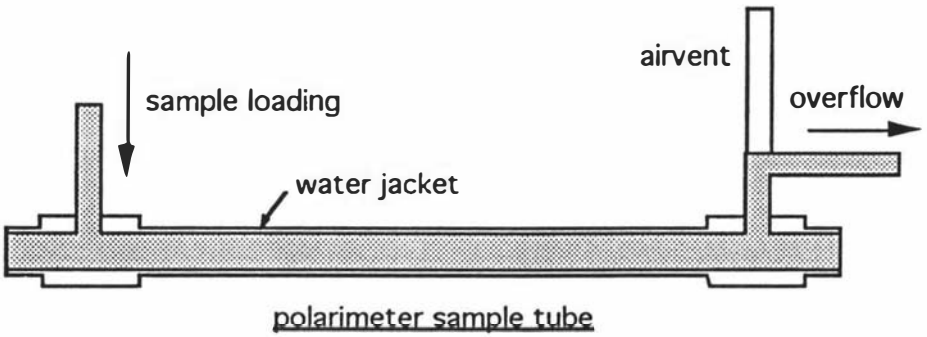

Figure 3.2. Setup used to load the aqueous sample into the temperature controlled polarimeter tube.

The anhydrous weight fraction of lactose was derived from the equilibrium reading, R_∞. The specific equilibrium rotation, $[R_\infty]$ of lactose is[10]

$$[R_\infty] = \frac{100R_\infty}{Lc} \qquad [3.1]$$

where L is the length of the polarimeter tube in decimeters (2 dm), c = anhydrous concentration of lactose in g/100ml, and $[R_\infty] = 55.48°$ for pure lactose. Having determined c, the anhydrous weight fraction, W_a may be found by

$$W_a = \frac{w_\infty}{c} \qquad [3.2]$$

Samples were found to have an anhydrous weight fraction in the range of 0.94-1.00. The hydration fraction is due to the water of crystallisation of the alpha lactose monohydrate component[9].

To measure the optical rotation immediately after dissolution, 5 grams of lactose was accurately weighed (w_t) into a 200 ml beaker in the waterbath, and 80 ml of distilled water added at which point timing commenced. This point (t=0) represents the start of mutarotation. The lactose solution was transferred to a 100 ml volumetric flask and made to the mark with distilled water. Vigorous agitation of the flask dissolved the powder within 30 seconds of solvent contact. The polarimeter tube was flushed three times with lactose solution and filled as before. The first polarimeter reading (R_t) was taken 3 minutes after solvent contact and subsequent optical readings taken at 1 minute intervals for a further 20 minutes. All measurements were carried out in triplicate so that reproducibility could be established.

The mutarotation of alpha lactose monohydrate dissolved in water at 20 °C is demonstrated clearly from the optical rotation readings depicted in Figure 3.3. The corresponding semi-logarithmic plot is presented in Figure 3.4. Since mutarotation is first order[36] (single exponential), the plot is linear. The fact that it is linear (Figure 3.4) confirms the temperature stability.

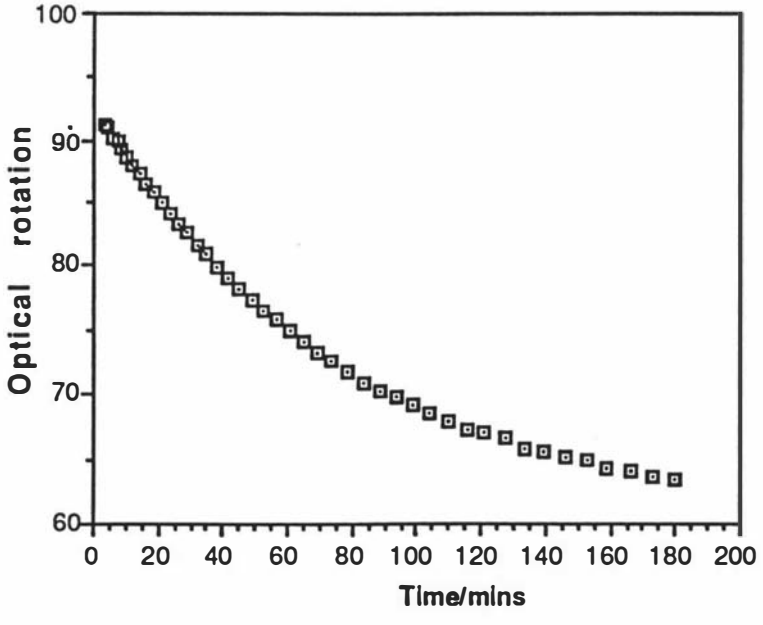

Figure 3.3. The mutarotation curve of alpha lactose monohydrate dissolved in water at 20 °C.

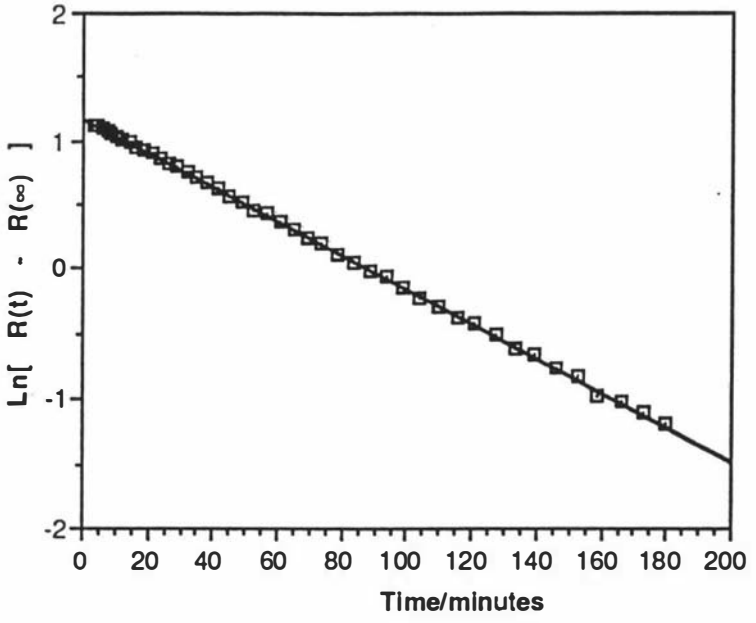

Figure 3.4. The corresponding semi-logarithmic plot of Figure 3.3.

The specific optical rotation at the moment of solvent contact is found from the y-intercept of a plot of $Ln([R_t]-[R_\infty])$ v t, where $[R_t]$ and $[R_\infty]$, the specific optical rotations at times t = t and t = ∞ respectively, are given by the relation,

$$[R_x] = \frac{100R_x}{LW_aw_x} \qquad x = t,\infty \quad [3.4]$$

The specific rotation at solvent contact, $[R_0]$ determines the anomeric composition of the powder from

$$\alpha = \frac{([R_0]-[\beta])}{([\alpha]-[\beta])}\times 100\% \qquad [3.5]$$

where $[\alpha]$ = 91.1, and $[\beta]$ = 33.5 are specific rotations of pure alpha and beta lactose respectively, and α is the percentage of alpha lactose in the sample. Results of lactose powder measurements will be covered in Section 3.6.

3.3.4 Temperature dependence of the mutarotation rate

The mutarotation rate is strongly temperature dependent[36]. The control of solution temperature may be used to manipulate the anomeric composition of an aqueous lactose solution. Heating to 65-70 °C quickly establishes equilibrium, whereas cooling to a few degrees above freezing

point strongly inhibits mutarotation. The temperature dependency was established by polarimetry.

Mutarotation of alpha lactose monohydrate in solution was followed to equilibrium by polarimetry. The rate constant of mutarotation k was obtained by fitting a single exponential[36] to the data (Equation [3.6]) using the Marquardt-Levenberg algorithm[32]. The method follows that described in Section 3.3.3 with some changes. In particular, optical readings spanned approximately four time constants and equilibration (to obtain R_∞) was established by heating the solution after measurement to 90 °C and cooling.

The mutarotation curve was normalised as

$$R_t' = \frac{R_t - R_\infty}{R_0} \qquad [3.6]$$

where R_t' represents the datum points of the normalised mutarotation curve. Assuming a first order rate constant k for mutarotation, then a plot of $\ln[R_t']$ *versus* t should be a straight line of slope = -k (typically as per Figure 3.4).

Polarimetric measurements were performed in duplicate at 21.5, 30, 40, and 51 °C. The temperature dependence is depicted in Figure 3.5 where it is clear that the data exhibit Arrhenius behaviour ($k = A\exp(-E_a/RT)$ with an activation energy E_a of 71900 J mol^{-1} K^{-1} and a pre-exponential factor A of 10.9 s^{-1}.

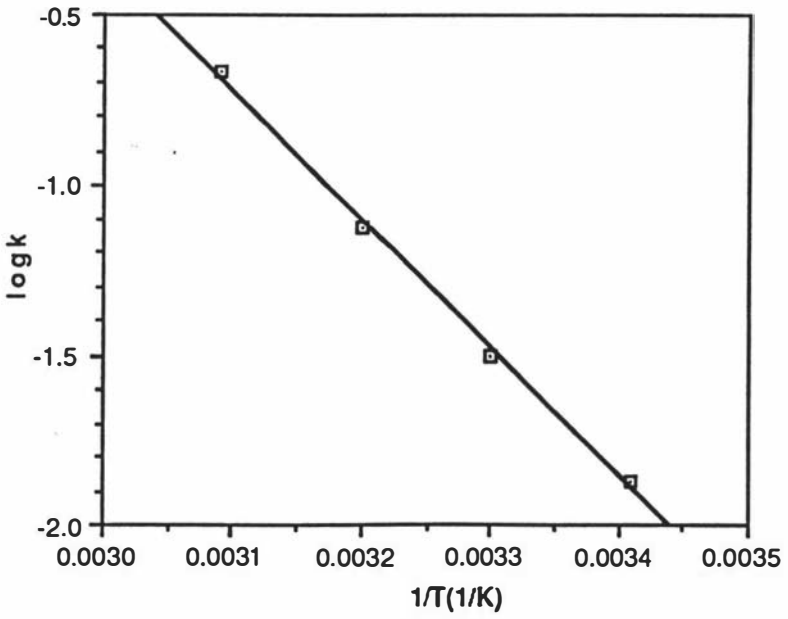

Figure 3.5. The temperature dependence of the mutarotation rate.

3.4 Gas liquid chromatography

Gas liquid chromatography (GLC) provides an efficient means of separating carbohydrates such as lactose. Each anomer expresses sufficiently different retention time[11] that separation over a column distance of 2 metres is readily achieved. As pure lactose does not readily volatilise at normal column injection temperatures (200-300 °C), samples must be derivatised to a more volatile compound, typically a trimethylsilylated (TMS) ether. This is readily performed with the various proprietary solutions available on the market. It is during derivatisation that anomeric conversion of lactose is likely to occur with conventional solvents such as pyridine[49], resulting in the anomeric composition at the detector not accurately reflecting that which existed in the powder. In this section various solvent/reagent mixtures are trialed and results of peak integrations compared to the resulting anomeric composition obtained by polarimetry.

3.4.1 Materials and method

Derivatisation to a TMS ether not only improves sample volatility, but also enhances the interaction between the mobile gaseous phase and the column, resulting in superior component separation and more accurate quantitative interpretation of the detector signal[50]. The high volatility expressed by TMS ethers means that a lower column temperature may be utilised, and therefore thermal degradation of samples is reduced. The derivatising reaction is,

$$3ROH + Me_3SiNHSiMe_3 + Me_3SiCl \rightarrow 3ROSiMe_3 + NH_4Cl \qquad [3.7]$$

where the terminal hydroxyl groups (ROH) are trimethylsilylated to yield the TMS ether ($ROSiMe_3$).

Lactose powders were dehydrated to remove the adsorbed water which severely inhibits derivatising action[51]. Ten milligrams of lactose was weighed into a micro test-tube, 1 ml of isopropanol added, and the mixture heated to 75 °C until dry. One ml of solvent (see next paragraph) and 0.3 ml of Tri-Sil concentrate™ was added to the powder, and the mixture gently heated to promote rapid dissolution. After 30 minutes and the completion of derivatisation, each sample was injected into the column.

Two solvent/reagent mixtures were trialed to investigate the extent, if any of anomeric conversion. The mutarotation-inhibiting solvent DMSO[11,52], and a mixture of DMSO/pyridine[11], which dissolves lactose more quickly, were compared. Sample preparation involving each solvent/reagent mixture was identical.

The GLC instrument was a SHIMADSU series 15A CHROMATOGRAPH with a CHROMATOPAC C-R6A integrator, and flame ionisation detector. One µL of sample was injected into the column at 255 °C. The column consisted of a 2 m x 2 mm glass tube packed

with 5% OV-17 chromosorp W-HP 80/100 mesh. The carrier gas was nitrogen and the flow rate 50 ml/minute.

A typical chromatograph of a powder mixture of alpha monohydrate and beta lactose is presented in Figure 3.6. Each peak was readily identified from the known anomeric composition of the powder. The concentration of each anomer was determined by integration, and the anomeric composition determined assuming the response of each species at the detector to be equal[11]. Measurements of the series of lactose powders will be presented in section 3.6.

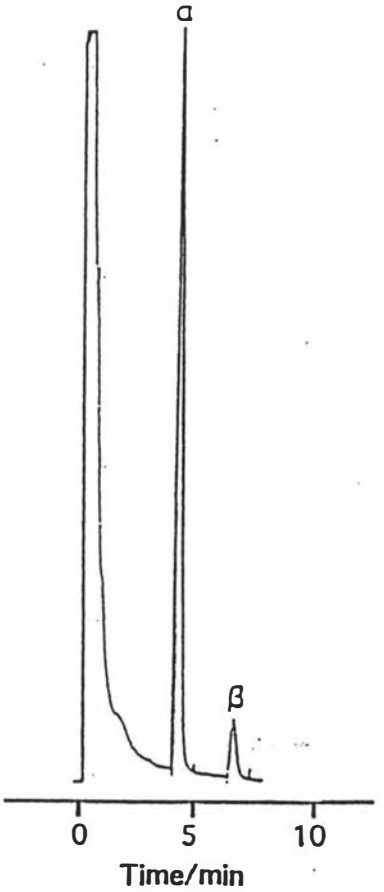

Figure 3.6. A typical gas chromatogram of a mixture of alpha lactose monohydrate and conventional beta lactose

3.5 High resolution NMR spectroscopy

High resolution NMR spectroscopy is inherently suited to the investigation of dissolved solids since resonance lines are motionally narrowed, and relatively good spectral resolution (compared with solid spectra) enables simple quantitative interpretation. Each anomer of lactose demonstrate chemically shifted proton and carbon-13 spectra[53] from which peak integrals may be easily determined, and anomeric compositions calculated. In proton spectra, the anomeric composition is easily determined by integrating any two peaks corresponding to each anomer. In carbon-13 spectra, where proton rf irradiation (decoupling) is used to remove the complicating effect of C-H coupling, some amplitude distortion of peaks invariably occurs, (this is a consequence of the Nuclear Overhauser Effect), and the calculation of the relative abundance of each species in solution from the relative peak intensities is not generally

possible. Both proton and carbon-13 NMR spectroscopy are investigated as a possible characterisation methodology of powdered lactose.

3.5.1 Materials and method

Samples were prepared for NMR measurement by dissolving 20 milligrams of lactose powder in 1 ml of solvent in a 5 mm NMR tube. The lactose samples were alpha lactose monohydrate, and conventional beta lactose as described in Chapter 2. For dynamic experiments in which the changing anomeric composition is monitored (as with polarimetry), the appropriate solvent is D_2O, whereas for static experiments DMSO-d6 is used. Each experimental protocol is described separately .

Proton and carbon-13 spectra were obtained using a JEOL JNM-GX270 FT NMR spectrometer operating at a field strength of 6.34 tesla (270 MHz for ^1H and 67.9 MHz for ^{13}C nuclei). A 5mm temperature controlled dual band probehead was used.

3.5.2 Dynamic measurements and calculation of the anomeric composition

Typical proton and carbon-13 spectra of alpha and beta lactose at 20 °C are presented in Figures 3.7 to 3.10. All ^{13}C spectra are proton decoupled. Proton spectra are the result of 20 signal averaged FID's whereas ^{13}C spectra were derived from 100 FID's. Proton and carbon-13 chemical shifts are available from the literature[53]. Chemical shifts which are given in parts per million (ppm) from TMS were actually measured using either water ($\delta = 4.7 ppm$) or the residual solvent peak of DMSO ($\delta = 2.6 ppm$) as the reference peak.

Figures 3.7 and 3.8 exhibit well resolved glucose 1β and superposed galactose $[1\alpha + 1\beta]$ peaks, both suitable for integration, along with a partially solvent-masked glucose 1α peak. The ^{13}C spectra of Figures 3.9 and 3.10 demonstrate excellent peak resolution albeit with a reduction in the signal:noise (S:N) ratio compared to proton spectra. Since the relative isotopic abundance of ^{13}C is only 1% the spectra require greater signal averaging to compete with the S:N ratio obtained from the more abundant proton nucleus. In addition, the lower nuclear gyromagnetic ratio of ^{13}C nuclei (6.7×10^7 rad s^{-1} T^{-1}) compared with ^1H nuclei (2.6765×10^8 rad s^{-1} T^{-1}) accounts for a significant reduction of sensitivity. A larger sample volume (10 mm versus 5 mm sample tubes) increases the S:N level but improvements are marginal. Because of the low S:N ratio and the inability to use ^{13}C intensities as a direct measure of spin concentration, it was decided to use proton spectroscopy as the sole liquid state characterisation method.

Reduction in the intensity of the solvent (H_2O) peak would prove advantageous to peak integration (of the glucose 1α resonance line), and calculation of anomeric compositions. Solvent signal suppression pulse sequences effectively reduce the amplitude and peak width of

the H_2O resonance, and unmask the peak of interest (see Figure 3.12). Alternatively, the solvent peak may be shifted upfield by a reduction in temperature. Since lactose proton chemical shifts demonstrate less temperature dependency than water, a reduction in temperature provides a relatively simple means of separating the residual H_2O and glucose 1 α resonance lines (Figure 3.13). Furthermore, temperature reduction during measurement has the added advantage of reducing the rate of mutarotation. Each of these techniques is discussed in turn.

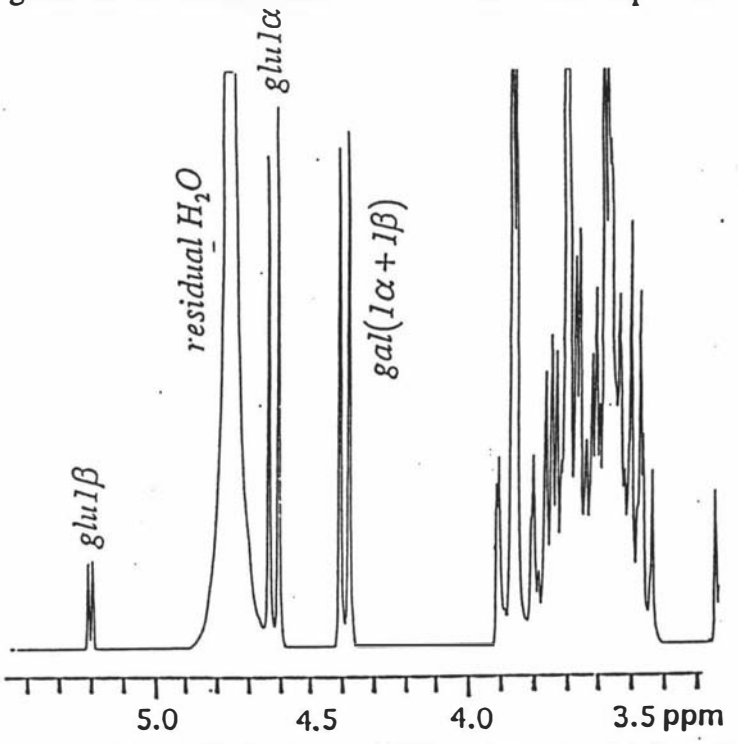

Figure 3.7. Proton spectra of alpha lactose in D_2O at 20 °C. **The poor quality of some spectra was caused by catastrophic failure of the JEOL harddrive prior to writting of this thesis. Therefore, most spectra had to be reproduced from hard copies.**

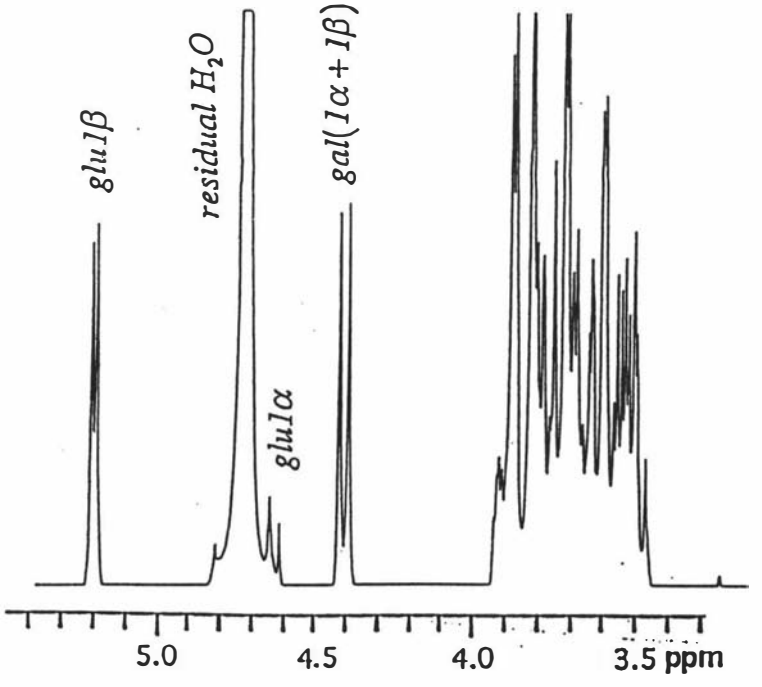

Figure 3.8. Proton spectra of beta lactose in D_2O at 20 °C

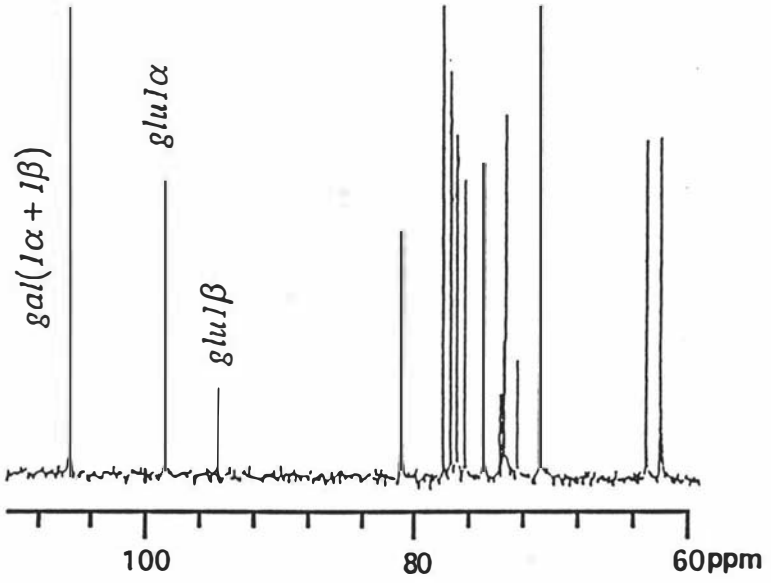

Figure 3.9. ^{13}C spectra of alpha lactose in D_2O at 20 °C

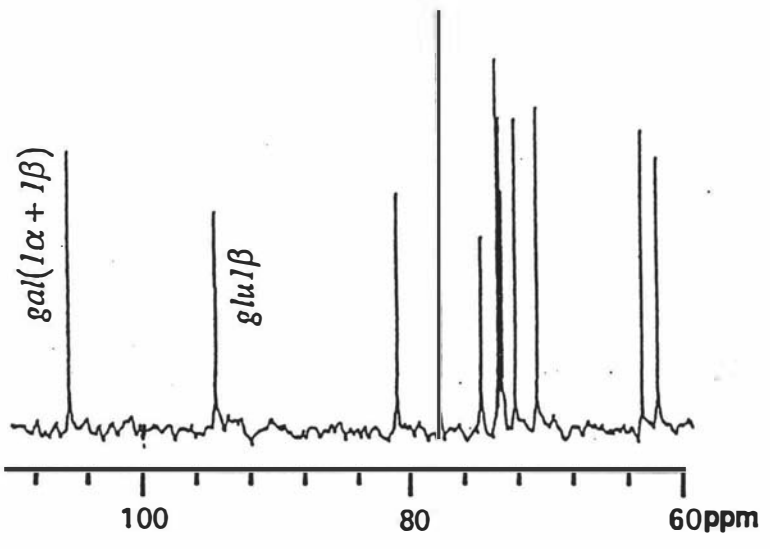

Figure 3.10. ^{13}C spectra of beta lactose in D_2O at 20 °C

3.5.2.1 Solvent suppression

Several solvent suppression pulse sequences were investigated[54] including inversion recovery, selective non-excitation, selective excitation and destruction, double quantum filter, and a hard-soft pulse combination. The hard-soft pulse combination proved most effective in quenching the solvent signal. The pulse sequence, illustrated in Figure 3.11, uses a succession of three selective "soft" 90° pulses of frequency coincident with the solvent resonance causing repeated solvent magnetisation flips and ultimately dephasing in the transverse plane. With a pulse duration of 200 ms (which gives an effective bandwidth of a few hertz), a pulse amplitude attenuation of 250 dB gave the required 90° flip angle. A delay of 200 ms was introduced between pulses to allow dephasing of the proton signal due to T_2 relaxation. The "hard" 90° pulse which follows excites lactose protons and an FID is generated. The effect of solvent suppression is demonstrated in Figure 3.12.

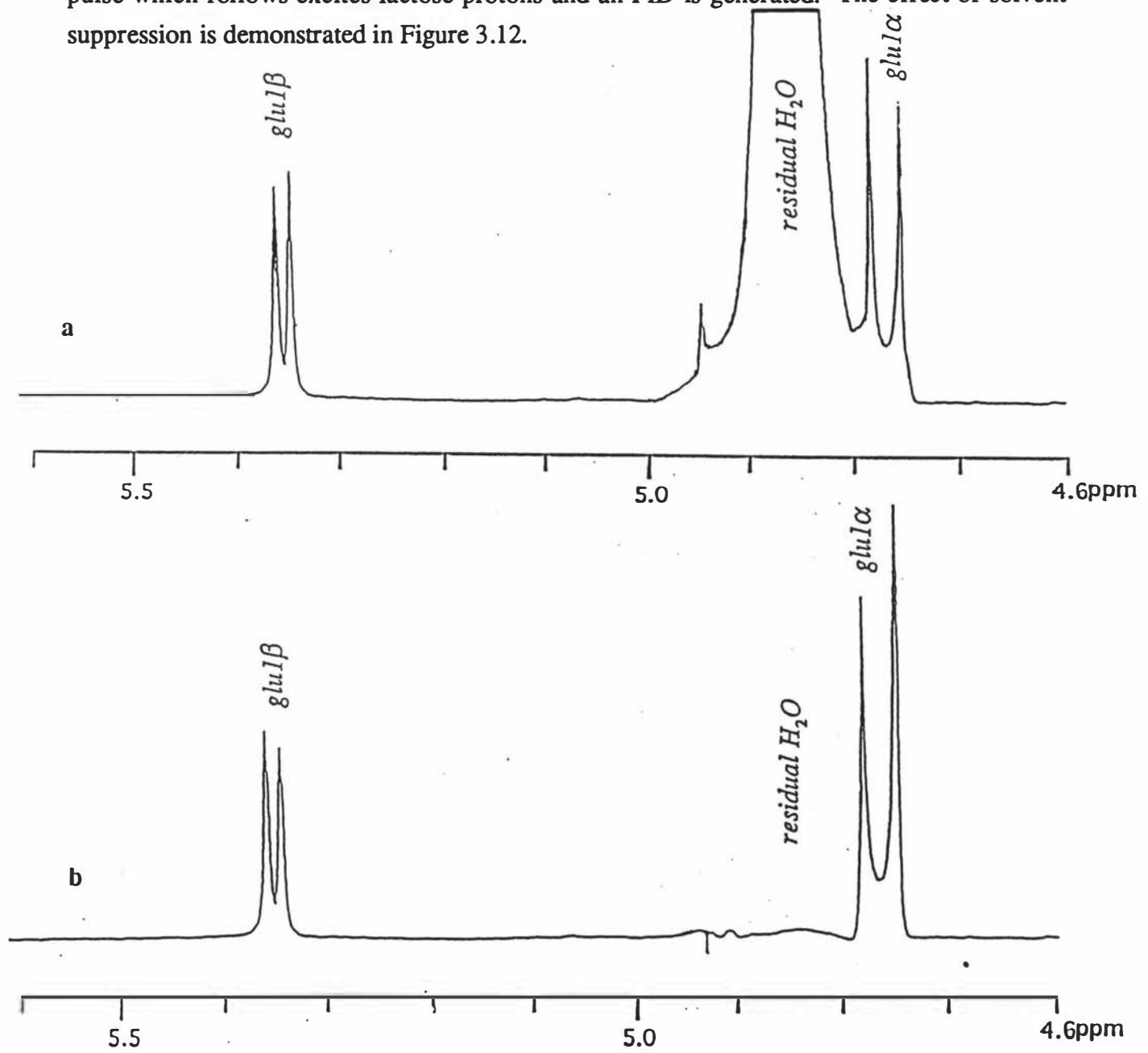

Figure 3.12. Comparison of the 4.6-5.6 ppm region of the proton spectrum of a mixture of alpha and beta lactose in D_2O at 20 °C with the normal (a) and hard-soft pulse (b) combination.

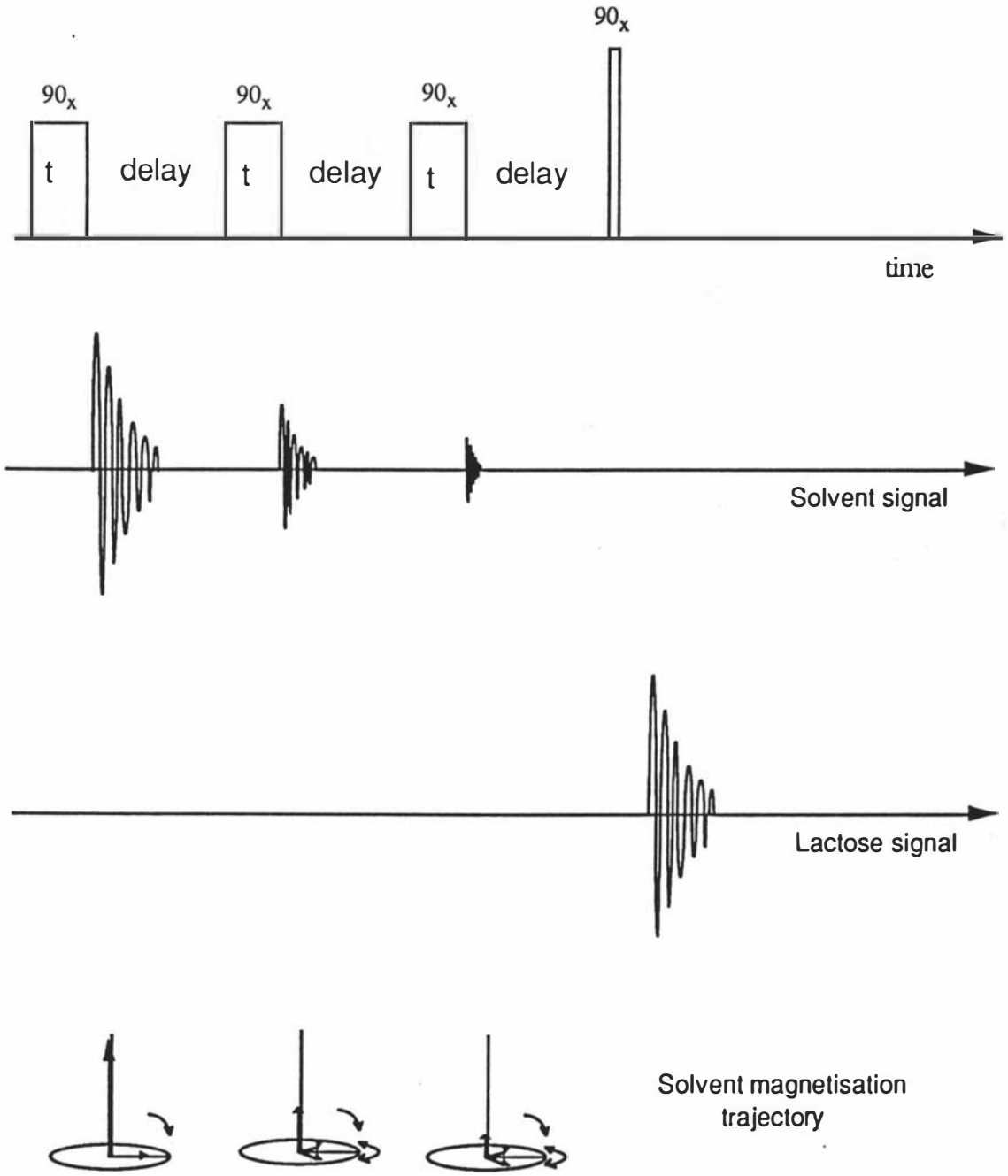

Parameters: attenuation = 250 (OBA)
delay and t = 200 ms

Figure 3.11. Hard-soft combination solvent suppression pulse sequence and magnetisation trajectories.

To measure the anomeric composition of lactose powders, twenty milligrams of sample was dissolved in 1 ml of D_2O in a 5 mm NMR tube. The first measurement commenced 3 minutes after solvent contact with the lactose powder. Twenty FID's were collected and the anomeric composition determined from peak integrations according to Equations [3.8]. Measurements were repeated at 5 minute intervals for a further 40 minutes.

$$anomeric\ composition = \frac{glucose1\alpha\ integral}{glucose1\alpha\ integral + glucose1\beta\ integral} \qquad [3.8]$$

The anomeric composition in the powder is determined as the intercept of a plot of $Ln(R(t) - R(\infty))$ v t, where R(t) and R(∞) are the anomeric compositions of the solution at time t, and equilibrium respectively. All samples were measured in triplicate. Results are discussed in Section 3.6.

3.5.2.2 Comparison of 20 °C spectra with 10 °C spectra

Temperature reduction to 10 °C sufficiently unmasked the glucose 1α peak to allow accurate integration. Figure 3.13 depicts the proton spectra of alpha lactose in D_2O at 10°C. Low temperature samples are cooled to 10 °C immediately after dissolution, and prior to NMR measurement.

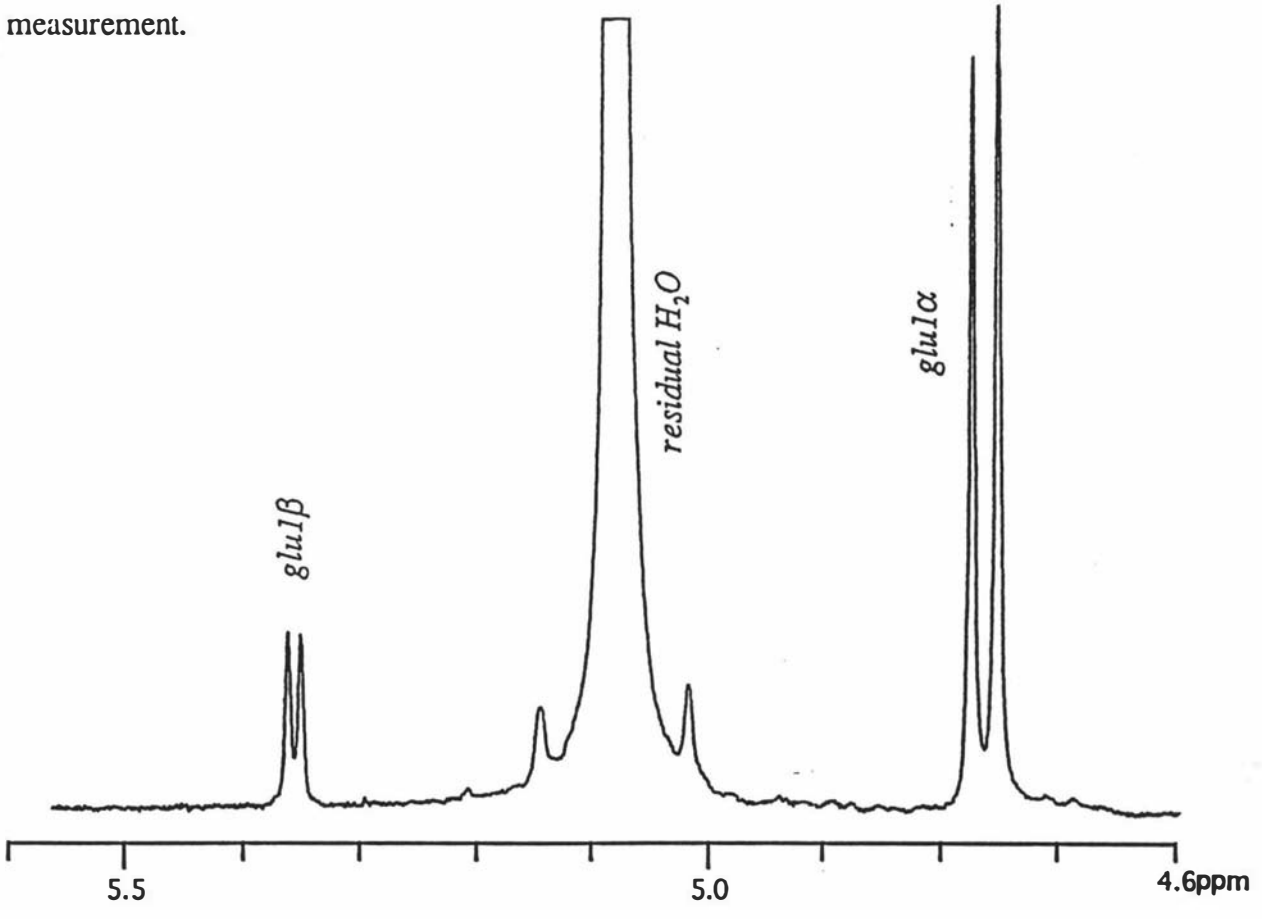

Figure 3.13. Proton spectra of alpha lactose in D_2O at 10 °C

The anomeric composition is determined at 10 °C and 20 °C according to Equations [3.10] and [3.11] respectively.

$$anomeric\ composition = \frac{glucose1\alpha\ integral}{glucose1\alpha\ integral + glucose1\beta\ integral} \qquad [3.10]$$

$$anomeric\ composition = \frac{glucose1\alpha\ integral}{galactose(1\alpha + 1\beta)\ integral} \qquad [3.11]$$

where the $galactose(1\alpha + 1\beta)$ integral corresponds to the superimposed $galactose1\alpha$ and $galactose1\beta$ peaks. The anomeric composition in the powder is determined from Equation [3.9]. Results of several powder measurements are presented in Section 3.6.

3.5.3 Static measurements using DMSO and calculation of the anomeric composition

In DMSO, mutarotation is suppressed[9,34,35] and the anomeric ratio of the solutes reflect that of the solid. It is therefore a simple matter to integrate the relative peak intensities from a single spectrum and calculate the anomeric ratio. ^{1}H NMR spectra of alpha and beta lactose are depicted in Figures 3.14 and 3.15 and ^{13}C spectra in Figures 3.16 and 3.17 respectively.

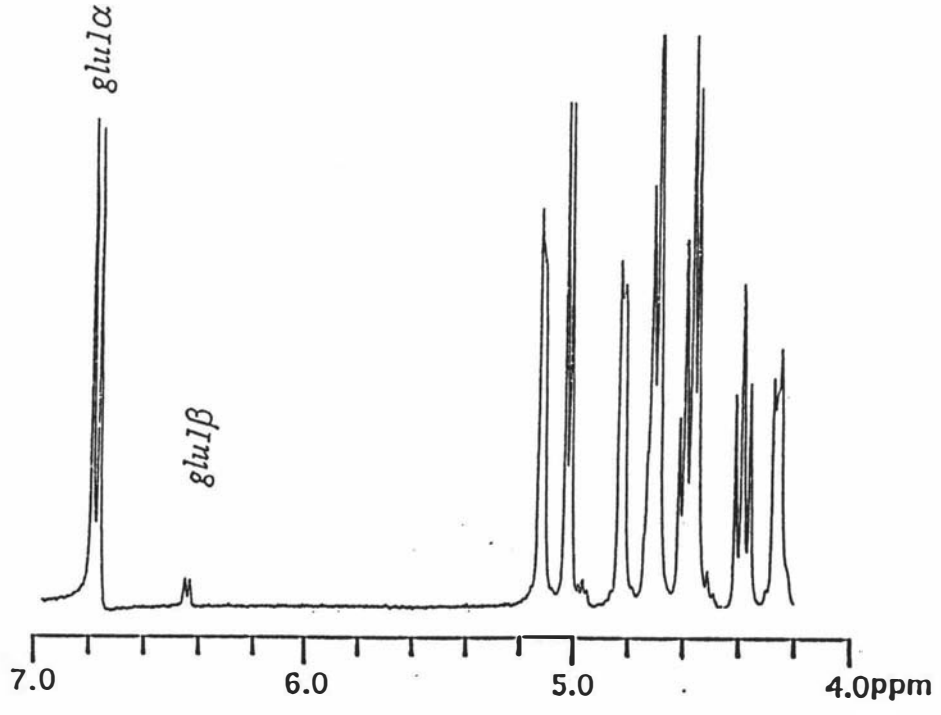

Figure 3.14. ^{1}H spectra of alpha lactose in DMSO-d6 at 20 °C

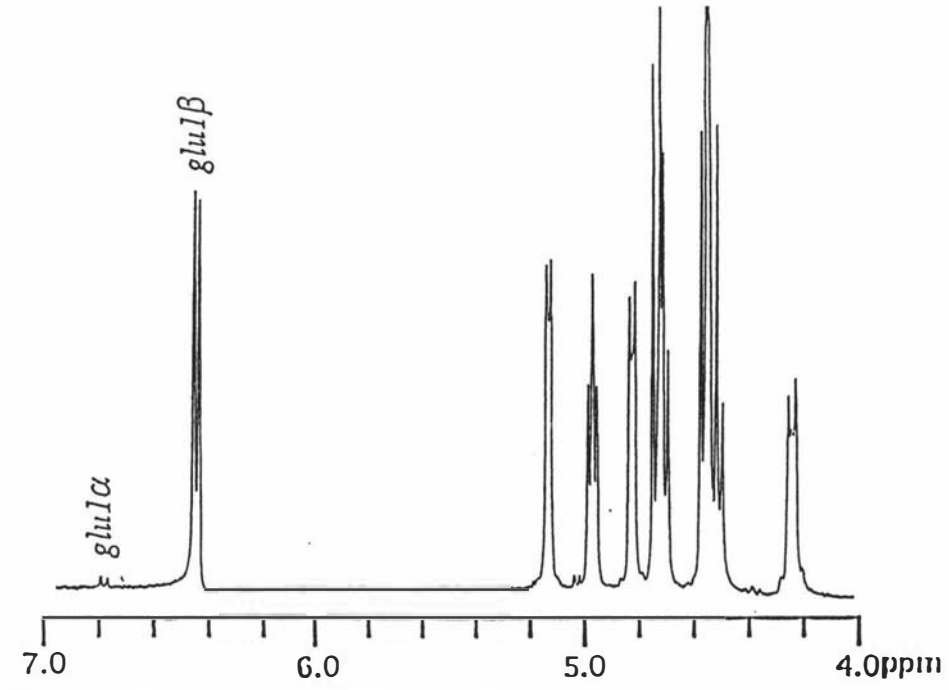

Figure 3.15. ^{1}H spectra of beta lactose in DMSO-d6 at 20 °C

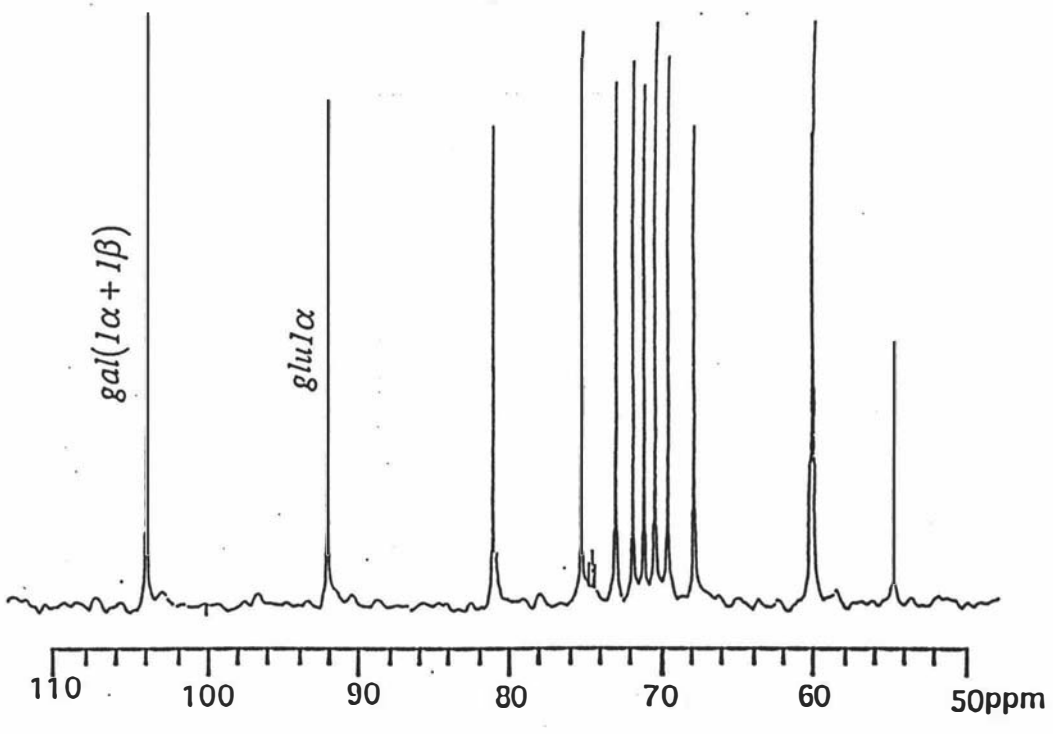

Figure 3.16. ^{13}C spectra of alpha lactose in DMSO-d6 at 20 °C

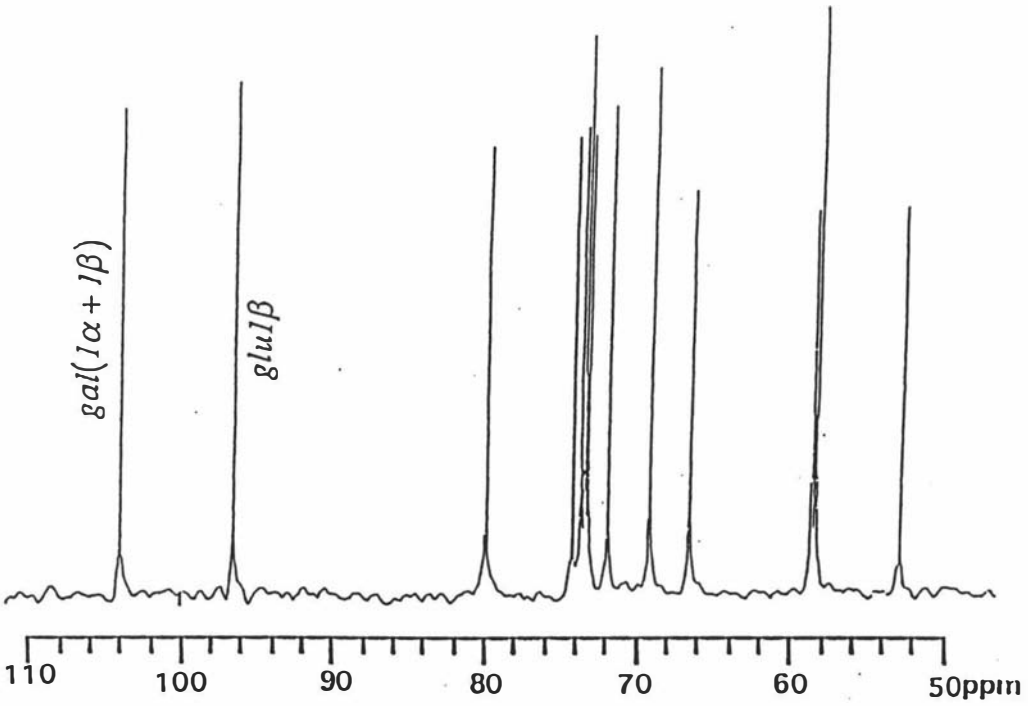

Figure 3.17. ^{13}C spectra of beta lactose in DMSO-d6 at 20 °C

Experimental protocol follows that described in Section 3.5.2, although solutions were momentarily heated to 40 °C to promote dissolution. The anomeric composition is determined according to Equations [3.8] and [3.9]. Results of powder measurements are presented in the next section.

3.6 Results of anomeric measurements

Table 3.2 and Figure 3.18 present a comparison of polarimetry, GLC, and high resolution ^1H NMR methodologies in measuring the powders prepared in Section 3.2.

3.7 Discussion

Apart from the NMR method using solvent suppression, most methodologies agree reasonably well. The large experimental error expressed by the NMR method using solvent suppression was caused by amplitude distortion of the respective resonance lines used for anomeric calculation. This effect is described further in Appendix 2. The magnitude of distortion was variable, increasing with stronger suppression, and difficult therefore to compensate for. Solvent suppression is not therefore a recommended methodology for accurate quantitative interpretation of proton spectra.

Table 3.2 The results of polarimetry, GLC and NMR to determine the anomeric composition of a series of powders

		GLC			PROTON NMR			
SAMPLE #	POL[a]	DMSO[b]	DMSO[c]	DMSO/ PYR	DMSO	20°C	10°C	SS[d]
1	95.6	95.1	94.4	95.2	95.9	95.8	94.4	94
2	94.6	93.9	92.8	94.8	94.0	92.8	93.8	92
3	60.9	57.8	56.1	58.4	58.9	56.1	58.0	59
4	17.2	17.0	19.4	16.9	16.9	15.6	17.0	14
5	15.7	15.0	17.1	14.9	15.9	14.1	15.6	13
6	5.5	5.6	-	5.5	5.0	5.9	5.8	-
SD[e]	0.3	0.5	0.8	0.3	0.4	0.9	0.6	2

a polarimetry
b lactose dissolved in DMSO at 60 °C
c lactose dissolved in DMSO at 40 °C
d solvent suppression
e standard deviation of triplicate measurements averaged over all samples

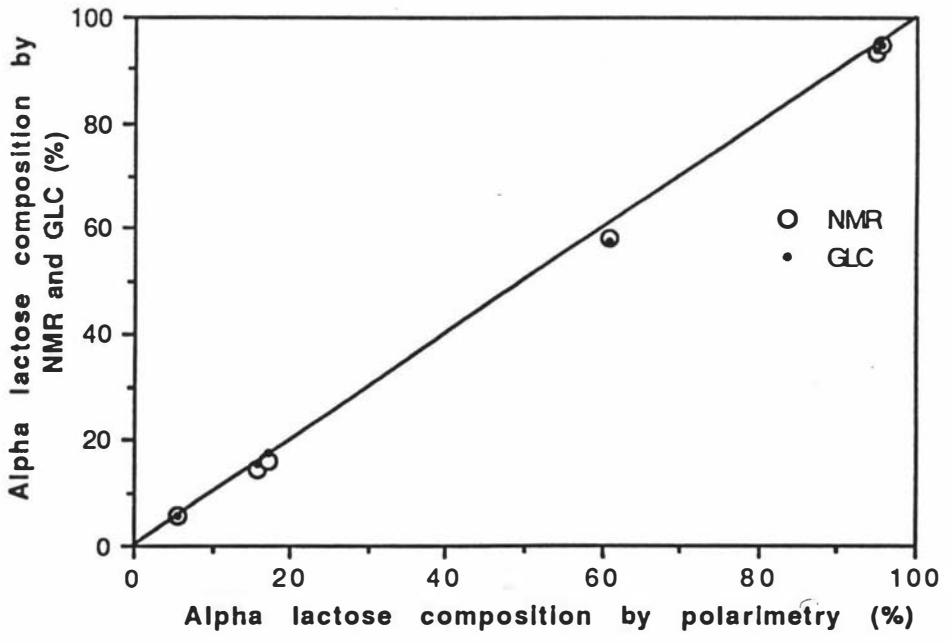

Figure 3.18. Comparison of polarimetry, NMR and GLC.

Polarimetry, the traditional methodology for lactose characterisation, is precise and reproducible. Its accuracy is confirmed by consistency with the other methods described here. In this sense, its use as a reference method is justified.

Gas liquid chromatography closely agrees with polarimetry when the solvent is DMSO or a DMSO/pyridine mixture. When DMSO is heated to 60 °C to promote dissolution of the powder, mutarotation appears to take place as the anomeric composition of all samples evolved slightly towards equilibrium. For GLC to be used with accuracy, the heating of solvents to promote dissolution must be done as quickly as possible.

Results of NMR spectroscopy at 20 °C and at low temperature (10°C) agree well with polarimetry. The higher random error associated with using a mutarotating solvent is probably due to the evolution of the anomeric composition over the time frame of spectral acquisition in conjunction with reduced signal averaging of the FID (to allow measurements at 5 minute intervals). This could be improved by increasing the sample volume and therefore reducing the noise level. Nonetheless, the method compares favourably with polarimetry, and offers the advantage that calculations are independent of concentration, and measurements are unaffected by optically active impurities. NMR spectroscopy using DMSO shows good agreement with other methodologies and excellent reproducibility. As only a single spectrum is required, a greater number of FID's may be collected and signal averaged to yield even higher precision.

3.8 Conclusions and summary

Polarimetry is confirmed as an accurate method for characterising the anomeric composition of lactose powders. The stability of solution temperature throughout optical measurement and the accurate definition of the solution concentration are essential to this accuracy and attainment of good reproducibility. Accurate polarimetry requires lactose samples to be free of glucose and other optically active impurities and powders must completely dissolve in 30 seconds. Both crude and refined lactose meet this purity criterion and careful grinding and sieving to 100 mesh ensures quick dissolution.

GLC is similarly confirmed as an appropriate characterisation method for lactose powders. No mutarotation was detected with the pyridine/DMSO solvent mixture or pure DMSO as long as overheating did not occur. In the interests of providing better dissolution of lactose and minimise mutarotation, the use of a cold pyridine/DMSO mixture is preferred to heating.

High resolution NMR spectroscopy is well suited to lactose characterisation. There is no need for time-consuming derivatisation, and unlike polarimetry, samples do not need to be accurately weighed. The use of D_2O as solvent causes mutarotation and the resulting curve must be followed over time before the anomeric composition of the powder can be obtained by

extrapolation. In using DMSO, a single spectrum suffices, and the determination of the anomeric composition of the powder is significantly simplified.

4. Relaxation of spin 1/2 nuclei in diamagnetic solids

4.1 Introduction

Relaxation of nuclear spins in a static magnetic field is caused by the distribution of local interactions that each nuclear spin experiences. The relaxation rate is sensitive to the magnitude *and* rate of fluctuation of these interactions[54]. The measurement of relaxation rates typically provides information about molecular structure[56] (by way of calculating internuclear distances).

The analysis of relaxation data according to current relaxation theory is complicated, requiring a deep understanding of quantum statistics[56]. In this chapter, some of the well-known formulae describing spin-lattice and spin-spin relaxation in diamagnetic insulators, such as lactose powder will be derived. The magnitude of spin-spin relaxation times (T_2) in solids is typically of order microseconds. Because of this, it is impractical to measure these relaxation times using a standard NMR spectrometer, and hence relaxation measurements of solid lactose is restricted here to spin-lattice relaxation, and its associated time constant, T_1. The identification of specific T_1 values corresponding to different crystalline structures of lactose provides the basis of powder assaying measurements. Relaxation measurements are also used to investigate structural rearrangements during the course of solid-state crystallisation of amorphous lactose, and to follow the changing molecular free volume and mobility that occur at the glass transition of amorphous lactose.

In Section 4.6 the practical measurement of T_1 using a wideline NMR machine will be described as will the methods for the calculation of relaxation time components from data using a selection of iterative and non-iterative linear inversion algorithms such as NNLS[30] (non-negative least squares (subsequently referred to as LH (Lawson-Hanson))), Marquardt-Levenberg[32] (ML) and Contin[57]. Each algorithm is extensively "tested" on simulated relaxation data incorporating Gaussian noise and baseline drift comparable in magnitude to that observed in real measurements to gauge the sensitivity of the algorithms to these factors.

Experimental protocol is discussed in Section 4.6 and the results of initial experiments on crystalline species of lactose are presented. These results are used to demonstrate the effect of drift in inversion recovery data (Section 4.3) on the relative amplitudes and times of relaxation components obtained from the T_1 spectra. A reduction in drift was achieved by modifying the pulse sequence to monitor "baseline" deviation during relaxation measurements followed by appropriate correction of the raw data. This involved modifications to the system hardware (upgraded input/output interface circuit boards), and the adoption of new software allowing the design and implementation of suitable pulse sequences, and storage of data. T_1 spectra derived from the two operating systems are compared to show the

significant improvement in reproducibility following the elimination (or reduction) of drift from IR data.

4.2 Spin lattice relaxation times in solids

This section introduces some basic concepts of NMR and includes a discussion of the process of spin-lattice and spin-spin relaxation of protons in solids and liquids close to room temperature.

4.2.1 Resonant excitation and the rotating frame

An ensemble[58] of equivalent nuclear spins in a polarising magnetic field, B_0 experiences an interaction energy described by the Zeeman Hamiltonian operator

$$H = -\gamma \hbar B_0 I_z \qquad [4.1]$$

where γ is the gyromagnetic ratio and I_z, the angular momentum operator, is in the direction of B_0 (z-axis). Application of an oscillating magnetic field of amplitude B_1 and frequency $\omega = \gamma B_0$ transverse to the direction of B_0 (in the x-y plane) yields the resonance phenomenon and the spin system is disturbed from equilibrium. In the static laboratory frame of reference the Hamiltonian due to B_0 and B_1 is[54]

$$H_{lab} = -\gamma B_0 I_z - 2\gamma B_1 \cos \omega t I_x \qquad [4.2]$$

The linearly polarised oscillatory field can be considered as the superposition of two counter-rotating circularly polarised components and, provided $B_1 \ll B_0$, the component rotating in the opposite sense to the nuclear precession may be ignored and B_1 may therefore be considered simply as a circularly polarised magnetic field rotating at ω. It is convenient to transform the coordinate system to the frame where B_1 is stationary since this makes the Hamiltonian time independent and the simple evolution operator,

$$U(t) = \exp(-iHt/h), \qquad [4.3]$$

applies to the quantum states. In the rotating frame, the Hamiltonian becomes

$$H_{rot} = -\gamma(B_0 - \omega/\gamma)I_z - \gamma B_1 I_x \qquad [4.4]$$

At resonance, where $\omega = \omega_0$, the apparent field in the direction of B_0 vanishes. The spins precess about the effective field which is positioned along the rotating frame x'-axis. In the rotating frame, the decay of nuclear magnetisation due to spin-lattice relaxation (T_2) is simply interpreted as a dephasing of individual nuclear spins with different precession frequencies in

the rotating frame x'-y' plane. Spin-lattice relaxation (T_1) is best described in the static laboratory frame since all magnetisation is aligned with the z-axis, and relaxation is simply observed as decay along this axis to equilibrium.

4.2.2 Semi-classical description of spin relaxation

The motion of the ensemble of independent spin 1/2 nuclei in a polarising magnetic field is conveniently described[54] in terms of the precession of the spin magnetisation vector, **M**. At thermal equilibrium **M** is aligned in the direction of **B**. Application of a resonant r.f. pulse disturbs **M** from equilibrium which is subsequently restored by a process known as spin-lattice relaxation. This process is described phenomenologically by the equation

$$\frac{dM_z}{dt} = -(M_z - M_0)/T_1 \qquad [4.5]$$

and has the solution

$$M_z(t) = M_z(0)\exp(-t/T_1) + M_0(1 - \exp(-t/T_1)) \qquad [4.6]$$

where M_z is the component of **M** in the direction of **B**. The constant T_1, known as the spin-lattice relaxation time, is used to characterise the rate of the relaxation process. In dielectric materials at room temperature, T_1 is typically in the range of 0.1 to 10 seconds.

The relaxation of transverse magnetisation ($M_{x,y}$) due to dephasing of nuclear spins is characterised by the time constant T_2 (the *spin-spin* relaxation time). The phenomenological description for spin-spin relaxation is

$$\frac{dM_{x,y}}{dt} = \frac{-M_{x,y}}{T_2} \qquad [4.7]$$

which has the corresponding solution

$$M_{x,y}(t) = M_{x,y}(0)\exp(-t/T_2) \qquad [4.8]$$

In solids where the interaction between the nuclear spins fluctuates very slowly, T_2 relaxation is observed to be exceedingly rapid (of order 10 μs). By comparison, the rapid tumbling experienced by nuclear spins in liquids causes much slower T_2 relaxation. T_2 values in liquids are typically in the range of 1 ms to 10 s.

Combining Equations [4.5] and [4.7], and with $d\mathbf{M}/dt = \gamma\mathbf{M} \times \mathbf{B}$, the decay of magnetisation in the rotating frame of reference due to spin relaxation may be restated by the set of relationships known as the Bloch equations[56]

$$\begin{aligned}
\frac{dM_x}{dt} &= \gamma\left(M_y B_0 + M_z B_1 \sin\omega t\right) - \frac{M_x}{T_2} \\
\frac{dM_y}{dt} &= \gamma\left(M_z B_1 \cos\omega t - M_x B_0\right) - \frac{M_y}{T_2} \\
\frac{dM_z}{dt} &= \gamma\left(-M_x B_1 \sin\omega t - M_y B_1 \cos\omega t\right) - \frac{\left(M_z - M_0\right)}{T_1}
\end{aligned} \qquad [4.9]$$

4.2.3 The dipolar Hamiltonian

The Hamiltonian of an ensemble of spin pairs may be written[54]

$$H_D = \frac{\mu_0}{4\pi}\sum_{i<j}\gamma_i\gamma_j\hbar r_{ij}^{-3}\left[\mathbf{I}_i \cdot \mathbf{I}_j - 3\left(\mathbf{I}_i \cdot \mathbf{r}_{ij}\right)\left(\mathbf{I}_j \cdot \mathbf{r}_{ij}\right)r_{ij}^{-2}\right] \qquad [4.10]$$

where $\mathbf{I}$ is the vector operator given by $I_x\mathbf{i} + I_y\mathbf{j} + I_z\mathbf{k}$, r_{ij} is the magnitude of the internuclear vector $\mathbf{r}_{ij}$, and the sum accounts for each pair of spins once. In the case of solids where the internuclear vectors have fixed orientation, the lineshape is dominated by the dipolar interaction. For protons with an average internuclear distance of order 0.15 nm, the interaction strength is about 100 kHz. NMR spectroscopy of solids typically yields broad resonances containing little or no spectroscopic detail.

Since the Zeeman interaction of the spins with the polarising field is largely dominant over the much weaker dipolar interaction, calculation of the H_D involves retention of secular, or diagonal terms only as these cause energy level shifts several orders of magnitude greater than non-secular elements. The fluctuating non secular elements can, however induce transitions between nuclear energy levels, and are important therefore in determining both spin-spin, and spin-lattice relaxation behaviour. Consequently, the thermal motion of nuclear spins is largely responsible for determining the efficiency of spin relaxation in materials such as lactose.

4.2.4 Relaxation and molecular motion

Relaxation behaviour can generally be divided into two broad regimes. The fast motion case representative of most liquids, and the slow motion regime representative of viscous liquids, polymers and solids. Spin lattice relaxation in the fast motion case is considered first (the Bloembergen-Purcell-Pound (BPP[29]) theory).

Dominance of the Zeeman field over the dipolar interaction allows use of time-dependent perturbation theory. The spin-lattice relaxation rate can be written as[59]

$$\frac{1}{T_1} = \frac{1}{2}\frac{\sum_{nm} W_{nm}(E_n - E_m)^2}{\sum_n E_n^2} \qquad [4.11]$$

where the transition rate W_{nm} between the two states n and m of energies E_n and E_m can be written in the limit $t \gg h/(E_n - E_m)$[54]

$$W_{nm} = \sum_{qq'}\left\{\int_{-\infty}^{\infty} \exp\left[i(E_n - E_m)\tau/h\right]\overline{F_2^q(0)F_2^{-q'}(\tau)}\,d\tau\right\}\langle n|T_2^q|m\rangle\langle m|T_2^{-q}|n\rangle \qquad [4.12]$$

The term in brackets is the Fourier transform of the autocorrelation function, $G^q(\tau)$. It is termed the spectral density function, $J^{(q)}(\omega)$ and represents the intensity of fluctuations in F_2^q at frequency ω. It has a characteristic frequency, τ_c^{-1}, with $J^{(q)}(\omega) \to 0$ as $\omega \gg \tau_c^{-1}$.

Because of the selection rule inherent in the matrix elements $\langle n|T_2^q|m\rangle$ (n-m = ±1 and ±2), the relevant frequencies for transitions are ω_0 and $2\omega_0$. Further manipulation of Equations [4.11] and [4.12] gives the equation describing spin-lattice relaxation for random isotropic motion

$$\frac{1}{T_1} = \left(\frac{\mu_0}{4\pi}\right)^2 \gamma^4 h^2 \frac{3}{2} I(I+1)\left[J^{(1)}(\omega_0) + J^{(2)}(2\omega_0)\right] \qquad [4.13]$$

The components of the spectral density function, $J^{(q)}(\omega)$, calculated for a simple rotational diffusion model are given by[56]

$$\begin{aligned} J^{(0)}(\omega) &= \frac{24}{15r_{ij}^6}\frac{\tau_c}{1+\omega^2\tau_c^2} \\ J^{(1)}(\omega) &= \frac{4}{15r_{ij}^6}\frac{\tau_c}{1+\omega^2\tau_c^2} \\ J^{(2)}(\omega) &= \frac{16}{15r_{ij}^6}\frac{\tau_c}{1+\omega^2\tau_c^2} \end{aligned} \qquad [4.14]$$

where τ_c is the rotational correlation time.

For the case of spin-lattice relaxation in solids, reorientation of the dipolar interaction slows sufficiently such that $M_2\tau_c^2 \geq 1$, and the line narrowing assumption of the BPP theory breaks down. However, the perturbation theory approach is still viable since $\omega_0 \gg M_2^{1/2}$, and Equation [4.13] therefore applies to solids as well.

Transverse relaxation cannot be described by perturbation theory[54] but is best handled using the density operator formalism[56]. The BPP theory assumes that $\overline{\langle H_D^2 \rangle}\tau_c^2 \ll 1$, ($M_2\tau_c^2 \ll 1$), such that the relevant time-scale for fast motions is the "precession period in the dipolar field".

The evolution of ρ in the rotating frame (ρ^*) may be deduced from the Schrødinger equation[54]

$$i\frac{d\rho^*(t)}{dt} = \left[H_D^*(t), \rho^*(t)\right] \qquad [4.15]$$

where H_D^* is the transformed dipolar Hamiltonian, $\exp[i\omega_0 t I_z] H_D(t) \exp[-i\omega_0 t I_z]$. Integration of Equation [4.15][56], yields an expression for the spin-spin relaxation time

$$\frac{1}{T_2} = \left(\frac{\mu_0}{4\pi}\right)\gamma^4 h^2 \frac{3}{2} I(I+1)\left[\frac{1}{4}J^{(0)}(0) + \frac{5}{2}J^{(1)}(\omega_0) + \frac{1}{4}J^{(2)}(2\omega_0)\right] \qquad [4.16]$$

where the $J^{(q)}(\omega)$ were given previously (Equation [4.14]). In contrast to Equation [4.13], the relevant frequencies for transitions causing spin-spin relaxation are the Larmor frequency, twice the Larmor frequency, and zero frequency terms.

Substituting the spectral density functions into the expressions for T_1 and T_2 (Equations [4.13] and [4.16] respectively) yields the relations shown in Figure 4.1.

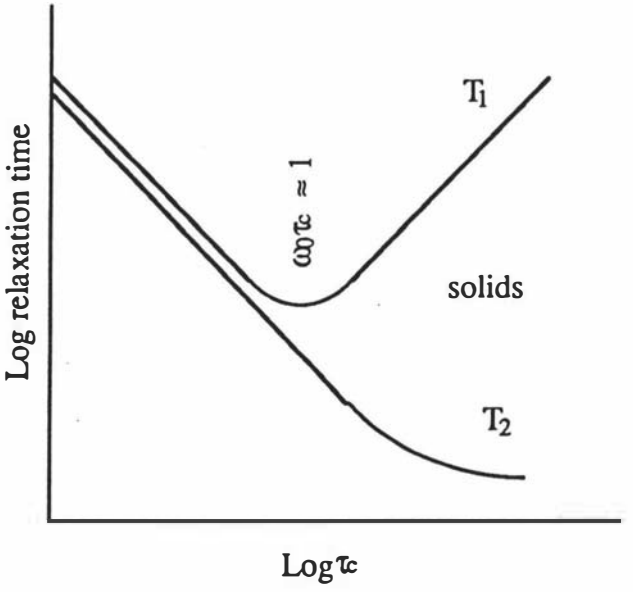

Figure 4.1. Schematic diagram showing the effect of molecular correlation times on the values of T_1 and T_2.

The T_1 minimum divides the regimes for τ_c into fast and slow in comparison with the Larmor frequency.

Equation [4.13] and Figure 4.1 may be used to determine the effect of glass transition and crystallisation pocesses (Chapters 6 and 7) on the magnitude of spin-lattice relaxation time values. Crystallisation of amorphous lactose causes a substantial decrease in molecular mobility as atomic centres assume rigid positions in the crystalline lactose. As atomic motions become slow, crystallisation lengthens τ_c and T_1 is therefore expected to increase. On the basis of correlation time, T_1 values should therefore differentiate crystalline from amorphous regions in an admixture of lactose powder.

In the slow motions regime, an increase in temperature shortens τ_c, and causes a corresponding decrease in T_1. When amorphous lactose passes from the glass to rubber state at the glass transition temperature T_g there is an increase in molecular mobility. Consequently, we expect that τ_c shortens, and T_1 would therefore be expected to decrease. However, free volume simultaneously increases, lengthening r_{ij} and increasing T_1 according to Equation [4.13] and [4.14]. The overall effect of a glass transition is somewhat difficult to predict, and cannot be discussed further without the benefit of experimental data. Nonetheless T_1 is expected to be a sensitive probe to the process of glass transition in amorphous lactose.

4.3 Measuring T_1 in solids

The measurement of proton relaxation times in solid lactose was performed on a model PC120 BRUKER MINISPEC wideline NMR machine with a permanent magnet system operating at a field strength of 0.47 T (20 MHz for ^1H nuclei). The standard 10 mm probehead was not temperature controlled, and samples would therefore equilibrate to the magnet system temperature of 40 ± 0.1 °C. A smaller 7 mm probehead with external water jacket was used for experiments requiring variable temperature control such as glass transition and crystallisation experiments. Temperature control was achieved using a model N4 HAAKE waterbath with a stability of ± 0.1 °C as tested with a calibrated mercury thermometer. The amplified analogue NMR signal is digitised using a 10 bit analogue to digital converter (ADC) with a maximum signal intensity of 5.12 V. Maximum signal resolution is therefore set at 0.005 V.

Proton spin lattice relaxation times were measured using the inversion recovery (IR) method[54]. The pulse sequence used for IR measurements is illustrated in Figure 4.2.

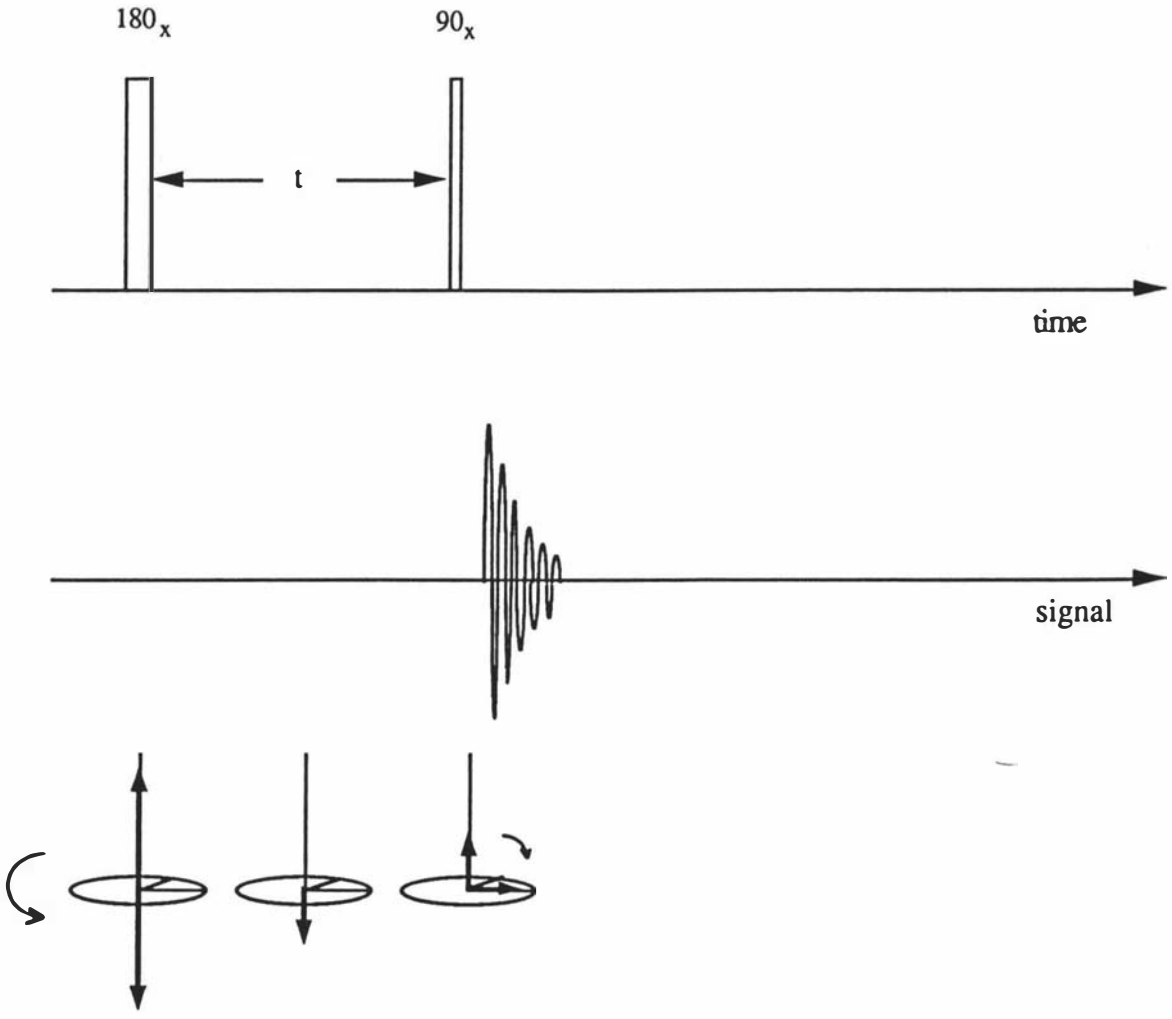

Figure 4.2. Illustration of the inversion recovery pulse sequence and the magnetisation trajectories. The interval t is a variable delay set to sample the z-magnetisation as it decays due to spin-lattice relaxation.

The first 180° r.f. pulse inverts the magnetisation vector, aligning it antiparallel with the field. Spin-lattice relaxation subsequently proceeds to restore thermal equilibrium of the spin system for a time, t following which a 90° pulse is used to sample the remaining longitudinal magnetisation. The free induction decay (FID) is sampled 10 μs after the 90° pulse to allow sufficient time for receiver coil "ringdown". Repetition of the IR pulse train is performed following a delay of approximately 5 times T_1 which allows complete thermal equilibration of the spin system. The delay, t is adjusted to sample different times during spin-lattice relaxation.

The signal amplitude in volts is proportional to the remaining magnetisation along the **z** axis. For the simple case of a system exhibiting uniform (monoexponential) relaxation, the remaining magnetisation is described by[54] (from Equation [4.6] assuming $M_z(0) = M_0$)

$$M(t) = M_0\left[1 - 2\exp(-t/T_1)\right] \qquad [4.17]$$

with exponential decay of M(t) from an initial amplitude of $-M_0$ to an equilibrium value of M_0. At a delay, t corresponding to a time of $0.6931T_1$, the magnetisation vector is passing through zero. For a system exhibiting monoexponential relaxation, determination of this crossover point can provide an accurate estimate of T_1. For lactose powders which may contain heterogeneous distributions of amorphous and/or crystalline lactose, and hence probably exhibit *multi*exponential relaxation, this method is not applicable. Instead, a large number of logarithmically spaced points must be measured and the spectrum of relaxation times obtained by multiexponential curve fitting.

The integrity of the multiexponential fitting method is strongly dependent on the assumption that the NMR signal obtained after amplification varies in direct proportion to M(t). In practice, it is found that the signal amplitudes at times, t = 0 and t = ∞ are not necessarily of equal absolute magnitude (see Figures 4.12 and 4.18, Sections 4.6.1 and 4.6.2 respectively). Some distortion of the decay curve inevitably occurs due to slight inaccuracy of pulse sequence timing (the 180° pulse may not invert the magnetisation exactly 180°), or nonlinearity of the detection system. These effects, however, tend to be weak and do not significantly affect the relaxation rate of the decay curve. More commonly, errors are caused due to drift of the broadband amplifiers which is evident as a d.c. offset which can change over time. The magnitude and direction of drift often varies in response to minor fluctuations in ambient temperature and can be difficult, therefore, to eliminate altogether. By taking representative measurements of M_∞ throughout the duration of an IR experiment, distortions in the IR data due to drift may be easily quantified, and appropriate measures taken in the data analysis to correct for these effects (see Figure 4.18)

Corrected magnetisation data (see Section 4.6.2 for details of the correction procedure) was fitted to a sum of exponentials

$$\sum_{i=1}^{N} A_i \exp\left(\frac{-t}{T_{1i}}\right) = M(t) \qquad [4.19]$$

where N ≥ number of expected phases. Often N is chosen large (≥100, but ≤ number of data points) so as not to bias the solution into a few relaxation components for which most of the expected A_i will be zero. Minimisation is carried out using the algorithms; Lawson-Hanson (LH), Marquardt-Levenberg (ML), and CONTIN[57]. Each minimise the misfit between the data points (M'(t)), and the model inherent in the left side of equation [4.19].

4.4 The use of computer algorithms to determine the spectrum of relaxation times

The general integral equation describing multiexponential relaxation is[60]

$$y(t_i) = y_i = \int s(T)\exp\left(\frac{-t_i}{T}\right)dT \qquad i = 1, 2, ..., N \qquad [4.20]$$

where the N data points y_i are measured at times t_i, and s(T) is the unknown amplitude of relaxation time T. Because of noise contaminating y_i, Equation [4.20] should not be solved exactly. Ideally the solutions should misfit the inaccurate data by an amount consistent with errors. The χ^2 statistic quantifies the misfit between the measured data, y_i and the constructed model. The χ^2 misfit is given by[32],

$$\chi^2 = \sum_{i=1}^{N}\left[\frac{(y_i - y_i')^2}{\sigma_i^2}\right] \qquad [4.21]$$

where σ_i^2 denotes the variance of datum point y_i, and y'_i describes the constructed model at time $t = t_i$. Two of the algorithms discussed in the following sections minimise Equation [4.21] to find the model s(T) (Equation [4.20]) which best describes the experimental data consistent with the noise level. The third method provides a fit consistent with the expected value of χ^2.

4.4.1 Marquardt-Levenberg

An excellent review of the Marquardt-Levenberg method may be found in "Numerical Recipes"[32]. A brief overview is reproduced here for convenience

The model described in Equation [4.20] depends nonlinearly on parameter T. With nonlinear dependencies, minimisation must proceed iteratively beginning with trial values for the parameters s(T) and T which collectively constitute the *starting model.* Given the trial solution, the ML algorithm proceeds to minimise the χ^2 statistic and improve the trial solution. This procedure is repeated iteratively until χ^2 stops (or effectively stops) decreasing.

The model described in Equation [4.20] can be generalised by the nonlinear equation

$$y = y(t;\mathbf{x}) \qquad [4.22]$$

where the column vector **x** has components which constitute the parameter set (the current estimate).

For **x** sufficiently close to the minimum, $\mathbf{x}_m$ the χ^2 statistic is well approximated by it's Taylor function[32]

$$\chi^2(\mathbf{x}) = \chi^2(\mathbf{x}_m) + \sum_i \left.\frac{\partial \chi^2}{\partial x_i}\right|_{x_m} a_i + \frac{1}{2}\sum_{ij} \left.\frac{\partial^2 \chi^2}{\partial x_i \partial x_j}\right|_{x_m} a_i a_j + \ldots \qquad [4.23]$$

$$\approx c - \mathbf{b}\cdot\mathbf{a} + \frac{1}{2}\mathbf{a}\cdot\mathbf{A}\cdot\mathbf{a} \qquad [4.24]$$

where $$\mathbf{a} = \mathbf{x} - \mathbf{x}_m, \quad c \equiv \chi^2(\mathbf{x}_m), \quad \mathbf{b} \equiv -\nabla\chi^2\big|_{\mathbf{x}}, \quad [\mathbf{A}]_{ij} \equiv \left.\frac{\partial^2 \chi^2}{\partial x_i \partial x_j}\right|_{\mathbf{x}} \qquad [4.25]$$

The matrix **A** whose components are the second partial derivatives of the function is called the *Hessian matrix* of the function (χ^2) at $\mathbf{x}_m$.

If the approximation, **x** is particularly close, the minimum can be obtained in a single step by solving Equation [4.24] as $\nabla\chi^2(\mathbf{x}) \to 0$, ie. when

$$\nabla\chi^2(\mathbf{x}) = \mathbf{A}\cdot\mathbf{a} - \mathbf{b} = \mathbf{0} \qquad [4.26]$$

This leads to an expression giving the finite step required to get the exact minimum

$$\mathbf{a} = \mathbf{A}^{-1}\cdot\mathbf{b} \qquad [4.27]$$

Equation [4.27] can be rewritten as the set of linear equations

$$\sum_{j=1}^{M} \alpha_{ij} a_j = \beta_i \qquad [4.28]$$

where $$\alpha_{ij} \equiv \frac{1}{2}\frac{\partial^2 \chi^2}{\partial x_i \partial x_j} \quad \textit{and} \quad \beta_i \equiv -\frac{1}{2}\frac{\partial \chi^2}{\partial x_i} \qquad [4.29]$$

Equation [4.28] is solved for the increment a_j that, added to the current approximation, gives the next approximation. (Equation [4.28] cannot be solved exactly due to truncation of the Taylor series [4.23]).

For the case where Equation [4.23] is a poor approximation such as when $\mathbf{x}_i$ is far from $\mathbf{x}_m$, (**a** is large) iteration according to Equation [4.28] does not provide a suitable path to convergence. In such cases, it is best to iterate in the direction of steepest decent ($\left|-\nabla\chi^2(\mathbf{x}_i)\right|$) according to

$$\mathbf{x}_{next} = \mathbf{x}_i - const \times \nabla\chi^2(\mathbf{x}_i) \qquad [4.30]$$

or, by using the definitions of Equation [4.29] and letting $const = \frac{1}{\lambda\alpha_{jj}}$,

$$a_j = \frac{1}{\lambda\alpha_{jj}}\beta_j \qquad [4.31]$$

By setting $\lambda >> 1$ (see Appendix 3 for the setting of λ), the step size is reduced such that the downhill direction is not exhausted. Equations [4.28] and [4.31] can be combined if a new matrix α' is defined by the following prescription

$$\begin{aligned} \alpha'_{jj} &= \alpha_{jj}(1+\lambda) \\ \alpha'_{jk} &= \alpha_{jk} \qquad (j \neq k) \end{aligned} \qquad [4.32]$$

Both equations can then be replaced by

$$\sum_{j=1}^{M} \alpha'_{ij} a_j = \beta_i \qquad [4.33]$$

When λ is very large, the matrix α' is forced into being diagonally dominant, so Equation [4.33] approximates Equation [4.31], and the convergence proceeds via the steepest decent method. This approach is adopted in the initial stages of convergence where $\mathbf{x}_i$ is usually far from $\mathbf{x}_m$. As λ approaches zero, signalling Equation [4.23] as a good approximation to the model, Equation [4.33] goes over to Equation [4.28], and convergence continues until χ^2 fails to diminish by a significant amount.

The ML method is readily implemented as a computer algorithm and provides an efficient and fast solution to most problems. The algorithm is listed and further described in Appendix 4. The ML method requires that the starting model be specified. In particular, the number of relaxation components must be pre-assigned. The following methods require no such specification.

4.4.2 Lawson-Hanson

Consider the case where the relaxation time parameter, T (Equation [4.20]) is allowed to assume a finite number of discrete values bounded by a maximum and minimum relaxation time (arising from possible *a priori* knowledge of the system). Discretisation of Equation [4.20] then gives the linear system of equations described by[60]

$$y_i = \sum_{j=1}^{M} s_j e^{-t_i/T_j}, \qquad i = 1, 2, ...,N \qquad [4.34]$$

where N is chosen large enough so as not to bias the solution into a small number of relaxation times. This can be rewritten in matrix form as

$$y_i = \sum_{j=1}^{M} A_{ij} s_j, \qquad i = 1, 2, ..., N \qquad [4.35]$$

where the rows and columns of the matrix A_{ij} correspond with the discrete points of the constructed model, and s_j are the spectral amplitudes corresponding with discrete relaxation times, T_j. Additional linear constraints are easily incorporated into the matrix **A**, and unknown variables such as baseline offset, or drift can be included by adding extra columns.

The LH algorithm solves Equation [4.35], using linear inversion techniques. These have the advantage of not requiring a starting model and are non-iterative and therefore do not suffer from many of the problems that plague iterative methods such as non-convergence, or convergence only to a local minimum. Equation [4.35] is solved using stable Householder transformations[30] and is guaranteed to find a solution in a finite number of these operations. A detailed description of general linear inverse techniques may be found in Lawson and Hanson[30].

The problem of least squares can be restated in the matrix equation[30]

$$\mathbf{A} \cdot \mathbf{x} = \mathbf{b}, \qquad \mathbf{x_i} \geq 0 \qquad [4.36]$$

where vector **b** is constructed from the N measured data points, and $\mathbf{x_i}$ is the set of parameter values which minimise Equation [4.36]. In the context of relaxation time analysis, vector components $\mathbf{x_i}$ constitutes the amplitudes of respective relaxation times implicit in the matrix **A**.

The successful computational minimisation of Equation [4.36] is dependent on the reduction of accumulated machine errors, and the avoidance of singularities. In the situation where two or more of the constructed data equations are nearly linearly dependent (when two relaxation times

are very similar), roundoff errors during computations can render them linearly dependent during the minimisation process, and the algorithm fails. Furthermore, accumulated roundoff errors can swamp the true solution (particularly where N is large), in which case the returned set of x_i's will be wrong. The special properties of Householder transformation matrices allow complex mathematical operations to be performed with the minimum of computational steps.

Consider the **QR** decomposition[30] of the matrix **A** described by the equation

$$\mathbf{Q}\mathbf{A}_k = \begin{bmatrix} \mathbf{R}_k \\ \mathbf{0} \end{bmatrix} \qquad [4.37]$$

Here $\mathbf{R}_k$ is a $k \times k$ upper triangular matrix, and is non singular (no linear dependencies), and Q is orthogonal. Once Q and R have been determined, the least squares solution of the system

$$\mathbf{A} \cdot \mathbf{x} = \mathbf{b} \qquad x_i \geq 0 \qquad [4.38]$$

is given by

$$\mathbf{x} = \left[\mathbf{R}_k^{-1} \quad \mathbf{0}\right]\mathbf{Q}\mathbf{b} \qquad [4.39]$$

which is easily solved algorithmically. Since $\mathbf{R}_k^{-1}$ is also upper triangular, Equation [4.50] can be solved by back substitution[32].

The special properties of matrix Q are obtained with Householder transformation matrices. An m x m Householder orthogonal transformation can be represented in the form

$$\mathbf{Q} = \mathbf{I}_m + \mathbf{b}^{-1}\mathbf{u}\mathbf{u}^T \qquad [4.40]$$

where **u** is any m vector satisfying $|\mathbf{u}| \neq 0$ and $\mathbf{b} = -|\mathbf{u}|^2/2$. The matrix, Q will transform a given vector (say **v**) by the following definition

$$\mathbf{Qv} = \begin{bmatrix} v_1 \\ \cdot \\ \cdot \\ v_{p-1} \\ -\sigma\left(v_p^2 + \sum_{i=l}^{m} v_i^2\right) \\ v_{p+1} \\ \cdot \\ \cdot \\ v_{l-1} \\ 0 \\ \cdot \\ \cdot \\ 0 \end{bmatrix} \equiv \mathbf{y} \qquad [4.41]$$

This vector operation is best described in terms of the following functions,

1: If $p > 1$, components 1 through p - 1 remain unchanged
2: Component p is permitted to change. This is called the *pivot element*
3: If $p < l - 1$, components p + 1 through l - 1 remain unchanged
4: If $l \leq m$, components l through m are zeroed.

Householder operations on an m x n matrix, **A** with appropriate choices of the condition parameters p, l, and m allow Equation [4.37] to be satisfied (the **QR** decomposition of **A**) where **R** will be upper triangular as required. The computational steps required to produce an m x m orthogonal matrix, **Q** that satisfies these conditions can be found in Lawson and Hanson[30].

Computation of Matrix **R** leads to the solution vector, x via Equation [4.39]. The inverse of R, R^{-1} is found algorithmically by solving the linear equations implicit in the matrix product

$$\mathbf{RR^{-1}} = \mathbf{I} \qquad [4.42]$$

The LH algorithm is described more fully in Appendices 5 and 6.

4.4.3 Contin

Contin uses the same linear inversion techniques to solve the least squares problem expressed in Equation [4.36]. The approach taken by Contin also allows for a finite number of discrete components (relaxation times) bounded by maximum and minimum values and constrained to

be non-negative. Due to the close similarities with LH, the algorithm itself will not be described here. A good description can be found in Provencher[57].

By incorporating additional constraints into matrix A, Equation [4.36] can be modified to alter the discrete character of the basic least-squares solution. A general form is to minimise[60]

$$|\mathbf{A}\cdot\mathbf{x}-\mathbf{b}|^2+\mu|\mathbf{H}\cdot\mathbf{x}-\mathbf{c}|^2 \qquad [4.43]$$

for fixed $\mu > 0$, where **A** in an m x n matrix, **H** is an k x n matrix representing the K additional constraints, and **c** is the corresponding n vector of right hand side values. The larger the value of μ, the more the algorithm attempts to satisfy the constraints implicit in matrix **H** at the expense of increasing the overall χ^2 misfit. In the limit of large μ, the data equations are ignored completely. In practice, μ is adjusted until the misfit is near it's expected value of N, which results in the preferred model in the absence of other information.

The matrix **H** can take many forms. If **H** is an M x M identity matrix, and **c** is the zero vector, the K = M constraints minimise the "energy" in the spectrum:

$$\sum_{j=1}^{M} s_j^2 \qquad [4.44]$$

If **c** is nonzero, then the constraints minimise the difference between the constructed spectrum, and the a priori estimate **c**. Another possibility is to set the rows of **H** equal to finite difference approximations of first, or second-order derivatives of s(T). When **c** is zero, these cases respectively minimise the energy in the spectrum derivative

$$\sum_{j-1}^{M-1}\left|s_{j+1}-s_j\right|^2 \qquad [4.45]$$

or curvature

$$\sum_{j=1}^{M-2}\left|s_{j+2}-2s_{j+1}+s_j\right|^2 \qquad [4.46]$$

The algorithm Contin uses the second derivative formulation to construct smooth s(T). The additional constraint in the form of Equation [4.46] are essential to regularise the solution where

the data is extremely noisy[60]. In practice, these constraints compromise some spectral details, but this is greatly offset by consistent solutions of s(T) obtained from closely related data sets.

This completes the theoretical presentation of the three algorithms which will be used to reduce the raw inversion recovery data to a spectrum of spin lattice relaxation times. We now investigate the performance of each algorithm on simulated data which has been corrupted with noise and baseline drifts of varying magnitudes.

4.5 Testing the algorithms

Testing of the inversion algorithms on simulated data was initiated for two important reasons. Firstly, early measurements had shown inconsistencies in the T_1 spectra derived from identical samples, and these concerns naturally lead to investigations of the susceptibility of the inversion algorithms to noise and baseline drift inherent in IR data. Secondly, the general performance of each algorithm could be readily compared under controlled conditions.

Data sets were generated to coincide with a lactose mixture consisting of equal parts of amorphous lactose, alpha lactose monohydrate, and coventional beta lactose with T_1 components of 0.1 s, 4 s, and 10 s respectively. The linear combination of the corresponding exponential functions produced one hundred data points which were then corrupted with Gaussian noise and drift effects of varying magnitude. The generation of Gaussian noise is described in Appendix 7. Baseline offset and variations of baseline drift (linear, exponential, and sinusoidal (spanning two periods)) was also introduced into the test data. The magnitude and sign of drift stated in the legends of thes following graphs represents the shift in the value of M_∞ (Equation [4.23]) as measured over time relative to the final measurement of M_∞ (see Appendix 7). The results of ML, LH and Contin treatment of the relaxation data are given in Figures 4.3-4.5, 4.6-4.8, and 4.9-4.11 respectively. The amplitudes of the relaxation time components of the following graphs have been normalised to sum to unity.

4.5.4 Discussion

As seen in Figures 4.3 to 4.11, the extraction of multiple relaxation time constants from inversion recovery data containing noise and drift is a non-trivial problem, and interpretation is often required. Confidence is improved markedly when *a priori* knowledge is available concerning the effects of data inaccuracies on the convergence path chosen by a particular algorithm. With reference to Figures 4.3 to 4.11, the information gained from these trial solutions will be used to gain a more informed interpretation of results from real lactose powder measurements.

4.5.1 Marquardt-Levenberg

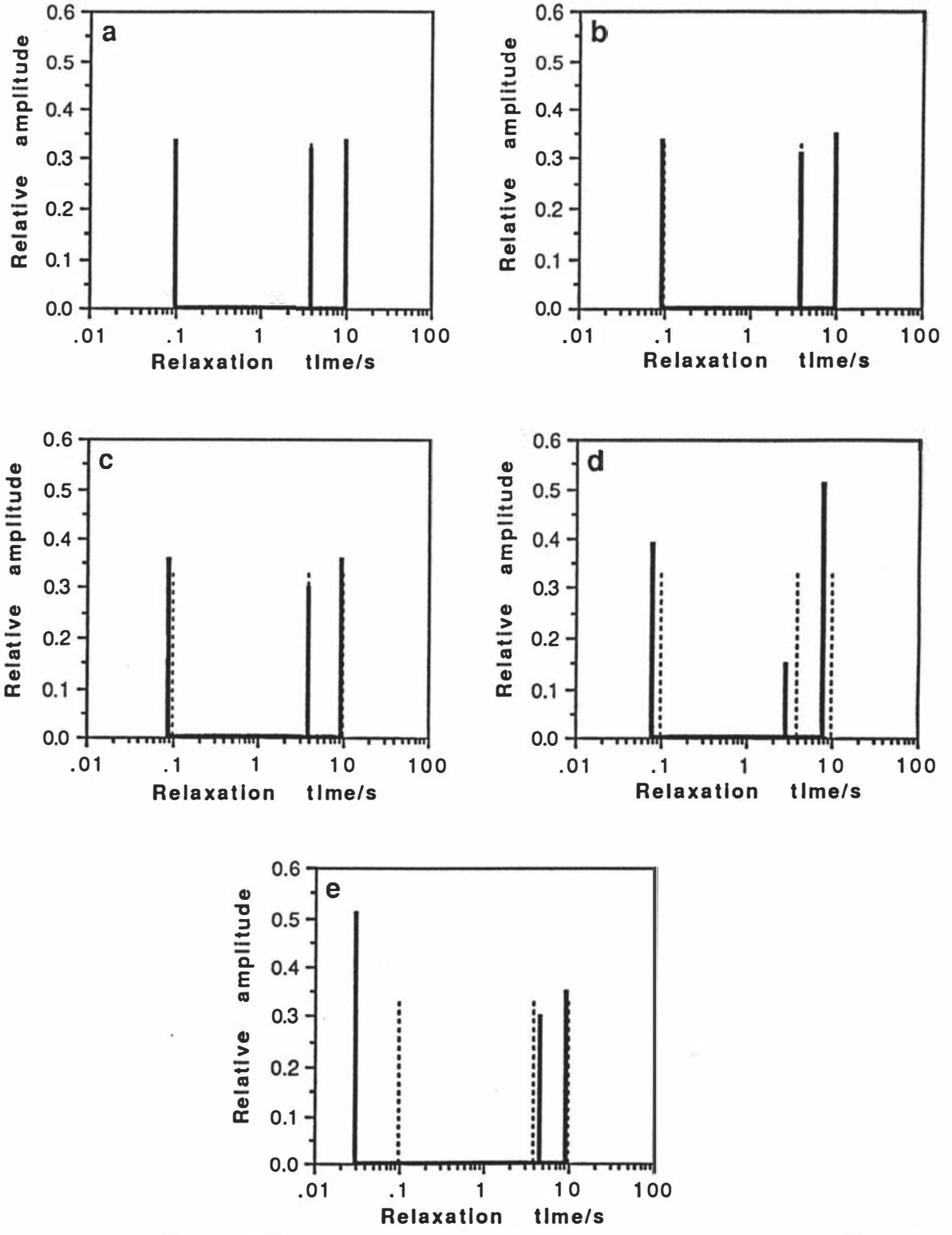

Figure 4.3. Treatment of data containing a 0.25%, b 0.5%, c 1%, d 2%, and e 4% Gaussian noise with the ML algorithm constrained to three components. The dotted lines represent the true solution.

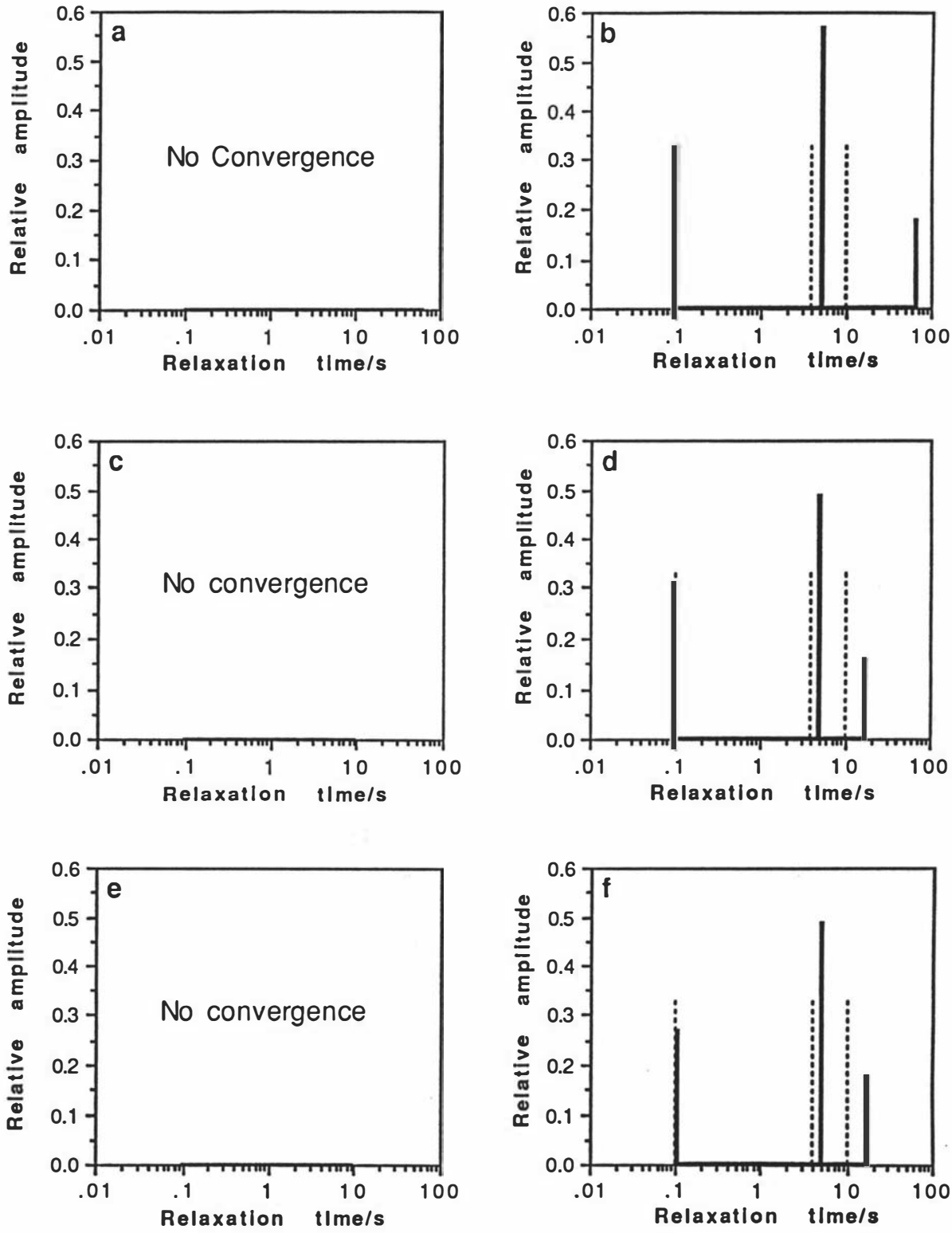

Figure 4.4. Treatment of data containing **a** +10% baseline offset, **b** -10% baseline offset, **c** +10% linear drift, **d** -10% linear drift, **e** +10% exponential drift, and **f** -10% exponential drift with the ML algorithm.

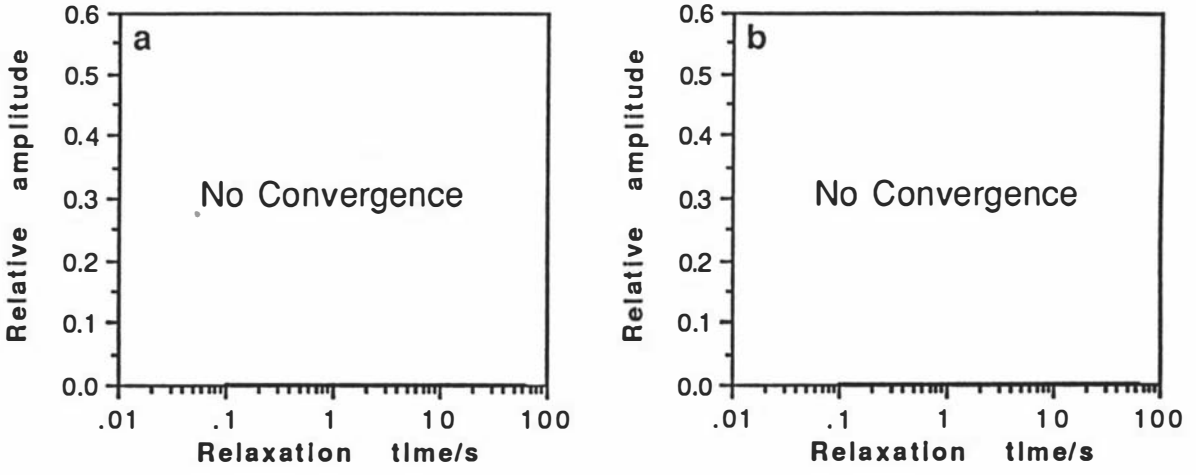

Figure 4.5. Further treatment by the ML algorithm **a** with +10 % sinusoidal drift and **b** -10% sinusoidal drift. In both cases, M-L did not converge. The sine function has a period of 25 s (see Appendix 7). A change in sign (from +10 % to -10% is equivalent to a phase shift of 180 °).

4.5.2 Lawson-Hanson

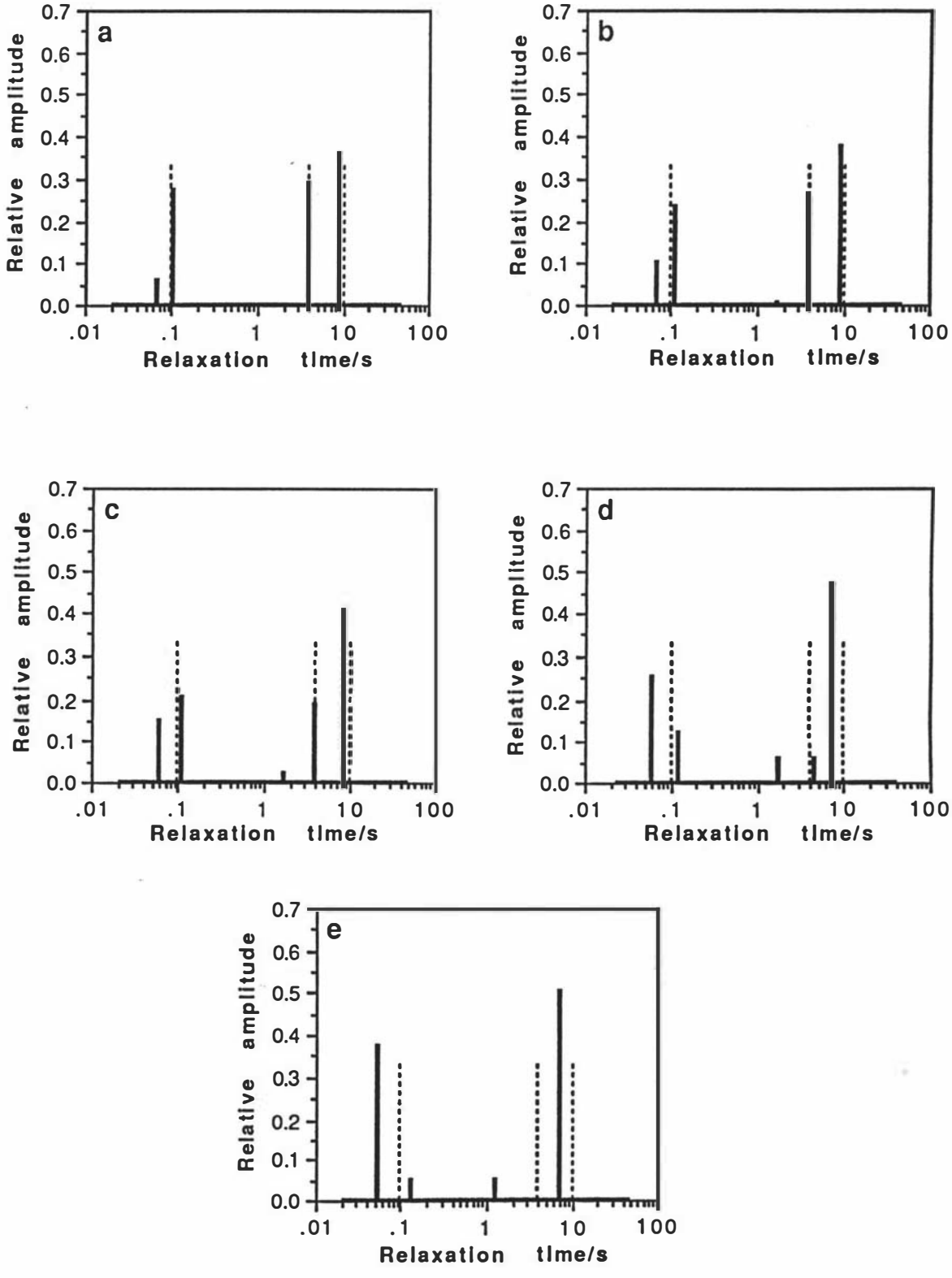

Figure 4.6. Treatment of data containing a 0.25%, b 0.5%, c 1%, d 2%, and e 4% Gaussian noise with the Lawson-Hanson algorithm. The dotted lines represent the true solution.

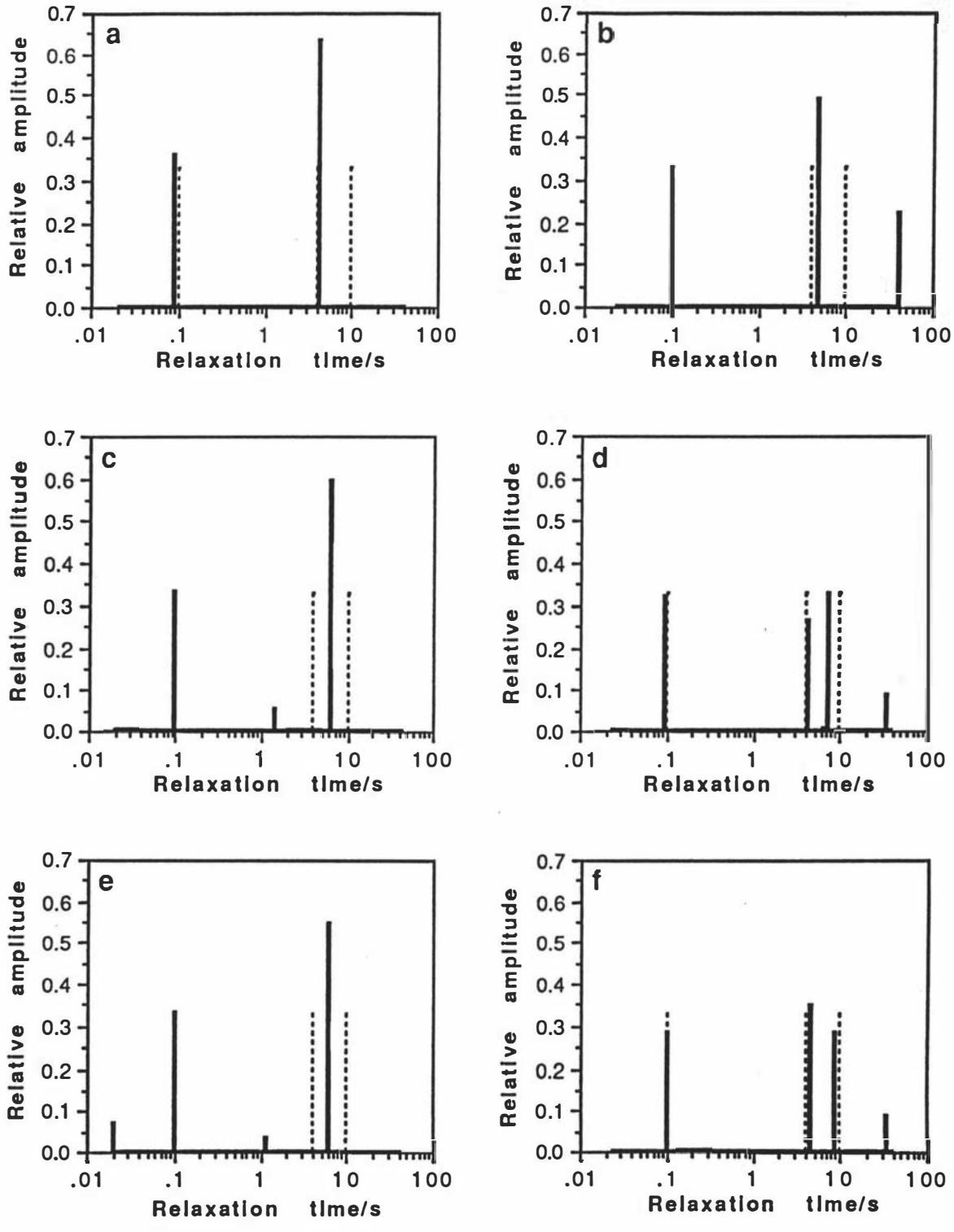

Figure 4.7. Treatment of data containing **a** +10% baseline offset, **b** -10% baseline offset, **c** +10% linear drift, **d** -10% linear drift, **e** +10% exponential drift, and **f** -10% exponential drift with the Lawson-Hanson algorithm. Notice the convergence of close components (4 s and 10 s) and generation of spurious lines where the offset is positive (ie. some data points are negative.)

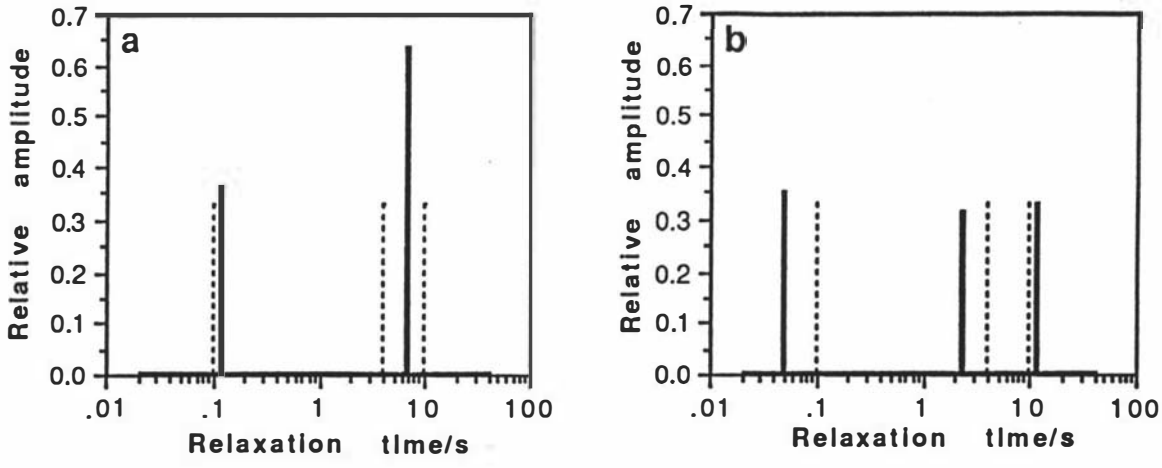

Figure 4.8. Further treatment by the Lawson-Hanson algorithm **a** with +10 % sinusoidal drift and **b** -10% sinusoidal drift. The sine function has a period of 25 s (see Appendix 7). A change in sign (from +10 % to -10% is equivalent to a phase shift of 180 °).

4.5.3 Contin

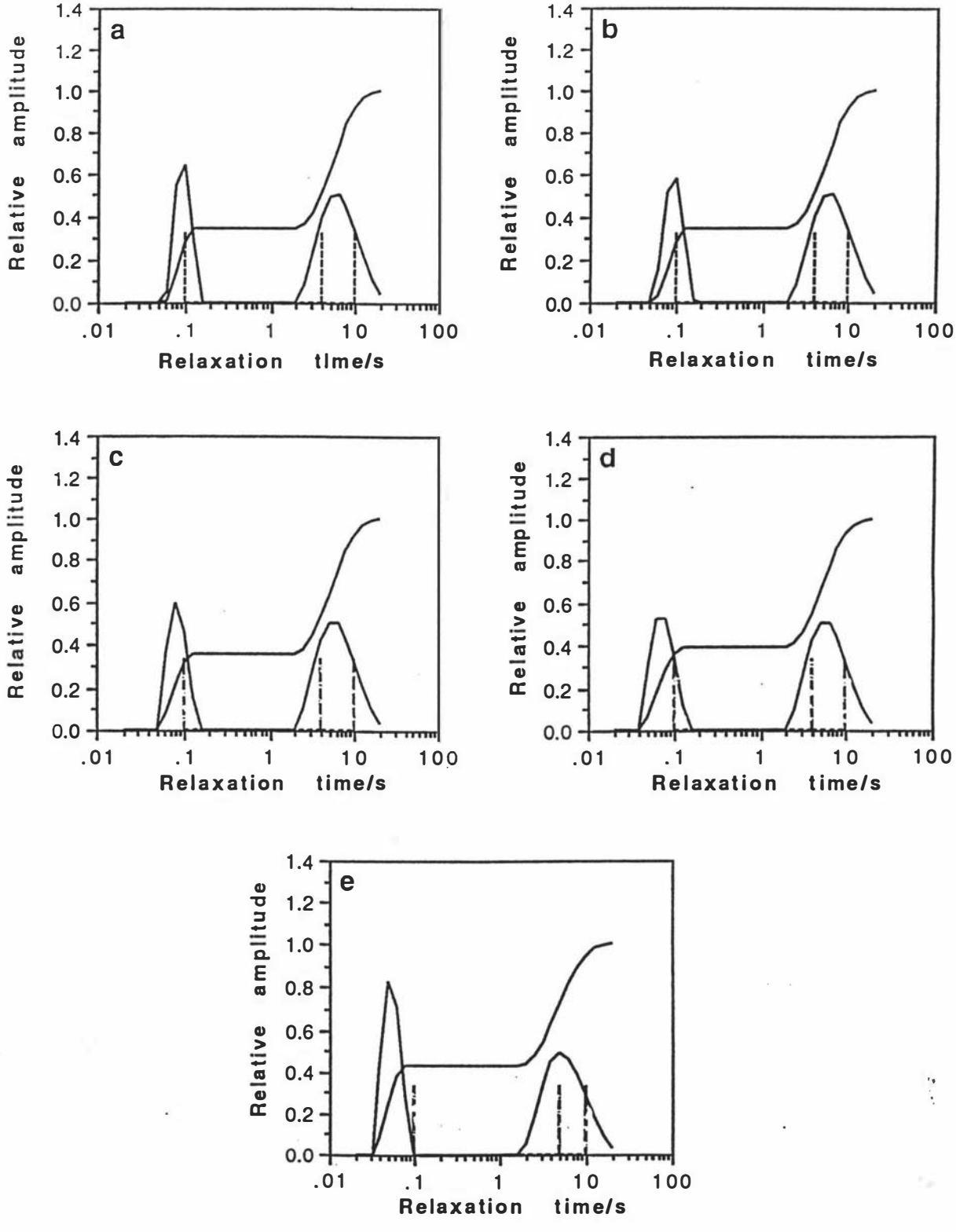

Figure 4.9. Treatment of data containing a 0.25%, b 0.5%, c 1%, d 2%, and e 4% noise with the Contin algorithm. The dotted lines represent the true solution. The integral of area is also shown.

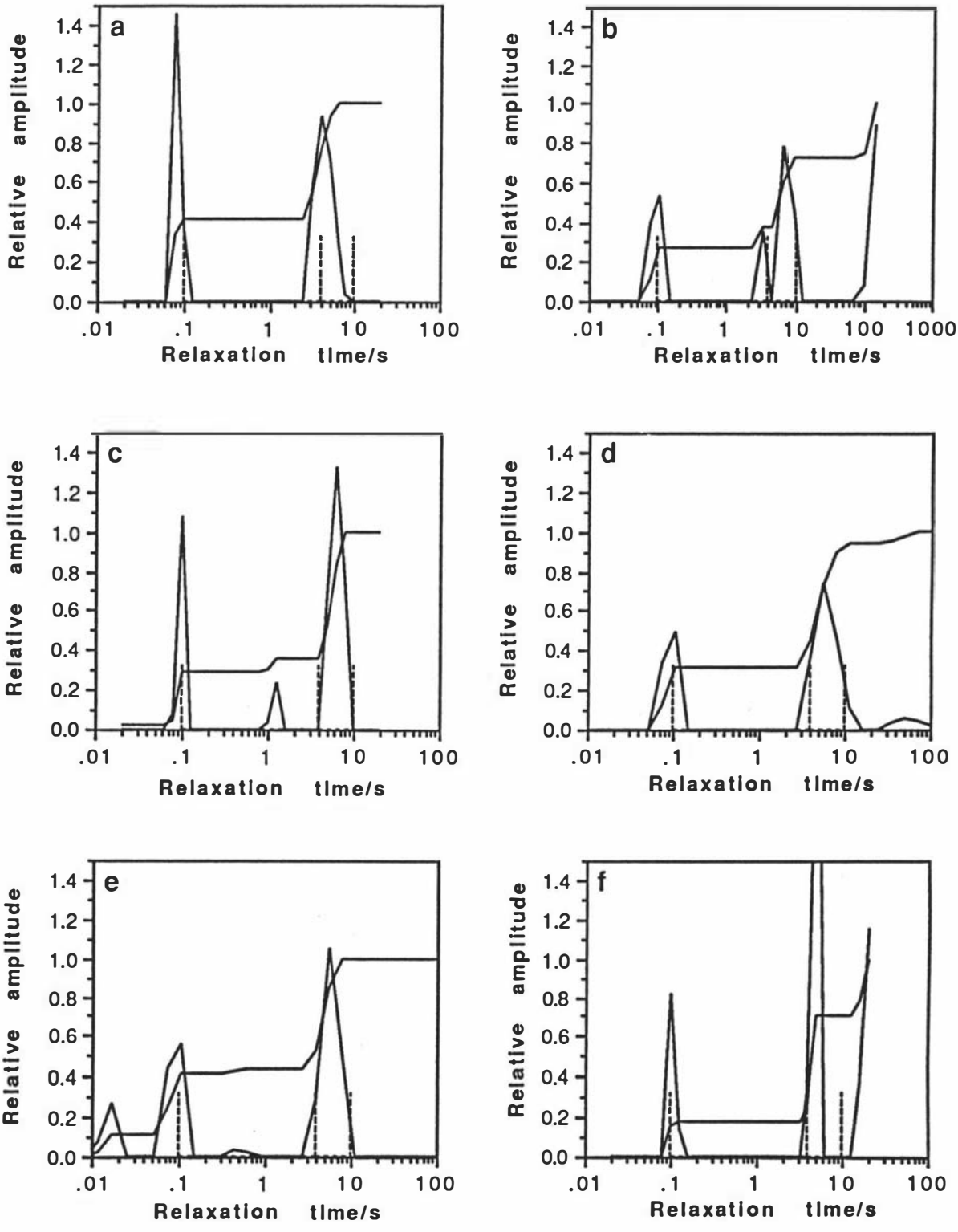

Figure 4.10. Treatment of data containing **a** +10% baseline offset, **b** -10% baseline offset, **c** +10% linear drift, **d** -10% linear drift, **e** +10% exponential drift, and **f** -10% exponential drift with the Contin algorithm. The integral of area is also shown. The 4 s and 10 s components are converged in most cases

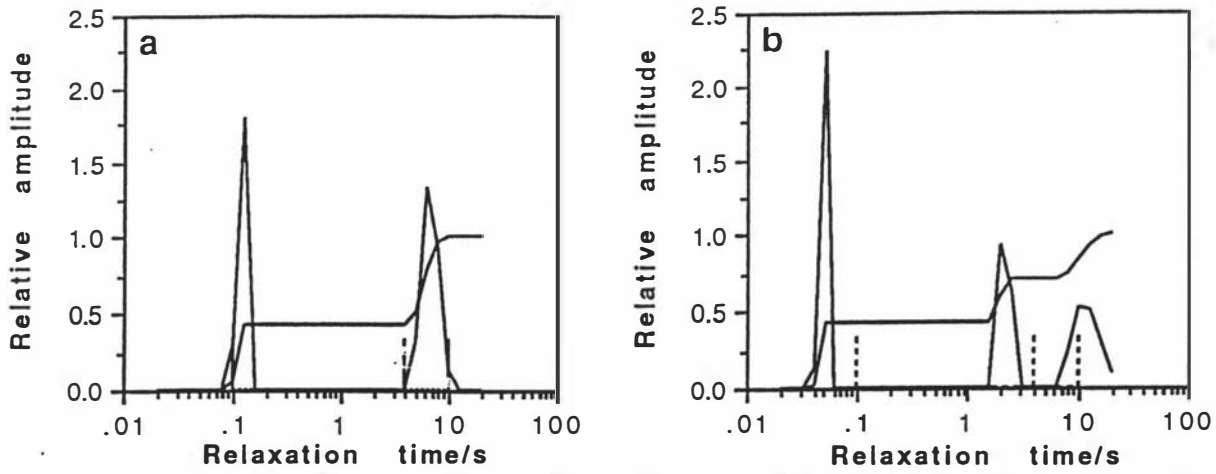

Figure 4.11. Further treatment by the Contin algorithm **a** with +10 % sinusoidal drift and **b** -10% sinusoidal drift. The sine function has a period of 25 s (see Appendix 9). A change in sign (from +10 % to -10% is equivalent to a phase shift of 180 °).

The consistent failing of the ML algorithm where data is corrupted by variations of baseline drift or offset is notable in Figures 4.4, and 4.5. When the starting model used equates to the known relaxation spectrum (of relaxation times 0.1, 4, and 10 s), it is found that ML divergences from this to produce a solution where χ^2 is unacceptably large (by many orders of magnitude) with no resemblance to the known relaxation spectrum. In contrast, ML achieves accurate convergence with Gaussian noise (Figure 4.3), with a progressive deterioration in accuracy with increasing noise levels. This contrasts markedly with the linear inverse schemes which often demonstrate convergence of close components where the noise level is high (Figures 4.6 and 4.9). ML is constrained in these tests to fitting three relaxation time components, which may explain the excellent handling of Gaussian noise, where in contrast, Lawson-Hanson, and Contin are not constrained, and convergence of close components sometimes occur.

The Lawson-Hanson algorithm performs well where baseline drift and offset errors exist in the data. In the case of negative baseline offset, the algorithm attempts to minimise the misfit by producing a component at the longest allowable relaxation time (Figures 4.7 and 4.8). The algorithm is similarly affected by negative linear and exponential drift where it attempts to compensate by fitting a long component, leaving the "true" components more or less intact. In contrast, positive drift (where data points lying on the tail become negative) causes convergence of the close (4 s and 10 s) components, reflecting the inability of the algorithm to interpret negative data points. The Lawson-Hanson algorithm handles sinusoidal drift (over two cycles) reasonably well (Figure 4.8). A phase shift of 180° (compare Figures 4.8a and 4.8b) causes convergence of the 4s and 10s components suggesting that this type of data error is not necessarily averaged out over the duration of an experiment. Gaussian noise greater than 0.5 %

has a detrimental effect causing the generation of spurious peaks, and finally convergence of close components (4 s and 10 s) at a 2 % noise level. This noise result will be used to establish an acceptable minimum signal:noise ratio for relaxation measurements, hence reducing the probability of generating spurious peaks which may otherwise be interpreted as arising from the physical system under investigation .

The Contin algorithm performs more conservatively where noise and baseline effects affect data. Convergence of close components occurs at a lower noise level (< 0.25 %) than Lawson-Hanson which is consistent with the second derivative formulation of the constraint matrix, H (Section 4.4.3). The constraint matrix, H forces the algorithm to accept the solution which (partially) minimises the curvature in s(T), and hence minimise the generation of noise or drift artefacts. Convergence occurs for most forms of baseline drift. Some spurious components are generated (linear drift, Figure 4.10), although relative amplitudes tend to be low. Performance on sinusoidal drift (Figure 4.11) is slightly inferior to Lawson-Hanson.

The most noticeable feature of the Lawson Hanson and Contin algorithms, is that the use of a non-iterative linear inverse method (compared to the nonlinear method of ML) to minimise the misfit between the generated model, and the raw data guarantees convergence for non-ideal data where noise and baseline effects often inhibit convergence for non-linear techniques.

4.6 Fitting of experimental data

Clearly, the accuracy of T_1 measurements deteriorates rapidly when noise levels rise above 0.25 - 0.5%, and baseline offset or drift occurs. The interpretation of "real" T_1 spectra can be further complicated by the appearance of spurious relaxation components which often cause amplitude and time domain distortions of remaining "true" components. The collection of inversion recovery data free of drift, and low in noise is therefore paramount to the use of relaxation measurements as an analytical method and the accurate assaying of lactose powders. The experimental protocol used to reach this objective will be described in Section 4.6.2.

4.6.1 Hardware-based experiments

The hardware system operates from a library of EPROM (Erasable Programmable Read Only Memory) integrated circuits. The variable delay, t is calculated automatically by the hardware routine to vary logarithmically once the estimated relaxation time and required number of data points have been established. Signal enhancement is possible by defining a loop parameter, N. At each delay setting t (Figure 4.2) a single averaged value of the FID amplitudes is recorded in the memory register. Although measurement of the baseline during T_1 measurement is possible, the hardware does not allow these values to be stored concurrently with IR signal data. In this, and many other respects, the hardware limits the user to performing "conventional" T_1 experiments with little or no flexibility.

Experiments measuring relaxation times were performed on alpha lactose monohydrate and conventional beta lactose. One hundred data points were collected and inverted to the relaxation time domain using the Lawson-Hanson algorithm. Two separate sets of data were obtained per sample, and the corresponding relaxation time components obtained by LH were averaged. The results of these experiments are presented in Figures 4.12 to 4.16. A typical magnetisation curve for alpha lactose monohydrate is presented in Figure 4.12.

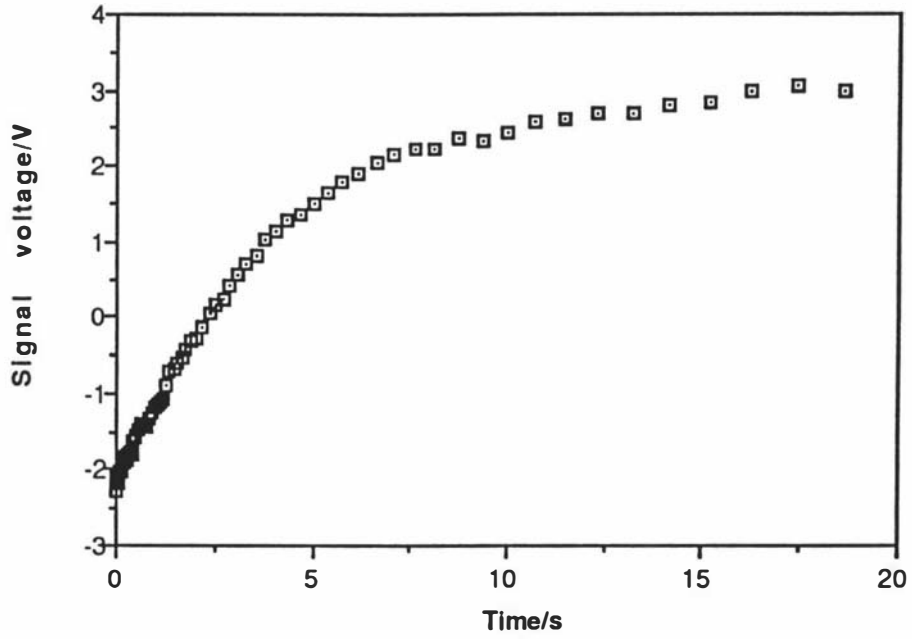

Figure 4.12. A typical magnetisation curve from alpha lactose monohydrate.

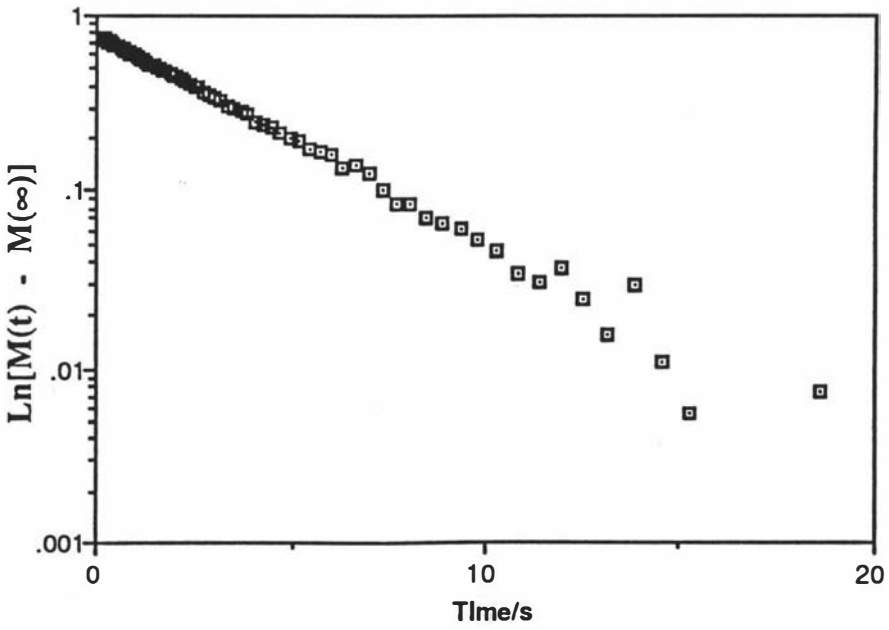

Figure 4.13. Corresponding semi-logarithmic plot of Figure 4.12. The linearity of the data is indicative of (predominantly) monoexponential relaxation. As expected experimental noise increases markedly for long delay times, t.

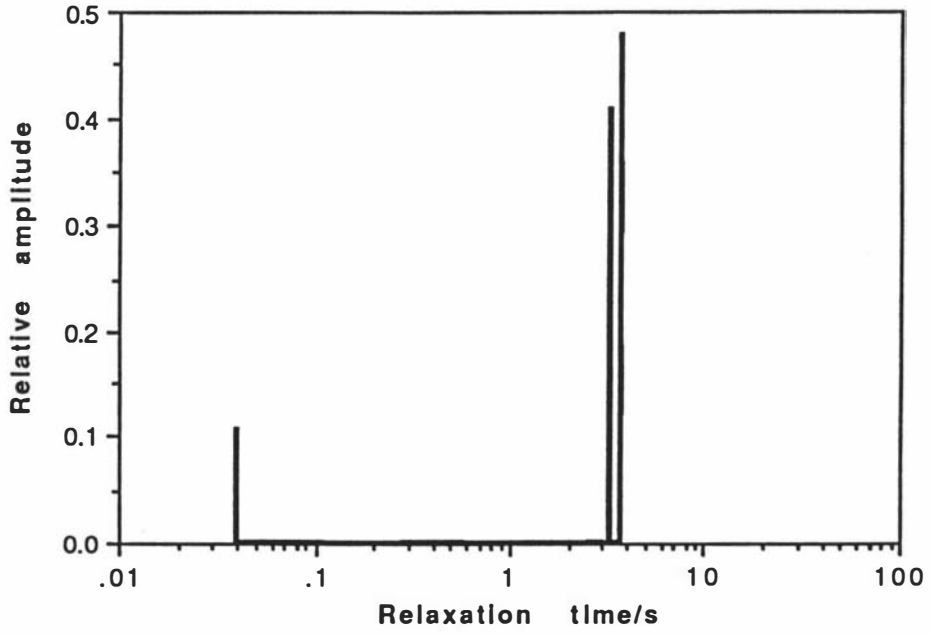

Figure 4.14. Relaxation time components obtained from the data of Figure 4.13 using the Lawson-Hanson algorithm. The short relaxation component at 0.04 s is probably caused by slow drift of the signal amplifiers (see Section 4.6.2) during the early stages of measurement.

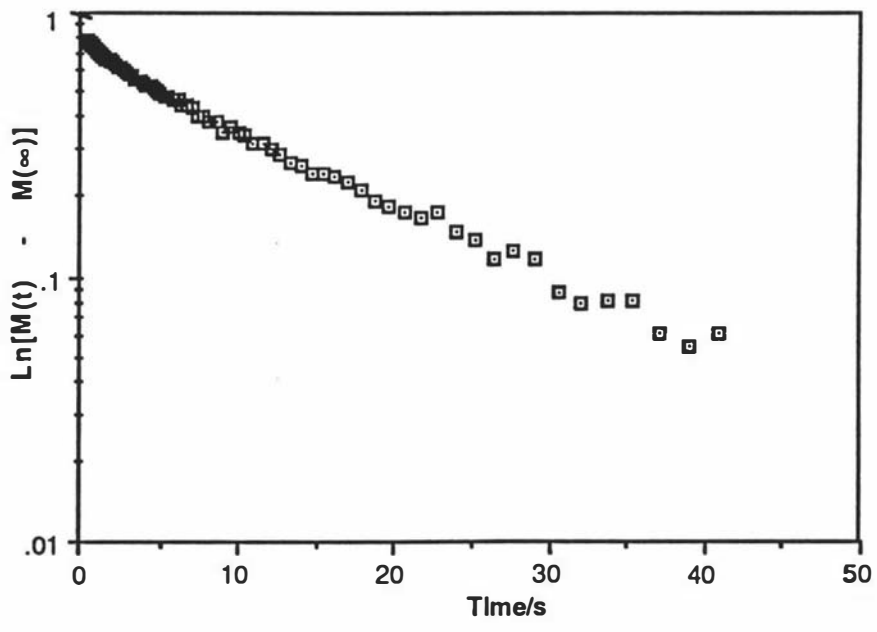

Figure 4.15. Semilogarithmic plot representing the inversion recovery of conventional beta lactose. The curvature is indicative of multiexponential relaxation.

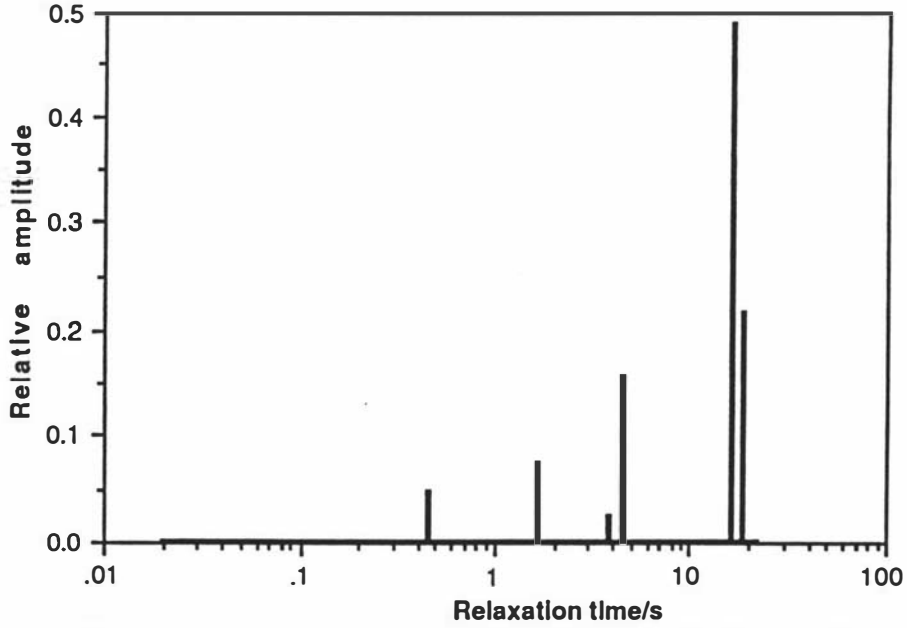

Figure 4.16. Corresponding relaxation time components (from Figure 4.15) of conventional beta lactose obtained using the Lawson-Hanson algorithm. The short relaxation time components around 0.45 and 1.5 s varied substantially in both relaxation time and amplitude between consecutive measurements of the same sample.

Figures 4.13 and 4.14 show that alpha lactose monohydrate exhibits essentially a single relaxation time constant. The 0.04 second component varied substantially in both time and amplitude between repeat measurements and was tentatively attributed to noise and drift fluctuations during measurement. Later improvements in drift control resulted in the elimination of such relaxation components (Section 4.6.2).

The demonstration of monoexponential relaxation of all protons on the alpha lactose molecule suggests spin energy exchange between neighbouring protons during the time frame of an NMR experiment. In such cases, the result is the averaging of the discrete relaxation times of individual protons to a single component; a process known as spin diffusion. Lactose mixtures containing a mixture of chemical species (alpha and beta), or proportions of structurally different lactose (amorphous, and various crystalline species) should exhibit a multiplicity of relaxation components no greater than the number of chemically or physically distinct lactose species.

Component "splitting" (Figures 4.14 and 4.16) due to the discrete nature of the relaxation time axis causes bounding of the "true" relaxation time component by a doublet. In such cases, the "true" relaxation time may be *estimated* from the weighted averaged of the two components. The production of four components from "pure" crystalline beta lactose was unexpected. Polarimetric determinations established a contamination of the sample by 10% alpha lactose

monohydrate which may account for the 4 second component (17%). Amplitude distortion of the 4 second component due to the proximity of the 1.5 second component may account for the poor agreement with the "known" amount of alpha lactose monohydrate. It was found that a repeat relaxation measurement gave a similar result, although a third experiment gave only three relaxation components. The variability of results (alluded to earlier) prompted investigations into the noise and possible baseline offset and drift generated during a typical relaxation experiment.

The measurements of ten M_∞ (M(t) as $t \rightarrow \infty$) datum points for alpha lactose monohydrate over a twenty minute period established a noise level around 1 - 2 %. This level coincides with a deterioration in the Lawson-Hanson algorithm as indicated in Figure 4.11, and the generation of spurious components. Further measurement of M_∞ over a 9 hour period (typical for a single experiment) established large baseline drift to the order of 10% (Figure 4.18).

The signal:noise ratio can be increased with signal averaging, where repeated FID signals are coadded when random phase components such as noise tend to cancel out. In such cases, the signal:noise ratio improves as $N^{\frac{1}{2}}$, where N denotes the number of coadded signals and therefore improvements in the S:N ratio occur at the expense of a greatly lengthened experimental runtime. In this study, a good compromise was established with N = 4 for crystalline lactose measurements (T_1's of order seconds) and N = 9 for amorphous lactose powders (T_1's of order tenths of seconds).

The effects of baseline drift and/or offset are less readily overcome. Drift is caused by variations in amplifier gain or offset in response to fluctuating ambient temperatures. Placing the spectrometer in a temperature controlled environment is not often practical. Magnitude and phase information concerning drift can be collected by simply measuring M_∞ over the duration of a relaxation experiment, and deconvoluted from the raw M(t) data prior to inversion to the relaxation time domain. These random fluctuations can appear in the T_1 spectrum (Section 4.5) as extra relaxation components, and often cause amplitude distortions of "true" components associated with true constituents of the sample. For accurate assaying, which is one objective of these relaxation experiments, baseline drift must be reduced to a level below the existing signal to noise ratio (1-2%), where it effectively becomes invisible.

The magnitude of drift may be determined by repeated measurements of M_0 over a nine hour period (which is typical of an IR experiment for crystalline lactose powders) using the standard hardware-based measuring procedure outlined in Section 4.6.1. However, to determine the phase of the baseline drift, it is necessary to concurrently measure M_0 and M(t). This posed several problems with respect to programming the EPROM based pulse sequencer. The

adoption of the "Experimental Supervisor" software supplied on request from BRUKER and upgraded input/output interface boards provided the necessary flexibility to perform these measurements.

4.6.2 "Experimental Supervisor" software and experimental procedure

The "EXP-SUP" software allows MINISPEC operation from any IBM compatible personal computer, and therefore increases flexibility in the design of pulse sequences and the storing of datum points.

To overcome the problem of baseline drift, the following pulse sequence (Figure 4.17) was implemented,

$$[180°|_x - t - 90°|_x - M_t - PD - 90°|_x - M_\infty]_N \qquad [4.47]$$

where M_∞ and M_t represent measurement of the baseline and the inversion recovery data points respectively and N = 100 data points were measured. The pulse delay, PD is approximately 5 times the longest expected T_1 component to allow the magnetisation vector complete thermal equilibration with the lattice.

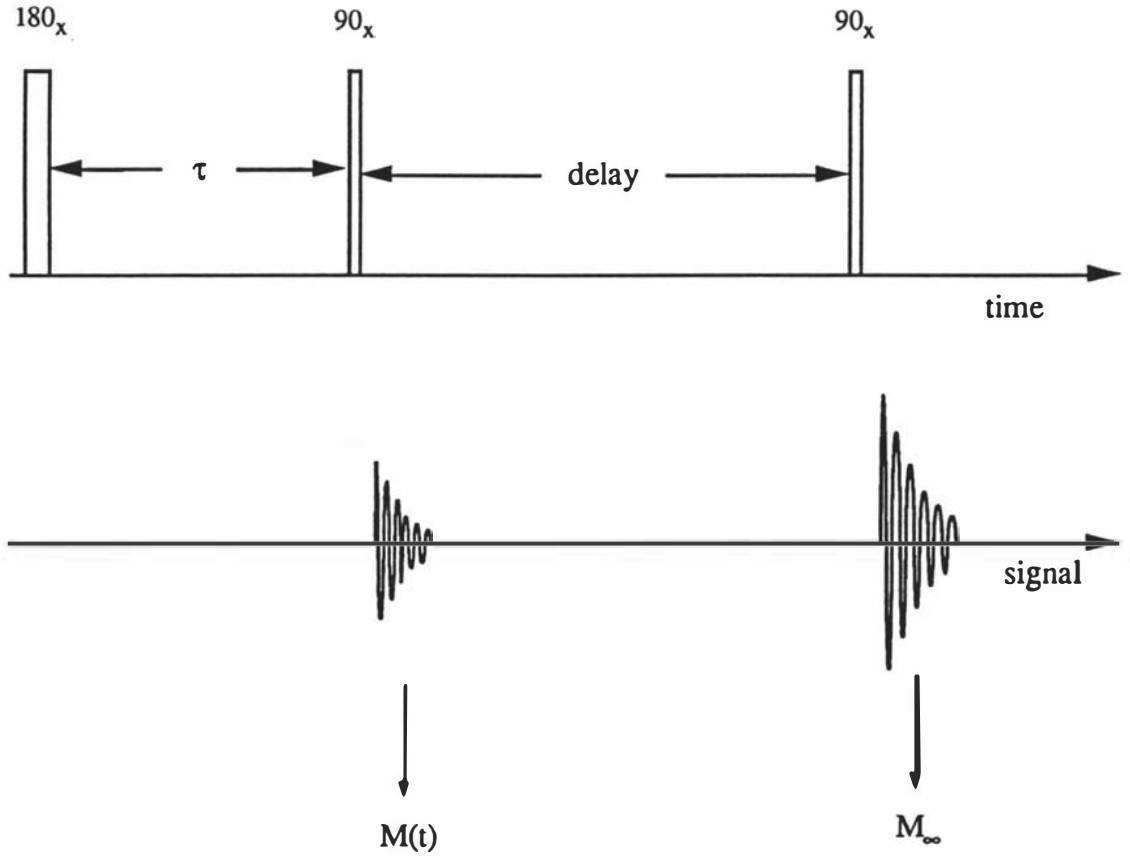

Figure 4.17. The modified IR pulse sequence designed to measure the baseline concurrently with measurement of the IR decay curve (M(t)). The delay is chosen to allow for complete thermal equilibration of the spin system (ie. 5 times T_1).

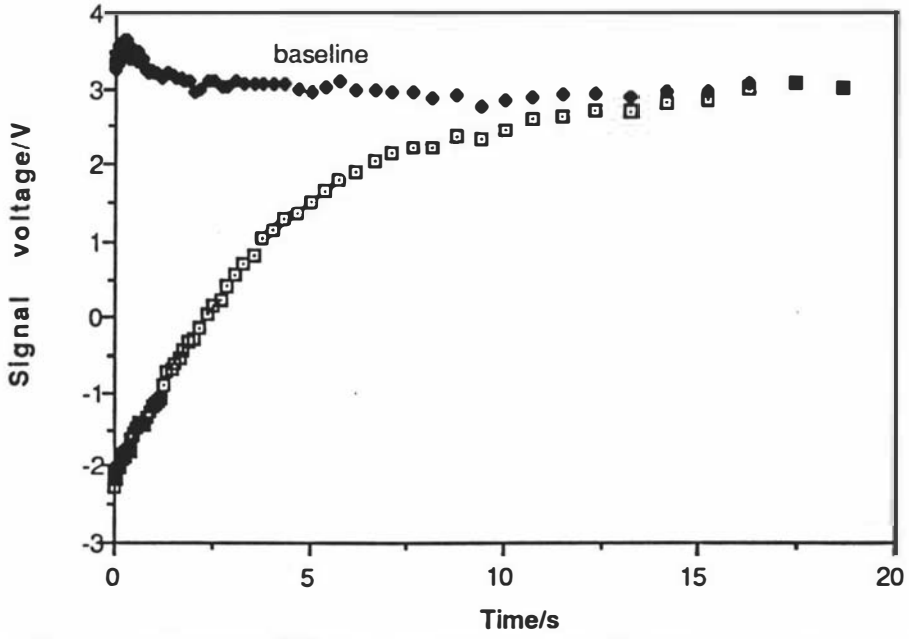

Figure 4.18. Illustrating the considerable drift that occurs during a single relaxation experiment (about nine hours)

Figure 4.18 demonstrates some correlation in drift between baseline and M(t) data, suggesting the origin of drift is a fluctuation in amplifier *offset* and not due to fluctuating amplifier *gain*, since for gain drifts one would expect an antiphase relationship between M(t) and M_∞ for values of M(t) < 0. Consequently, correction was carried out by calculating

$$M'(t) = -\left[M(t) - M_\infty(t)\right] \qquad [4.18]$$

where $M'_\infty(t)$ represents the linearly interpolated baseline point corresponding to datum point M(t). $M'_\infty(t)$ is determined from the FID following a single 90° pulse applied some time after an M(t) measurement (Figure 4.17). As measurements of $M'_\infty(t)$ typically follow M(t) by several minutes (over which time some drift occurs), the correction inherent in Equation [4.18] cannot be exact. Linear interpolation of $M'_\infty(t)$ values partially overcomes this, although some error may still exist. Nonetheless, implementation of the new pulse sequence, in conjunction with the correction of Equation [4.18], and interpolation of $M'_\infty(t)$ yielded marked improvements in results suggesting that any remaining errors were small. This is illustrated by comparing the T1 spectra for alpha lactose monohydrate (Figure 4.19) and beta lactose (Figure 4.20) obtained using the pulse sequence of Equation [4.47] with the corresponding spectra (Figures 4.14 and 4.16) respectively obtained by the conventional IR method (Figure 4.2). The disappearance of the spurious components is attributed to reduction of baseline drift.

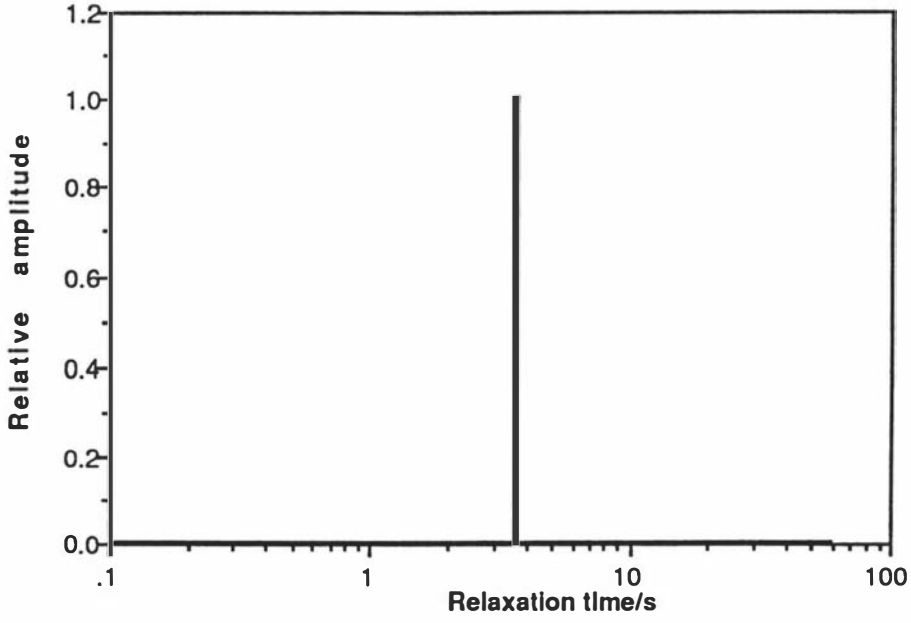

Figure 4.19. A typical T_1 spectra of alpha lactose monohydrate obtained from the relaxation data generated by the "EXP-SUP" software to correct for baseline drift and offset, and inverted using the LH algorithm. (Compare this result to Figure 4.14).

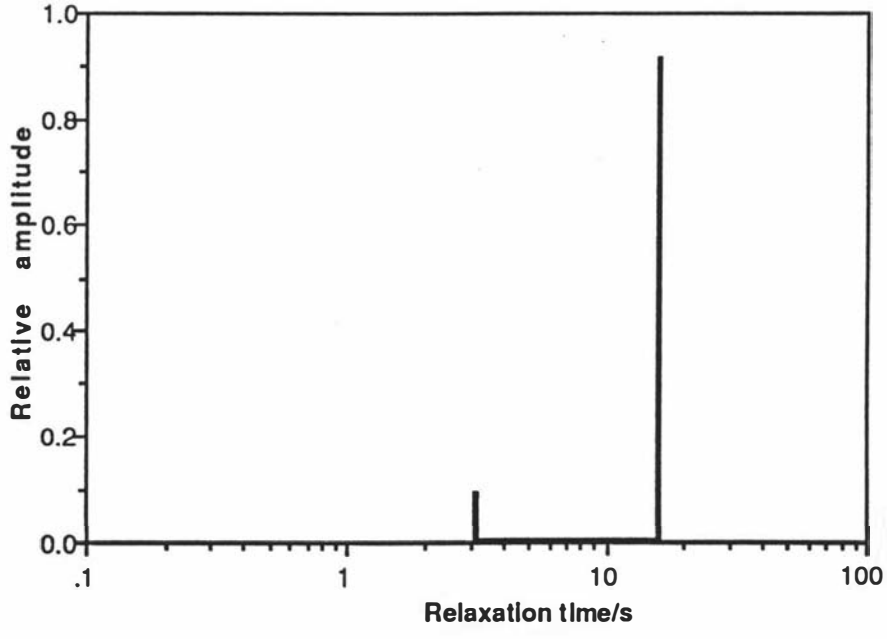

Figure 4.20. A typical T_1 spectra from conventional beta lactose correcting for baseline drift and offset as for Figure 4.19. (Compare this result to Figure 4.16). The "impurity" alpha lactose monohydrate is clearly indicated at around 3 seconds.

The relative amplitudes of components from beta lactose shown in Figure 4.20 agree with polarimetric determinations of the anomeric composition (10% alpha lactose monohydrate). The accuracy of relaxation measurements in determining the anomeric composition of lactose powders will be ascertained in Chapter 5.

4.7 Conclusions and summary

T_1 is sensitive to variations in molecular structure and dynamics and should, therefore, be of use in assaying a sample in terms of chemical composition and structural (crystalline) variations. Preliminary relaxation measurements on crystalline species of lactose (alpha and beta) established a marked difference in relaxation times with the possibility of quantifying these species in a real powder mixture. Relaxation measurements to determine the anomeric composition of powders will be investigated in Chapter 5. The investigation of spin-lattice relaxation times around the glass transition of amorphous lactose will be the subject of Chapter 6.

The algorithms LH, ML, and Contin each demonstrated specific advantages in handling data affected by noise and baseline drift and offset. Those utilising linear inverse operations to find the solution of best fit performed particularly well on data affected by large baseline drift, whereas ML had an advantage in overcoming the destabilising effects of noise. Linear inverse methods perform well in general where the noise level is less than 1-2%. For spin-lattice relaxation time measurements, where noise and drift are always present, the use of linear inverse methods to gain accurate physical and chemical information about the system is entirely appropriate.

5. Identification of crystalline forms of lactose

5.1 Introduction

Crystalline lactose produced by conventional refining techniques (utilising aqueous crystallisation) forms either alpha lactose monohydrate or (conventional) beta lactose (crystallisation temperature < 93.5°C and > 93.5°C respectively)[2]. Consequently, the crystalline state of commercial grade lactose powder can be simply inferred by determining the anomeric composition in solution: a task which is easily achieved with polarimetry.

However, there are many more crystalline species of lactose besides those known to be formed during the commercial manufacture of lactose. Many of these form by solid-state recrystallisation of alpha lactose monohydrate under extreme dehydration conditions[20-28] (Chapter 2). These conditions potentially exist during lactose refining (Figure 1.2) and food manufacture, and the formation of these crystalline species is therefore suspected[15,18]. Obviously, the method used to characterise mixtures where these "non-conventional" forms of lactose are present must identify the different crystalline variations of the same anomeric form. Solution methodologies are simply not capable of achieving this.

In this chapter, the spin-lattice relaxation times of the crystalline species of lactose produced in Chapter 2 are measured. In each case the magnetisation decay is represented by a distribution of exponentials corresponding to a spectrum of relaxation times. Differences in the relaxation time spectra provided the basis for the differentiation of crystalline species. An experimental protocol was developed to determine the anomeric composition of a series of mixed alpha and beta lactose powders in the solid state, and the limit of sensitivity of the method was investigated.

5.2 Analysis of the crystalline composition of lactose powders

5.2.1 T_1 measurements

Measurements were performed on a model **PC120 BRUKER MINISPEC** with a 0.47 Tesla (20 MHz) temperature-controlled (40°C) permanent magnet. Spin-lattice relaxation times were measured by the drift-compensated IR method described in Section 4.3. One hundred logarithmically distributed relaxation data points were measured from t = 20 ms to 50 s (Figure 4.4), and four Free Induction Decays (FID's) signal averaged to improve the signal:noise ratio. Relaxation data was drift-corrected according to Equation[4.18], and inverted to the relaxation time domain using the ML, LH and Contin algorithms discussed in Chapter 4.

Where the "true" relaxation time value did not correspond closely with the points on the discretised relaxation time axis, it was observed that a doublet spanning the true relaxation time

occurred. In such cases, the weighted average of the two relaxation time components was calculated and a single relaxation time displayed. Three T_1 spectra were obtained for each crystalline species. The relaxation time spectra of crystalline lactose are presented in Figures [5.1] to [5.12].

5.2.2 The T_1 spectra

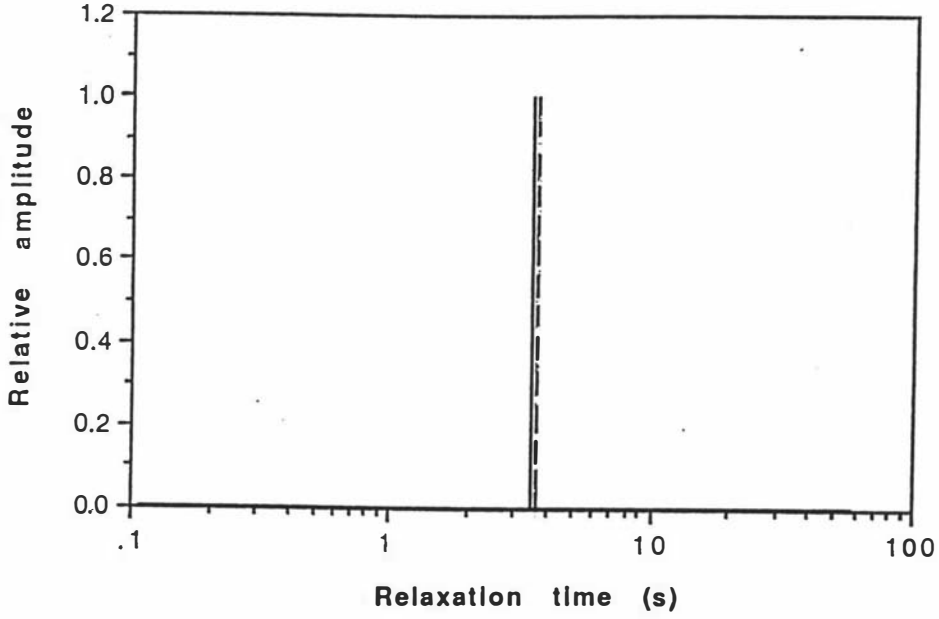

Figure 5.1. T_1 components of alpha lactose monohydrate. The dashed and solid lines correspond to the ML and LH solutions respectively.

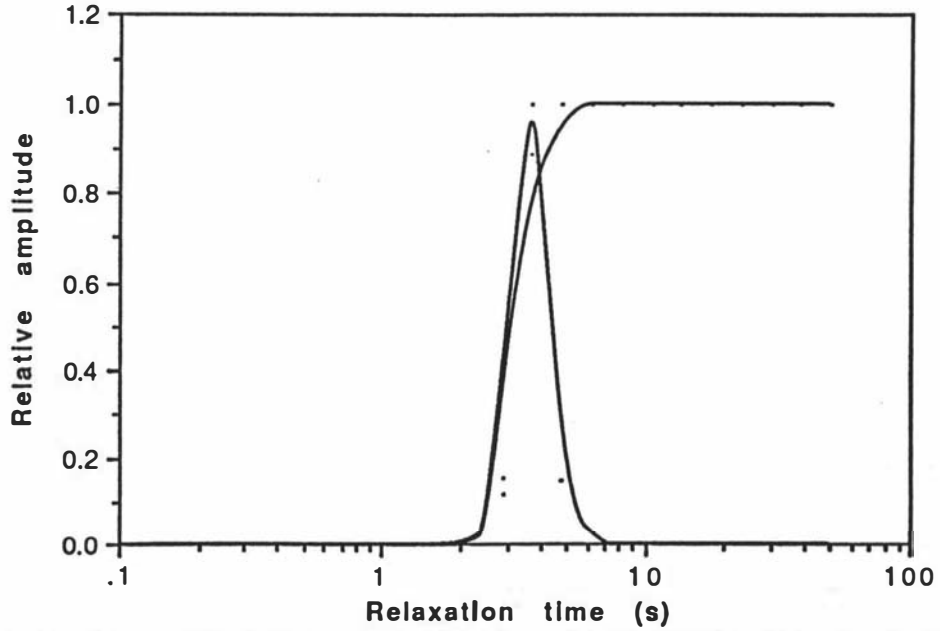

Figure 5.2. T_1 components of alpha lactose monohydrate determined by Contin. The integral of area is also shown. Note that each curve (of subsequent Contin figures) is obtained by interpolation using Cricket Graph™. Due to limitations of this software, the curve does not necessarily go through all points. The amplitude axis has been normalised for each curve.

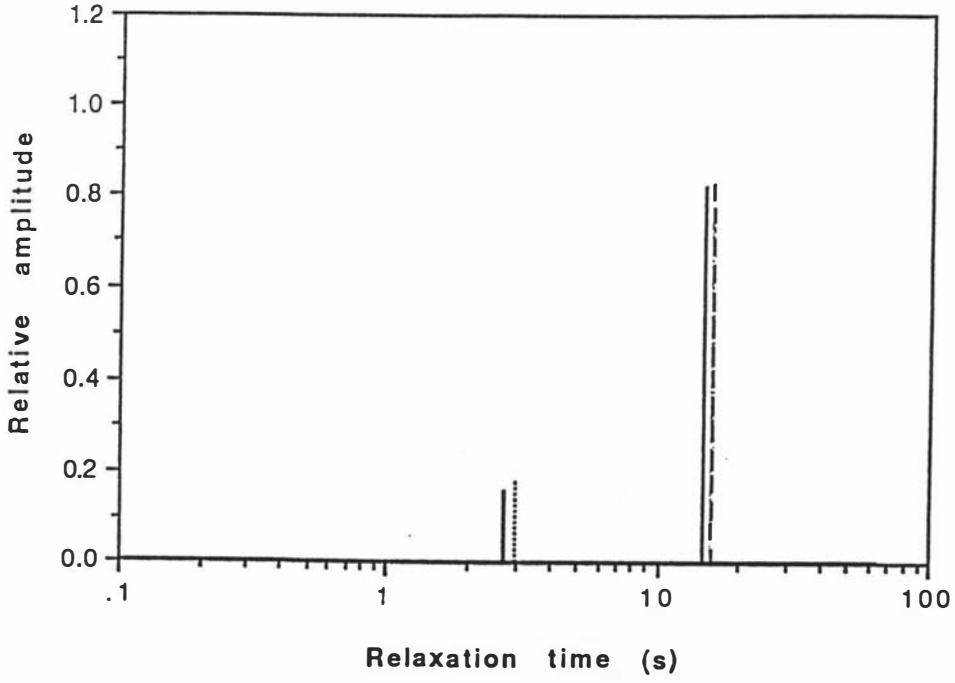

Figure 5.3. T_1 components (M-L & L-H) for conventional beta lactose

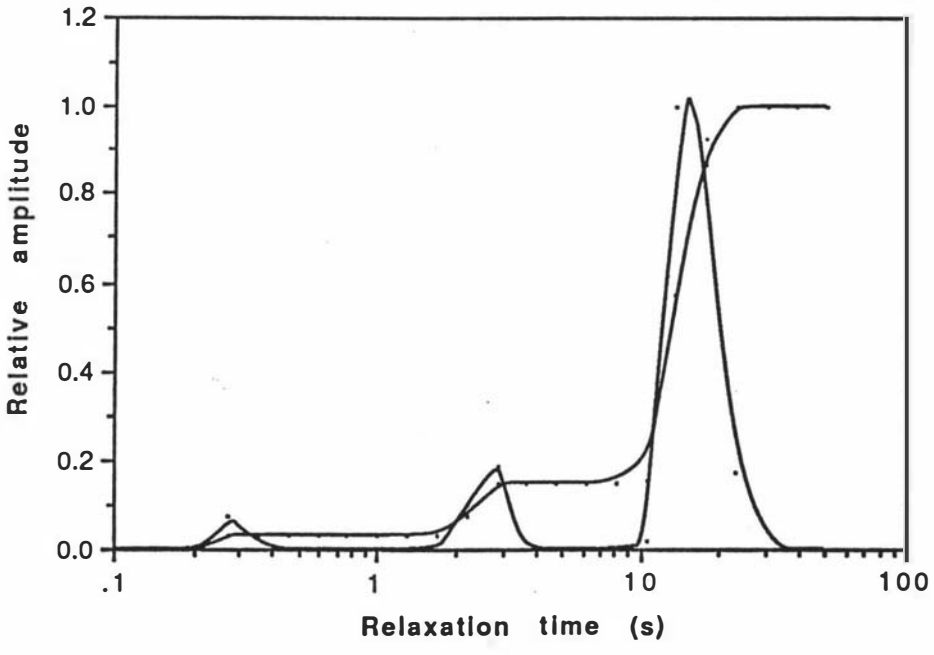

Figure 5.4. T_1 components of beta lactose determined by Contin. The integral of area is also shown. Note the amplitude axis has been normalised for each curve.

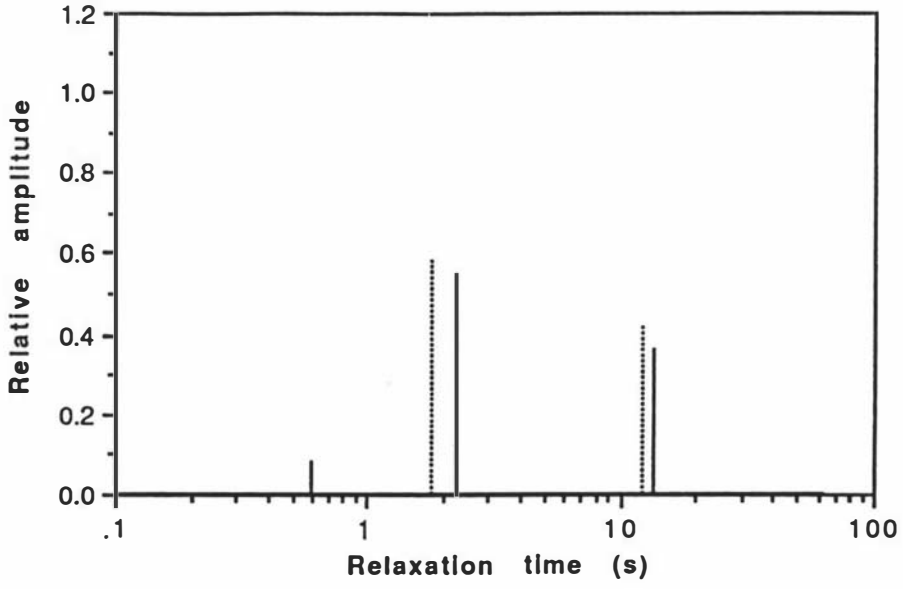

Figure 5.5. T_1 components of S-lactose. The dashed and solid lines correspond to the ML and LH solutions respectively.

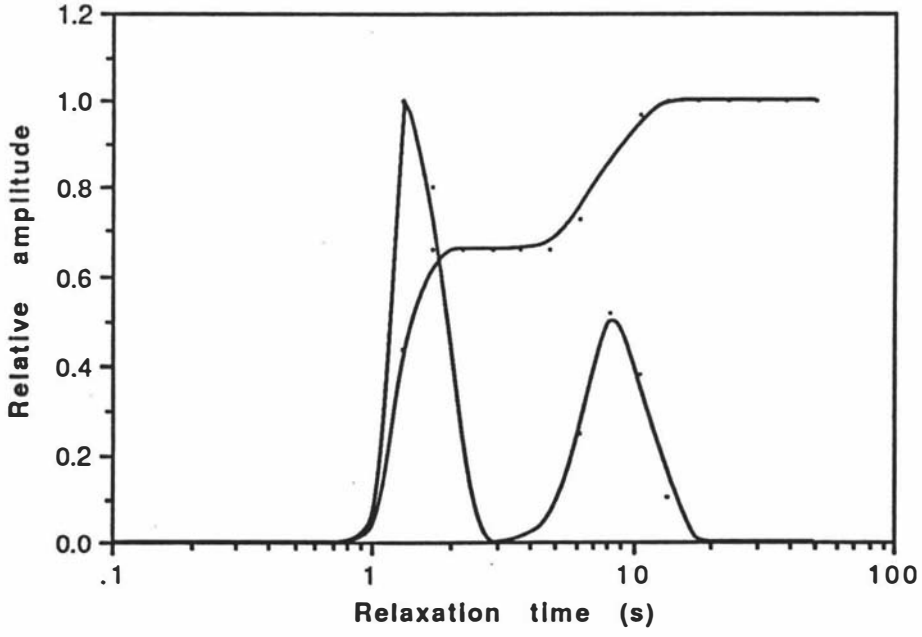

Figure 5.6. T_1 components of S-lactose determined by Contin. The integral of area is also shown. Note the amplitude axis has been normalised for each curve.

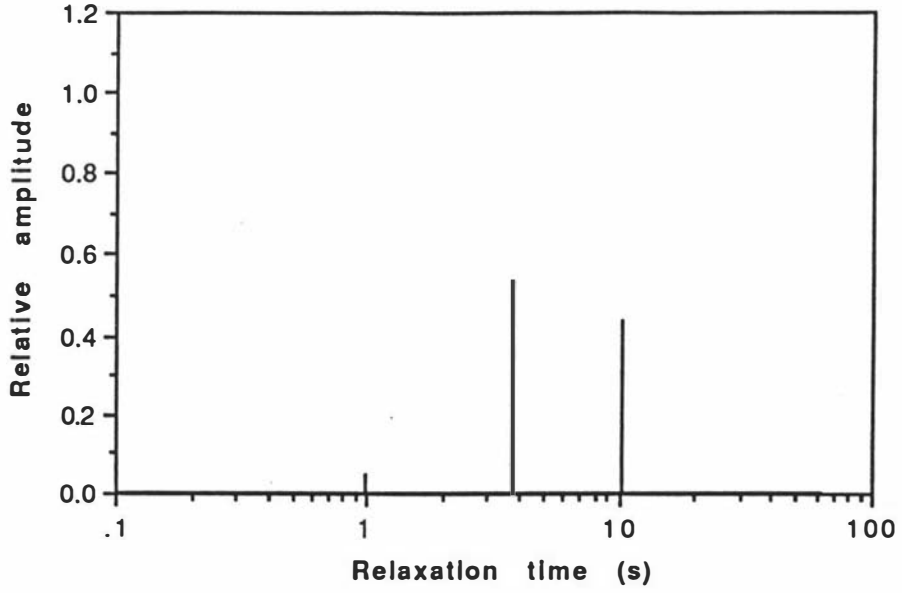

Figure 5.7. T_1 components of Beta (methanol prep) lactose. The dashed and solid lines correspond to the ML and LH solutions respectively.

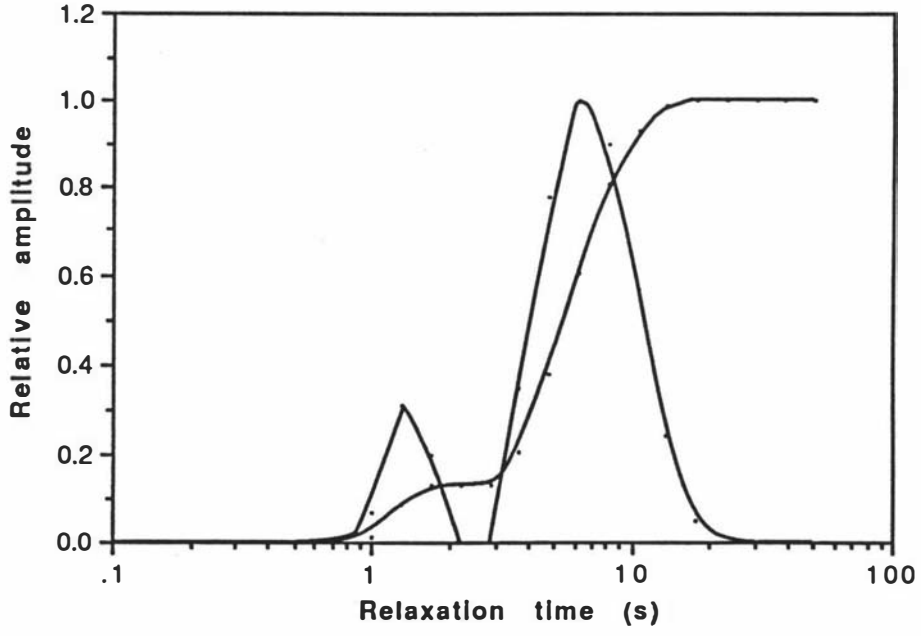

Figure 5.8. T_1 components of beta (methanol prep) lactose determined by Contin. The integral of area is also shown. Note the amplitude axis has been normalised for each curve.

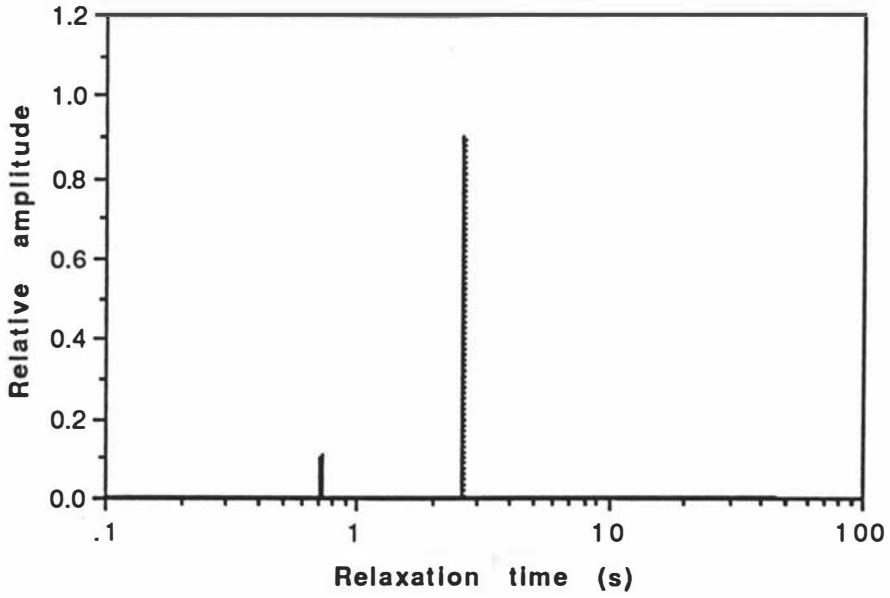

Figure 5.9. T_1 components of U-lactose. The dashed and solid lines correspond to the ML and LH solutions respectively.

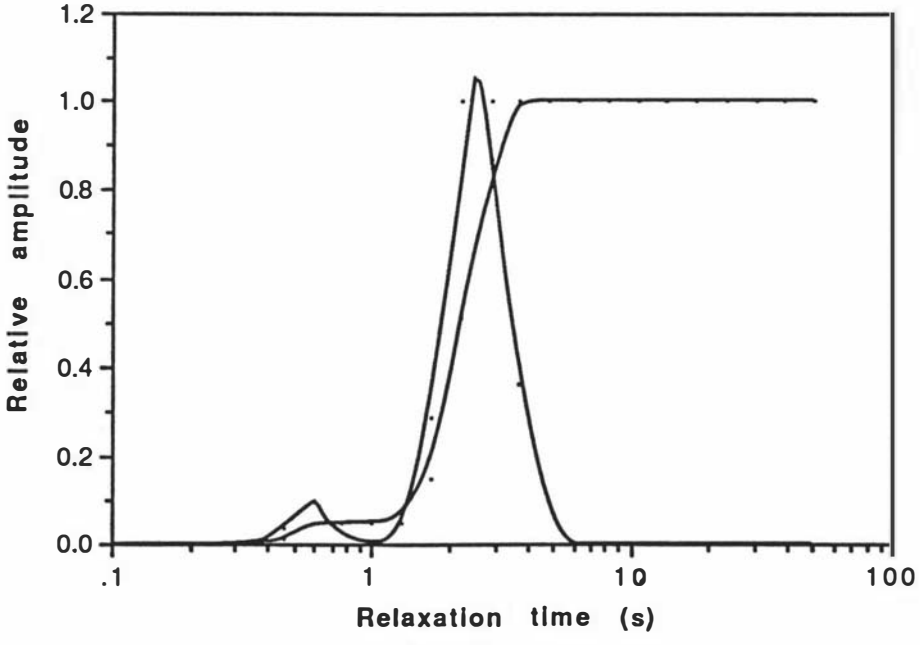

Figure 5.10. T_1 components of U-lactose determined by Contin. The integral of area is also shown. Note the amplitude axis has been normalised for each curve.

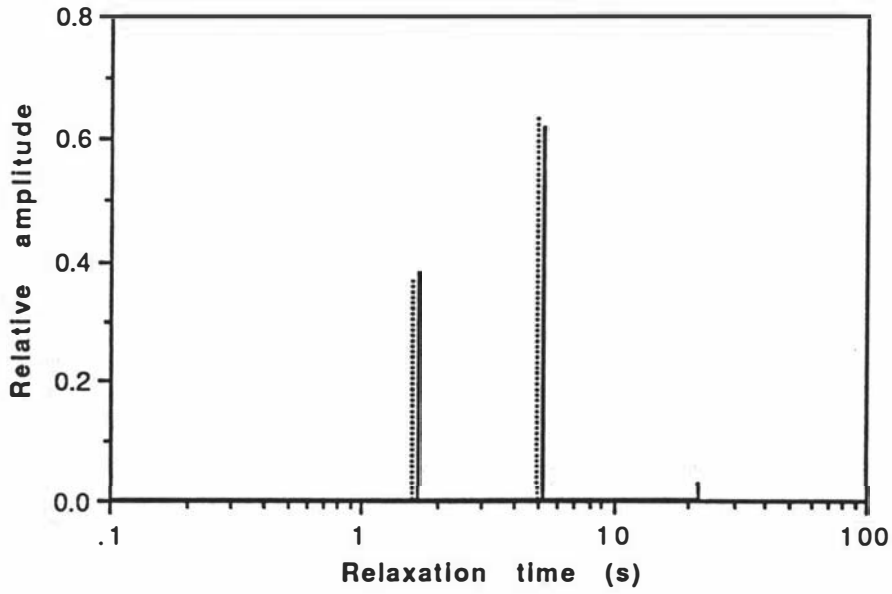

Figure 5.11. T_1 components of 5:3 lactose. The dashed and solid lines correspond to the ML and LH solutions respectively.

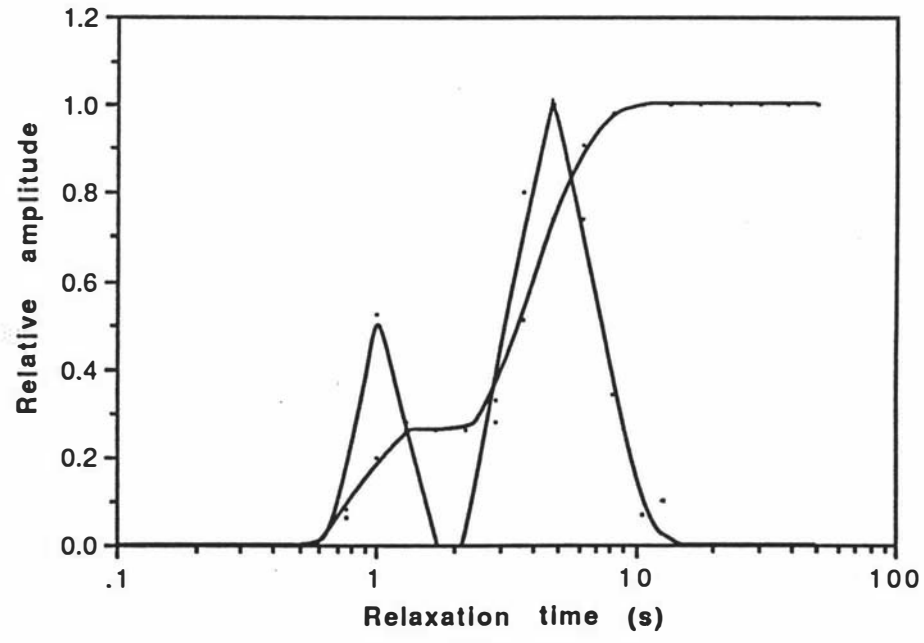

Figure 5.12. T_1 components of 5:3 lactose determined by Contin. The integral of area is also shown. Note the amplitude axis has been normalised for each curve.

In most cases, there is good agreement of relaxation time values obtained by the LH and ML algorithms. Spectra obtained using the Contin algorithm sometimes demonstrate convergence of close relaxation components (Figures 5.7 and 5.8 where 4 and 10 s components have been averaged to 7 s), however most Contin spectra agree with those obtained using the LH and ML algorithms. Incidentally, this convergence behaviour is consistent with the continuum formulation (Equation [4.43]) of Contin, which provides enhanced stability against random noise effects[57,60] albeit a slight reduction in "energy" of the relaxation time spectrum; ie a reduction of component multiplicity.

Alpha lactose monohydrate exhibits a single relaxation component around 3.5 s (Figures 5.1 and 5.2). Beta lactose manufactured by conventional aqueous crystallisation (Figures 5.3 and 5.4) exhibits components around 13 and 3 s. Since the beta lactose powder was contaminated with approximately 8% alpha lactose (determined by polarimetry), the 3 s component (9% relative amplitude, Figure 5.3) is assumed to be due to contaminating alpha lactose monohydrate. The existence of discrete relaxation time components (multi-exponential relaxation) suggests that alpha and beta crystalline regions are not exchanging spin energy during the time frame of relaxation measurement on the order of T_1. In such cases, the relative amplitude of respective relaxation time components may be unambiguously correlated with the weight fraction of each crystalline species in the powder. Multi-exponential relaxation may occur because the distances between anomeric nuclei are unable to be spanned by spin diffusion during the relevant time scale (of order T_1). A possible conclusion is that the contaminating crystalline alpha species is concentrated into discrete macroscopic regions.

For beta lactose manufactured by methanolic reflux, the LH spectrum (Figure 5.7) exhibits relaxation components of 1, 3.8 and 10 s. This spectrum is entirely different from that of conventional beta lactose (aqueous crystallisation) suggesting these species have different crystalline structures. Methanolic beta lactose was contaminated with 3% alpha lactose (polarimetric measurement) which tentatively agrees with the amplitude of the 1 s component (5%). Contaminating alpha lactose is expected to be of the anhydrous form (due to methanolic dehydration), although the corresponding relaxation time spectrum does not agree closely with the relaxation times of S-, M-, or U-lactose.

S lactose exhibits relaxation time components of 0.6, 2.2 and 11 s (Figures 5.5 and 5.6). The S-lactose powder was contaminated with 2% beta lactose (determined by polarimetric measurement) which does not agree with the relative amplitude (9%) of the 0.6 s component. It appears that this component arises from anhydrous alpha lactose.

U lactose exhibits relaxation time components of 0.6 and 2 s (Figures 5.9 and 5.10). The 0.6 s component agrees in time and relative amplitude with the matching relaxation component of S

lactose but not with the known concentration of contaminating beta lactose (3% by polarimetric measurement). It is notable that heat desiccation of lactose at reduced pressure (10^{-1} torr) has yielded a product with a relaxation spectra different from S lactose. It may be concluded that the crystalline structure of each species is unique.

The relaxation time spectrum of the 5:3 "mixed crystal" form of lactose exhibits components at 1.7 and 5 s in an amplitude ratio of 5.1:3 respectively (Figure 5.11). This agrees with the anomeric composition determined by polarimetry (alpha:beta = 4.9:3), and by implication, it has been decided that these correspond to beta and alpha lactose respectively. It is noted that here beta lactose has a shorter relaxation time than alpha lactose which contrasts with the relative relaxation times of alpha monohydrate and beta lactose (3 and 13 s respectively). It can be inferred that the crystalline structure of beta lactose in the 5:3 mixture is markedly different to that of conventional beta lactose.

The demonstration of discrete relaxation time components and the agreement of the relative amplitudes of these components with the results of polarimetric measurement suggests that the crystalline regions corresponding to alpha and beta lactose are not coupled by spin-diffusion. This behaviour was similarly demonstrated by aqueous-crystallised beta lactose (Figure 5.3). The implication of this result is that the crystalline domains of alpha and beta lactose are separated by distances greater than that spanned by spin diffusion in the frame of T_1. Consequently, no molecular "bonding" is believed to exist between alpha and beta regions as suggested by others[47]. This is further supported from the result of DSC measurement (Figure 5.13).

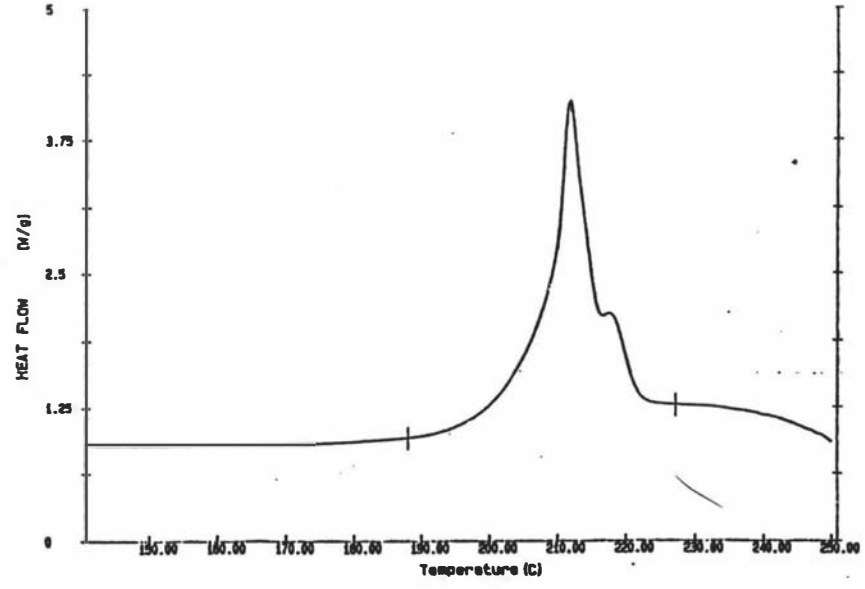

Figure 5.13. DSC thermograph of the "5:3" crystalline mixture of alpha and beta lactose.

Here, the demonstration of a biphasic melting endotherm suggests the existence of a binary mixture of crystalline species. It appears that the unique anomeric composition obtained by this method of preparation is a result of kinetic, not equilibrium mechanisms.

The T_1 components of each crystalline species are summarised in Table 5.1. The experimental error is estimated from the standard deviation of three measurements.

Table 5.1 Spin-lattice relaxation time components of the crystalline species of lactose determined from the LH algorithm

Crystalline species	Relaxation times (s)	Relative amplitude (%)	Anomeric species
alpha monohydrate	3 ± 1	100 ± 0	alpha
conventional beta	3 ± 1	9 ± 2	alpha(impurity)
	13 ± 2	91 ± 2	beta
methanol beta	1.0 ± 0.3	5 ± 1	beta(impurity)
	3.8 ± 1	53 ± 3	beta
	10 ± 2	42 ± 3	beta
S lactose	0.6 ± 0.1	9 ± 2	alpha
	2.2 ± 0.6	57 ± 3	alpha
	11 ± 1	34 ± 3	alpha
U lactose	0.6 ± 0.3	9 ± 2	alpha
	2.0 ± 0.5	91 ± 2	alpha
5:3 mixed crystal	1.7 ± 0.5	37 ± 3	beta
	5.0 ± 0.8	63 ± 3	alpha

5.2.3 The effect of adsorbed moisture on relaxation times of crystalline lactose

The spread of relaxation times and relative amplitudes for each crystalline species, as evident from Table 5.1, is expected to result from experimental noise, and the associated non-uniqueness of solutions found by χ^2 minimisation[60] (Chapter 4). However, T_1 variations were observed in amorphous lactose subjected to moisture adsorption/desorption (Chapter 4) processes after being subjected to changes in the ambient relative humidity (RH). Here, the

effect of adsorbed ambient moisture on the relaxation time values of crystalline species of lactose is described. Experiments are performed on the hygroscopic species of S- and U-lactose.

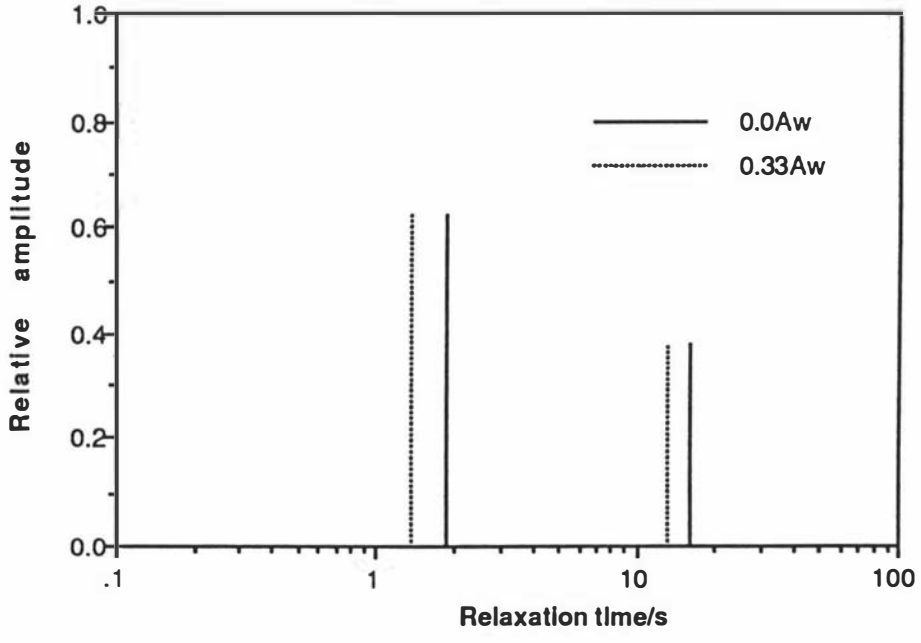

Figure 5.14. Comparison of S lactose equilibrated to 0.0 A_w and 0.33 A_w.

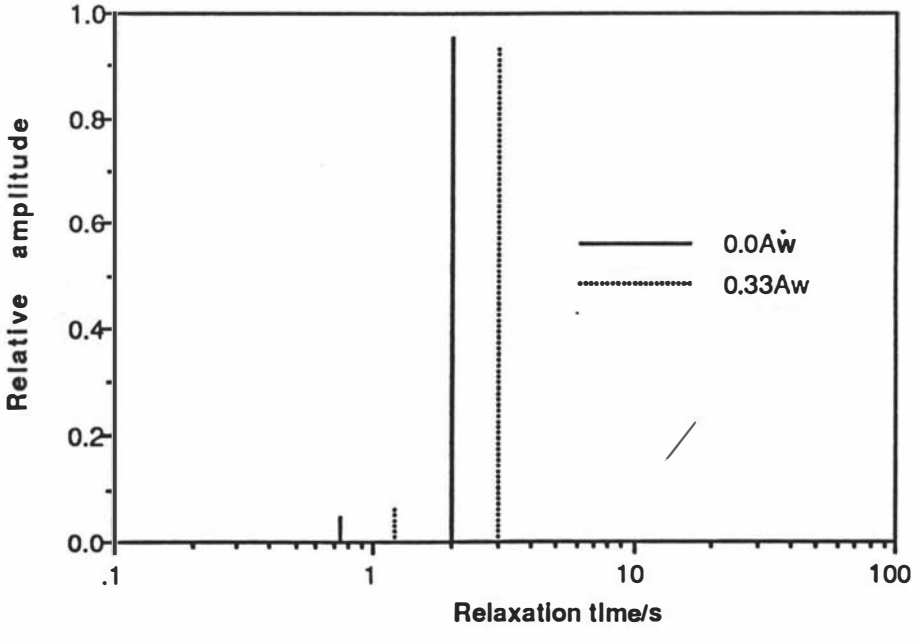

Figure 5.15. Comparison of U lactose equilibrated to 0.0 A_w and 0.33 A_w.

Freshly prepared S- and U-lactose was sealed in vacuum desiccators maintained at 0% RH and 33% RH and equilibrated for three weeks at 15 ± 4°C. Data inversion to the relaxation time domain was achieved using the LH algorithm. The results are depicted in Figures 5.14 and 5.15. Relaxation spectra represent the average (relaxation time values and relative amplitude) of two measurements.

The relaxation time spectra of S- and U-lactose exhibit displacement of relaxation components to shorter and longer time values respectively as moisture levels are increased, whereas the relative amplitudes of individual components are only slightly affected. The time displacements of the S-lactose spectrum are no greater than experimental error (Table 5.1). U-lactose demonstrates the largest relaxation time value displacements which is consistent with greater moisture adsorption. In view of this apparent moisture-dependency of U-lactose relaxation spectra and, as a precaution, future preparations of all crystalline lactose were desiccated over P_2O_5 for 48 hr prior to relaxation measurement.

5.2.4 High resolution solid state NMR of crystalline lactose

Solid state ^{13}C spectra of several crystalline species of lactose were obtained to determine whether spectroscopic differences could be used to identify and possibly quantify the various crystalline forms of alpha and beta lactose[47]. At the time, alpha monohydrate, conventional beta, methanolic beta and S-lactose were available for measurement. Amorphous lactose was also measured.

Due to the static dipolar broadening of ^{13}C nuclei in solids, conventional NMR spectroscopy yields broad, overlapping resonance lines which merge to form a single broad resonance known as a powder pattern[54]. Often, little or no spectroscopic detail is evident. However, by spinning the sample at high rotational speed (exceeding the static line width (several kHz)) at an inclined angle of 54.7° to the static field axis, dipolar interactions are averaged to zero, and narrow resonance lines may be obtained[61-63]. In conjunction with signal:noise enhancement by cross polarisation (CP, which transfers magnetisation from the abundant ^{1}H to dilute ^{13}C nuclei) and high power dipolar decoupling of ^{1}H from ^{13}C nuclei, a high resolution spectrum may be obtained[64]. Cross polarisation may be achieved utilising "Hartmann-Hahn contact"[64] where two rf fields are simultaneously applied in resonance with the respective ^{1}H and ^{13}C rotating frames. The increase in signal follows from the ratio of the gyromagnetic ratios, $\gamma_H/\gamma_C = 4$, and the shorter relaxation times (T_1) of ^{1}H nuclei (allowing faster signal recovery and repetition). A 20 fold improvement in the signal:noise ratio is readily obtained. In practice, the "contact" produced by the two resonant fields may be optimised by observing the increase in signal strength of the ^{13}C resonance lines as a function of time, t.

5.2.4.1 Method and results

Cross-polarisation Magic-angle-spinning (CP-MAS) ^{13}C measurements were performed on a model XL 200 BRUKER NMR spectrometer located at Industrial Research Limited (IRL), Gracefield. The MAS probe consisted of a twin bearing air-driven Al_2O_3 sample spinner[102]. Crystalline lactose was packed in the rotor (homogeneity is vital to balance) and capped. Rotor frequency was 3000 Hz. The Hartmann-Hahn contact time (1 ms) was optimised (as previously described), and one hundred FID's were collected and signal averaged. Because of the long T_1's of alpha monohydrate and conventional beta lactose (41 and 79 s respectively), repetition times of order 200-400 s were required to prevent saturation of the ^{13}C resonance. Consequently, each spectrum required 8-12 hr of signal aquisition. Spectra of alpha monohydrate, conventional beta, methanolic beta, S-lactose and amorphous lactose are presented in Figures 5.16 to 5.20. Chemical shift information has previously been published[47].

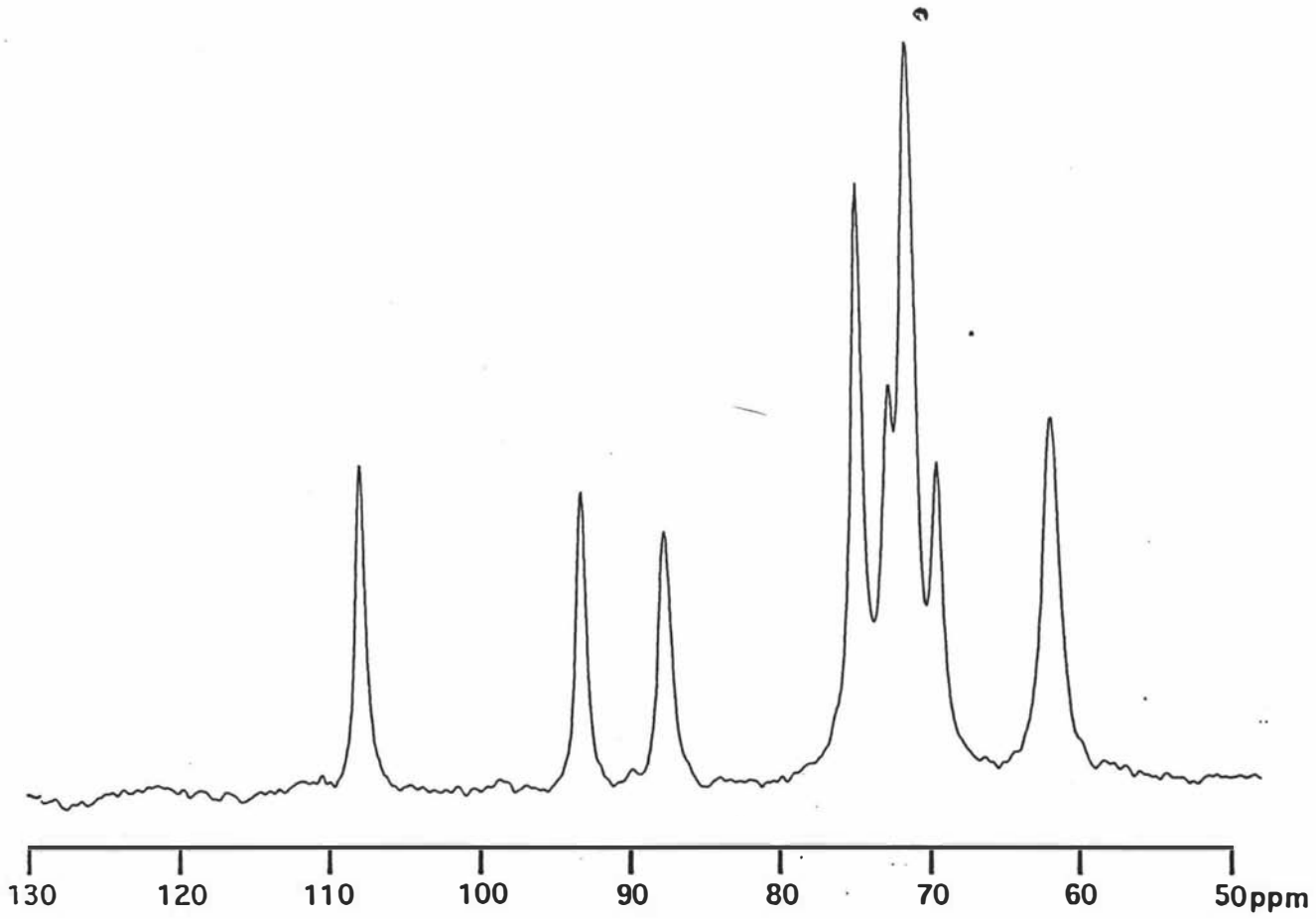

Figure 5.16 ^{13}C spectra of alpha lactose monohydrate

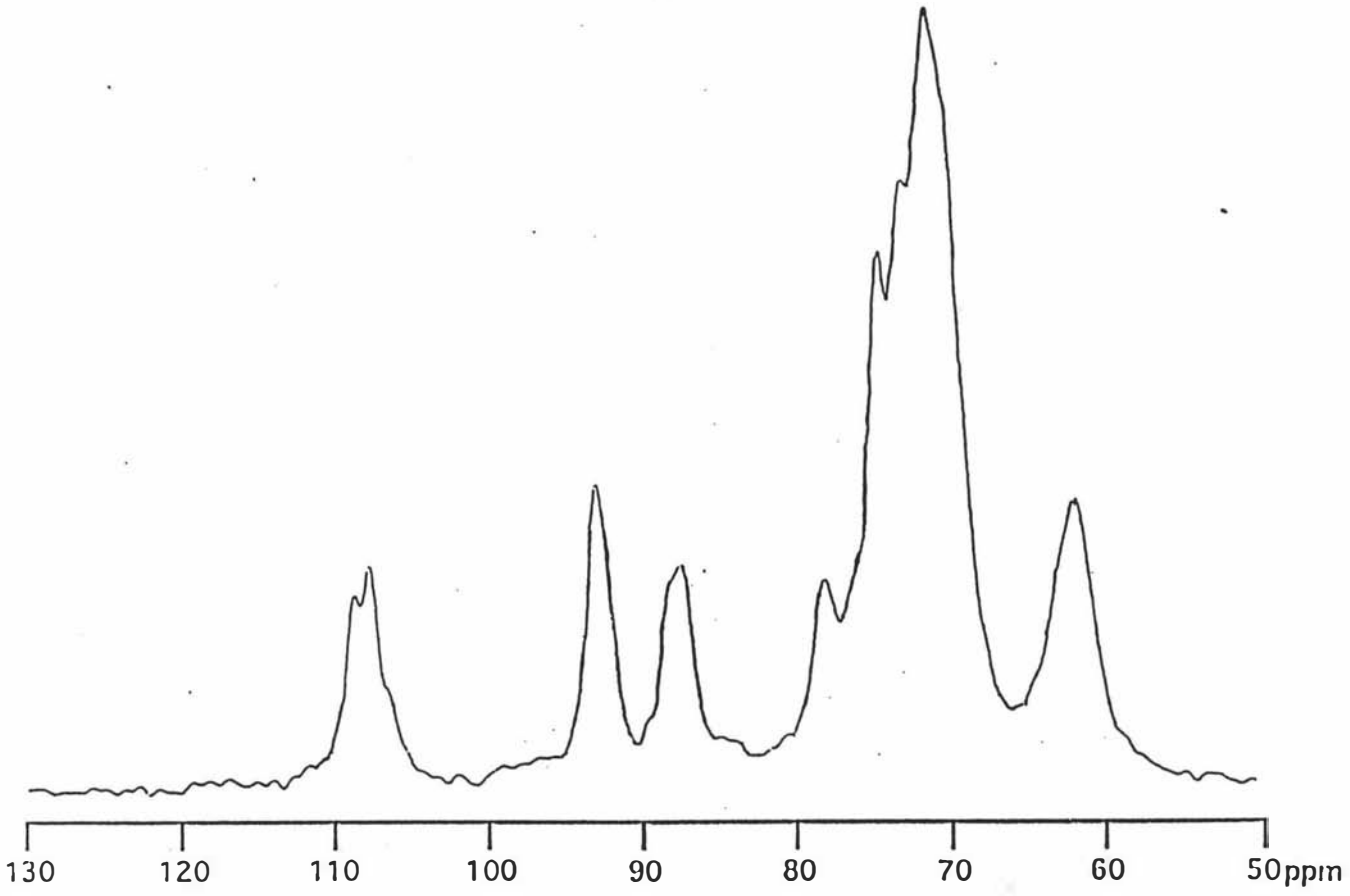

Figure 5.17 ^{13}C spectra of S lactose

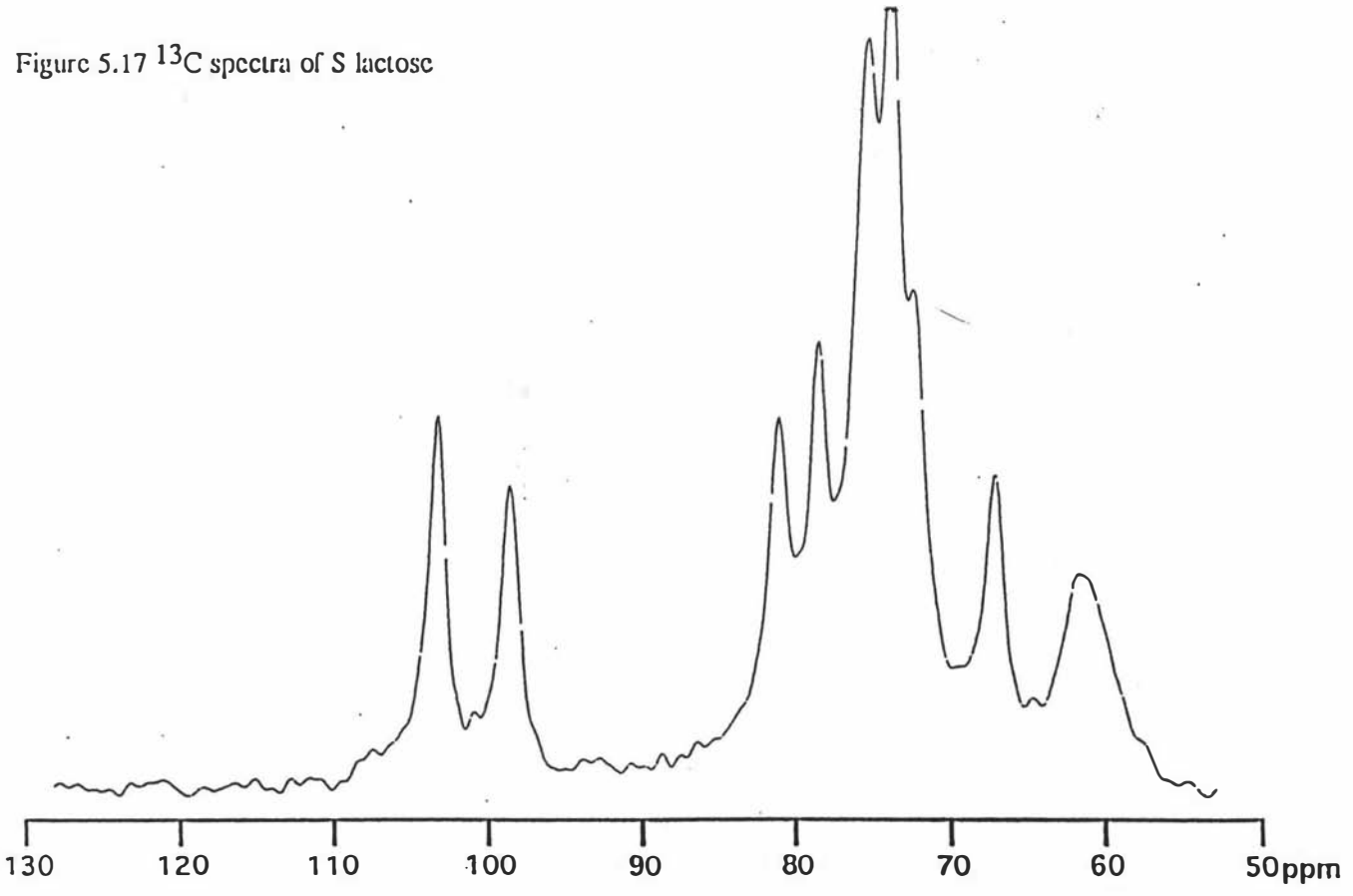

Figure 5.18 ^{13}C spectra of conventional beta lactose

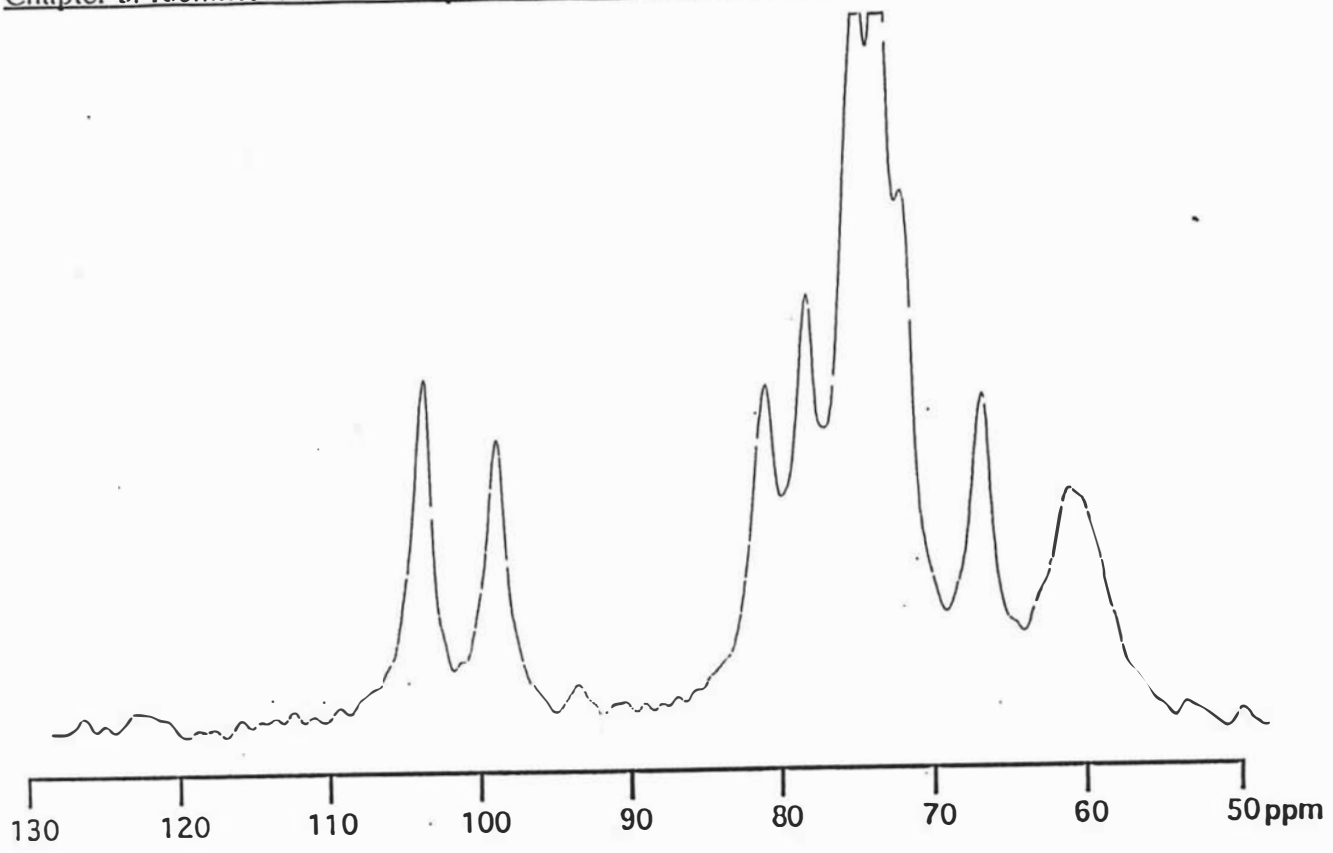

Figure 5.19 ^{13}C spectra of beta lactose from methanol

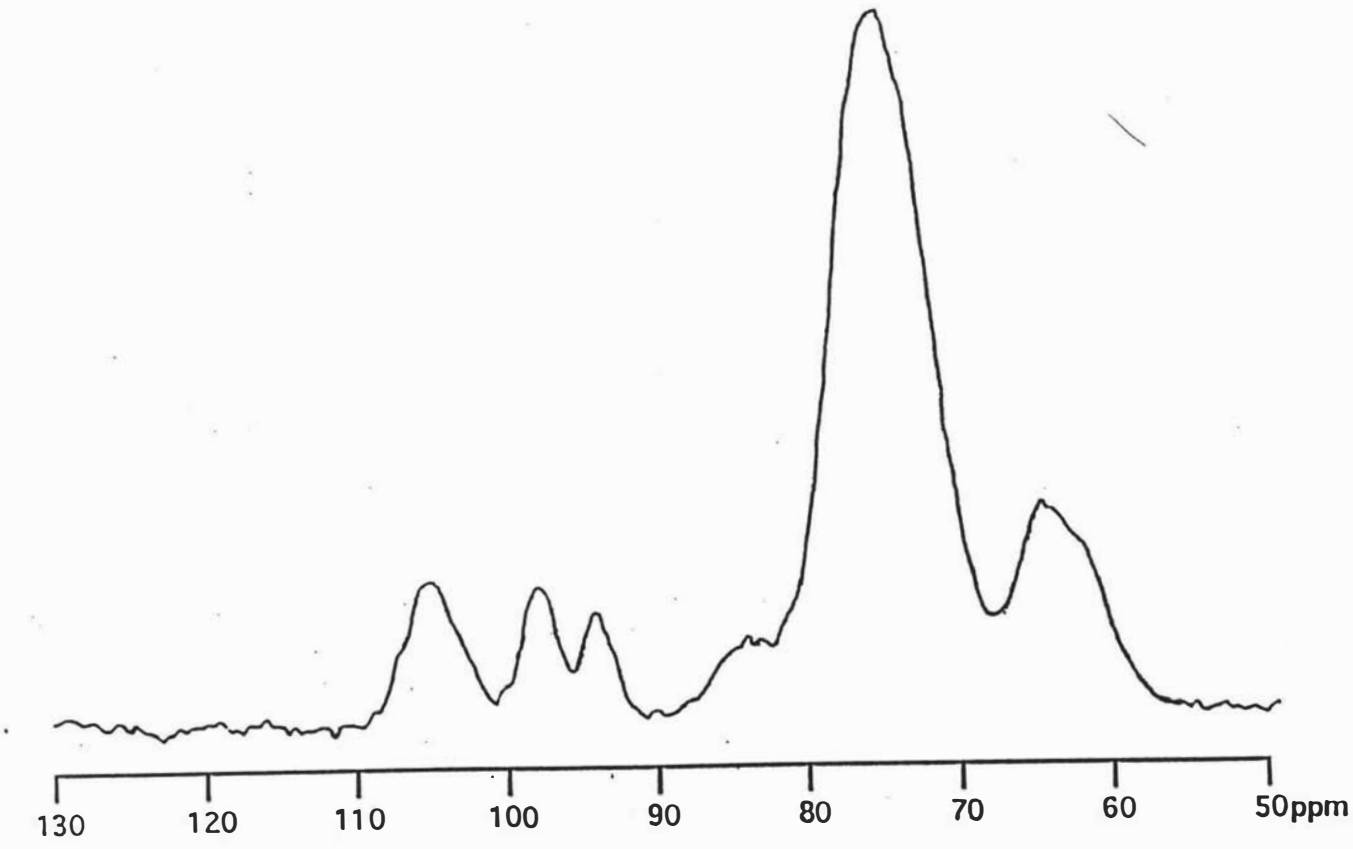

Figure 5.20 ^{13}C spectra of amorphous lactose

Figure 5.20 depicts the broad, poorly resolved resonance lines characteristic of amorphous materials[47]. Alpha lactose monohydrate and S lactose exhibit significant spectroscopic differences due to the different crystal ordering of nuclei[18]. S lactose demonstrates lower spectral resolution than alpha monohydrate. This is probably due to chemical-shift dispersion as a result of physical inhomogeneity of the crystalline lattice[47] due to lattice destruction during dehydration.

The two species of beta lactose demonstrate no significant spectroscopic differences. Since each crystal structure is unique (each demonstrated unique T_1 spectra), this result is unexpected. Because of the insensitivity of CP-MAS to differences in crystalline structure between beta lactose species, the method was not pursued further as a characterisation methodology.

5.2.5 Analysis of the anomeric composition of lactose powders by T_1 value analysis

By contrast to polarimetry, the determination of the anomeric composition of lactose directly in the solid state by T_1 value measurement offers the advantage that information concerning crystalline structure is retained, and the sample is not altered in any way. In this section, the relaxation spectra of lactose powders of known anomeric composition (by polarimetry) are obtained, and the anomeric composition determined from the relative amplitude of respective relaxation time components. The sensitivity of the method to dilute components is determined.

Five powders were blended from alpha monohydrate and beta lactose and the anomeric compositions were determined by polarimetry (Table 5.2). All samples were desiccated over P_2O_5 for 48 hr. Data inversion to the relaxation time domain was achieved using the LH algorithm. The LH algorithm was constrained to perform a two component fit (ie. determine the relative amplitudes of the two assumed relaxation time components) with fixed relaxation times of 3 s and 13 s corresponding to alpha monohydrate and conventional beta lactose respectively. The results of these calculations are presented in Table 5.2.

Table 5.2 Anomeric compositions of lactose powders determined by polarimetry and spin-lattice relaxation

Alpha lactose content by polarimetry (%)	Alpha content by T_1 value measurement (%)
5.5 ± 0.3	6.2 ± 0.8
10.8 ± 0.3	9.6 ± 1
13.5 ± 0.2	14.6 ± 1
54.5 ± 0.2	54.0 ± 0.7
94.8 ± 0.2	94.3 ± 1
97.8 ± 0.2	97.1 ± 1

The anomeric composition determined by polarimetry and T_1 analysis agree within experimental error for all samples. It is noted that relaxation measurements exhibit higher experimental error than polarimetry. Perhaps because of the proximity of the two relaxation components (3 and 13 s) relatively minor relaxation data errors may cause proportionately greater amplitude distortion of the relaxation time components and therefore a correspondingly higher experimental error. In such cases, reproducibility may be enhanced by improving the signal:noise ratio of relaxation data by increasing the signal averaging, although the analysis time may becomes prohibitively long. Alternatively, analysis time may be shortened by measuring fewer points, and advantage taken of the reduced analysis time to undertake more signal averaging. This approach, and it's resultant improvement in experimental error and reproducibility is investigated more fully in Chapter 7.

5.3 Summary

CP-MAS NMR ^{13}C spectroscopy did not differentiate the two crystalline species of beta lactose, and was therefore not pursued as a characterisation method. Spin-lattice relaxation time values differentiated all crystalline species of lactose. Relaxation times in S- and U-lactose were found to be weakly correlated to free moisture concentration. Co-crystallised alpha and beta lactose exhibited bi-exponential relaxation and no magnetisation transfer between alpha and beta regions was observed. Thus, spin-lattice relaxation spectra of binary or higher order lactose mixtures may be used to determine the relative concentration of crystalline species according to the relative amplitude of relaxation time components.

The spin-lattice relaxation time method of determining the anomeric composition of lactose powders demonstrated good agreement with polarimetry. Precision was inferior to polarimetry

but adequate for general routine analysis of powders. The method offers the possibility of detecting and quantifying other crystalline species not detected by polarimetry; eg. S-lactose versus alpha monohydrate, or conventional beta versus methanolic beta.

6. Determination of the glass transition and crystallisation temperatures of amorphous lactose powders

6.1 Introduction

The rapid cooling of viscous carbohydrate melts on a time scale shorter than the average rate of molecular diffusion inhibits the formation of crystalline domains, and an amorphous "solid" or glass is formed[65,66]. By definition, a glass exists in a supercooled liquid state where the viscosity is sufficiently high (of the order of 10^{13} N s m^{-2})[65] that the material behaves much like a solid (will support its own weight). Glassy materials are characterised by randomly orientated molecular domains, but short range molecular ordering, reminiscent of the liquid state, is believed to exist[65,67]. The distances spanned by these ordered domains are smaller than the resolving power of soft X-rays (20 Å) which scatter diffusely from the amorphous substrate[19,65].

Simple carbohydrate glasses are prepared commercially by rapid concentration of an aqueous solution[68]. The time frame for glass formation is necessarily short (seconds) so that rapid drying techniques[38] such as spray atomisation (spray drying, Chapter 1) or thin film evaporation (roller drying) must be used to inhibit crystallisation. The formation of amorphous lactose by these methods, and under optimum drying conditions, yields a white, finely divided, free-flowing powder.

At ambient temperatures and humidities, amorphous carbohydrate powders (in particular, lactose) are sufficiently close to the glass transition temperature (T_g)[69,70] for their behaviour to be affected by environmental changes such as temperature and humidity[13]. The glass transition affects the behaviour of carbohydrates by several means. The material changes from a brittle to a rubbery state, and there is a large associated decrease in modulus (or rigidity) as T_g is exceeded[71]. Functional behaviour is affected[72] by the dramatic slowing of diffusive processes as the material is cooled towards T_g[73]. In powders, the rate of diffusive processes dramatically affects the stability to crystallisation, and the rate of drying/rehydration[74] and spoilage reactions.

Traditionally, the glass transition has been detected using differential scanning calorimetry (DSC) which detects the subtle endothermic shift in specific heat capacity around T_g[13,74]. The method is generally sensitive and reproducible provided that strict protocol concerning sample preparation is followed[75]. In this chapter, the sensitivity of spin-lattice relaxation time (T_1) values to the glass transition in amorphous lactose is described. The T_1 method is used to determine T_g in a range of moisture-equilibrated lactose powders and results are compared with DSC analyses. The phenomenon of solid-state crystallisation at temperatures approaching T_g +

50°C[13] is also investigated. The resultant stepwise change in the T_1 value at crystallisation is used to determine the onset temperature (T_c) of crystallisation, and also the product of crystallisation.

6.2 The glass transition phenomenon

6.2.1 Background

The T_g value of a quenched glass is dependent on the rate of cooling[67]. Furthermore, mechanical and electrical relaxation[71] may occur in carbohydrate glasses below (but close to) T_g. Consequently, a glass is not in a state of thermodynamic equilibrium relative to the crystal[76]. However, if time constants are long and deviations from equilibrium are slight, the glass may assume a state of quasi-equilibrium, and the theories of thermodynamics, which potentially offer much insight into the phenomenological properties of the glass transition, may be applied with negligible error.

The transformation between the glassy state and the liquid (or rubber) state is accompanied by characteristic changes in the physical state of the system. The most dramatic occur in the volume expansivity and the heat capacity, defined respectively as follows[67]:

$$\alpha_p = \left(\frac{\partial V}{\partial T}\right)_{p,z} \qquad C_p = \left(\frac{\partial H}{\partial T}\right)_{p,z} \qquad [6.1]$$

at constant pressure, p and order parameter, z[67] (the order parameter represents the order frozen into the glass and is a function of the rate of cooling during glass formation. It's incorporation normalises Equation [6.1] in terms of the dependency of T_g on the rate of cooling). These quantities undergo a stepwise change at T_g (Figure 6.1) reminiscent of a second-order phase transition. Viscosity and dielectric constant quantities undergo similar changes.

The discontinuity in α_p is naturally explained by free volume effects[76]. This theory assumes that all transport properties of the liquid are controlled by a parameter known as the free volume (defined as the unoccupied voids that exist between molecules), and that the glass transition occurs at a temperature at which the free volume drops to a value equalling that of the crystal. Hence, restricted molecular mobility below T_g causes an increase in the observed viscosity[68] (of the order of 10^3 N s m^{-2} (Figure 6.2)). By contrast, the entropy model[76] of the glass transition depicts a change in slope of the entropy-temperature curve around T_g . As the temperature (and therefore entropy) is reduced, a temperature at which the liquid entropy becomes equal to that of the crystal is reached. As it is not possible for the entropy of a disordered liquid to fall below that of a crystal (the Kauzmann paradox[77]), the entropy line

must undergo a change of slope, and a second-order phase transition occurs - the glass transition.

The glass transition is a function of three thermodynamic variables - composition, pressure and temperature. There is a region in the composition-pressure-temperature space of the supercooled liquid where the volume, enthalpy, entropy *etc.* approach values corresponding to those of the crystal and where a glass transition may potentially occur.

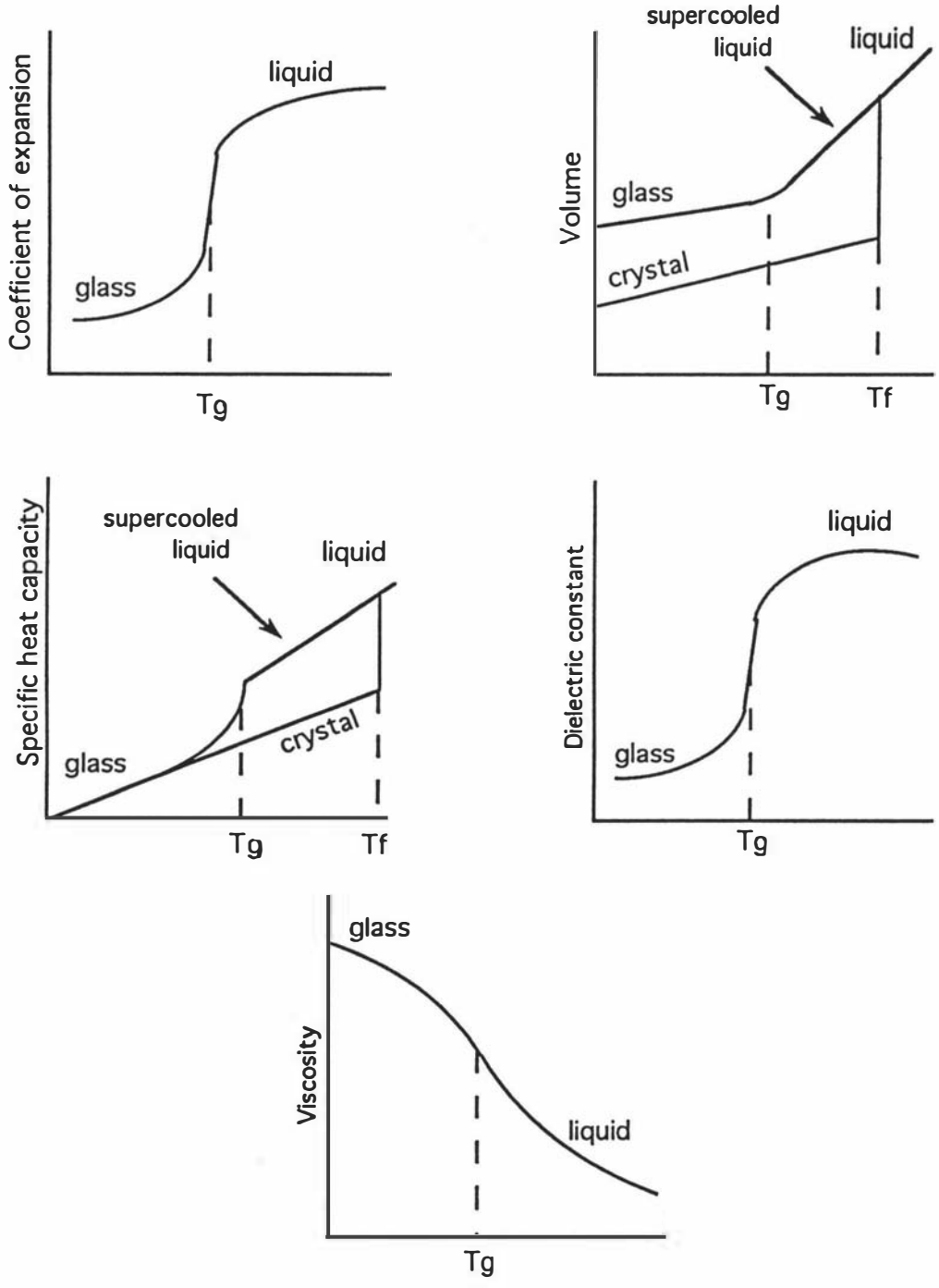

Figure 6.1. The physical changes that occur at the glass transition in amorphous materials. The x-axis represents the temperature scale. (Adapted from reference [58])

At constant pressure, the temperature-composition relationship of the glass transition of binary mixtures of fixed chemical composition has been shown[13,78] to obey

$$T_g = \frac{w_1 T_{g1} + k w_2 T_{g2}}{w_1 + k w_2} \qquad [6.2]$$

where k is a constant and T_g, T_{g1} and T_{g2} are the glass transition temperatures of the mixture and the individual components of weight fractions w_1 and w_2 respectively. The composition dependence of T_g is represented by the phase diagram of Figure 6.2.

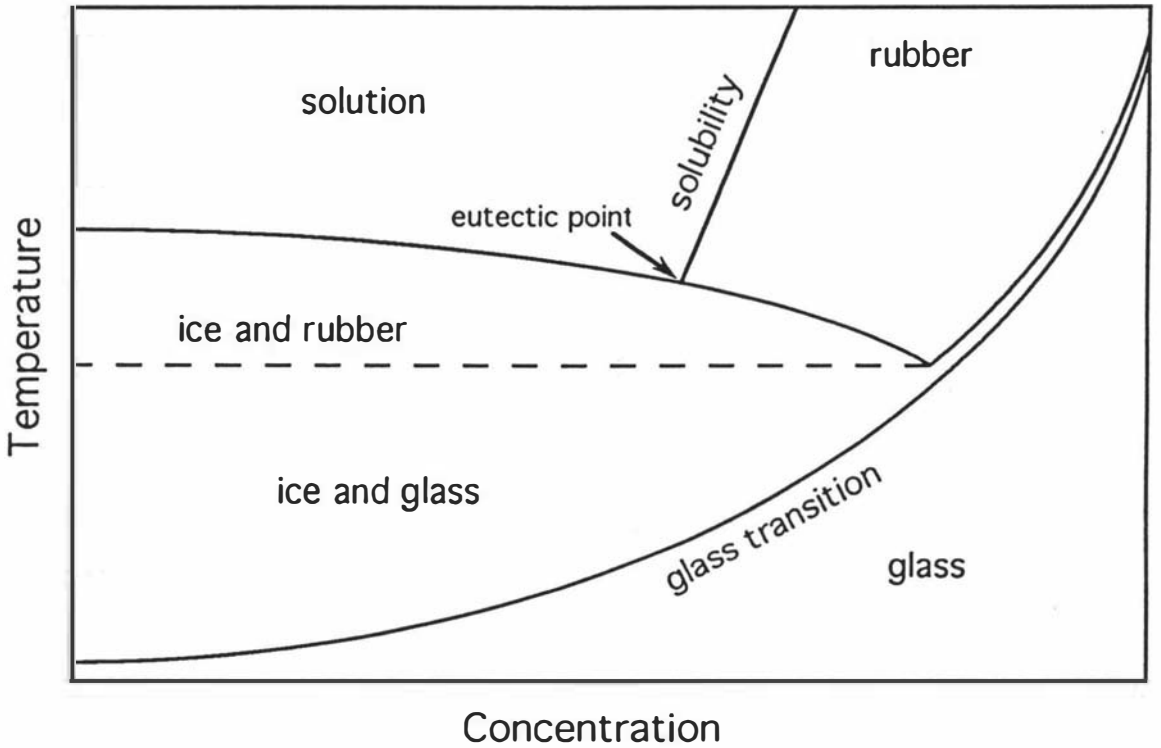

Figure 6.2. A representative phase diagram of a binary carbohydrate-water mixture. The ice component is assumed to be in the amorphous state. For a lactose-water system, T_g varies from -137°C (pure water[96]) to 101°C (pure lactose[81]).

The dependence of T_g on composition has practical relevance to the control of the physical properties of carbohydrate blends. The stability of a carbohydrate system may be enhanced by the addition of high T_g glassy compounds (typically of higher molecular weight)[79,80] that elevate T_g of the blend above normally encountered ambient temperatures. Typically, maltodextrins are used to improve dehydration characteristics, to decrease stickiness, and to improve product stability.[14,70,81] The dilution of amorphous carbohydrates by non-glassy compounds can also affect T_g. Small, highly mobile molecules such as water act as "plasticisers" and their adsorption into the amorphous matrix causes a substantial depression of the T_g value[74]. As amorphous carbohydrates are often hygroscopic, ambient moisture levels play an important role in determining the stability and functionality of powders[82].

For the purposes of spin-lattice relaxation measurements and the detection of T_g, the free volume theory provides useful insight into the expected change in T_1 value. Temperatures higher than T_g cause free volume[69] and hence average intermolecular distances to increase. As a consequence, the mobilities of molecular sites (most importantly, those that control relaxation behaviour due to spin diffusion) are expected to increase and relaxation rates are affected. Spin-lattice relaxation in solids is described by (from Equations[4.13] and [4.14])

$$\frac{1}{T_1}=\left(\frac{\mu_0}{4\pi}\right)^2\gamma^4h^2\frac{1}{10r_{ij}^6}I(I+1)\left[\frac{\tau_c}{1+\omega^2\tau_c^{\,2}}+\frac{4\tau_c}{1+4\omega^2\tau_c^{\,2}}\right] \qquad [6.3]$$

where for the solid state $\omega\tau_c >> 1$. At the glass to rubber transition, r_{ij} (average intermolecular distance) increases whereas τ_c (average correlation time for molecular motion) decreases in magnitude. It is clear that changes in both r_{ij} and τ_c will contribute to opposing changes in the relaxation time value. For lactose, which demonstrates "solid-like" T_1 relaxation and a negative temperature dependence of T_1 (see Section 6.3.3) it is expected that the glass transition will be evident as a discontinuity in the smoothly changing T_1 values.

6.2.2 Effect of glass transition on food structure

Below the glass transition temperature, glassy materials exhibit mechanical and electrical relaxation times sufficiently long that all time-dependent processes are essentially stationary[83]. In the rubber state, the relaxation times become strongly temperature dependent as represented by the Williams-Landel-Ferry (WLF)[69] equation

$$\log_{10}\left[\frac{\tau(T)}{\tau(T_g)}\right]=\frac{C_1^g(T-T_g)}{C_2^g+(T-T_g)} \qquad [6.4]$$

where $\tau(T)$ and $\tau(T_g)$ are the relaxation times at temperatures $T = T$ and $T = T_g$ respectively and C_1^g and C_2^g are arbitrary constants (for many polymers $C_1^g = -17.4$ and $C_2^g = 51.6$ give good agreement with experimental results[69] although others have suggested that the constants be allowed to vary according to the material[85,86]. Close to (and above) T_g, $\tau(T)$ changes by many orders of magnitude, and the rate of time dependent processes becomes significant.

In lactose powders, these relaxation processes account for many observed physical changes during processing and storage at $T > T_g$. Changes occur due to processes such as sticking, collapse and loss of binding ability.[72,82,83] (Crystallisation[84] is also a time-dependent process, but is not included here as it is discussed in detail in Section 6.4.)

The phenomenon of sticking occurs due to the adherence of neighbouring powder particles[82] and is characterised by agglomeration, a reduction in powder flowability and the formation of soft lumps. As powders are commonly transferred through ducting during manufacture and processing by air suspension, the maintenance of free-flowing characteristics is vital for the efficient mass transport of materials. Electron microscopy of sticky powders suggests that particle agglomeration is due to the formation of interparticle powder bridges at natural points of contact[82]. It is postulated that this coalescence phenomenon is accomplished through viscous flow of the plasticised powder, and is driven by surface energy. The rate-limiting step (diffusion) is viscosity dependent[82], and hence sticking is expected to be time and temperature ($T-T_g$) dependent. Indeed, the sticking time diminishes abruptly as $T-T_g$ exceeds 10-20°C.

Collapse occurs commonly in sugar-containing powders and many freeze-dried materials that have experienced temperatures higher than T_g[87-91,99]. It causes loss of food structure which, for frozen systems, results in complete change in the product characteristics. In lactose powders, collapse is observed as shrinkage of individual powder particles, which causes a substantial increase in bulk density[92]. Collapse is postulated to be diffusion limited, and is therefore a function of time and temperature ($T-T_g$)[83]. As collapse in powders is usually preceded by sticking, it appears that the two processes represent different stages of essentially the same phenomenon.

The diffusivity of small organic molecules (*eg.* flavour and aroma compounds) through the amorphous matrix increases dramatically at temperatures above T_g[13,73,93]. As diffusion kinetics determine the rate of mass transport of volatiles out of the matrix, the apparent binding capacity of amorphous carbohydrates is diminished rapidly as $T-T_g$ is increased. At temperatures around T_g + 50°C, crystallisation will cause the complete expulsion of all organic volatiles. Volatile loss leads to the dilution of flavour and aroma in foods and degrades the perceived quality of the product. Below T_g, the rate of release of organic volatiles is so low as to be unmeasurable[92].

6.3 Determination of T_g using T_1 and DSC measurements

6.3.1 Sample preparation and investigations of moisture content hysteresis

Spin-lattice relaxation time measurements were performed on a series of moisture-containing amorphous lactose powders. Spray-dried amorphous lactose powder was manufactured in a pilot plant located at the New Zealand Dairy Research Institute (NZDRI). Drying conditions are listed in Appendix 8. The powders were hermetically sealed in aluminium foil bags and stored at 4°C.

The dependence of T_g on moisture content (MC) was investigated by preparing a range of amorphous lactose powders containing 0-5 % (w/w) moisture. In this narrow composition range, T_g varies linearly[13] with MC. Powder samples weighing about 20 g were distributed to five vacuum desiccators maintained at various relative humidities (RH) and equilibrated for 3 weeks (equilibrated to constant weight) at 15 ± 4°C. Powder samples were stirred twice during this period to reduce MC inhomogeneity. Humidity levels were maintained by using the saturated salt solutions listed in Table 6.1

Table 6.1 Relative humidity (RH) of lactose equilibrated over saturated salt solutions expressed as the water activity (A_w) measured on a model N4 Novasina water activity meter (at equilibrium $RH = A_w \times 100\%$)

Salt solution	Expected A_w	Measured A_w
P_2O_5	0.00	a
LiCl	0.11	0.149
CH_3COOK	0.22	0.224
$MgCl_2$	0.33	0.324
K_2CO_3	0.44	b

a Unmeasurable
b Partial crystallisation of lactose occurred at this water activity

The discrepancy in A_w for lactose equilibrated over LiCl remains unexplained, with further equilibration for 2 weeks demonstrating no measurable change in A_w.

Many hygroscopic materials exhibit hysteretic moisture absorption/desorption behaviour. Lactose exhibits a hysteresis envelope which can give MC differences of the order of 1% w/w for powders equilibrated by converging pathways[94]. This hysteresis behaviour was investigated by subjecting lactose powders to stepwise changes in humidity levels, and observing changes in MC after equilibration. Powder samples were equilibrated at 0.00 A_w and 0.33 A_w for 3 weeks, redistributed to the 0.11 A_w and 0.22 A_w desiccators and then equilibrated for a further 3 weeks. The results of MC and A_w measurements are presented in Figure 6.3.

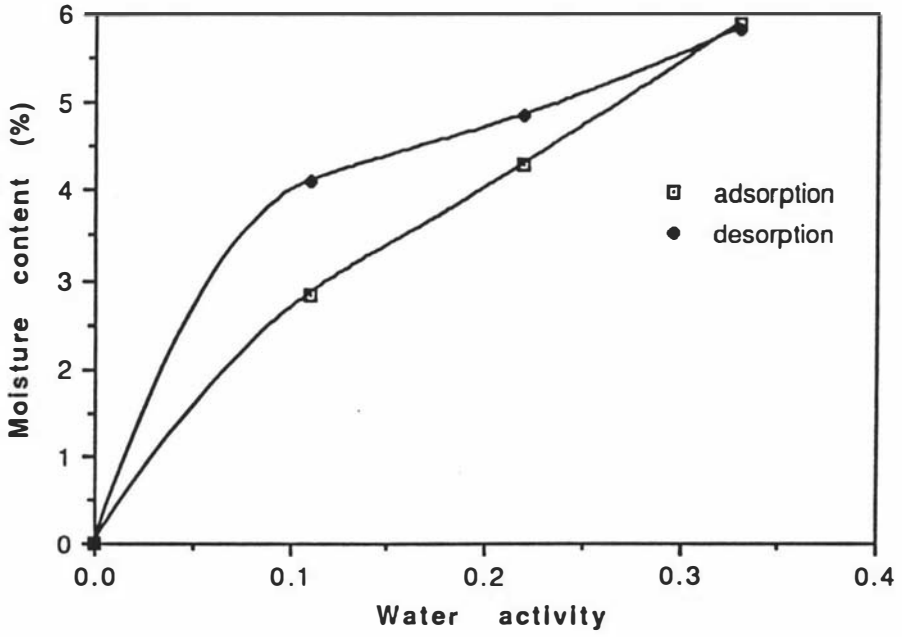

Figure 6.3. Adsorption/desorption isotherm for amorphous lactose at room temperature (15 ± 4 °C).

It can be seen that convergence occurred at 0.33 A_w as the powders were not subjected to higher humidities because of the crystallisation potential at ambient temperatures. Around 0.11-0.22 A_w, MC hysteresis of the order of 1% w/w was observed.

The existence of temperature gradients across powder particles or the bulk powder generally causes diffusion of moisture from high to low temperature regions[95]. An isolated powder mass that is subject to a transient RH (Figure 6.3) or temperature gradient, or a transient admixture of both, will ultimately equilibrate to uniform RH. Such conditions are likely to lead to MC heterogeneity, in which case the powder will exhibit a distribution of T_g values. In preliminary DSC and T_1 experiments, temperature cycling of the powder prior to measurement appeared to subdue the discontinuities expected around the glass transition temperature. This result was credited to MC heterogeneity formation during moisture equilibration. Consequently, the following modifications were carried out to reduce the effects of MC heterogeneity.

All lactose powders produced by spray drying were initially dehydrated to 0.00 A_w and rehydrated to the desired water activity. In addition, equilibration was carried out under temperature controlled conditions (20 ± 0.2°C). As a result of these changes, T_1 measurements demonstrated improved sensitivity to the glass transition.

6.3.2 The DSC method

The DSC method is used to detect the glass transition by determining the temperature at which the specific heat capacity undergoes a stepwise discontinuity[81]. The method measures the enthalpy required to heat a few milligrams of material under a linearly increasing temperature program with reference to an empty chamber. The differential that appears at the output is due to enthalpy changes of the material as a function of temperature.

Measurements were performed on a model DSC7 Perkin-Elmer differential scanning calorimeter fitted with a nitrogen-purged dry box and subambient temperature attachment. Lactose samples weighing 20-30 mg were hermetically sealed in stainless steel pans and scanned from 25 to 160°C at a rate of 5°C/min. Stepwise enthalpy transitions were investigated for reversibility by temperature cycling the lactose sample. Typical twin scans are presented in Figure 6.4.

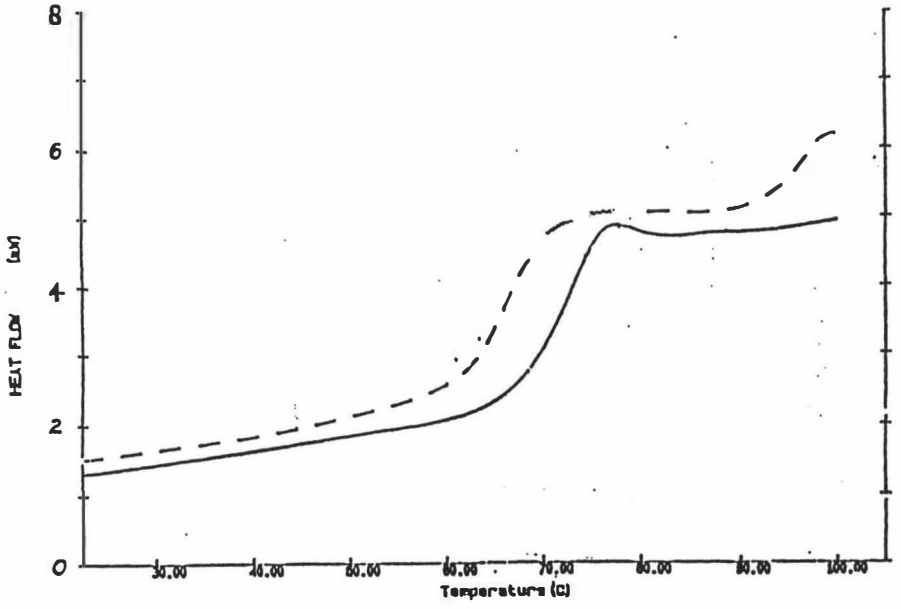

Figure 6.4. The result of repeated DSC scans at an increasing temperature rate of 5°C/min. The superposability of the scans confirms the transitions as glass transitions. In this and all subsequent thermograms, the vertical axis corresponds to endothermic heat flow.

Despite a small displacement to higher temperature (possibly due to dehydration), the transition was reversible. The fact that the transition extended over several degrees is partly to do with the time-dependence of the glass transition phenomenon[76]. The endothermic overshoot is thought to be caused by structural rearrangement, because of higher molecular mobility above T_g, or alternatively by stress relaxation[33]. As the overshoot effect occurs at $T > T_g$, it is assumed that these processes have a negligible effect on the determination of T_g from such a thermogram.

T_g is determined arbitrarily by two simple methods. The first-derivative methodology[33], as the name implies, calculates the first derivative and determines T_g at the point of steepest slope. This method provides excellent sensitivity to the subtle endothermic shifts that typically occur in multi-component systems where sudden enthalpy deviations due to a glass transition can be strongly buffered by other enthalpic changes within the sample. In lactose powders, where the endothermic shift is well defined, the mid-point methodology[33] provides a simple, reproducible estimate of T_g. This method finds the point on the endothermic transient that lies midway between the extrapolated baselines preceding and following the discontinuity. Reference to Figure 6.6 provides a clear understanding of the method.

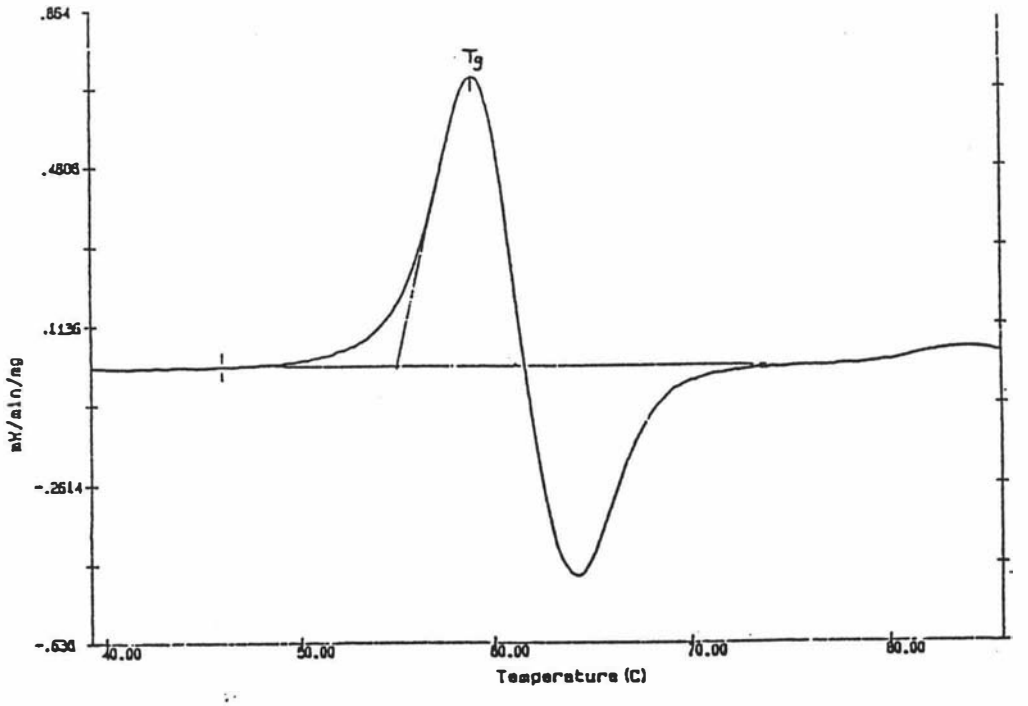

Figure 6.5. Determination of Tg using the first-derivative method.

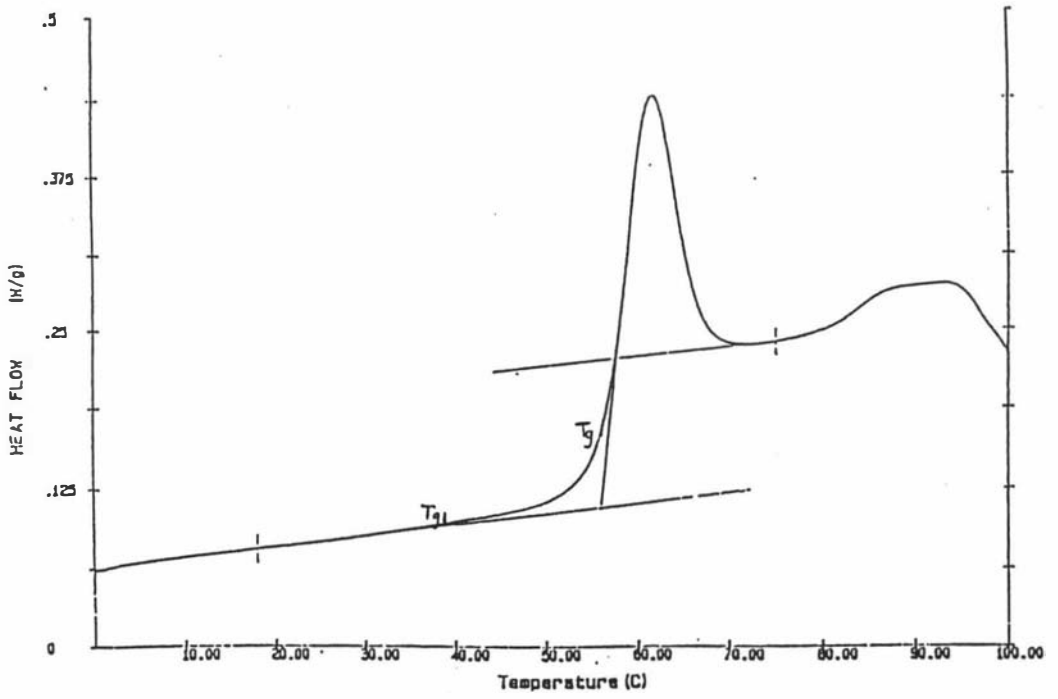

Figure 6.6. Determination of Tg using the "mid-point" method.

The five lactose powders previously equilibrated over saturated salt solutions were analysed by DSC and the T_g was determined. Triplicate determinations provided an estimate of the errors associated with the method. Typical thermograms of each sample are presented in Figure 6.7, and glass transition temperatures determined by the mid-point method are given in Table 6.2. An estimate of the onset glass transition temperature, T_{g1}, was determined at the onset of the endothermic deviation.

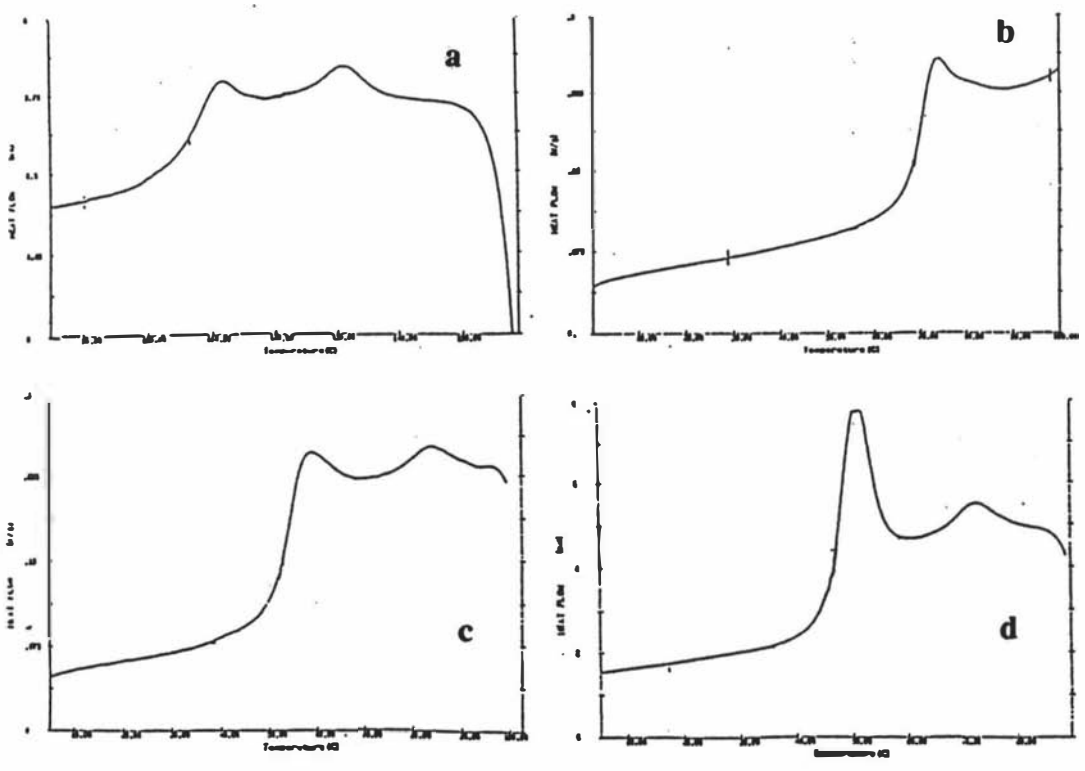

Figure 6.7. **Typical DSC thermograms of amorphous lactose equilibrated to a; 0.0 Aw, b; 0.11 Aw, c; 0.22 Aw, d; 0.33 Aw.**

Table 6.2. Glass transition temperatures determined by the DSC mid-point method

Sample	Glass transition temperature/°C	
	T_{g1}	T_g
0.00 A_w	85 ± 5	101 ± 5
0.149 A_w	60 ± 5	72 ± 5
0.224 A_w	40 ± 5	53 ± 5
0.324 A_w	30 ± 5	45 ± 5

6.3.3 The T_1 method

Spin-lattice relaxation time measurements were carried out on the five amorphous lactose powders equilibrated in the MC range of 0-5% w/w. The experimental protocol has been described in Chapter 4. Temperature control was achieved using a water-jacketed 7.5 mm probehead and closed circuit circulation system connected to a model N4 HAAKE water bath containing a 50:50 water:glycol mixture. The available temperature range was 0-100°C and stability was better than 0.2°C as determined with a calibrated mercury thermometer.

Temperature control of the sample in the probehead was achieved by heat radiation from the water jacket located outside of the NMR receiving coil. As the rate of heat transfer was limited, temperature changes were undertaken gradually so as not to introduce appreciable temperature hysteresis into the system. Amorphous samples were removed from the desiccator immediately prior to measurement and were hermetically sealed in the 7.5 mm NMR tubes.

Relaxation time measurements were performed at 5°C intervals over a temperature range spanning the expected T_g from DSC measurements. Inversion of data to the relaxation time domain (T_1) was achieved using the LH algorithm constrained to fit 95 logarithmically distributed relaxation time components from 0.02 to 1.0 s. T_1 measurements were performed in duplicate at each designated temperature. All T_1 spectra exhibited monoexponential relaxation according to the LH algorithm. Typical T_1 vs temperature graphs are presented in Figure 6.8.

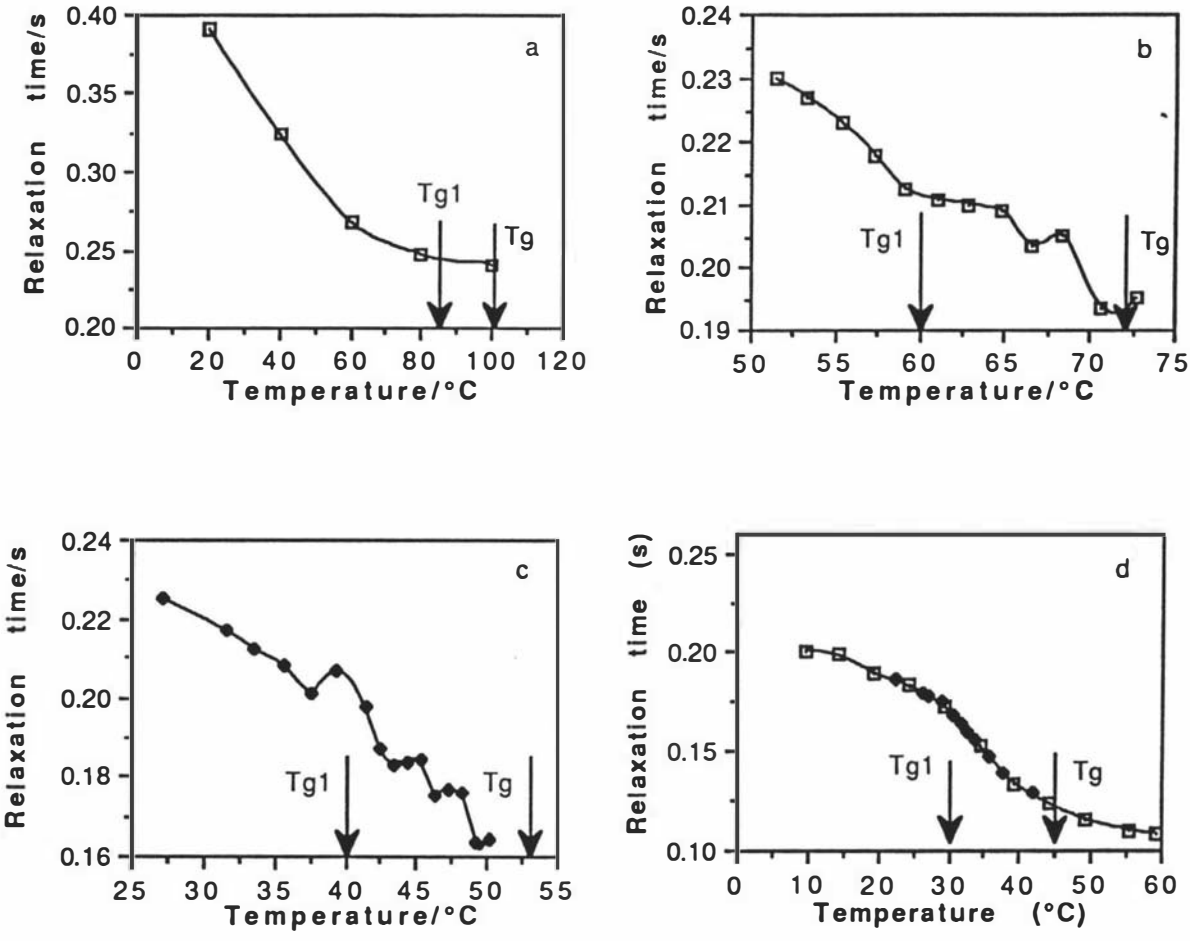

Figure 6.8. Spin-lattice relaxation time spectra for amorphous lactose experiencing a glass transition. The T_g and T_{gl} values determined using DSC are shown. Powders exhibited a water activity of **a** 0.00 A_w, **b** 0.149 A_w, **c** 0.224 A_w, **d** 0.324 A_w.

The sample equilibrated to 0.00 A_w exhibited a smooth descent towards an apparent T_1 minimum. The onset of glass transition (85°C) was not detected. Figures 6.8b to 6.8d show departure from the smoothly varying T_1 baseline at temperatures that broadly correspond with DSC determinations of T_{gl}. The low moisture samples (0.149 and 0.224 Aw) exhibited an initial positive departure followed by fluctuation, whereas the high moisture sample demonstrated a smooth negative descent reminiscent of an inverted DSC enthalpic discontinuity. The T_{gl} was determined at the point of initial deviation away from the smoothly varying temperature-dependent change in T_1. It was noted that the oscillatory behaviour shown in Figures 6.8b and 6.8c appeared to be time dependent because repeat measurements using reduced temperature increments resulted in a change in oscillatory behaviour. It was difficult, therefore, to increase the density of measuring points to obtain a more detailed analysis of these oscillations. By contrast, the high moisture sample (Figure 6.8d) demonstrated good reproducibility when measurements were repeated at smaller incremental spacings.

6.3.4 Comparison of DSC and T_1 measurements

A comparison of T_{g1} determinations from DSC analysis and T_1 measurement is presented in Table 6.3. Experimental error was calculated from the 95% confidence interval for duplicate determinations. All T_{g1} results agreed within the experimental error.

Table 6.3 A comparison of DSC and T_1 value determinations of the onset glass transition temperature of amorphous lactose

	Onset glass transition temperature, T_{g1}/°C	
Sample	DSC	T_1 measurement
0.0 A_w	85 ± 5	-
0.149 A_w	60 ± 5	58 ± 5
0.224 A_w	40 ± 5	37 ± 5
0.324 A_w	30 ± 5	30 ± 5

6.4 Determination of the crystallisation temperatures (T_c) by T_1 value analysis and DSC measurement

6.4.1 Background

Solid state crystallisation of amorphous lactose is time dependent[84]. As in solution, the rate-limiting step is the rate of diffusive encounter which, in turn, is determined by local molecular viscosity[69]. As the viscosity of amorphous materials is strongly temperature dependent, it is not surprising that crystallisation kinetics are also strongly temperature dependent. Roos and Karel[13] have demonstrated that the temperature-time interdependence of lactose crystallisation (and other amorphous carbohydrate materials) is closely approximated by the WLF equation alluded to in Section 6.2.2, and restated here as

$$\log\frac{\phi_{CR}}{\phi_g} = \frac{C_1^g\left(T - T_g\right)}{C_2^g + \left(T - T_g\right)} \qquad [6.5]$$

where ϕ_{CR} and ϕ_g are the relaxation times of crystallisation at temperatures T = T and T = T_g respectively. The relaxation time of crystallisation of amorphous lactose at T = T_g is of the order of 4600 years[13] and converges to zero time at temperatures around T_g + 50°C. The temperature at which crystallisation is instantaneous is defined as the crystallisation temperature, T_c. In practice, T_c(measured) < T_c(true) because crystallisation will be initiated at temperatures below T_c(instantaneous). The onset of crystallisation and the determination of T_c

will therefore depend on the rate of temperature increase, which itself may be a function of the methodology used to detect crystallisation, as indicated in later experiments.

6.4.2 Sample preparation

Sample preparation was as previously described in Section 6.3.1 with the addition of an extra sample equilibrated over K_2CO_3 (A_w = 0.44) and maintained at 10°C to inhibit crystallisation.

6.4.3 The DSC method

Crystallisation is readily detected by DSC as an intense and well-defined exothermic release of crystallisation enthalpy[13,84] (Figure 6.9) that extends over a finite temperature range. As crystallisation is time dependent, T_c is usually taken at the point at which the enthalpy initially deviates away from the baseline.

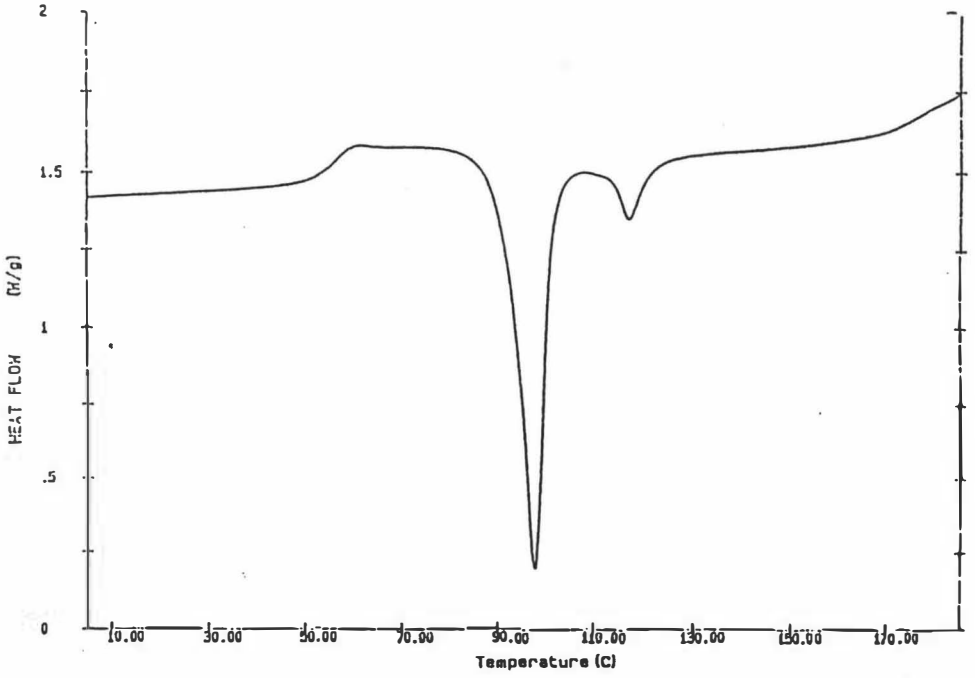

Figure 6.9. A typical DSC thermogram illustrating the intense exotherm produced at the crystallisation of amorphous lactose.

DSC measurements of all powders were performed from 25 to 140°C at a rate of 5°C/min. DSC scans were obtained in duplicate, and experimental error was estimated from the range of T_c values. T_c determinations are presented in Table 6.4.

Table 6.4 Crystallisation temperatures of amorphous lactose powders as determined by DSC

Sample number	Measured water activity ($\pm$ 0.001 A_w)	Crystallisation temperature (°C)
1	0.149	118 ± 4
2	0.224	100 ± 4
3	0.324	90 ± 3
4	0.382	75 ± 3

6.4.4 The T_1 method

The onset of crystallisation is readily detected from the appearance and subsequent growth of relaxation time components longer than 1 s (Noting that all crystalline relaxation times from Chapter 5 were longer than 1 s). The relaxation time value may also be used to determine the particular crystalline species (Table 5.2). The experimental protocol used to measure the moisture-equilibrated amorphous powders was modified from previous T_g-T_1 experiments. To sample the large range of relaxation times, delay t was logarithmically varied from 0.02 to 50 s. T_1 experiments were performed at 5°C intervals from 20-30°C to 100°C and an average temperature scan was completed in approximately 2 h. Data inversion to the relaxation time domain was achieved with the LH algorithm and T_1 components were constrained between 0.02 and 50 s. Typical T_1 versus temperature plots are collectively presented in Figure 6.10 and T_c determinations are presented in Table 6.5.

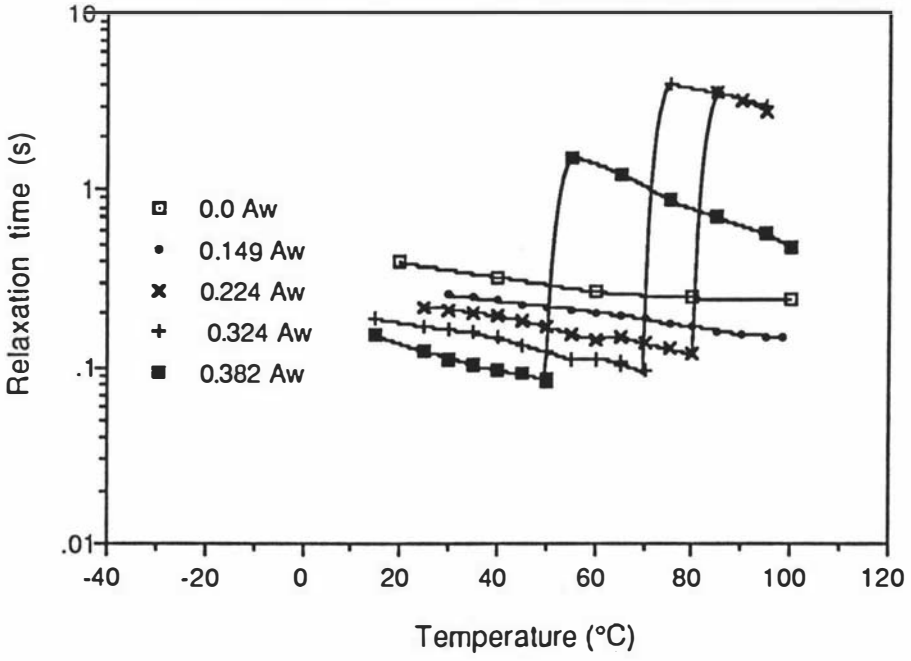

Figure 6.10. Detecting crystallisation of amorphous lactose by the change in T_1 value.

Table 6.5 The crystallisation temperature of several amorphous lactose powders determined by spin-lattice relaxation time measurement

Sample number	Measured water activity (± 0.001 A_w)	Crystallisation temperature (°C)
2	0.224	83 ± 3
3	0.324	74 ± 3
4	0.382	52 ± 3

T_c values determined by T_1 value measurement correspond (on average) to T_g(DSC) - 20°C. For identical powders, the T_1 methodology gives T_c values 20°C lower than those obtained by DSC. As the effective rate of temperature increase for T_1 measurements is 0.67°C/min (due to the slowness of measurements), the time dependence of crystallisation means that crystallisation will occur at a lower temperature for NMR.

The different relaxation times for crystalline products formed at low temperature suggest the formation of different crystalline species. Extrapolation to 40°C gives relaxation times of 3 s and 9 s respectively, which correspond to the relaxation times of alpha lactose monohydrate and

beta lactose determined in Chapter 5. This conclusion is supported by polarimetric measurements.

Vuatez[97] showed that crystallisation of lactose in milk powder yielded beta and alpha monohydrate crystalline forms at correspondingly low and high temperatures respectively. In conjunction with these results, a phase diagram that outlines the interrelation of temperature, moisture and the crystalline product has been established (Figure 6.11). The phase boundaries are only approximate.

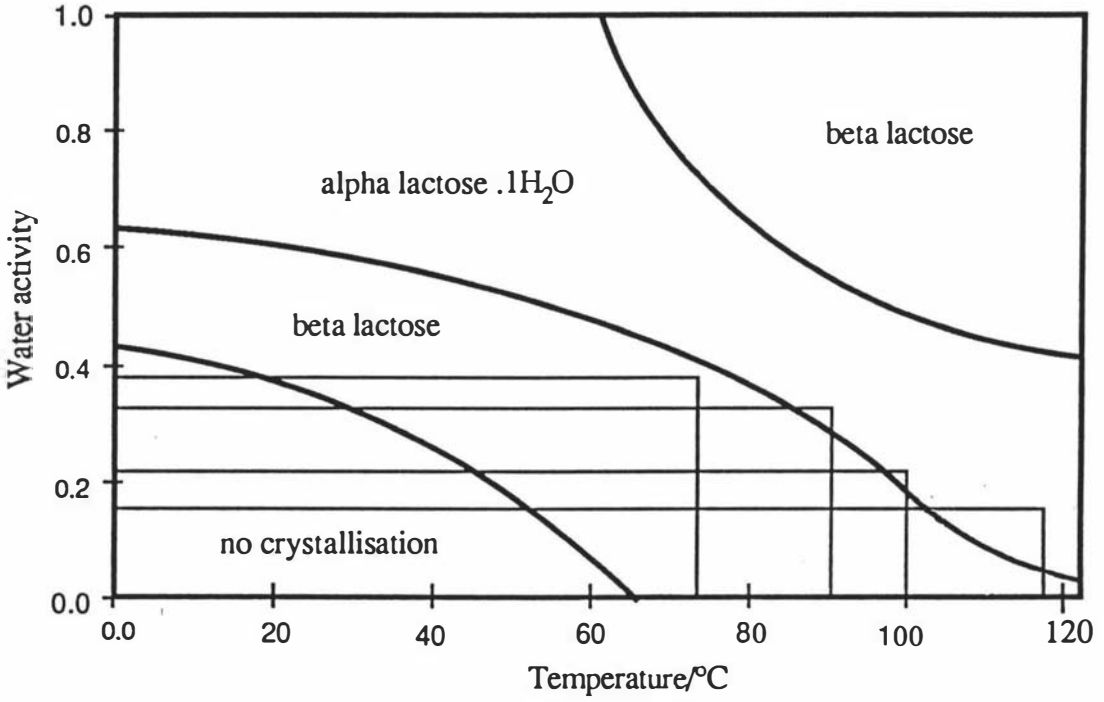

Figure 6.11. Schematic phase diagram representing the temperature-moisture dependence of the product of amorphous lactose crystallisation. The product of crystallisation for each of the four samples (0.149, 0.224, 0.324 and 0.382 A_w) is found at the intersection with the crystallisation temperature.

The region of inhibited crystallisation is clearly evident. The high moisture-high temperature phase boundary, where beta lactose is formed, was not crossed during the crystallisation experiments reported here. Vuatez demonstrated that crystallisation on a phase boundary allowed the interconversion of crystalline species in the solid state[97].

6.5 Summary

The use of spin-lattice relaxation time measurement to detect the glass transition and crystallisation and to quantify both offers no significant advantage over the presently used DSC methodology. The T_1 methodology allows the determination of the water content of amorphous samples (Figure 6.8) and of the product of crystallisation. However, this is easily and accurately determined by polarimetry in most cases. T_g determination by T_1 value analysis

was difficult because of the subtlety of the T_1 discontinuity, which competed with experimental noise. The determination of a rotating frame relaxation time, $T_{1\rho}$, may provide increased sensitivity to the glass transition process since relaxation rates are sensitive to motions corresponding to the frequency of the rotating frame which is typically in the range of several kHz. This frequency window may provide enhanced sensitivity to the changing mobility and correlation times of the nuclear relaxation sites at the glass transition.

7. Determination of the crystallinity of lactose and lactose-containing powders

7.1 Introduction

In isolation, the state of amorphous lactose may be accurately characterised and it's future behaviour predicted from the measurement of moisture content (MC) and water activity (A_w), and/or from the determination of the glass transition temperature (T_g) of the powder[13,72,73,81,83,84,91]. Long term stability may be achieved by keeping moisture levels and storage temperatures sufficiently low that the powder is maintained in the glassy state[83]. By contrast, pure crystalline species (disregarding anhydrous forms) are less affected by the elevated humidity and temperature levels commonly encountered during storage. Provided that humidity levels are maintained below 80-90% (condensation and dissolution of the crystalline surface occurs at 85-100% RH[98]), crystalline lactose may be stored indefinitely without the caking, sticking and crystallisation problems encountered with amorphous lactose under similar conditions.

Commercial methods of powder manufacture do not necessarily yield a purely amorphous or crystalline product. The slower rate of drying encountered by larger powder particles during spray drying may allow partial crystallisation of lactose, and the drying and milling processes used during the manufacture of alpha lactose monohydrate are believed to produce a surface coating of amorphous lactose[81]. Because powder particle interactions are dominated by surface effects, it is predicted that the inclusion of relatively minute quantities of contaminating lactose can cause a significant change in powder properties. Incorporation of lactose crystals into spray-dried amorphous lactose and milk powder is believed to be responsible for reducing the storage qualities and lowering the rate of solubility in water, and the subsequent moisture absorption and crystallisation of the amorphous layer resident on alpha lactose monohydrate crystals is assumed to be responsible for sticking and caking problems encountered with some batches.

In this chapter, spin-lattice relaxation time measurements are used to determine the ratio of crystalline to amorphous lactose in a range of prepared lactose powders and the limit of sensitivity is investigated. The developed methodology is applied to a range of commercially produced milled crystalline lactose samples in an attempt to detect amorphous contaminants and to caked milk powder samples to detect the occurrence of lactose crystallisation.

7.2 Sample preparation

Samples were prepared by mechanically hand blending alpha lactose monohydrate and spray-dried amorphous lactose (manufactured at the New Zealand Dairy Research Institute (NZDRI))

to a composition ranging from 0 to 100% w/w (crystalline basis) and a total weight of approximately 50 g. Samples were stored over P_2O_5 at 4°C until required for measurement.

7.3 T_1 measurements and crystallinity determination of pure lactose powders

7.3.1 Measurements

Initial relaxation experiments were performed at a temperature of 40°C using the 10 mm probe, to maximise the signal:noise ratio. As crystallisation was observed for some samples (see Section 7.3.2), subsequent measurements were performed at 20°C. The experimental protocol for T_1 measurement has been described previously (Section 4.3). Raw relaxation decay data were corrected for drift and offset as previously described. One hundred logarithmically distributed relaxation points were measured with τ varies from 0.02 to 20 s (Figure 4.4), and data inversion was performed using the LH algorithm constrained to fit relaxation time components at 0.25 s and 3.5 s, corresponding to T_1 amorphous (0% moisture at 20°C) and T_1 alpha monohydrate (20°C) respectively. Crystallinity was determined by the ratio

$$crystallinity = \frac{crystalline\ amplitude}{crystalline + amorphous\ amplitude} \qquad [7.1]$$

The effect of inaccuracy of the assumed relaxation time values on the crystallinity values of powders is discussed in Appendix 9.

7.3.2 Results and discussion

The results of crystallinity determinations performed at 40°C are presented in Table 7.1. The "known" crystallinity was estimated from the weight fractions of the amorphous and crystalline components, assuming each to be 100% pure.

As indicated, the sensitivity to concentrations of amorphous lactose below 10% was extremely poor, contrasting strongly with the excellent sensitivity to low concentrations of crystalline lactose (better than 2%). There are two possible explanations for this anomaly. It is feasible that dilution of amorphous material by crystalline lactose in conjunction with unintentional absorption of ambient moisture by the amorphous fraction during sample preparation, storage and measurement may depress T_c sufficiently that crystallisation occurs at or below 40°C. This would cause a reduction in the weight fraction of amorphous lactose, or, in extreme cases, complete loss from the sample altogether.

Table 7.1 Crystallinity of prepared lactose powders determined by equation [7.1] and gravimetric analysis (NMR measurements were performed at 40°C).

Sample number	Estimated crystallinity (±0.05%)	Measured crystallinity (%)
1	0.0	0.0 ± 0.0
2	2.0	1.8 ± 0.1
3	5.1	4.8 ± 0.5
4	9.7	8.9 ± 0.4
5	50.8	49.3 ± 1
6	90.1	93.7 ± 1
7	95.1	100 ± 0
8	98.1	100 ± 0
9	100.0	100 ± 0

Alternatively, it may be an artefact of the methodology that the sensitivity to dilute amorphous components is naturally poor. The rationale for this idea is based on the fact that dilute amorphous signals decay relatively quickly and are therefore absorbed by the background noise level of the decay curve more rapidly than an equally dilute crystalline component which decays slowly and is consequently detected by a greater number of measuring points. In such cases, concentration of measuring points around the "amorphous region" of the decay curve may increase the sensitivity (this is investigated later).

To investigate the sensitivity of the LH algorithm to dilute short T_1 components, a simulated data set was constructed matching a lactose sample of 95% crystallinity. Two exponential decay components of relaxation time 0.25 s and 3.5 s respectively were coadded in the amplitude ratio of 5:95, corrupted with 3% mean deviation Gaussian noise and inverted to the relaxation time domain using the LH algorithm configured as previously described. The result (Figure 7.1) indicates good sensitivity and relatively accurate quantitative interpretation. Furthermore, it adds support to the idea that sensitivity may in fact be limited by amorphous crystallisation prior to and possibly during measurement.

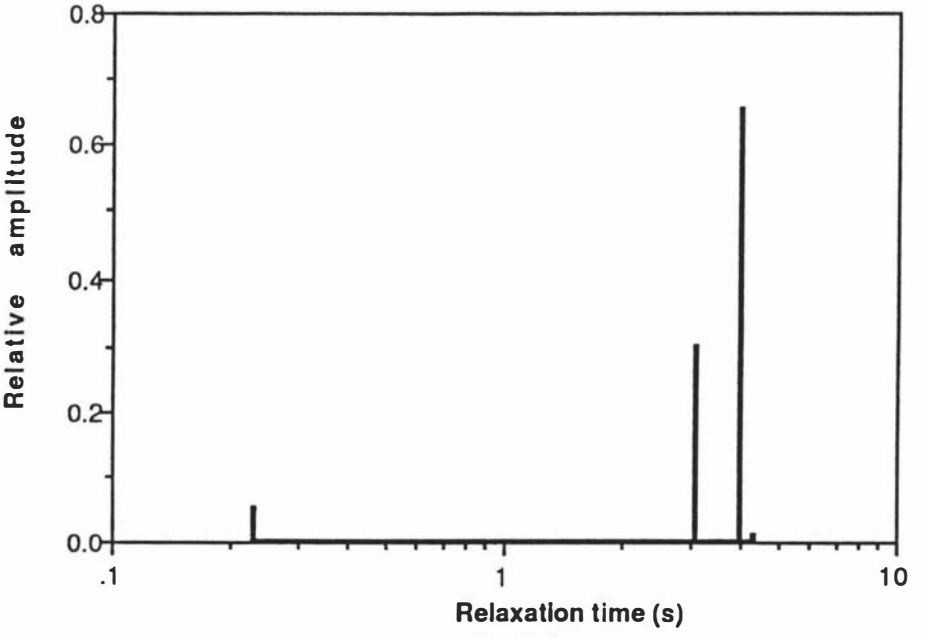

Figure 7.1. LH relaxation time components of simulated relaxation data corresponding to a lactose sample of 95% crystallinity. The 0.22 s component has a relative amplitude of 4.8%.

Table 7.2 Crystallinity of prepared lactose powders determined by Equation [7.1] and gravimetric analysis (NMR measurements were performed at 20°C).

Sample number	Estimated crystallinity (±0.05%)	Measured crystallinity (%)
1	0.0	0 ± 0
2	2.0	1.9 ± 0.2
3	5.1	4.6 ± 0.6
4	9.7	9.1 ± 0.6
5	50.8	55.2 ± 1
6	90.1	89.7 ± 1
7	95.1	97.0 ± 2
8	98.1	100 ± 0
9	100.0	100 ± 0

Crystallisation of the amorphous component was investigated by changing the measurement temperature from 40°C to 20°C. The results of measurements at 20°C are presented in Table 7.2.

The improvement in sensitivity to dilute amorphous lactose is consistent with a reduction (or elimination) of crystallisation as a result of the lower measurement temperature. Still lower temperatures are possible, but this lengthens the relaxation times, and therefore the duration of an experiment. As the relaxation time method is being promoted as an analytical method, further depression of the measuring temperature is not appropriate. The alternative is to elevate T_c of the amorphous component simply by desiccation. Amorphous lactose was desiccated over P_2O_5, weighed into glass capillary tubes which were sealed, and surrounded with pure crystalline alpha lactose monohydrate in an NMR tube. Three samples were prepared in the crystallinity range 90-98% and measurements were performed in duplicate at 20°C (see Table 7.3).

Table 7.3 Crystallinity determined with physical separation of the amorphous and crystalline lactose phases

SAMPLE NUMBER	ESTIMATED CRYSTALLINITY/%±0.05%	MEASURED CRYSTALLINITY
1	88.7	88.5 ± 1%
2	95.6	96.0 ± 1%
3	97.9	100 ± 0%

It is clear that the sensitivity is now limited by factors other than crystallisation. Possibilities include masking of the weak amorphous signal by random noise (mean = 0.25%) and limited sensitivity of the LH inversion algorithm to weak components. To improve the detection sensitivity, the measuring sequence was altered to concentrate measuring points about the "amorphous region" (10-500 ms) of the relaxation decay curve. Fifty points were distributed logarithmically between 10 and 500 ms and a further 50 points were distributed logarithmically between 3 and 35 s. Measurements were performed in triplicate on gravimetrically prepared powders containing approximately 4, 2, and 1% w/w amorphous lactose. The results are presented in Table 7.4.

Table 7.4 Crystallinity determined with concentration of measuring points between τ = 10 and 500 ms

Gravimetric composition (±0.05%)	Crystallinity by NMR (%)
96.0	94 ± 4
98.0	99 ± 1
99.0	100 ± 0

The results indicate a marginal improvement in sensitivity and a marked decrease in reproducibility. Further improvement is probably limited by the present noise level (0.25%). As this increases at the rate of $N^{1/2}$, where N is the number of coadded signal acquisitions, this approach provides a very inefficient means of improvement. However, as it is the amplitudes of relaxation time components, and not the relaxation time values, that are of importance, it is possible to reduce the number of measuring points substantially with little or no loss of information. This approach is invoked by the "three-point" methodology.

7.3.3 The three-point methodology

At time t = 0 (or close to t = 0), the amplitude of the inversion recovery signal is described by (from Equation [4.17]):

$$M(t=0) = M_0\left[A_{am} + A_{cr}\right] \qquad [7.2]$$

where A_{am} and A_{cr} represent the amplitude of amorphous and crystalline regions respectively. The NMR signal after a delay greater than five times $T_{1amorphous}$, say 1.5 s is

$$M(t=1.5) \approx M_0\left[A_{cr}\left(1-2\exp\left(-1.5/T_{1cr}\right)\right)\right] \qquad [7.3]$$

and after a long delay allowing complete decay of the crystalline and amorphous signals, say 35 s, M(t) will be

$$M(t=35) = M_0 \qquad [7.4]$$

The crystallinity of the measured sample may be determined by combining Equations [7.2], [7.3], and [7.4] and with T_{1cr} accurately known (6.4 s at 20 °C):

$$X_{cr} = \frac{1}{\exp[-1.5/6.4]}\left[\left[M(t=35)-M(t=1.5)\right]/\left[M(t=35)-M(t=0)\right]\right] \qquad [7.5]$$

where X_{cr} is the relative crystallinity. Measurements were performed in triplicate on a series of freshly prepared lactose powders. The results are given in Table 7.5.

Table 7.5 Crystallinity of a series of lactose powders determined by the "three-point" method

"Known" crystallinity	Measured crystallinity (%)	Standard deviation
90	90.3	0.2
95	95.5	0.2
98	98.2	0.2
99	98.7	0.3
99.5	99.3	0.03
100	100.0	0.03

The results of Table 7.5 demonstrate a substantial improvement in sensitivity (better than 0.5%) and good reproducibility (better than 0.3%). Furthermore, the time required for a single analysis was reduced from several hours to 30 min.

7.4 Detection of contaminating lactose in crystalline alpha lactose monohydrate and spray-dried milk powder

The detection sensitivity of the "three-point" methodology to contaminating amorphous lactose in alpha lactose monohydrate and crystalline lactose in fresh spray-dried milk powder is now described. Milk powders that had exhibited caking after storage in humid conditions were also analysed for lactose crystallisation.

7.4.1 Sample preparation

Fresh whole milk powder was heated to 50°C for 3 h over a saturated K_2CO_3 solution to promote partial crystallisation of the amorphous fraction. Other whole milk powder samples were stored for several months at ambient temperature and humidity to invoke caking. Caked powders were sampled using a 7 mm diameter core borer. Refined lactose powders were supplied by Lactose New Zealand and transported to the NZDRI in sealed aluminium foil bags at ambient temperature. It was assumed that little or no change in composition occurred during transport[98]. Spray-dried whole and skim milk powder was supplied by the NZDRI. All powder samples were packed in 7.5 mm NMR tubes to a height of 35-40 mm.

7.4.2 Measurements

Multiexponential relaxation measurements were performed on whole milk powder to determine the relaxation times of the fat, protein and lactose constituents. One hundred relaxation time data points were measured from τ = 0.02 to 20 s, and data inversion was achieved using the LH algorithm constrained to fit 95 components from 0.02 to 20 s. Measurements were performed at 20°C.

Crystallinity determinations were performed by the "three-point" method at 20°C. All crystalline material contained in the lactose samples was assumed to be alpha lactose monohydrate with a relaxation time of 6.4 s. Crystalline material contained in the milk powder was assumed to be beta lactose with a relaxation time of 1.8 s (Figure 7.2). The relaxation time expressed by the amorphous fraction is not significant to crystallinity determinations. The amplitude of the decay curve was determined at τ = 0.01, 2 and 35 s for the milk powders (see section 7.4.3) and τ = 0.01, 1.5 and 35 s for the lactose powder samples.

7.4.3 Results and discussion

The relaxation time spectrum of caked whole milk powder is presented in Figure 7.2.

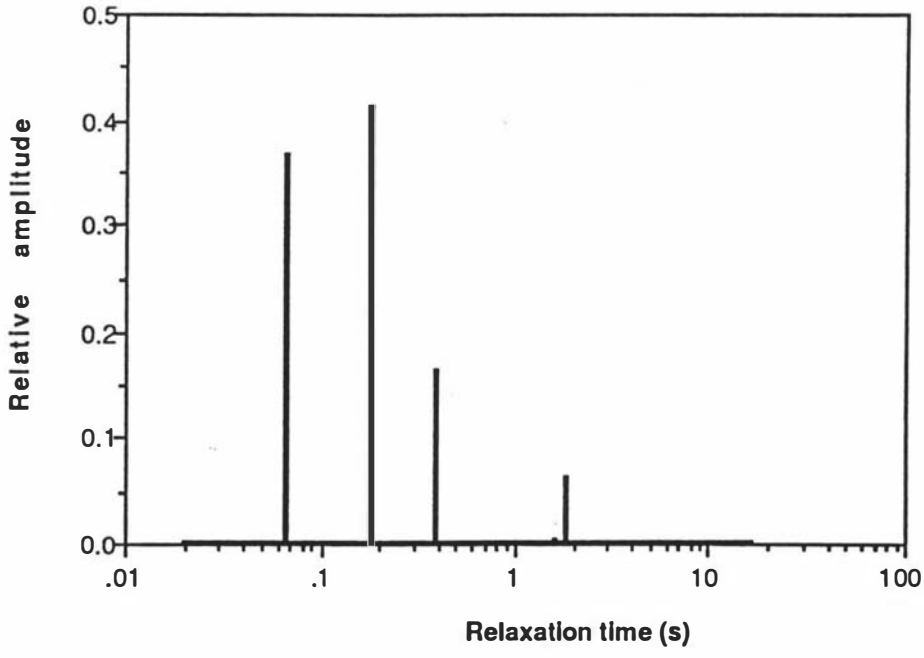

Figure 7.2. Spin-lattice relaxation time spectrum of caked whole milk powder. Caking was induced by heating a sample of standard whole milk powder to 50 °C over saturated K_2CO_3 for 3 hours. The component around 2 s is attributed to crystalline lactose (assumed to be beta lactose).

The relaxation time components at 0.07, 0.2 and 0.4 s correlate with the fat, protein and amorphous lactose constituents of the sample. The relaxation component at 1.8 s is consistent with the formation of crystalline beta lactose at 50°C and 44% RH (Section 6.4.4).

The results of crystallinity determinations of the lactose powders and caked amorphous lactose and milk powders are presented in Tables 7.6 and 7.7 respectively.

Table 7.6 Crystallinity determinations of lactose supplied by Lactose New Zealand

Sample	Crystallinity by NMR (%)	Increase in amorphous content (%)
Drier feed	-	
Drier discharge (main)	98.7	-
Drier discharge (fines)	99.1	-
ACM mill feed	99.4	
ACM mill discharge	98.1	1.3
BM1 mill feed	99.5	
BM1 mill discharge	97.8	1.7
BM2 mill feed	99.5	
BM2 mill discharge	97.1	2.4
Final product	96.9	

All the lactose powders in Table 7.6 demonstrated contamination by amorphous lactose. There was a consistent increase in the amorphous content across the three milling stages, which agrees with the findings of others[15]. The amorphous lactose and caked milk powder samples showed no significant crystalline contamination. Interestingly, lumps discovered in the spray-dried amorphous lactose had a high crystallinity. They accounted for less than 0.5% of the total amorphous powder.

Table 7.7 Crystallinity determinations of lumped powders and fresh spray-dried amorphous lactose

Sample	Measured crystallinity (%)	Standard deviation
Whole milk powder lumps/Site #1	0.0	0.3
Whole milk powder lumps/Site #2	0.0	0.3
Skim milk powder lumps/Laboratory	0.2	0.4
Chocolate powder lumps/Laboratory	0.1	0.2
Spray-dried lactose powder	0.0	0.4
Lactose lumps (> 500 μm)	95	0.6

7.5 Summary

The characterisation of a binary mixture of amorphous and crystalline lactose on the basis of differences in the spin-lattice relaxation times may be achieved by two methods. The multiexponential approach measures the spectrum of relaxation times and sample composition may be easily determined from the relative amplitudes of the relaxation time components. The relaxation time of the amorphous phase gives an indication of moisture content (Figure 6.8). Where the determination of the spin-lattice relaxation time values is unnecessary, the "three-point" methodology provides improved sensitivity and reduced analysis time. This method measures three points on the relaxation curve and fits a biexponential model. Typically, ten signal-averaged three-point measurements can detect amorphous fractions more dilute than 0.5% w/w with a reproducibility of better than 0.3%, and the analysis time is of the order of 30 min. The method offers the flexibility of enhanced reproducibility through greater signal averaging. In real measurements, the three-point method detected the presence of amorphous lactose in alpha lactose monohydrate, and showed that milk powder caking is not necessarily caused by lactose crystallisation.

8. Summary

The chemical composition of lactose, which is characterised in the anomeric composition , is easily determined by solution-state methodologies such as polarimetry, gas liquid chromatography, and high-resolution ^1H NMR spectroscopy. Analysis of the anomeric composition of identical powders by each method yielded consistent results that confirmed the accuracy of all three. Polarimetry emerged as the most precise method, but is sensitive to solvation delay, sample weighing inaccuracy, and contamination of the lactose sample with optically active species. With GLC and NMR measurements, the use of a mutarotation-inhibiting solvent such as DMSO eliminates the complicating effect of solvation delay and mutarotation, and simplifies experimental procedure and calculation of the anomeric composition.

Structural differences of lactose are readily detected by measuring the NMR spin-lattice relaxation time (T_1) values. The T_1 spectra of several crystalline and amorphous species of lactose demonstrated significant spectroscopic differences that formed the basis of a new characterisation methodology. Crystalline beta lactose generally demonstrated longer relaxation times than crystalline alpha species although this was not always the case. The relaxation times of amorphous lactose were shorter than all crystalline forms by at least an order of magnitude. The spectrum of relaxation times was obtained using linear NNLS and Contin algorithms which gave repeatable and unbiased relaxation spectra despite the distorting effects of noise and drift of the inversion recovery data. The subsequent analysis of a series of mechanically blended lactose samples of varying crystallinity and anomeric composition demonstrated excellent correlation between the known composition and the relative amplitude of respective T_1 components.

The T_1 spectra of co-crystallised species of alpha and beta lactose (notably the 5:3 "mixed" crystal, and alpha lactose incorporated during crystallisation of conventional beta lactose) exhibited discrete relaxation components with a relative amplitude ratio that agreed closely with the known anomeric composition (from polarimetry). This result indicated the absence of spin-diffusion between anomeric species in the crystal which would otherwise result in amplitude distortion, or the averaging of both T_1 values to a single component. The correlation of relative T_1 component amplitudes to the weight fraction of crystalline species in co-crystallised powder samples is therefore justified from this result.

Relaxation measurements of amorphous lactose containing adsorbed moisture demonstrated a single relaxation time that varied with moisture content. The T_1 value decreased with increasing water content and temperature. A subtle T_1 discontinuity was observed around the expected glass transition temperature (T_g). In future work, it is worth considering the possible

sensitivity of a rotating-frame relaxation time ($T_{1\rho}$) as, in this case the relaxation rate is sensitive to motions corresponding to the frequency of the rotating frame which is typically in the range of several kHz. This frequency window may provide enhanced sensitivity to the changing mobility and correlation times of the nuclear relaxation sites at the glass transition.

A large T_1 value discontinuity was detected at a temperature corresponding to the onset of crystallisation (T_c) of amorphous lactose. However, because of the time-dependence of crystallisation, the T_c value determined at the T_1 discontinuity occurred some 30 °C below the T_c value determined by DSC analyses. The T_1 value after crystallisation was dependent on the product of crystallisation (alpha or beta).

Where the lactose sample consisted of a binary mixture of amorphous and crystalline lactose, a simple biexponential model was fitted to the relaxation data. In such cases, and assuming total relaxation of the amorphous phase after a time delay of 5 times $T_{1\,amorphous}$, the relative amplitude of each relaxation component was determined by measuring three points on the decay curve. This method gave improved sensitivity, and a reduced analysis time (of order 30 min). A series of test measurements on lactose and milk powders showed that this improved method detected concentrations of unwanted lactose species down to 0.5% w/w.

As a characterisation method, T_1 analysis is sensitive and accurate. The potential exists for its application in many industrial fields including lactose refining, milk powder manufacture, and general food processing where lactose is a vital ingredient. The detection and quantisation of contaminating seed crystals of lactose in milk powder and amorphous lactose would provide a basis for improvements to the drying and agglomeration stages such that lactose crystallisation is eliminated. Correspondingly, the detection of contaminating amorphous lactose during crystalline lactose manufacture would allow manufacturing parameters to be optimised with the view of eliminating this contaminating compound.

In confectionary production, the identification and isolation of lactose crystallisation during the manufacture and storage of icecream and chocolate offers the possibility of better product control and the improvement of keeping qualities. On a broader scale, the multi-exponential T_1 method of compositional analysis is applicable to other food systems where significant differences in the T_1 values exist for the food constituents of interest. A typical example is the detection and quantisation of milkfat, protein and water components of cheese and the measurement of fat melting at elevated temperatures[100]. There is evidence to suggest that the T_1 values of the various whey protein fractions contained in whey are sufficiently different that quantisation by the T_1 method is possible[101].

References

1. Pritzwald-Stegmann, B. F. (1986). *J. of Soc. of Dairy Tech.*, **39**, 91-97.
2. Nickerson, T. A. (1970). *By-products from milk,* AVI publishing company, Westport.
3. O'Donnell, J. (1991). *Dairy Foods.* **92**, 71-73.
4. Igwilo, C., and Pilpel, N. (1988). *J. Pharm. pharmacol.* **40**, 825-828.
5. Sagawa, Y. (1983). *J. Powder Tech. Jap.*, **20**, 738-743.
6. Chuy, L. T., and Labuza, T. E. (1994). *J. Food Sci.* **59**, 43-46.
7. Jouppila, K., and Roos, Y. H. (1994). *J. Dairy Sci.* **77**, 1798-1808.
8. Roos, M. (1991). *Drying '91.* Elsevier Science Publishers, Amsterdam.
9. Buma, T. J. and van der Veen, H. K. C. (1974). *Neth. Milk Dairy J.* **28,** 175-185.
10. Sharp, P. F., and Doob, H. (1941). *J. Dairy Sci.* **24**, 589.
11. Dwivedi, S. A. (1989). *J. Pharm. Sci.* **78**, 1055.
12. Susi, H. and Ard, J. S. (1973). *J. of the A.O.A.C.*, **56**, 177.
13. Roos, Y. and Karel, M. (1991). *J. of Food Sci.* **56,** No. 1, 38-42.
14. Roos, Y. and Karel, M. (1991). *J. of Food Sci.* **56,** No. 6, 1676-1681.
15. Otsuka, M., Ohtani, H., Kaneniwa, N. and Higuchi, S. (1991). *J. Pharm. Pharmacol.* **43,** 148-153.
16. Morita, M,. Nakai, Y., Fukuoka, E. and Nakajima, S. (1984). *Chem. Pharm. Bull.* **32,** 4076-4083.
17. Ruland, W. (1961). *Acta. Cryst.* **14,** 1180-1185.
18. Lerk, C. F., Andrae, A. C., de Boer, A. H., de Hoog, P., Kussendrager, K., van Leverink, J. (1984). *J. of Pharm. Sci.* **73,** 856-857.
19. Huttenrauch, R. (1978) *Acta Pharm. Technol.* **6**, 55
20. Hockett, R. C. and Hudson, C. S. (1931). *J. Am. Chem. Soc.* **53,** 4455-4456.
21. Simpson, T. D., Parrish, F. W., Nelson, M. L., (1982). *J. of Food Sci.* **47,** 1948-1954.
22. Olano, A., Bernhard, R. A., Nickerson, T. A. (1977). *J. of Food Sci.* **42,** 1066-1083.
23. Parrish, F. W., Ross, K. D. and Valentine, K. M. (1980). *J. of Food Sci.* **45,** 68-70.
24. Olano, A. and Rios, J. J. (1978). *J. Dairy Sci.* **61,** 300-302.
25. Olano, A. (1978). *J. Dairy Sci.* **61,** 1622-1623.
26. Ross, K. D., (1978). *J. Dairy Sci.* **61,** 152-158.
27. Buma, T. J. and Wiegers, G. A., (1967). *Neth. Milk and Dairy J.* **21,** 208-213.
28. Itoh, T., Satoh, M. and Adachi, S. (1977). *J. Dairy Sci.* **60,** 1230.
29. Bloembergen, N., Purcell, E. M., and Pound, R. V. (1948). *Phys. Rev.*, **73**, 679.
30. Lawson, C. L. and Hanson, R. J. (1974). *Solving least squares problems*, Pentice-Hall, Englewood Cliffs, new Jersey.

31. Recipe for the manufacture of conventional beta lactose; supplied by Lactose New Zealand.
32. Press, W. H., Flannery, B. P., Teukolsky, S. A., and Vetterling, W. T. (1989). *Numerical recipes*, Cambridge University Press, Cambridge.
33. Perkin Elmer DSC7 application notes.
34. Brittain, G. D. (1971). *Recent advances in Gas Chromatography*, Marcel Dekker, New York.
35. Suryanarayanan, R. (1984). *J. Pharm. Sci.*, **73**, 78.
36. Haase, G. and Nickerson, T. A. (1966). *J. Dairy Sci.*, **49**, 127.
37. Zadow, J. D. (1993). "Whey and Lactose Processing", Elsevier Applied Science, London and New York.
38. Caric, M. and Kalab, M. (1987). *Food microstructure*, **6**, 171.
39. Roetman, K. and Van Schaik, M., (1975). *Neth. Milk Dairy J.* **29,** 225-237.
40. Whittier, E. O. (1944). *J. Dairy Sci.* **27**, 504.
41. Shi, Y., Hartel, R. W., and Liang, B. (1989) *J. Dairy Sci.* **72,** 2906-2915.
42. Visser, R. A. (1980). *Neth. milk Dairy J.* **34,** 255-275.
43. Lerk, C. F., Andreae, A. C., de Boer, A. H., Bolhuis, G. K., Zuurman, K., de Hoog, P., Kussendrager, K., and van Leverink, J. (1983). *J. Pharm. Pharmacol.* **35**, 747-748.
44. Fries, D. C., Rao, S. T. and Sunaralingam, M. (1971). *Acta. Cryst.* **B27,** 994-1005.
45. Beevers, C. A. and Hansen, H. N. (1971). *Acta. Cryst.* **B27,** 1323-1325.
46. Hirotsu, K. and Shimada, A. (1974). *Bull. of the Chem. Soc. of Japan* **47,** 1872-1879.
47. Earl, W. L. and Parrish, F. W. (1983). *Carb. Res.* **115,** 23-32.
48. Analytical method of "Determining the anomeric ratio of lactose by polarimetry", supplied by the New Zealand Lactose Company.
49. Newstead, D. F., and Gray, I. K. (1972). *New Zealand J. Dairy Sci. Technol.*, **7**, 161-172.
50. Poole, C. F., and Shuette, S. S. (1984). *Contemporary practice of chromatography,* Elsevier, New York.
51. Li, B.W., Schuhmann, P. J., Holden, J. M. (1983). *J. Ag. Fd. Chem.*, **31**, 985
52. Olling, C. C. J. (1973). Unpublished results, C. C. F. laboratory.
53. Breg, J., Romijn, D., Van Halbeek, H., Vliegenthart, J. F. G., Visser, R. A., Hassnoot, C. A. G. (1988). *Carb. Research* **174,** 23-36.
54. Callaghan, P. T. (1991). *Principles of nuclear magnetic resonance microscopy*, Clarendon Press, Oxford.
55. Provencher, S. W. (1982). *Comput. Phys. Commun.* **27**, 229.
56. Abragam, A. (1961). *Principles of nuclear magnetism*, Clarendon Press, Oxford.
57. Provencher, S. W. (1976). *Biophys. J.*, **16**, 27.

58. Slichter, C. P. (1963). *Principles of magnetic resonance*, Harper and Row, New York.
59. Hebel, L. C. and Slichter, C. P. (1959). *Phys. Rev.* **116**, 583.
60. Whittal, K. P. and MacKay, A. L. (1989). *J. of Mag. Res.*, **84**, 134.
61. Andrew, E. R., Bradbury, A., and Eades, R. G. (1958). *Nature*, **182**, 1659.
62. Andrew, E. R., Bradbury, A., and Eades, R. G. (1958). *Nature*, **183**, 1802.
63. Andrew, E. R. (1971). *Prog. NMR Spectr.*, **8**, 1.
64. Mehring, M. (1982). *High resolution NMR in solids*, Springer, Berlin.
65. White, G. W. and Cakebread, S. H. (1966). *J. Fd. Technol.*, **1**, 73.
66. Parks, G. S., and Reagh, J. D. (1937). *J. Chem. Phys.*, **5**, 364.
67. Allen, G. (1993). Chapter 1 *The glassy state in foods*, Nottingham University Press, UK.
68. Roos, Y., and Karel, M. (1991). *Food Technol.*, **45**, 66-107.
69. Williams, M. L., Landel, R. F., and Ferry, J. D. (1955). *J. Am. Chem. Soc.* 77, 3701.
70. Levine, H., and Slade, L. (1986). *Carboh. Polym.*, **6**, 213.
71. Noel, T. R., Ring, S. G., Whittam, M. A. (1993). Chapter 8, *The glassy state in foods*, Nottingham University Press, UK.
72. Peleg, M. (1993). Chapter 21, *The glassy state in foods*, Nottingham University Press, UK.
73. Roos, Y., and Karel, M. (1993). Chapter 2, *The glassy state in foods*, Nottingham University Press, UK.
74. Roos, Y. (1987). *J. food Sci.*, **52**, 146.
75. Hargreaves, J. B. (1995). NZDRI report no. MP94R06
76. Mansfield, M. L. (1993). Chapter 4, *The glassy state in foods*, Nottingham University Press, UK.
77. Kauzmann, W. (1948). *Chemical Reviews*, **43**, 219-256.
78. Gordon, M., and Taylor, J. S. (1952). *J. Appl. Chem.*, **2**, 493.
79. Levine, H., and Slade, L. (1990). *Dough Rheology and Baked Product Texture.*, AVI publishing company, New York.
80. Fox, T. G., and Flory, P. J. (1950). *J. Appl. Phys.*, **21**, 581.
81. Roos, Y. and Karel, M. (1990). *Biotech. prog.*, **6**, 159.
82. Wallack, D. A. and King, C. J. (1988). *Biotech. Prog.*, **4**, 31.
83. Roos, Y., and Karel, M. (1993). Chapter 10, *The glassy state in foods*, Nottingham University Press, UK.
84. Roos, Y., and Karel, M. (1992). *J. Food Sci.*, **57**, No. 3, 775.
85. Ferry, J. D. (1980). *Viscoelastic properties of polymers*, John Wiley and sons, New York.
86. Peleg, M. (1991). *Food Res.*, **26**, 604
87. Flink, J. M., and Karel, M, (1970). *J. Food Sci.*, **35**, 444-446.

88. Tsourouflis, S., Flink, J. M., and Karel, M. (1976). *J. of the Science of Food and Ag.*, **27**, 509-519.
89. To, E. C., and Flink, J. M. (1978). *J. of Food Tech.*, **13**, 551-565.
90. To, E. C., and Flink, J. M. (1978). *J. of Food Tech.*, **13**, 567-581.
91. To, E. C., and Flink, J. M. (1978). *J. of Food Tech.*, **13**, 583-594.
92. Lloyd, R. J., and Chen, D. (1993). NZDRI report no. MP93R05
93. Niediek, E. A. (1979). *Gordian*, **79**, 35.
94. Lloyd, R. J. and Chen, D. (1993). *Unpublished data.*
95. Bronlund, J. (1993). *Unpublished data.*
96. Johari, G. P., Hallbruker, A., and Mayer, E. (1987). *Nature*, **330**, 552.
97. Vuatez, G. (1988). *Food preservation by moisture control*, Elsevier applied science, London.
98. Bronlund, J. (1993). *Unpublished data.*
99. To, E. C., and Flink, J. M. (1978). *J. Fd. Technol.* **13**, 551.
100. Hargreaves, J. B. (1995). Unpublished data.
101. Hargreaves, J. B. (1995). Unpublished data.
102. Gidley, M. J. (1992). *Trends in Fd. Sci. and Technol.*, **3**, 231-235.

Appendix 1

Simulated model of the effect of solvation delay on polarimetric readings

The effect of solvation delay on the optical rotation of a lactose solution can be modeled by convoluting the rate of mass transfer from the solid to solution with the known rate of mutarotation at a fixed temperature.

Beginning with a sample composed of pure alpha lactose monohydrate and assuming first order kinetics (and a temperature of 20 °C), the optical rotation at time t (where t=0 represents the point of solvent contact with the powder) is given as

$$specific\ optical\ rotation = \frac{100}{2C} R(t) = A\exp(-k_1 t) \qquad [8.1]$$

where R(t) is the optical rotation at time t, k_1 is the rate constant (0.012 at 20°C (Figure 3.5)), A is the specific optical rotation of alpha lactose (91.1°), and C is the concentration of lactose in solution (g/100 ml).

A simplistic model of particle dissolution assumes a spherical dissolving fragment. In the limit $\Delta t \rightarrow 0$, the rate of mass of material entering solution for a spherical particle of radius r and density ρ is

$$\frac{dM}{dt} = \rho 4\pi r^2 \frac{dr}{dt} = \frac{3M}{r}\frac{dr}{dt} \qquad [8.2]$$

Since the solution is well agitated during dissolution, it is assumed that there is no effective diffusion layer around the particle. By assuming the rate of change of the radius to be constant with time, ie.

$$r = r_0 - kt \qquad [8.3]$$

then $dr/dt = -k$, and Equation [8.2] reduces to

$$\frac{dM}{dt} = \frac{-3kM}{r} \qquad [8.4]$$

Collecting terms and integrating

$$\int_{M_0}^{M} \frac{dM}{M} = \int_0^t \frac{-3k}{r_0 - kt} dt \qquad [8.5]$$

where M_0 is the initial mass of the particle. Letting $x = r_0 - kt$, Equation [8.5] gives

$$\int_{M_0}^{M} \frac{dM}{M} = 3\int_{r_0}^{r_0 - kt} \frac{dx}{x} \qquad [8.6]$$

This has solution

$$\frac{M}{M_0} = \left(\frac{r_0 - kt}{r_0}\right)^3 \qquad 0 \le t \le \frac{r_0}{k} \qquad [8.7]$$

where M is the undissolved mass of lactose at time, t and M_0 is the initial mass of lactose. The mass of lactose in solution is simply

$$M_s = M_0\left(1-\left(\frac{r_0-kt}{r_0}\right)^3\right) \qquad 0 \le t \le \frac{r_0}{k} \qquad [8.8]$$

As the lactose enters solution, mutarotation is initiated. By discretising the process of the dissolution, it is possible to simply determine the evolution of the optical rotation of the entire solution by summing the current optical rotation of each increment. Figure 8.1 demonstrates the evolution of the optical rotation for the first five increments to dissolve prior to summation.

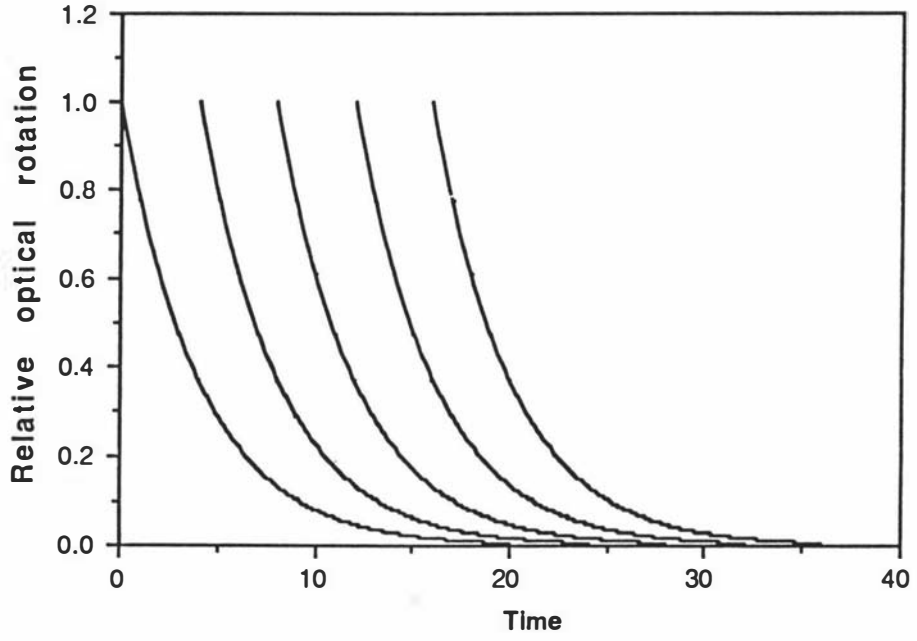

Figure 8.1 Evolution of the optical rotation for the first five increments to dissolve. Note that the optical rotation axis has been normalised and that the time axis is arbitrary.

Assuming 100 equal increments of mass Mo/100, then the time of dissolution of increment N is found by solving Equation [8.8] for t, ie.

$$t_N = \frac{r_0}{k}\left[1-\sqrt[3]{1-\frac{M_{S,N}}{M_0}}\right] = \frac{r_0}{k}\left[1-\sqrt[3]{1-\frac{N}{100}}\right] \qquad 1 \le N \le 100 \qquad [8.9]$$

Substituting Equation [8.9] into Equation [8.1] yields

$$specific\ rotation = 91.1\sum_{N=1}^{N_N}\frac{1}{100}\exp\left[-k_1\left(t-\left(\frac{r_0}{k}\left(1-\sqrt[3]{1-\frac{N}{100}}\right)\right)\right)\right] \qquad 1 \le N_N \le 100 \qquad [8.10]$$

r_0/k is simply the time for complete dissolution. Figure 3.1 represents the form of Equation[8.10] for $k_1 = 0.012$ and dissolution times of 1, 2, and 3 min respectively.

Appendix 2

Solvent Suppressed High Resolution NMR Spectroscopy

Preliminary experiments indicated that the anomeric ratio determined according to Equation[3.8] varied significantly in response to the strength of solvent suppression employed to unmask the glucose 1β peak. In an attempt to quantify these effects, anomeric measurements were performed on an aqueous lactose solution of known composition (an aqueos lactose solution at mutarotation equilibrium has an anomeric ratio of alpha:beta = 38.1:61.9 at 20°C), and the pulse sequence parameters OBA, delay, and t (Figure 3.11) were varied. The response is depicted in Figure 8.2.

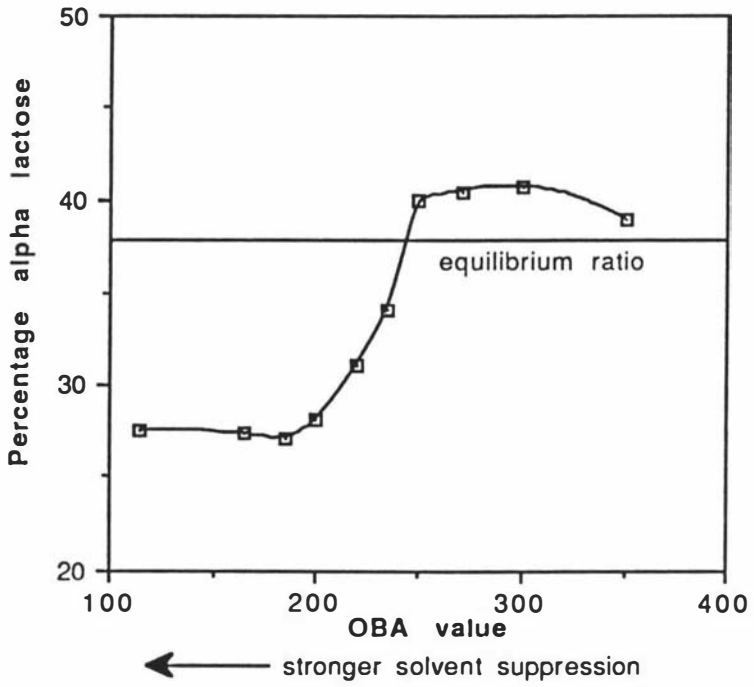

Figure 8.2. The effect of solvent suppression strength on the outcome of anomeric ratio determination.

The calculated anomeric ratio deviates from the known value mostly in the region of strongest solvent suppression. It is not clear at this time as to the cause of the distortion of the relative integrals of the *glucose1α* and *glucose1β* peaks. However, the conclusion was drawn that the solvent suppression method was unsuitable for anomeric determinations of aqueous solutions of lactose.

Appendix 3

Operation of the Marquardt Levenberg algorithm

The ML algorithm achieves convergence according to the following prescription. Given an initial guess for the set of fitted parameters, a the algorithm

1 Computes χ^2
2 Picks a modest value for λ say $\lambda = 0.001$
3 Solves the linear Equations [4.33] for a_i and evaluate $\chi^2(x + a)$
4 If $\chi^2(x + a) \geq \chi^2(a)$ then λ is increasedby a factor of 10 and the algorithm returns to (3)
5 If $\chi^2(x + a) < \chi^2(a)$ then λ is increasedby a factor of 10, the trial solution is updated ($x \rightarrow x + a$), and the algorithm returns to (3)

Appendix 4

The Marquardt-Levenberg Algorithm

The ML algorithm used to perform the multiexponential fitting tasks in Chapter 4 is listed here in PASCAL language.

Sane

```
{}
{Created: Saturday, October 15, 1988 at 8:46 AM}
{   SANE.p}
{   Pascal interface for Standard Apple Numeric Environment}
{}
{         Copyright © Symantec Corporation 1989}
{   Copyright Apple Computer, Inc.  1985-1988}
{   All rights reserved}
{}


unit SANE;
interface


{ Elems881 mode set by -d Elems881=true on Pascal command line }

{$IFC UNDEFINED Elems881}
{$SETC Elems881 = FALSE}
{$ENDC}


const
{$IFC OPTION(MC68881)}

{*=============================================================*}
{ *  The interface specific to the MC68881 SANE library  *}
{ *=============================================================*}

 Inexact = 8;
 DivByZero = 16;
 Underflow = 32;
 Overflow = 64;
 Invalid = 128;
 CurInex1 = 256;
 CurInex2 = 512;
 CurDivByZero = 1024;
 CurUnderflow = 2048;
 CurOverflow = 4096;
 CurOpError = 8192;
 CurSigNaN = 16384;
 CurBSonUnor = 32768;


{$ELSEC}

{*=============================================================*}
{ *  The interface specific to the software SANE library   *}
{ *=============================================================*}

 Invalid = 1;
 Underflow = 2;
 Overflow = 4;
 DivByZero = 8;
```

```
 Inexact = 16;
 IEEEDefaultEnv = 0;    {IEEE-default floating-point environment constant}


{$ENDC}

{*=============================================================================*}
{ *  The common interface for the SANE library   *}
{ *=============================================================================*}

 DecStrLen = 255;
 SigDigLen = 20;        {for 68K; use 28 in 6502 SANE}


type

 RelOp = (GreaterThan, LessThan, EqualTo, Unordered);

 NumClass = (SNaN, QNaN, Infinite, ZeroNum, NormalNum, DenormalNum);

 RoundDir = (ToNearest, Upward, Downward, TowardZero);

 RoundPre = (ExtPrecision, DblPrecision, RealPrecision);

 DecimalKind = (FloatDecimal, FixedDecimal);

{$IFC OPTION(MC68881)}

{*=============================================================================*}
{ *  The interface specific to the MC68881 SANE library  *}
{ *=============================================================================*}
 Exception = LONGINT;

 Environment = record
  FPCR: LONGINT;
  FPSR: LONGINT;
 end;

 Extended80 = array[0..4] of INTEGER;

 TrapVector = record
  Unordered: LONGINT;
  Inexact: LONGINT;
  DivByZero: LONGINT;
  Underflow: LONGINT;
  OpError: LONGINT;
  Overflow: LONGINT;
  SigNaN: LONGINT;
 end;

{$ELSEC}

{*=============================================================================*}
{*  The interface specific to the software SANE library   *}
{*=============================================================================*}

 Exception = INTEGER;

 Environment = INTEGER;

 Extended96 = array[0..5] of INTEGER;

{$ENDC}

{*=============================================================================*}
```

```
{* The common interface for the SANE library   *}
{*=============================================================================*}

 DecStr = string[DecStrLen];

 DecForm = record
  style: DecimalKind;
  digits: INTEGER;
 end;

 Decimal = record
  sgn: 0..1;
  exp: INTEGER;
  sig: string[SigDigLen];
 end;

 CStrPtr = ^CHAR;


{$IFC OPTION(MC68881)}

{ return IEEE default environment }
function IEEEDefaultEnv: environment;
procedure SetTrapVector (Traps: trapvector);
{ FPCP trap vectors <-- Traps }

{-------------------------------------------------------------------}
{  * FUNCTIONs for converting between SANE Extended formats}
{  -------------------------------------------------------------------}


procedure GetTrapVector (var Traps: trapvector);
{ Traps <-- FPCP trap vectors }

function X96toX80 (x: Extended): extended80;
{ X96toX80 <-- 96 bit x in 80 bit extended format }

function X80toX96 (x: extended80): Extended;
{ X80toX96 <-- 80 bit x in 96 bit extended format }

{$IFC Elems881 = false}

function Sin (x: Extended): Extended;
{ sine }

function Cos (x: Extended): Extended;
{ cosine }

function ArcTan (x: Extended): Extended;
{ inverse tangent }

function Exp (x: Extended): Extended;
{ base-e exponential }

function Ln (x: Extended): Extended;
{ base-e log }

function Log2 (x: Extended): Extended;
{ base-2 log }

function Ln1 (x: Extended): Extended;
{ ln(1+x) }

function Exp2 (x: Extended): Extended;
```

```
{ base-2 exponential }

function Exp1 (x: Extended): Extended;
{ exp(x) - 1 }

function Tan (x: Extended): Extended;
{ tangent }

{$ENDC}

{$ELSEC}

{ return halt vector }
function GetHaltVector: LONGINT;
procedure SetHaltVector (v: LONGINT);
{ halt vector <-- v }


function X96toX80 (x: Extended96): Extended;
{ 96 bit x in 80 bit extended format }

function X80toX96 (x: Extended): Extended96;
{ 80 bit x in 96 bit extended format }
{------------------------------------------------------------------}
{* SANE library functions}
{ ------------------------------------------------------------------}

function Log2 (x: Extended): Extended;
{ base-2 log }

function Ln1 (x: Extended): Extended;
{ ln(1+x) }

function Exp2 (x: Extended): Extended;
{ base-2 exponential }

function Exp1 (x: Extended): Extended;
{ exp(x) - 1 }

function Tan (x: Extended): Extended;
{ tangent }

{$ENDC}


{*==================================================================*}
{*  The common interface for the SANE library   *}
{*==================================================================*}

{-------------------------------------------------}
{* Conversions between numeric binary types.}
{-------------------------------------------------}

function Num2Integer (x: Extended): INTEGER;
function Num2Longint (x: Extended): LONGINT;
function Num2Real (x: Extended): real;
function Num2Double (x: Extended): DOUBLE;
function Num2Extended (x: Extended): Extended;
function Num2Comp (x: Extended): Comp;
{ -------------------------------------------------}
{* Conversions between binary and decimal.}
{-------------------------------------------------- }

procedure Num2Dec (f: decform; x: Extended; var d: decimal);
{ d <-- x according to format f }
```

```
function Dec2Num (d: decimal): Extended;
{ Dec2Num <-- d }

procedure Num2Str (f: decform; x: Extended; var s: DecStr);
{ s <-- x according to format f }

function Str2Num (s: DecStr): Extended;
{ Str2Num <-- s }

{------------------------------------------------}
{* Conversions between decimal formats.}
{------------------------------------------------}

procedure Str2Dec (s: DecStr; var Index: INTEGER; var d: decimal; var ValidPrefix: BOOLEAN);
{ On input Index is starting index into s, on output Index is}
{one greater than index of last character of longest numeric}
{substring;}
{d <-- Decimal rep of longest numeric substring;}
{ValidPrefix <-- "s, beginning at Index, contains valid numeric}
{string or valid prefix of some numeric string" }

procedure CStr2Dec (s: CStrPtr; var Index: INTEGER; var d: decimal; var ValidPrefix: BOOLEAN);
{ Str2Dec for character buffers or C strings instead of Pascal}
{strings: the first argument is the the address of a character}
{buffer and ValidPrefix <-- "scanning ended with a null byte" }

procedure Dec2Str (f: decform; d: decimal; var s: DecStr);
{ s <-- d according to format f }

{------------------------------------------------}
{* Arithmetic, auxiliary, and elementary functions.}
{------------------------------------------------}

function Remainder (x: Extended; y: Extended; var quo: INTEGER): Extended;
{ Remainder <-- x rem y; quo <-- low-order seven bits of integer}
{quotient x/y so that -127 < quo < 127 }

function Rint (x: Extended): Extended;
{ round to integral value }

function Scalb (n: INTEGER; x: Extended): Extended;
{ scale binary;  Scalb <-- x * 2^n }

function Logb (x: Extended): Extended;
{ Logb <-- unbiased exponent of x }

function CopySign (x: Extended; y: Extended): Extended;
{ CopySign <-- y with sign of x }

(* FUNCTION NextReal(x: real;y: real): real; *)
function NextReal (x: Extended; y: Extended): real;
(* FUNCTION NextDouble(x: DOUBLE;y: DOUBLE): DOUBLE; *)
function NextDouble (x: Extended; y: Extended): DOUBLE;
function NextExtended (x: Extended; y: Extended): Extended;
{ return next representable value from x toward y }

function XpwrI (x: Extended; i: INTEGER): Extended;
{ XpwrI <-- x^i }

function XpwrY (x: Extended; y: Extended): Extended;
{ XpwrY <-- x^y }

function Compound (r: Extended; n: Extended): Extended;
{ Compound <-- (1+r)^n }
```

```
function Annuity (r: Extended; n: Extended): Extended;
{ Annuity <-- (1 - (1+r)^(-n)) / r }

function RandomX (var x: Extended): Extended;
{ returns next random number and updates argument;}
{x integral, 1 <= x <= (2^31)-2 }

{-------------------------------------------------}
{* Inquiry routines.}
{-------------------------------------------------}

(* FUNCTION ClassReal(x: real): NumClass; *)
function ClassReal (x: Extended): NumClass;

(* FUNCTION ClassDouble(x: DOUBLE): NumClass; *)
function ClassDouble (x: Extended): NumClass;

(* FUNCTION ClassComp(x: Comp): NumClass; *)
function ClassComp (x: Extended): NumClass;

function ClassExtended (x: Extended): NumClass;
{ return class of x }


function SignNum (x: Extended): INTEGER;
{ 0 if sign bit clear, 1 if sign bit set }

{-------------------------------------------------}
{* NaN function.}
{-------------------------------------------------}

function NAN (i: INTEGER): Extended;
{ returns NaN with code i }

{-------------------------------------------------}
{* Environment access routines.}
{-------------------------------------------------}

procedure SetException (e: Exception; b: BOOLEAN);
{ set e flags if b is true, clear e flags otherwise; may cause halt }

function TestException (e: Exception): BOOLEAN;
{ return true if any e flag is set, return false otherwise }

procedure SetHalt (e: Exception; b: BOOLEAN);
{ set e halt enables if b is true, clear e halt enables otherwise }

function TestHalt (e: Exception): BOOLEAN;
{ return true if any e halt is enabled, return false otherwise }

procedure SetRound (r: RoundDir);
{ set rounding direction to r }

function GetRound: RoundDir;
{ return rounding direction }

procedure SetPrecision (p: RoundPre);
{ set rounding precision to p }

function GetPrecision: RoundPre;
{ return rounding precision }


procedure SetEnvironment (e: environment);
```

```
{ set environment to e }

procedure GetEnvironment (var e: environment);
{ e <-- environment }

procedure ProcEntry (var e: environment);
{ e <-- environment;  environment <-- IEEE default env }

procedure ProcExit (e: environment);
{ temp <-- exceptions; environment <-- e;}
{signal exceptions in temp }

{-------------------------------------------------}
{* Comparison routine.}
{-------------------------------------------------}

function Relation (x: Extended; y: Extended): RelOp;
{ return Relation such that "x Relation y" is true }


implementation
end.
```

MRQCOF

```
unit MRQCOF;

interface


type
 glndata = array[1..2000] of extended;
 glmma = array[1..20] of extended;
 gllista = array[1..20] of integer;
 glnalbynal = array[1..20, 1..20] of extended;
 glndataPtr = ^glndata;

const
 pi = 3.1415926536;

var
 glochisq, aa, bb: extended;
 glbeta, a: glmma;
 mfit, ma, fitFunction: integer;
 x, y, sig: glndataPtr;



procedure funcs (fitFunction: integer; xx: extended; var y: extended; var dyda: glmma);
(* Programs using routine FGAUSS must define the type}
{TYPE}
{   glnparam = ARRAY [1..na] OF extended;}
{in the main routine.  *)


procedure mrqcof (ndata: integer; lista: gllista; var alpha: glnalbynal; var beta: glmma; nalp: integer; var
chisq: extended);
(* Programs using routine MRQMIN must provide a}
{PROCEDURE funcs(xx:extended; a:glmma; yfit:extended; dyda:glmma; mma:integer);}
{that evaluates the fitting function yfit and its derivatives dyda}
{with respect to the parameters a at point xx.  Also they}
{must define the types}
{TYPE}
{   glndata = ARRAY [1..ndata] OF extended;}
{   glmma = ARRAY [1..mma] OF extended;}
```

```
{  gllista = ARRAY [1..mma] OF integer;}
{  glnalbynal = ARRAY [1..nalp,1..nalp] OF extended;}
{in the main routine *)


procedure covsrt (var covar: glnalbynal; ncvm: integer; lista: gllista);
(* Programs using routine COVSRT must define the types}
{TYPE}
{  glcovar = ARRAY [1..ncvm,1..ncvm] OF extended;}
{  gllista = ARRAY [1..mfit] OF integer;}
{in the calling program. *)

implementation

procedure funcs;

 var
  i: integer;
  fac, ex, arg, phi: extended;

begin
 case fitFunction of
  1:   {2 Parameter Fit}
   begin
    y := a[1] * exp(-3.33 * xx) + a[2] * exp(-0.121 * xx);
    dyda[1] := exp(-3.33 * xx);
    dyda[2] := exp(-0.121 * xx);
   end;
  2:   {2 Parameter Fit}
   begin
    y := a[1] * exp(-3.33 * xx) + a[2] * exp(-0.121 * xx);
    dyda[1] := exp(-3.33 * xx);
    dyda[2] := exp(-0.121 * xx);
   end;
  3:   {2 Parameter Fit}
   begin
    y := a[1] * exp(-3.33 * xx) + a[2] * exp(-0.121 * xx);
    dyda[1] := exp(-3.33 * xx);
    dyda[2] := exp(-0.121 * xx);
   end;
 end;
end;


procedure mrqcof;

 var
  k, j, i: integer;
  ymod, wt, sig2i, dy, xx: extended;
  dyda: glmma;

begin
 for j := 1 to mfit do
  begin
   for k := 1 to j do
    begin
     alpha[j, k] := 0.0
    end;
   beta[j] := 0.0
  end;
 chisq := 0.0;
 for i := 1 to ndata do
  begin
   xx := x^[i];
   funcs(fitFunction, xx, ymod, dyda);
```

```
    sig2i := 1.0 / (sig^[i] * sig^[i]);
    dy := y^[i] - ymod;
    for j := 1 to mfit do
     begin
      wt := dyda[lista[j]] * sig2i;
      for k := 1 to j do
       begin
       alpha[j, k] := alpha[j, k] + wt * dyda[lista[k]]
       end;
      beta[j] := beta[j] + dy * wt
     end;
    chisq := chisq + dy * dy * sig2i
   end;
  for j := 2 to mfit do
   begin
    for k := 1 to j - 1 do
     begin
      alpha[k, j] := alpha[j, k]
     end
   end
end;


procedure covsrt;

 var
  j, i: integer;
  swap: extended;

begin
 for j := 1 to ma - 1 do
  begin
   for i := j + 1 to ma do
    begin
     covar[i, j] := 0.0
    end
  end;
 for i := 1 to mfit - 1 do
  begin
   for j := i + 1 to mfit do
    begin
     if (lista[j] > lista[i]) then
      begin
      covar[lista[j], lista[i]] := covar[i, j]
      end
     else
      begin
      covar[lista[i], lista[j]] := covar[i, j]
      end
    end
  end;
 swap := covar[1, 1];
 for j := 1 to ma do
  begin
   covar[1, j] := covar[j, j];
   covar[j, j] := 0.0
  end;
 covar[lista[1], lista[1]] := swap;
 for j := 2 to mfit do
  begin
   covar[lista[j], lista[j]] := covar[1, j]
  end;
 for j := 2 to ma do
  begin
   for i := 1 to j - 1 do
```

```
    begin
     covar[i, j] := covar[j, i]
    end
   end
 end;

end.
```

Gauss.J

```
unit GAUSSJ;

interface

 uses
  MRQCOF;


 procedure gaussj (var a: glnalbynal; n, np: integer; var b: glnalbynal; m, mp: integer);
(* Programs using GAUSSJ must define the types)
{TYPE}
{   glnpbynp = ARRAY [1..np,1..np] OF extended;}
{   glnpbymp = ARRAY [1..np,1..mp] OF extended;}
{   glnp = ARRAY [1..np] OF integer;}
{in the main routine. *)

implementation

 procedure gaussj;
  var
   big, dum, pivinv: extended;
   i, icol, irow, j, k, l, ll: integer;
   indxc, indxr, ipiv: gllista;
 begin
  for j := 1 to n do
   begin
    ipiv[j] := 0
   end;
  for i := 1 to n do
   begin
    big := 0.0;
    for j := 1 to n do
     begin
      if (ipiv[j] <> 1) then
       begin
       for k := 1 to n do
       begin
       if (ipiv[k] = 0) then
       begin
       if (abs(a[j, k]) >= big) then
       begin
       big := abs(a[j, k]);
       irow := j;
       icol := k
       end
       end
       else if (ipiv[k] > 1) then
       begin
       writeln('pause 1 in GAUSSJ - singular matrix');
       readln
       end
       end
       end
     end;
    ipiv[icol] := ipiv[icol] + 1;
```

```
    if (irow <> icol) then
     begin
      for l := 1 to n do
       begin
       dum := a[irow, l];
       a[irow, l] := a[icol, l];
       a[icol, l] := dum
       end;
      for l := 1 to m do
       begin
       dum := b[irow, l];
       b[irow, l] := b[icol, l];
       b[icol, l] := dum
       end
     end;
    indxr[i] := irow;
    indxc[i] := icol;
    if (a[icol, icol] = 0.0) then
     begin
      writeln('pause 2 in GAUSSJ - singular matrix');
      readln
     end;
    pivinv := 1.0 / a[icol, icol];
    a[icol, icol] := 1.0;
    for l := 1 to n do
     begin
      a[icol, l] := a[icol, l] * pivinv
     end;
    for l := 1 to m do
     begin
      b[icol, l] := b[icol, l] * pivinv
     end;
    for ll := 1 to n do
     begin
      if (ll <> icol) then
       begin
       dum := a[ll, icol];
       a[ll, icol] := 0.0;
       for l := 1 to n do
       begin
       a[ll, l] := a[ll, l] - a[icol, l] * dum
       end;
       for l := 1 to m do
       begin
       b[ll, l] := b[ll, l] - b[icol, l] * dum
       end
       end
     end
   end;
  for l := n downto 1 do
   begin
    if (indxr[l] <> indxc[l]) then
     begin
      for k := 1 to n do
       begin
       dum := a[k, indxr[l]];
       a[k, indxr[l]] := a[k, indxc[l]];
       a[k, indxc[l]] := dum
       end
     end
   end
 end;
end.
```

MRQMin

```
unit MRQMIN;


interface

 uses
  MRQCOF, GAUSSJ;

 procedure mrqmin (ndata: integer; lista: gllista; var covar, alpha: glnalbynal; nca: integer; var chisq, alamda:
extended);
(* Programs using routine MRQMIN must define the types}
{TYPE}
{     glndata = ARRAY [1..ndata] OF extended;}
{     glmma = ARRAY [1..mma] OF extended;}
{     gllista = ARRAY [1..mma] OF integer;}
{     glncabynca = ARRAY [1..nca,1..nca] OF extended;}
{and the variables}
{VAR}
{     glochisq: extended;  glbeta: glmma;}
{in the main routine. Also note that this routine calls MRQCOF, which}
{requires a user-defined procedure FUNCS, described in that routine.          *)

implementation

 procedure mrqmin;

  label
  99;

  var
  k, kk, j, ihit: integer;
  da: glmma;
  oneda: glnalbynal;

begin
 if alamda < 0.0 then
  begin
   alamda := 0.001;
   mrqcof(ndata, lista, alpha, glbeta, nca, chisq);
   glochisq := chisq;
  end;
 for j := 1 to mfit do
  begin
   for k := 1 to mfit do
    begin
     covar[j, k] := alpha[j, k]
    end;
   covar[j, j] := alpha[j, j] * (1.0 + alamda);
   oneda[j, 1] := glbeta[j]
  end;
 gaussj(covar, mfit, nca, oneda, 1, 1);
 for j := 1 to mfit do
  da[j] := oneda[j, 1];
 if (alamda = 0.0) then
  begin
   covsrt(covar, nca, lista);
   goto 99
  end;
 for j := 1 to mfit do
  begin
   a[lista[j]] := a[lista[j]] + da[j]
  end;
 mrqcof(ndata, lista, covar, da, nca, chisq);
 if (chisq < glochisq) then
```

```
  begin
   alamda := 0.1 * alamda;
   glochisq := chisq;
   for j := 1 to mfit do
    begin
     for k := 1 to mfit do
      begin
      alpha[j, k] := covar[j, k]
      end;
     glbeta[j] := da[j];
    end
  end
 else
  begin
   alamda := 10.0 * alamda;
   chisq := glochisq
  end;
99:
 end;
end.
```

Curvefit

```
program CurveFit (input, output);

 uses
  MRQCOF, MRQMIN, SANE;

 var
  view, box: Rect;
  fileName, txt, txt1, params: str255;
  ndata, i, j, k, nca, numberOfPoints, itemType, itemHit, start, finish: integer;
  alamda, chisq, lastchisq, x1, x2, y2, increment, z, ex, phi: extended;
  quit, cancel, allPoints: boolean;
  f: text;
  lista: gllista;
  covar, alpha: glnalbynal;
  ch, answer: char;
  item: Handle;
  theDialog: DialogPtr;
  numSt, paramNumber: DecStr;
  form: DecForm;
  paramName: array[1..9] of str255;


function ConvertToInteger (strng: str255): integer;

 var
  i, l, value, factor: integer;
  ch: char;

begin
 l := length(strng);
 factor := 1;
 value := 0;
 for i := l downto 1 do
  begin
   ch := copy(strng, i, 1);
   if (ch >= '0') and (ch <= '9') then
    begin
     value := value + (ord(ch) - 48) * factor;
     factor := factor * 10;
    end;
  end;
```

```
 ConvertToInteger := value;
end;


function OpenFile: Str255;

 var
  where: point;
  prompt: Str255;
  reply: SFReply;
  Typelist: SFTypelist;
  myfileinfo: FInfo;
  err: OSErr;


begin
 where.v := 50;
 where.h := 100;
 prompt := ' OPEN which file ?';
 Typelist[0] := 'TEXT';
 SFGetFile(where, prompt, nil, 1, typelist, nil, reply);
 if (reply.good = true) then
  begin
   err := GetFInfo(reply.fName, reply.vRefNum, myfileinfo);
   err := SetVol(nil, reply.vRefNum);
   OpenFile := reply.fname;
  end
 else
  OpenFile := chr(0);
end;


begin
 x := glndataPtr(NewPtr(SizeOf(glndata)));
 y := glndataPtr(NewPtr(SizeOf(glndata)));
 sig := glndataPtr(NewPtr(SizeOf(glndata)));
 InitGraf(@thePort);
 InitFonts;
 FlushEvents(EveryEvent, 0);
 InitWindows;
 InitMenus;
 InitCursor;
 TEInit;
 InitDialogs(nil);
 quit := false;
 repeat
  cancel := false;
  theDialog := GetNewDialog(150, nil, POINTER(-1));
  SetPort(theDialog);
  GetDItem(theDialog, 1, itemTYPE, item, box);
  PenSize(3, 3);
  InsetRect(box, -4, -4);
  FrameRoundRect(box, 16, 16);
  for i := 4 to 9 do
   begin
    GetDItem(theDialog, i, itemType, item, box);
    SetCtlValue(ControlHandle(item), 0);
   end;
  GetDItem(theDialog, 3, itemType, item, box);
  SetCtlValue(ControlHandle(item), 1);
  fitFunction := 1;
  GetDItem(theDialog, 8, itemType, item, box);
  SetCtlValue(ControlHandle(item), 1);
  allPoints := true;
  SelIText(theDialog, 10, 0, 32767);
```

```
 for i := 1 to 9 do
  paramName[i] := '';
 repeat
  ModalDialog(nil, itemHit);
  if (itemHit > 2) and (itemHit < 8) then
   begin
    for i := 3 to 7 do
     begin
      GetDItem(theDialog, i, itemType, item, box);
      SetCtlValue(ControlHandle(item), 0);
      GetDItem(theDialog, itemHit, itemType, item, box);
      SetCtlValue(ControlHandle(item), 1);
      fitFunction := itemHit - 2;
     end;
    case itemHit of
     3:
      begin
      txt := '2';
      txtl := '2';
      paramName[1] := 'ampl1';
      paramName[2] := 'ampl2';
      end;
     4:
      begin
      txt := '2';
      txtl := '2';
      paramName[1] := 'ampl1';
      paramName[2] := 'ampl2';
      end;
     5:
      begin
      txt := '2';
      txtl := '2';
      paramName[1] := 'ampl1';
      paramName[2] := 'ampl2';
      end;
    end;
    GetDItem(theDialog, 10, itemType, item, box);
    SetIText(item, txt);
    GetDItem(theDialog, 11, itemType, item, box);
    SetIText(item, txtl);
   end;
  if itemHit = 8 then
   begin
    GetDItem(theDialog, 9, itemType, item, box);
    SetCtlValue(ControlHandle(item), 0);
    GetDItem(theDialog, 8, itemType, item, box);
    SetCtlValue(ControlHandle(item), 1);
    allPoints := true;
    SelIText(theDialog, 10, 0, 32767);
   end
  else if (itemHit = 9) or (itemHit = 16) or (itemHit = 17) then
   begin
    GetDItem(theDialog, 8, itemType, item, box);
    SetCtlValue(ControlHandle(item), 0);
    GetDItem(theDialog, 9, itemType, item, box);
    SetCtlValue(ControlHandle(item), 1);
    allPoints := false;
    if itemHit = 9 then
     SelIText(theDialog, 16, 0, 32767);
   end;
  if itemHit = 2 then
   quit := true;
 until (itemHit = 1) or (itemHit = 2);
 if not quit then
```

```
 begin
  GetDItem(theDialog, 10, itemType, item, box);
  GetIText(item, txt);
  ma := ConvertToInteger(txt);
  GetDItem(theDialog, 11, itemType, item, box);
  GetIText(item, txt);
  mfit := ConvertToInteger(txt);
  if not allPoints then
   begin
    GetDItem(theDialog, 16, itemType, item, box);
    GetIText(item, txt);
    start := ConvertToInteger(txt);
    GetDItem(theDialog, 17, itemType, item, box);
    GetIText(item, txt);
    finish := ConvertToInteger(txt);
   end;
 end;
DisposDialog(theDialog);
if not quit then
 begin
  params := chr(0);
  form.style := fixedDecimal;
  form.digits := 0;
  for i := 1 to ma do
   if not quit and not cancel then
    begin
     theDialog := GetNewDialog(151, nil, POINTER(-1));
     SetPort(theDialog);
     GetDItem(theDialog, 1, itemTYPE, item, box);
     PenSize(3, 3);
     InsetRect(box, -4, -4);
     FrameRoundRect(box, 16, 16);
     SelIText(theDialog, 3, 0, 32767);
     Num2Str(form, i, paramNumber);
     ParamText(paramNumber, params, paramName[i], '');
     GetDItem(theDialog, 5, itemTYPE, item, box);
     PenSize(2, 2);
     InsetRect(box, -4, -4);
     FrameRect(box);
     repeat
     ModalDialog(nil, itemHit);
     until (itemHit = 1) or (itemHit = 2);
     if itemHit = 2 then
     cancel := true;
     if not quit and not cancel then
     begin
     GetDItem(theDialog, 3, itemType, item, box);
     GetIText(item, txt);
     a[i] := Str2Num(txt);
     params := concat(params, chr(13), txt);
     end;
     DisposDialog(theDialog);
    end;
 if not quit and not cancel then
  begin
   fileName := OpenFile;
   if fileName = chr(0) then
    cancel := true;
   if not quit and not cancel then
    begin
    SetRect(view, 20, 40, 400, 240);
    SetTextRect(view);
    ShowText;
    writeln('Reading ''', fileName, ''' ...');
    writeln;
```

```
reset(f, fileName);
if allPoints then
begin
i := 1;
readln(f, x^[1], ch, y^[1]);
while not eof(f) do
begin
i := i + 1;
readln(f, x^[i], ch, y^[i]);
end;
ndata := i;
end
else
begin
ndata := finish - start + 1;
for i := 1 to start do
readln(f);
for i := 1 to ndata do
begin
readln(f, y^[i]);
y^[i] := 240 - y^[i];
x^[i] := i + start - 1;
end;
end;
close(f);
writeln('Number of data points is ', ndata : 5);
writeln;
for i := 1 to ndata do
sig^[i] := 1;
for i := 1 to ma do
lista[i] := i;
alamda := -1.0;
mrqmin(ndata, lista, covar, alpha, nca, chisq, alamda);
writeln('After iteration number 1:');
writeln('CHI SQUARED = ', chisq : 10 : 4);
for k := 1 to ma do
writeln('Parameter', k : 2, ' = ', a[k] : 10 : 4);
writeln;
i := 1;
repeat
lastchisq := chisq;
i := i + 1;
mrqmin(ndata, lista, covar, alpha, nca, chisq, alamda);
writeln('After iteration number', i : 2, ' :');
writeln('CHI SQUARED = ', chisq : 10 : 4);
for k := 1 to ma do
writeln('Parameter', k : 2, ' = ', a[k] : 10 : 4);
writeln;
until abs(lastchisq - chisq) < 0.0001;
alamda := 0;
i := i + 1;
mrqmin(ndata, lista, covar, alpha, nca, chisq, alamda);
writeln('After iteration number', i : 2, ' :');
writeln('CHI SQUARED = ', chisq : 10 : 4);
writeln;
writeln('The final parameters for "', fileName, '" are :');
writeln;
for i := 1 to ma do
writeln('Parameter', i : 2, ' = ', a[i] : 10 : 4, sqrt(covar[i, i]) : 10 : 4);
theDialog := GetNewDialog(152, nil, POINTER(-1));
SetPort(theDialog);
GetDItem(theDialog, 1, itemTYPE, item, box);
PenSize(3, 3);
InsetRect(box, -4, -4);
FrameRoundRect(box, 16, 16);
```

```
    form.digits := 3;
    Num2Str(form, x^[1], numSt);
    GetDItem(theDialog, 3, itemType, item, box);
    SetIText(item, numSt);
    Num2Str(form, x^[ndata], numSt);
    GetDItem(theDialog, 4, itemType, item, box);
    SetIText(item, numSt);
    increment := (x^[ndata] - x^[1] + 1) / ndata;
    Num2Str(form, increment, numSt);
    GetDItem(theDialog, 5, itemType, item, box);
    SetIText(item, numSt);
    SelIText(theDialog, 3, 0, 32767);
    repeat
    ModalDialog(nil, itemHit);
    until (itemHit = 1) or (itemHit = 2);
    if itemHit = 2 then
    cancel := true;
    if not quit and not cancel then
    begin
    GetDItem(theDialog, 3, itemType, item, box);
    GetIText(item, txt);
    x1 := Str2Num(txt);
    GetDItem(theDialog, 4, itemType, item, box);
    GetIText(item, txt);
    x2 := Str2Num(txt);
    GetDItem(theDialog, 5, itemType, item, box);
    GetIText(item, txt);
    increment := Str2Num(txt);
    end;
    DisposDialog(theDialog);
    if not quit and not cancel then
    begin
    numberOfPoints := round((x2 - x1) / increment) + 1;
    writeln;
    writeln('The number of points is ', numberOfPoints : 8);
    writeln;
    writeln('Calculating values...');
    rewrite(f, 'Best Fit');
    for i := 1 to numberOfPoints do
    begin
    x2 := x1 + (i - 1) * increment;
    case fitFunction of
    1:  {2 Parameter Fit}
    begin
    y2 := a[1] * exp(-3.333 * x2) + a[2] * exp(-0.121 * x2);
    end;
    2:  {2 Parameter}
    begin
    y2 := a[1] * exp(-3.333 * x2) + a[2] * exp(-0.121 * x2);
    end;
    3:  {2 Parameter}
    begin
    y2 := a[1] * exp(-3.333 * x2) + a[2] * exp(-0.121 * x2);
    end;
    end;
    writeln(f, x2 : 20 : 8, chr(9), y2 : 20 : 8);
    end;
    close(f);
    end;
    writeln;
    writeln;
    HideAll;
   end;
  end;
end;
```

```
 until quit;
end.
```

Appendix 5

Operation of the LH algorithm

The LH algorithm finds the solution vector, x in the following way. Given the m x n matrix A, the intergers m and n, and the m vector b, the algorithm solves equation[*] for vector x. The n-vectors w and z provide working space. Index sets P and Z are defined and modified during execution of the algorithm.

$$A.x \approx b \qquad x \geq 0 \qquad [8.11]$$

step	description
1	Define set P = Null: Set Z = {1, 2, 3, ..., n}, and x = 0. {Elements indexed in set P during execution correspond to $x_j > 0, j \in P$}
	LOOP A begins here
2	Compute the n-vector $w = A^T(b - Ax)$. {vector z is the negative gradient vector of the function $\varphi(x) = |A.x - b|^2/2$ at x = x}
3	If the set Z is empty or if $w_j \leq 0$ for all $j \in Z$, goto 12 {this step terminates the algorithm either when the gradient becomes zero, or all elements, j have been indexed in set P}
4	Find an index $t \in Z$ such that $w_t = \max[w_j : j \in Z]$ {this step determines the path of steepest decent}
5	Move the index t from set Z to set P {once in set P, index j designates the next trial vector component $z_j, j \in P$}
6	Let E' denote the the m x n matrix defined by $Column\ j\ of\ \mathbf{A}' := \begin{cases} column\ j\ of\ \mathbf{E} & if\ \mathbf{j} \in \mathbf{P} \\ \mathbf{0} & if\ \mathbf{j} \in \mathbf{Z} \end{cases}$ {this isolates the columns of matrix A corresponding to a specific relaxation time tested in this (and previous) iterations. The respective amplitude (x_j) is calculated next}
	Compute the n-vector as a solution of the least squares problem (†) $A'z \approx b$. {This is performed by a QR decomposition of matrix A using Householder transformations as previously described. Vector z is the tentative solution vector for x. Only the components $z_j, J \in P$ are determined here.}
7	If $z_j > 0$ for all $j \in P$, set x = z and goto 2. {If successful, this indicates that the elements z_j are a good approximation to the final solution vector. If some elements of z_j become ≤ 0 (possibly due to machine roundoff errors) the algorithm changes each component of z_j (as described next) and attemptes to solve equation (†) again}
	LOOP B begins here
8	Find an index $q \in P$ such that $x_q/(x_q - z_q) = \min[x_j/(x_j - z_j): z_j \leq 0, j \in P]$ {In steps 8 - 10, the previous x_j's are incremented by an amount less than $(z_j - x_j)$ such that all new x_j's indexed in set P will be non-negative. Step 8 establishes the index q from set P such that α (calculated next) will be the smallest possible consistent with keeping all new x's (step 10) nonnegative. The most negative component will be removed from set P (step 11).}

9 Set $\alpha = x_q/(x_q - z_q)$

10 Set $\mathbf{x} = \mathbf{x} + \alpha(\mathbf{z} - \mathbf{x})$ {Here, all new x's will be non-negative (except the most negative component of vector z)}

11 Move from set P to set Z all indices $j \in P$ for which $x_j = 0$. Goto 6 {Here all indices for which x_j have become zero from a previously positive value are moved back to set Z. On returning to step 6, a new tentative solution vector z is calculated. If components of z indexed in set P are still negative, Loop B is repeated until it successfully exits at step 7.}

12 *Comment*: The computation is complete.

On termination, the solution vector x satisfies

$$x_j > 0 \qquad j \in P \qquad [8.12]$$
$$x_j = 0 \qquad j \in Z \qquad [8.13]$$

The finiteness of Loop B can be proved by observating that at least one more index (q) is removed from set P each time Step 11 is executed. Thus exit from Loop B at step 7 must occur after π - 1 iterations where π denotes the number of indices in set P when Loop B was entered. In practice Loop B usually exits immediately on reaching Step 7 and does not reach Steps 8 - 11 at all.

The finiteness of Loop A can be proved* by showing that the value of the residual norm function

$$r(x) = |\mathbf{A} \cdot \mathbf{x} - \mathbf{b}| \qquad [8.14]$$

is smaller each time step 2 is reached, and hence the vector x and it's associated set, P are distinct from all previous instances of x and P at Step 2. Since there are a finite number of subsets from the set [1, 2, ..., n), Loop A must terminate after a finite number of iterations. For small n, Loop A typically terminates after 0.5n iterations.

Appendix 6

The LH Algorithm

The LH algorithm used to perform the multiexponential fitting tasks in Chapter 4 is listed here in PASCAL language.

NNLS

```
program NNLS;

 uses
  sane;

 label
  10, 30, 60, 70, 100, 130, 140, 170, 190, 210, 220, 240, 260, 261, 262, 265, 290, 330, 350, 370, 390, 400,
410, 450;


 const
  zero = 0.0;
  one = 1.0;
  two = 2.0;
  factor = 0.01;
  mda = 100;
  nda = 95; {number of relaxation times>=n}
  lowReltime = 0.02;
  highReltime = 20;

 type
  thearray = array[1..mda, 1..nda] of extended;
  arrpt = ^thearray;
  arrhand = ^arrpt;

 var
{A: array[1..mda, 1..nda] of extended; }
{relaxation time matrix}
  A: arrhand;
  b, time: array[1..mda] of extended; {input data vector}
  x, RelaxT: array[1..nda] of extended; {solution vector for relaxation times}
  w: array[1..nda] of extended; {working space n vector}
  zz: array[1..mda] of extended; {working space m vector}
  index: array[1..nda] of integer;  {working array}
  exit, selected: boolean;
  itemtype, thenum, num: Integer;
  item: Handle;
  box: Rect;
  dumstr: Str255;
  dstr: Decstr;
  myform: Decform;


  mode: integer; {success failure flag}
  i, ii, ip, j, jj, jz, l, m, n, iz, izmax, iz1, iz2, nsetp, npp, npp1, iter, itmax, sgn: integer;
  Asave, aa, bb, alpha, sm, wmax, unorm, test, ztest, t, cc, ss, xr, yr, rnorm, up, multfact: extended;


{=============================================================
==}


procedure Opendata;

 var
```

```
  f: text;
  where: point;
  prompt: Str255;
  reply: SFReply;
  count: integer;
  err: OSerr;
  d1, d2, sdev1: extended;
  Typelist: SFTypelist;
  dumtab: char;
  myfileinfo: FInfo;


 begin

  where.v := 50;
  where.h := 200;
  prompt := ' OPEN which file ?';
  Typelist[0] := 'TEXT';

  SFGetFile(where, prompt, nil, 1, typelist, nil, reply);
  if (reply.good = true) then
   begin
    err := GetFInfo(reply.fName, reply.vRefNum, myfileinfo);
    err := SetVol(nil, reply.vRefNum);
    Reset(f, reply.fName);
    count := 1;
    repeat
     Readln(f, d1, d2);
     time[count] := d1;
     b[count] := d2;
     count := count + 1;
    until (Eof(f) or (count = 200));
    num := count - 1;
    Close(f);
    selected := true;
   end
  else
   begin
    selected := false;
   end;
 end;

{=========================================================================
==}


 procedure SaveSpectrum;

  label
   290, 300, 310;

  var
   f: text;
   count, countd, j: integer;
   thedel, ampl, Sum, relaxtim, rads, dees: extended;
   tab: char;
   dumstra, title: str255;
   creat, ctype: OSType;
   myfileinfo: FInfo;
   err: OSerr;

   where: point;
   prompt: Str255;
   reply: SFReply;
   theDialog: DialogPtr;
```

```
 begin
  tab := char($09);
  prompt := 'Save this Data As';
  title := 'name of file';

  where.v := 50;
  where.h := 200;

  SFPUTFile(where, prompt, title, nil, reply);
  if (reply.good = true) then
   begin
    Sum := 0;
    count := 0;
    err := SetVol(nil, reply.vrefnum);
    creat := 'CGRF';
    Rewrite(f, reply.fName);
    WriteLn(f, '*');
    WriteLn(f, 'relaxtime', tab, 'ampl', tab);

    for j := 1 to nda do
     begin
      Sum := Sum + x[j];
     end;

    for j := 1 to nda do
     begin
      WriteLn(j, x[j], x[j + 1]);
      if (x[j] > 0.01) and (x[j + 1] > 0.01) then
       goto 300;
290:
     end;
    goto 310;

300:
    RelaxT[j] := ((x[j + 1] / (x[j + 1] + x[j])) * (RelaxT[j + 1] - RelaxT[j])) + RelaxT[j];
    x[j] := x[j + 1] + x[j];
    RelaxT[j + 1] := RelaxT[j];
    x[j + 1] := 0;
    goto 290;

310:
    for j := 1 to nda do
     begin
      ampl := x[j];
      relaxtim := RelaxT[j];
      WriteLn(f, relaxtim : 9 : 4, tab, ampl : 9 : 3, tab);
     end;

    Close(f);

    err := GetFInfo(reply.fName, reply.vRefNum, myfileinfo);
    myfileinfo.fdcreator := creat;
    err := SetFInfo(reply.fName, reply.vRefNum, myfileinfo);

   end;

 end;

{=========================================================================
==}
 procedure triangulate;

  label
   420;
```

```
 var
  ltr, iitr: integer;

begin
 for ltr := 1 to nsetp do
  begin
   ip := nsetp + 1 - ltr;
   if ltr = 1 then
    goto 420;
   for iitr := 1 to ip do
    begin
     zz[iitr] := zz[iitr] - A^^[iitr, jj] * zz[ip + 1];
    end;
420:
   jj := index[ip];
   zz[ip] := zz[ip] / A^^[ip, jj];
  end;
end;


{=============================================================================}

function amax1 (paramx, paramy: extended): extended;


begin
 if paramx > paramy then
  amax1 := paramx
 else
  amax1 := paramy;
end;

{=============================================================================}
procedure H12first (hmode, lpivot, l1, icc, icv, ncv: integer);
{works on column j of global variable array A(i,j) where in fortran U(1,1)=A(1,j),}
{U(1,2)=A(2,j) etc}

 label
  1050, 1060, 1070, 1130;

 const
  zero = 0.0;
  one = 1.0;

 var
  j0: integer;
  cl, clinv: extended;
  sm, b, dummy: extended;



begin
 if (lpivot <= 0) or (lpivot >= l1) or (l1 > m) then
  goto 1130;
 cl := abs(A^^[lpivot, j]);
 if (hmode = 2) then
  goto 1060;

{construct the transformation}
 for j0 := l1 to m do
  begin
   cl := amax1 (abs(A^^[j0, j]), cl);
```

```
  end;
  if (cl <= 0) then
   goto 1130;
  clinv := one / cl;
  sm := (A^^[lpivot, j] * clinv) * (A^^[lpivot, j] * clinv);
  for j0 := l1 to m do
   begin
    sm := sm + (A^^[j0, j] * clinv) * (A^^[j0, j] * clinv);
   end;

  cl := cl * sqrt(sm);
  if (A^^[lpivot, j] <= zero) then
   goto 1050;
  cl := -cl;
 1050:
  up := A^^[lpivot, j] - cl;
  A^^[lpivot, j] := cl;
  goto 1070;

 {apply the transformation I+u*(u**T)/b to c)}
 1060:
  if (cl <= 0) then
   goto 1130;
 1070:
  if (ncv <= 0) then
   goto 1130;

 {this is the case for H12 first}

 1130:
 end;

 {=============================================================================
 ==}
 procedure H12second (hmode, lpivot, l1, ice, icv, ncv: integer);
 {works on column j of global variable array A(i,j) where in fortran U(1,1)=A(1 j),}
 {U(1,2)=A(2,j) etc}


  label
   1060, 1070, 1120, 1130;

  const
   one = 1.0;

  var
   j0, hi, i2, i3, i4, incr: integer;
   cl, clinv, sm1: extended;
   sm, b: extended;



 begin
  if (lpivot <= 0) or (lpivot >= l1) or (l1 > m) then
   goto 1130;
  cl := abs(A^^[lpivot, j]);
  if (hmode = 2) then
   goto 1060;

 {this is the case with H12 second}

 {apply the transformation I+u*(u**T)/b to c)}
 1060:
  if (cl <= 0) then
   goto 1130;
```

```
1070:
 if (ncv <= 0) then
  goto 1130;
 b := up * A^^[lpivot, j];

{b must be non-positive here. If b=0 return}
 if (b >= 0) then
  goto 1130;
 b := one / b;
 i2 := 1 - icv + ice * (lpivot - 1);
 incr := ice * (l1 - lpivot);
 for j0 := 1 to ncv do
  begin
   i2 := i2 + icv;
   i3 := i2 + incr;
   i4 := i3;
   sm := zz[i2] * up;
   for hi := l1 to m do
    begin
     sm := sm + zz[i3] * A^^[hi, j];
     i3 := i3 + ice;
    end;
   if sm = 0 then
    goto 1120;
   sm := sm * b;
   zz[i2] := zz[i2] + sm * up;
   for hi := l1 to m do
    begin
     zz[i4] := zz[i4] + sm * A^^[hi, j];
     i4 := i4 + ice;
    end;
1120:
  end;
1130:
end;

{=============================================================================
==}
procedure H12third (hmode, lpivot, l1, ice, icv, ncv: integer);
{works on column j of global variable array A(i,j) where in fortran U(1,1)=A(1,j),}
{U(1,2)=A(2,j) etc}

{works on global variable array A(1,jj) where in fortran c(1)=A(1,jj),}
{c(2)=A(2,jj) etc}

 label
  1060, 1070, 1120, 1130;

 const
  one = 1.0;

 var
  j0, i0, i2, i3, i4, incr: integer;
  cl, clinv, sm1: extended;
  sm, b: extended;



begin
 if (lpivot <= 0) or (lpivot >= l1) or (l1 > m) then
  goto 1130;
 cl := abs(A^^[lpivot, j]);
 if (hmode = 2) then
  goto 1060;
```

```
{this is the case with H12third}

{apply the transformation I+u*(u**T)/b to c)}
1060:
 if (cl <= 0) then
  goto 1130;
1070:
 if (ncv <= 0) then
  goto 1130;
 b := up * A^^[lpivot, j];

{b must be non-positive here. If b=0 return}
 if (b >= 0) then
  goto 1130;
 b := one / b;
 i2 := 1 - icv + ice * (lpivot - 1);
 incr := ice * (l1 - lpivot);
 for j0 := 1 to ncv do
  begin
   i2 := i2 + icv;
   i3 := i2 + incr;
   i4 := i3;
   sm := A^^[i2, jj] * up;
   for i0 := l1 to m do
    begin
     sm := sm + A^^[i3, jj] * A^^[i0, j];
     i3 := i3 + ice;
    end;
   if sm = 0 then
    goto 1120;
   sm := sm * b;
   A^^[i2, jj] := A^^[i2, jj] + sm * up;
   for i0 := l1 to m do
    begin
     A^^[i4, jj] := A^^[i4, jj] + sm * A^^[i0, j];
     i4 := i4 + ice;
    end;
1120:
  end;
1130:
end;
{================================================================
==}


begin

        { Initialize all the needed managers. }

 Initcursor;
 ShowText;
 m := mda;
 n := nda;
 A := arrhand(NewHandle(SizeOF(thearray)));


{fetch data}

 WriteLn('opendata');
 Opendata;
 WriteLn('number of time points=');
 WriteLn(num);

{set dimensions of arrays}
 m := num;
```

```
{write data}
for i := 1 to m do
 begin
  WriteLn(time[i], b[i]);
 end;



{input relaxation times }
RelaxT[1] := lowReltime;
multfact := exp((1 / (nda - 1)) * Ln(HighReltime / lowReltime));
WriteLn(multfact);

for j := 2 to n do
 begin
  RelaxT[j] := RelaxT[j - 1] * multfact;
 end;

{for j := 1 to n do}
{begin}
{RelaxT[j] := j * 1;}
{end;}


{create A matrix}
for i := 1 to m do
 begin
  for j := 1 to n do
   begin
    A^^[i, j] := exp(-time[i] / RelaxT[j]);
   end;
 end;



mode := 1;
if (m > 0) and (n > 0) then
 goto 10;
mode := 2;
goto 400;
10:
iter := 0;
itmax := 3 * n;

{initialize the arrays index[] and x[]}
for i := 1 to n do
 begin
  x[i] := zero;
  index[i] := i;
 end;

iz2 := n;
iz1 := 1;
nsetp := 0;
npp1 := 1;

{main loop begins}
{quit if coefficients are already in the solution or if m cols of A have already been triangularized}
30:
if ((iz1 > iz2) or (nsetp >= m)) then
 goto 350;
```

```
{compute components of the dual (negative gradient) vector w[]}
 for iz := iz1 to iz2 do
  begin
   j := index[iz];
   sm := zero;
   for l := npp1 to m do
    begin
     sm := sm + A^^[l, j] * b[l];
    end;
   w[j] := sm;
  end;

{find largest positive w[j]}
60:
 wmax := zero;
 for iz := iz1 to iz2 do
  begin
   j := index[iz];
   if w[j] <= wmax then
    goto 70;
   wmax := w[j];
   izmax := iz;
70:
  end;

{if wmax<=0 go to termination-indicates satisfaction of Kuhn-Tucker}
 if wmax <= 0 then
  begin
   WriteLn('wmax<=0');
   goto 350;
  end;
 iz := izmax;
 j := index[iz];

{the sign of w[j] is ok for j to be moved to set p.}
{begin the transformation and check new diagonal element to avoid near linerar dependence}

 Asave := A^^[npp1, j];
 H12first(1, npp1, npp1 + 1, 1, 1, 0);
 unorm := zero;
 if nsetp = 0 then
  goto 100;
 for l := 1 to nsetp do
  begin
   unorm := unorm + A^^[l, j] * A^^[l, j];
  end;
100:
 unorm := sqrt(unorm);
 test := (unorm + abs(A^^[npp1, j]) * factor) - unorm;
 if test <= zero then
  goto 130;

{col j is sufficiently independent. Copy b into 11. }
{Update zz and solve for ztest (=proposed new value for }
{[j])}

 for l := 1 to m do
  begin
   zz[l] := b[l];
  end;
 H12second(2, npp1, npp1 + 1, 1, 1, 1);
 ztest := zz[npp1] / A^^[npp1, j];

{see if ztest is positive}
```

```
if ztest <= zero then
 goto 130
else
 goto 140;

{reject j as candidate to be moved from set z to set p. }
{Restore A[npp1,j]. }
{Set w[j]=0, and loop back to test dual coeffs again.}
130:
A^^[npp1, j] := Asave;
w[j] := zero;
goto 60;

{the index j=index[iz] has been selected to be moved from set z to set p. }
{ Update b. Update indices. }
{Apply householder transformations to cols in new set z.}
{ Zero subdiagonal elts in col j. Set w[j]=0}
140:
for l := 1 to m do
 begin
  b[l] := zz[l];
 end;

index[iz] := index[iz1];
index[iz1] := j;
iz1 := iz1 + 1;
nsetp := npp1;
npp1 := npp1 + 1;

if iz1 > iz2 then
 goto 170;
for jz := iz1 to iz2 do
 begin
  jj := index[jz];
  H12third(2, nsetp, npp1, 1, mda, 1);
 end;
170:
if nsetp = m then
 goto 190;
for l := npp1 to m do
 begin
  A^^[l, j] := zero;
 end;
190:
w[j] := zero;

{solve the triangular system. Store temporarily in zz[]}
triangulate;

{secondary loop begins here}
{iteration counter}
210:
iter := iter + 1;
WriteLn('iteration=', iter);
if iter <= itmax then
 goto 220;
mode := 3; {write that termination due to exceeding iteration count}
goto 410;

{see if all new constrained coeffs are feasible. If not compute alpha}
220:
alpha := two;
for ip := 1 to nsetp do
 begin
  l := index[ip];
```

```
  if zz[ip] > 0 then
   goto 240;
  t := -x[l] / (zz[ip] - x[l]);
  if alpha <= t then
   goto 240;
  alpha := t;
  jj := ip;
240:
 end;

{if all new constrained coeffs are feasible then alpha will still =2.}
{If so exit from secondary loop to main loop.}

 if alpha = 2 then
  goto 330;
{otherwise use alpha which will be between 0 and 1 }
{to interpolate between the old x and the new zz}
 for ip := 1 to nsetp do
  begin
   l := index[ip];
   x[l] := x[l] + alpha * (zz[ip] - x[l]);
  end;

{modify A and b and the index arrays to move coefficient i from set p to set z}
 i := index[jj];
260:
 x[i] := zero;
 if jj = nsetp then
  goto 290;
 jj := jj + 1;
 for j := jj to nsetp do
  begin
   ii := index[j];
   index[j - 1] := ii;
{equiv to subroutine G1}
   aa := A^^[j - 1, ii];
   bb := A^^[j, ii];
   if abs(aa) <= abs(bb) then
    goto 261;
   xr := bb / aa;
   yr := sqrt(one + xr * xr);
   if aa < 0 then
    sgn := -1;
   if aa > 0 then
    sgn := 1;
   if aa = 0 then
    sgn := 0;
   cc := sgn * one / yr;
   ss := cc * xr;
   A^^[j - 1, ii] := abs(aa) * yr;
   goto 265;
261:
   if bb = 0 then
    goto 262;
   xr := aa / bb;
   yr := sqrt(one + xr * xr);
   if bb < 0 then
    sgn := -1;
   if bb > 0 then
    sgn := 1;
   ss := sgn * one / yr;
   cc := ss * xr;
   A^^[j - 1, ii] := abs(bb) * yr;
   goto 265;
262:
```

```
  A^^[j - 1, ii] := 0;
  cc := zero;
  ss := one;



265:
  A^^[j, ii] := zero;
  for l := 1 to n do
   begin
    if l <> ii then
     begin
{equiv to subroutine G2}
      xr := cc * A^^[j - 1, l] + ss * A^^[j, l];
      A^^[j, l] := -ss * A^^[j - 1, l] + cc * A^^[j, l];
      A^^[j - 1, l] := xr;
     end;
   end;
{equiv to subroutine G2}
  xr := cc * b[j - 1] + ss * b[j];
  b[j] := -ss * b[j - 1] + cc * b[j];
  b[j - 1] := xr;
 end;
290:
 npp1 := nsetp;
 nsetp := nsetp - 1;
 iz1 := iz1 - 1;
 index[iz1] := i;

{see if the remaining coeffs in set p are feasible.}
{They should be because of the way alpha was determined}
{If any are unfeasible it is due to round-off error.}
{Any that are non-positive will be set to zero and moved from set p to set z.}

 for jj := 1 to nsetp do
  begin
   i := index[jj];
   if x[i] <= 0 then
    goto 260;
  end;

{copy b[] into zz[]. Then solve again and loop back}
 for i := 1 to m do
  begin
   zz[i] := b[i];
  end;

 triangulate;
 goto 210;
{end of secondary loop}

330:
 for ip := 1 to nsetp do
  begin
   i := index[ip];
   x[i] := zz[ip];
   WriteLn('ip,i,x[i]', ip, i, x[i]);
  end;

{all new coeffs are positive.  Loop back to beginning}
 goto 30;
{end of main loop}
{come here for termination}
{compute the norm of the residual vector}
350:
```

```
 sm := zero;
 if npp1 > m then
  goto 370;
 for i := npp1 to m do
  begin
   sm := sm + b[i] * b[i];
  end;
 goto 390;
370:
 for j := 1 to n do
  begin
   w[j] := zero;
  end;
390:
 rnorm := sqrt(sm);
WriteLn('finished');
 for j := 1 to n do
  begin
   WriteLn(j, RelaxT[j], x[j]);
  end;
 SaveSpectrum;
 goto 450;
400:
 WriteLn('the dimensions of the problem are bad');
 goto 450;
410:
 WriteLn('quitting on exceeding iteration count');
 goto 450;
450:
DisposHandle(handle(A));
end.
```

Appendix 7

Simulated drift distortion of Inversion Recovery data and the generation of Gaussian noise.

Inversion recovery data was distorted with "baseline offset" and "baseline drift" which varied linearly, exponentially and sinusoidally with time. The magnitude of offset and drift was set to 10 % of the initial M_0 value. Positive and negative drift is represented as an increase (Figure 8.7) or decrease (Figure 8.8) in the magnitude of the M_∞ value over time. The period of the sine function is 25 s. Positive and negative sinusoidal drift corresponds to an initial positive or negative deviation of the sine function from the initial M_0 value.

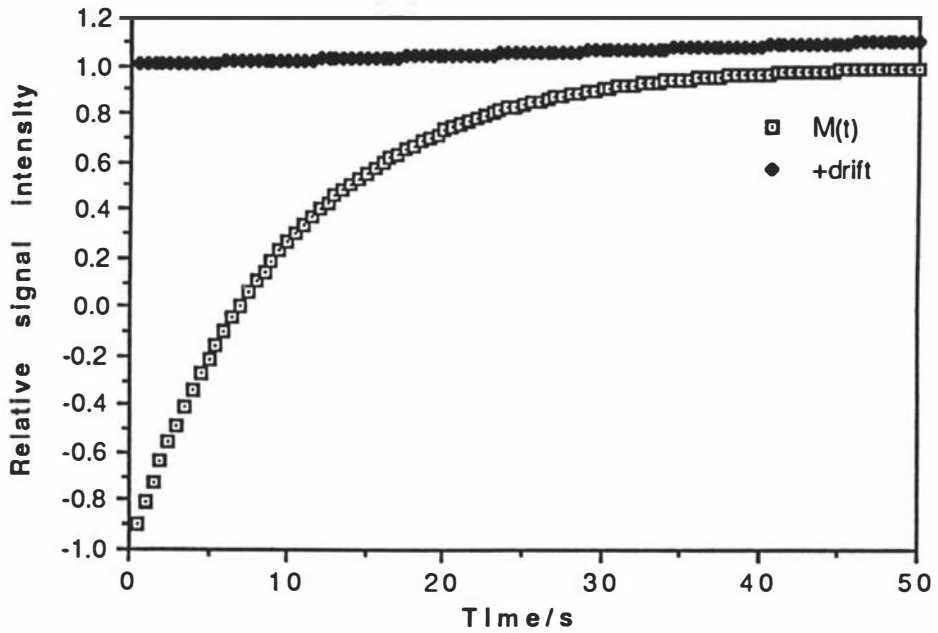

Figure 8.3. Representation of positive linear baseline dift where the magnitude of drift is 10 % of the M_0 value. Note the signal amplitude has been normalised.

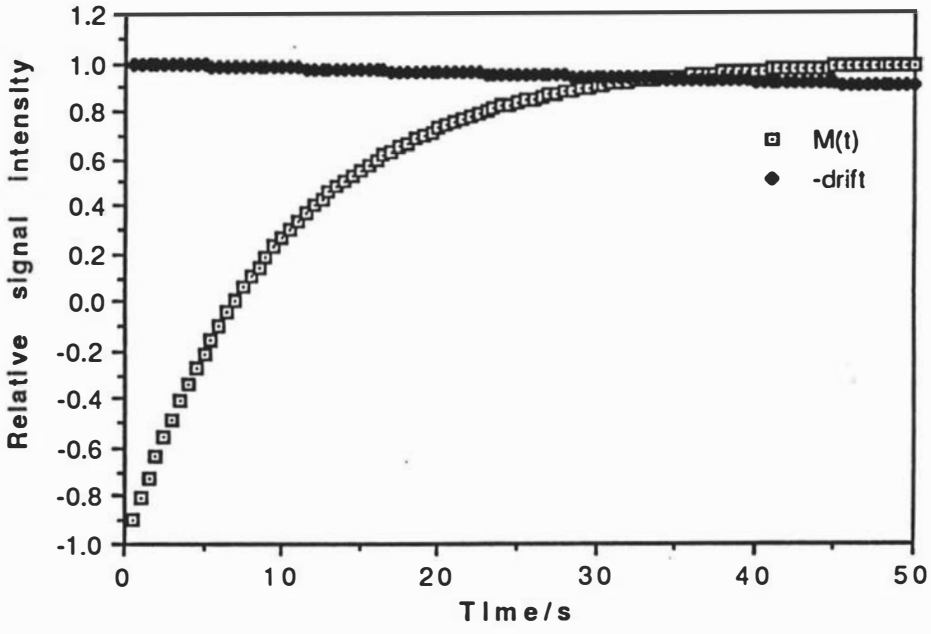

Figure 8.4. Representation of negative linear baseline drift where the magnitude of drift is 10 % of the M_0 value. Note the signal amplitude has been normalised.

Gaussian noise was calculated according to the following algorithm:

```
 REM GENERATEDATA-NOISE-BASELINE-DRIFT

 DIM T(200),X(200),Y(200),Z(200),MoDRIFT(200),NOISE(200),F(200),S(200)

 PARAMETERS:

 L=.04:H=40:I=100:S=400

 PRINT"No. OF T1'S?"
 INPUT J

  FOR N=1 TO J
     PRINT"T(";N;")";"VALUE?"
     INPUT T(N)
     PRINT"PERCENTAGE T(";N;")"
     INPUT X(N)
     LET X(N)=X(N)/100
  NEXT N

  PRINT"BASELINE?  (%)"
  INPUT BASELINE
  BASELINE=BASELINE/100

  PRINT"Mo DRIFT?  (%)?"
  INPUT D
  D=D/100
  PRINT" "
  PRINT"LINEAR?(L), EXP?(E), SIN?(S)"
  INPUT TYPE$

  PRINT"NOISE? (%)"
  INPUT P
  P=P/100
```

```
PRINT"SAVE AS?"
INPUT A$

 REM CALCULATE Mo DRIFT

 IF TYPE$ = "L" THEN
 MoDRIFT(1)=-(.25*D)
  FACTOR =(.5*D/(I-1))
   FOR N=1 TO I-1
     MoDRIFT(N+1)=MoDRIFT(N)+FACTOR
   NEXT N
 END IF

 IF TYPE$ = "E" THEN
     FOR N=0 TO I-1
       MoDRIFT(N+1)=(-.5*D*EXP((-5*N)/(I)))+.25*D
     NEXT N
 END IF

 IF TYPE$="S" THEN
  PERIOD=.5:PHASE=0
   FOR N=1 TO I
    MoDRIFT(N)=-.25*D*SIN(PHASE+6.283*(N/(PERIOD*I)))
   NEXT N
 END IF

 OPEN "COEFFS" FOR INPUT AS #1
  N=1
  WHILE NOT EOF(1)
    INPUT#1,S(N),F(N):PRINT S(N);F(N)
     N=N+1
  WEND
CLOSE #1

  FOR N=1 TO S
     RAND#=RND
  NEXT N

FOR R=1 TO I

   RAND#=RND

   IF RAND#>.5 AND RAND#<.9987 THEN
    N=1
     WHILE F(N)<RAND#
       N=N+1
     WEND
    NOISE(R)=S(N)*P
   END IF

   IF RAND#<.5 AND RAND#>.0013 THEN
    N=1
     WHILE F(N)<1-RAND#
       N=N+1
     WEND
    NOISE(R)=-1*S(N)*P
   END IF

   IF RAND#=.5 THEN
     NOISE(R)=0
   END IF

   IF RAND#<O.OO13 THEN
     NOISE(R)=-3
   END IF
```

```
    IF RAND#>.9987 THEN
      NOISE(R)=3
    END IF

    PRINT NOISE(R)

  NEXT R

REM LOG SCALE
LET D= LOG(H/L)/(I-1)
LET L=LOG(L)
FOR N=0 TO I-1
LET Y(N+1) =EXP(L+(N*D))
NEXT N

 FOR R=1 TO I
  FOR N=1 TO J
   LET Z(R)=Z(R)+(X(N)*EXP(-Y(R)/T(N)))
  NEXT N
   Z(R)=Z(R)+BASELINE+ NOISE(R)- MoDRIFT(R):PRINT"Z=";Z(R)
 NEXT R

OPEN A$ FOR OUTPUT AS #1
FOR N=1 TO I
PRINT #1,Y(N);CHR$(9);Z(N)
NEXT N
CLOSE #1
END
```

Appendix 8

Drying conditions of Spray-dried amorphous lactose powder

A solution of 13.04% w/w lactose was prepared by dissolving 12 kg of pharmaceutical grade lactose (Lactose Company of New Zealand) in 80 kg of water at 80 °C. The dissolved lactose was then spray dried using a pilot-scale disc drier, equipped with an intenal fluid bed, at the New Zealand Dairy Research Institute. The inlet air temperature was 200 °C and the exhaust temperature was 94 °C (see Figure 8.3). The fluid bed was supplied with dehumidified air at 25 °C to cool the product.

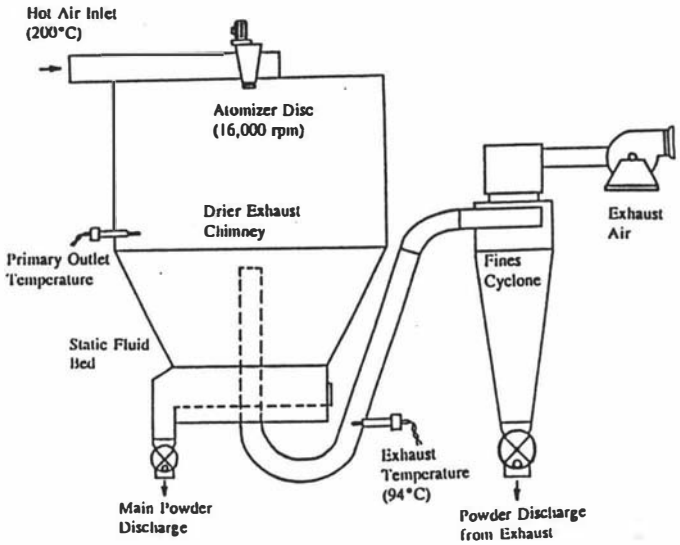

Figure 8.5. Schematic diagram of the pilot-scale drier used to spray dry amorphous lactose.

Appendix 9

Constraining the LH algorithm to a biexponential model

Figures 8.4 to 8.6 indicate the outcome of LH inversion of simulated biexponential relaxation data constructed from coadded 0.3 s and 8.9 s relaxation time constants in the amplitude ratio of 2:98 respectively. The LH algorithm is configured with the 8.9 s component fixed and the second component is varied from 0.1 s to 8.9 s. The result indicates the amplitude distortion of the short relaxation time component due to innacuracy of the relaxation time value in relation to random experimental noise.

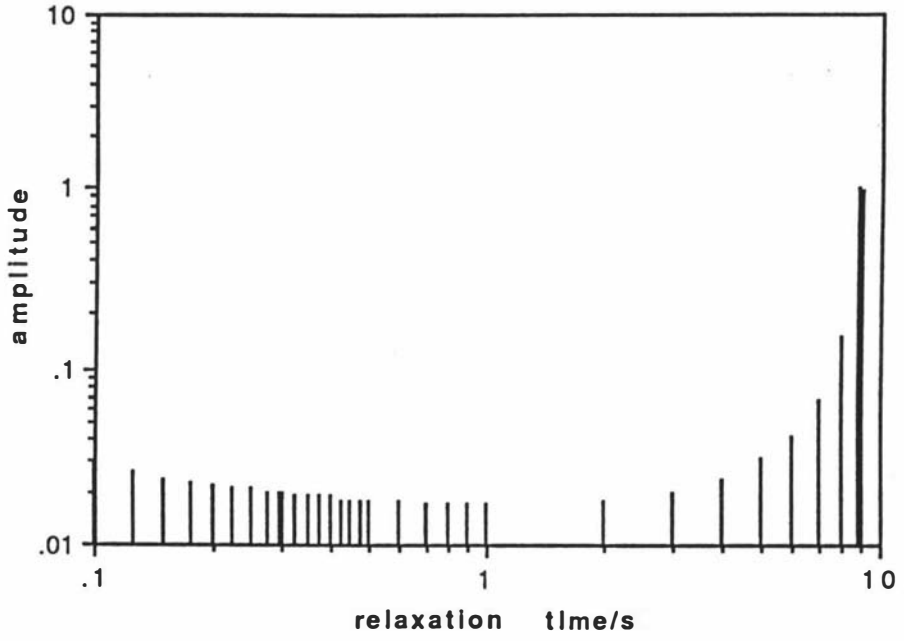

Figure 8.6. Biexponential relaxation data (as described in the text) corrupted with 0.5% mean deviation Gaussian noise

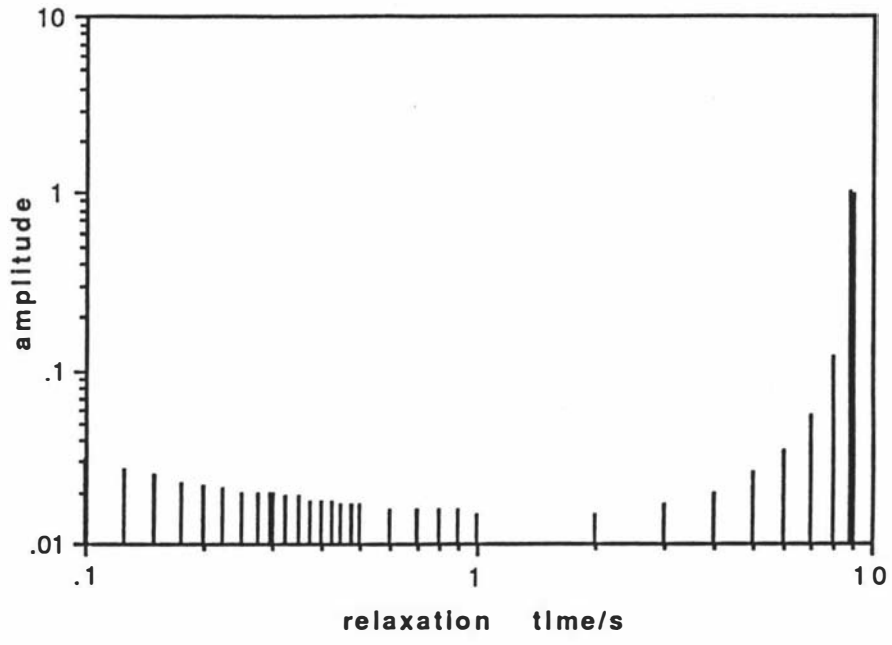

Figure 8.7. Biexponential relaxation data (as described in the text) corrupted with 1% mean deviation Gaussian noise

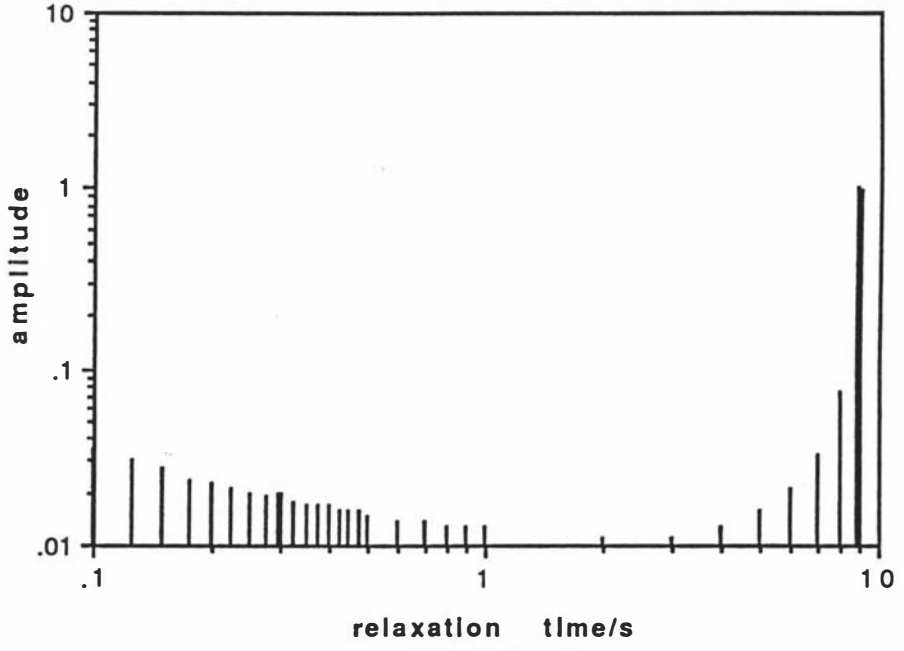

Figure 8.8. Biexponential relaxation data (as described in the text) corrupted with 2% mean deviation Gaussian noise

It is clear that amplitude distortion increases with experimental noise. An error of order 50% in the relaxation time value (corresponding to variations in $T_{1amorphous}$ due to variable moisture content (0.3 ± 0.15 s)) results in amplitude distortion of order 25% of the true value (2%) or 0.25% of the total amplitude of both components. This is less than the random experimental error of the multiexponential and "three-point" methodologies and is therefore not significant.